University of Glasgow

McCallum, Jennifer Elizabeth. (2014) *Investigation of a role for GPR35 as a novel therapeutic target in cardiovascular disease.* PhD thesis.

Investigation of a role for GPR35 as a novel therapeutic target in cardiovascular disease

Jennifer Elizabeth McCallum
B.Sc (Hons), MRes

Submitted in the fulfilment of the requirements of the degree of Doctor of Philosophy in the Institute of Molecular, Cell and Systems Biology and the Institute of Cardiovascular and Medical Sciences, University of Glasgow

J.E.McCallum
September 2014

Author's Declaration

I declare that this thesis has been written entirely by myself and is a record of my own work, with the exception of the collection of tissues derived from angiotensin II infused mice (Dr M. Flores-Munoz) and gene expression analysis of human tissue (Dr C. Clarke). This thesis has not been submitted for any other degree at the University of Glasgow or any other institution and has been completed under the supervision of Professor Graeme Milligan and Dr Stuart Nicklin at the Institute of Molecular, Cell and Systems Biology and Institute of Cardiovascular and Medical Sciences, respectively.

Signature _____

Printed name: Jennifer Elizabeth McCallum

Acknowledgments

First and foremost, I would like to thank Professor Graeme Milligan and Dr Stuart Nicklin for their tireless support, guidance and encouragement throughout the course of my research and during the write-up time. I am hugely appreciative of the generous time, advice and opportunities you have both given me over the years. I would also like to sincerely thank the British Heart Foundation for my funding and directors Profs. Andrew Baker and Godfrey Smith for their advice and guidance throughout the studentship.

Secondly, I would like to acknowledge Dr Andrew Cathcart, who is tragically no longer with us. Andy was the first person to recognise my potential in scientific research and I can truly say that it was an honour to work with him. His enthusiastic tutorials and passion for research inspired me to progress to the next step in scientific research and for this, I will be forever indebted to him.

I would also like to extend my gratitude to all of my friends and colleagues in the Milligan lab, past and present. Laura, thank you for teaching me all of the pharmacology basics, your help has been invaluable! A huge thank you to John for all his advice and training with microscopy and to Brian for his helpful discussions. Of course, my research journey would not have been bearable without the friendship of Laura, Elisa and Nicola (an honorary Milligan lab member) – thank you girls for all the tea chats, lunch chats and pub chats!

Equally, I would like to thank all of my friends and colleagues in the BHF lab. Thank you to Nicola and Gregor for all their help and guidance, Delyth Graham for her invaluable training in small animal surgery techniques and also to Elisabeth Beattie for her myography training and for introducing me to the wonders of Women's Hour (which I now listen to daily)! Thank you also to Carolyn for her time and patience, teaching me all things qRT-PCR based. Huge appreciation to Clare, Hollie, Lesley, Audrey, Jenny and Erin for their friendship, office hilarity and great advice, whenever it was needed.

I would like to acknowledge my wonderful friends - you have all been there throughout every important journey in life. My lovely Ya Ya's; Anna-Louise, Eleanor, Janet, Sarah, Karen, Ruth, Joanne and Catherine, thank you for your indelible support and for being the greatest inspiration a girl could ever need.

Last, but never least, I want to thank my entire family who have supported every decision I have made with gusto and pride. Mum and Dad, a special thank you for being my eternal champions. To my husband, Lorne, thank you for your unending support and light-hearted nature. You calm my soul.

List of Publications

MacKenzie AE, **Lappin JE**, Taylor DL, Nicklin SA, and Milligan G (2011) GPR35 as a novel therapeutic target. *Front. Endocrin. Molecular and Structural Endocrinology* **2**: 68.

Jenkins L, Harries N, **Lappin JE**, MacKenzie AE, Neetoo-Isseljee Z, McIver E, Taylor DL, and Milligan G (2012). Antagonists of GPR35 display high species ortholog selectivity and varying modes of action. *J Pharmacol Exp Ther 343:683–695.*

MacKenzie AE, Caltabiano G,Kent TC, Jenkins L, **McCallum JE**, Hudson BD, Nicklin SA, Fawcett L, Lane R, Charlton SJ and Milligan G (2013). Antiallergic mast cell stabilizers lodoxamide and bufrolin as the first high and equipotent agonists of human and rat GPR35. *Mol Pharmacol, 85**, 91-104.*

Abstracts:

Scottish Cardiovascular Forum (SCF)

University of Strathclyde, Glasgow, January 2013

GPR35 as a novel therapeutic target of cardiovascular disease. **Jennifer E. Lappin**,

Stuart A. Nicklin, Graeme Milligan.

(Poster communication)

BHF 4-year studentship meeting

University of Oxford, Oxford, May 2013

Investigating GPR35 function in human vascular smooth muscle cell migration. **Jennifer**

E. Lappin, Stuart A. Nicklin, Graeme Milligan.

(Oral presentation)

European Society of Cardiology (ESC)

Amsterdam, September 2013

Investigating GPR35 function in human vascular smooth muscle cell migration. **Jennifer E. Lappin**, Stuart A. Nicklin, Graeme Milligan.

(Oral presentation)

Table of Contents

List of Figures

List of Abbreviations and Definitions

7TMR	Seven-transmembrane receptor
AC	Adenylyl cyclase
ACE	Angiotensin converting enzyme
ADP	Adenosine diphosphate
Ang I	Angiotensin-I
Ang II	Angiotensin-II
AT_1R	Angiotensin II-type 1 receptor
ATP	Adenosine triphosphate
A.U.	Arbitrary unit
$β_2AR$	$β_2$-adrenoceptor
BHF	British Heart Foundation
BMS	Bare metal stent
BP	Blood pressure
BPM	Beats per minute
BRET	Bioluminescence resonance energy transfer
BrdU	5-Bromodeoxycytidine
BW	Body weight
C-	Carboxyl terminus
Ca^{2+}	Calcium
CABG	Coronary artery bypass-graft
CAD	Coronary artery disease
CAM	Constitutively active mutant
cAMP	Cyclic adenosine monophosphate
CCP	Clathrin coated pit
cGMP	Cyclic guanine monophosphate
COX	Cyclooxygenase
CRTH2	Chemoattractant receptor-homologous molecule
CVD	Cardiovascular disease
DAG	Diacyl glycerol
DBP	Diastolic blood pressure

DES	Drug eluting stent
DMR	Dynamic mass redistribution
DNA	Deoxyribonucleic acid
DOX	Doxycycline
EC	Endothelial cell
EC_{50}	Half maximal effective concentration
ECL	Extracellular loop
ECM	Extracellular matrix
Edg1	Sphingolipid G-protein-coupled Receptor 1
EGF	Epidermal growth factor
ELISA	Enzyme-linked immunosorbant assay
EPAC	Exchange proteins activated by cAMP
ERK	Extracellular signal-regulated kinases
eYFP	Enhanced-yellow fluorescent protein
g/mm	Grams/millimetre
g/g	Grams/grams
GABA	γ-aminobutyric acid
GAP	GTPase activating protein
GDP	Guanosine diphosphate
GEF	Guanine nucleotide exchange factor
GFP	Green fluorescent protein
GnRH	Gonadotrophin releasing hormone
GPCR	G protein-coupled receptor
GPR35	G protein-coupled receptor 35
GRK	GPCR Kinase
Gstm1	Glutathione S-transferase Mu 1
GTP	Guanosine triphosphate
GWAS	Genome-wide association study
HBD	Hormone binding domain
HFD	High fat diet
HIF-1	Hypoxia inducible factor-1
HR	Heart rate

HSV	Human saphenous vein
HTRF	Homogenous time resolved fluorescence
HUVEC	Human umbilical vein endothelial cell
HW	Heart weight
ICAM-1	Intracellular adhesion molecule-1
ICL	Intra-cellular loop
IP1	Inositol-1-phosphate
IP3	Inositol 1,4,5-trisphosphate
IVUS	Intravascular ultrasound
K^+	Potassium
K_i	Dissociation constant
KO	Knock-out
KYNA	Kynurenic acid
LAD	Left anterior descending
LDL	Low-density lipoprotein
LPA	Lysophosphatidic acid
LV	Left ventricle
LV+S	Left ventricle plus septum
MAP	Mean arterial pressure
MAPK	Mitogen Activated Protein Kinase
MLC	Myosin light chain
MLCP	Myosin light chain phosphatase
mg/g	Milligrams/grams
mg/mm	Milligrams/millimetre
MI	Myocardial infarction
MMA	Molecular mode of action
mmHg	Millimetres of mercury
MMP	Matrix metalloproteinase
MYPT-1	Myosin phosphatase-1
N-	Amino terminus
NA	Nor-adrenaline
ORF	Open reading frame

OxLDL	Oxidised low-density lipoprotein
PCR	Polymerase chain reaction
PE	Phenylephrine
PDE	Phosphodiesterase
PIP2	Phosphatidylinositol 4,5-bisphosphate
PI3K	Phosphatidylinositol-3 kinase
PKA	Protein kinase A
PKC	Protein kinase C
PLC-β	Phospholipase-C β
PHD	EGL nine homolog 3
PTCA	Percutaneous transluminal coronary angioplasty
PTX	*Pertussis* toxin
PP	Pulse pressure
qRT	Quantitative real-time
R	Inactive receptor conformation
R*	Active receptor conformation
Rluc	*Renilla* luciferase
RGS	Regulators of G-protein signalling
RNA	Ribonucleic acid
ROCK	Rho-associated coil kinase
ROS	Reactive oxygen species
RT	Reverse transcription
RQ	Relative quantification
RyR	Ryanodine receptor
S1P	Sphingosine-1-phosphate
SBP	Systolic blood pressure
SHRSP	Stroke-prone spontaneously hypertensive rat
SMC	Smooth muscle cells
SNP	Sodium nitroprusside
SNP	Single nucleotide polymorphism
SRF	Serum response factor
TAC	Transverse aortic constriction

TIMP	Tissue inhibitor of metalloproteinase
TMD	Transmembrane domain
TRITC	Tetramethylrhodamine
VCAM-1	Vascular cell adhesion molecule-1
VSMC	Vascular smooth muscle cell
WGA	Wheat germ agglutinin
WHO	World Health Organisation
WKY	Wistar-Kyoto rat
WT	Wild-type

Abstract

G protein-coupled receptors (GPCRs) are often described as 'gate-keepers' of the eukaryotic cell and their roles primarily involve translating extra-cellular stimuli via G-protein coupling and intracellular signalling to govern various physiological responses. These functional parameters are wide ranging and include the modulation of visual sensory organs, to the control of vasoreactivity and heart rate. Importantly, their flexible architecture can facilitate small molecule interaction within a 'binding-pocket' and GPCR research often focuses on this relationship to identify and design novel and effective ligands to manipulate GPCR activation and signalling.

GPR35 is a poorly characterised, Class A GPCR and despite reports of two potential endogenous activators; kynurenic acid (KYNA) and lysophosphatidic acid (LPA) in recent years, it is still widely acknowledged as an 'orphaned' GPCR. This is reflected by the propensity of its ligands, both endogenous and synthetic, to demonstrate extreme species orthologue-selective properties. Despite this, investigators have highlighted various roles for GPR35 relating to pain, inflammation, hypertension and heart failure, and investigations have suggested that activation of GPR35 leads to a selective coupling of $G\alpha_{13}$, a G-protein understood to mediate Rho A and ROCK 1/2 signalling. However, a lack of functional ligand pairs has hampered further research to examine a role for GPR35 and subsequent $G\alpha_{13}$ signalling in these disease models. In this study, we have characterised a series of highly-potent, synthetic ligands at human, rat and mouse orthologues of GPR35, revealing that GPR35 agonist, pamoic acid and antagonists, CID-2745687 and ML-145, are highly potent and selective for the human orthologue of GPR35. This has provided us with the opportunity to assess a functional role for GPR35 within a cardiovascular disease setting using functional ligand pairs in cells of a human origin, for the first time.

Vascular smooth muscle cell (VSMC) migration and proliferation are central to neointima formation in vein graft failure. Despite a detailed understanding of VSMC migration and proliferation mechanisms, there are no pharmacological interventions which effectively prevent vein graft failure through intimal occlusion. In this study, we demonstrated that primary vascular cells expressed robustly detectable levels of GPR35, and these were comparable to those demonstrated in the colon, which has been previously reported to highly express GPR35. Human GPR35 is potently activated by the selective agonist pamoic acid and reference ligand zaprinast and blocked by antagonists CID-2745687 and ML-145. Following exposure of VSMC to pamoic acid or zaprinast, cell migration was enhanced and these effects were blocked by co-incubation with CID-2745687 or ML-145. Pamoic acid induced HSV SMC migration was also blocked in the presence of two distinct Rho A pathway inhibitors, Y-16 and Y-27632. Activation of this pathway was also reflected by remodelling of the cytoskeletal architecture in HSV SMCs to significantly elongate the cell and promote a contractile, migratory phenotype following pamoic acid stimulation and this effect was also blocked following co-administration with either antagonist. Additionally, we also demonstrated that following exposure to pamoic acid or zaprinast, human saphenous vein endothelial cell (HSV EC) integrity and proliferation were significantly improved and this was blocked following co-administration with either antagonist, suggesting a protective role for GPR35 in the vascular endothelium.

Results from a previous study demonstrated that lack of GPR35 expression resulted in an elevation in systolic blood pressure (SBP) by up to 37.5mmHg in mice. The recent identification of mast-cell stabilising compounds as highly potent agonists at GPR35 provided the opportunity to pharmacologically target GPR35 within a rodent model of hypertension. Therefore, we also aimed to test if pharmacological manipulation of GPR35 via stimulation with the novel, rodent selective agonist amlexanox, modulated blood pressure and end-organ related damage in 6-12 weeks of age stroke prone spontaneously hypertensive rats (SHRSPs). Radiotelemetry acquisition of haemodynamic

properties highlighted that pharmacological agonism of GPR35 exacerbated hypertension and end-organ damage in the SHRSP and this was evident following an elevation in SBP by 20mmHg throughout the trial. Moreover, quantification of heart mass and cardiomyocyte size revealed that GPR35 agonism induced cardiac hypertrophy. Collagen staining revealed enhanced renal fibrosis in both the interstitial and perivascular regions of the kidney from amlexanox treated animals, compared to vehicle controls. Additionally, large vessel myography highlighted that endothelium-dependent vasorelaxation was reduced by 20% in amlexanox treated SHRSPs. Fundamentally, these results suggest that GPR35 is involved in regulating vascular tone and we hypothesise that this may involve the $G\alpha_{13}$-Rho A-ROCK1/2 signalling pathway demonstrated to mediate a contractile, migratory phenotype in human primary VSMCs.

Taking these data together, the results suggest that GPR35 antagonists might be of clinical use to therapeutically target and inhibit activation of GPR35 in the setting of vascular remodelling during acute vascular injury, and hypertension and its related end-organ damage.

1 Introduction

1.1 G Protein-Coupled Receptors

Since their discovery in the early twentieth century, G protein-coupled receptors (GPCRs) have become the most extensively studied class of cellular receptors. Comprising a 'super-family' with an extensive array of sub-classifications, all GPCRs share a common single polypeptide, seven-transmembrane domain structure and are therefore also termed seven-transmembrane domain receptors (7TMRs). Often described as 'gate-keepers' of the eukaryotic cell, members of the GPCR superfamily are activated by a diverse range of endogenous ligands which include neurotransmitters, hormones, and environmental stimuli such as light, smell and taste as well as synthetic small molecules (Kenakin, 2004).

Upon activation, the GPCR-ligand binding complex undergoes marked conformational changes to facilitate coupling to a heterotrimeric G-protein, which in turn, produces physiological effects via regulation of a broad group of intracellular signalling pathways. Pharmacological manipulation of GPCRs can provide the means to alter GPCR regulation, activation and downstream signalling in health and disease and, consequently, these receptors are widely considered as excellent therapeutic targets in a variety of pathological conditions. It is, therefore, unsurprising that GPCR research remains an integral aspect of efforts in translational medicine and, to this end, there are many examples of 'druggable' GPCRs for which ligands that either block or activate the receptor are widely used in clinical medicine. Examples of these include valsartan, an antagonist of the angiotensin II-type 1 receptor (AT_1R) which is utilised in the treatment of hypertension, coronary artery disease and heart failure and a range of β_2-adrenoceptor (β_2AR) ligands with broad application including relieving acute symptoms of asthma and chronic obstructive pulmonary disease as well as heart failure (DeWire and Violin, 2011).

1.1.1 GPCR structure

In their inactive state GPCRs are routinely situated within the lipid-rich plasma membrane and span the surface of virtually all eukaryotic cells. These surroundings provide structural stability for the relatively hydrophobic transmembrane domains (TMDs) of GPCRs. The seven helices are linked via extra and intra-cellular loops (E/ ICL) spanning the cell membrane and both the extracellular domains and the architectural organisation of the transmembrane helices provide flexible pockets into which GPCR ligands can bind (Kobilka, 2007).

The core domain of the seven transmembrane helices and linking intra- and extra-cellular loops is flanked by an extracellular amino (N)-terminus and an intracellular carboxyl (C)-terminus. Sequence alignments show the third intracellular loop between the fifth and sixth TMDs, along with the C and N-termini, are the most variable regions (Kobilka, 2007). GPCR termini can vary in both length and function and are often indicative of their GPCR classification, as discussed later.

Analysis of GPCR protein structure has also highlighted a number of highly conserved regions within the TMDs and, as anticipated from such conservation, these regions play key roles in receptor structure and function (Teller *et al.*, 2001). Perhaps the best known of these is the key 'DRY' motif. This amino acid sequence, which consists of glutamic acid/aspartic acid–arginine–tyrosine (i.e. E/DRY), is located at the interface between the bottom of the third TMD and second ICL of the 'rhodopsin-like' family of GPCRs (Ballesteros *et al.*, 1998). Due to its highly conserved nature, researchers have examined its structural and functional role within GPCRs and evidence is strongly suggestive of critical involvement in the governance of conformational stability, constitutive activity and G-protein coupling profiles (Alewijnse *et al.*, 2000, Rovati *et al.*, 2007). In recent years rapid advances in the ability to stabilise and obtain atomic level X-ray structures of

individual GPCRs has resulted in a previously unimaginable increase in understanding of the organisational structure of members of the GPCR family (see later).

1.1.2 GPCR classification

GPCRs are the largest family of cell surface receptors, with more than 800 identified following the completion of the human genome project in 2003 (Fredriksson *et al.*, 2003). Based on homology and potential ligand groups, they are organised into 5 broad sub-families, 'Rhodopsin-like/ Class A', 'Secretin', 'Glutamate', 'Adhesion' and 'Frizzled' (Fredriksson *et al.*, 2003, Krishnan *et al.*, 2012) – please see Figure 1-1 for a representative diagram of the 5 sub-families and a range of representative GPCRs which have been clinically targeted or where atomic level structures have been solved.
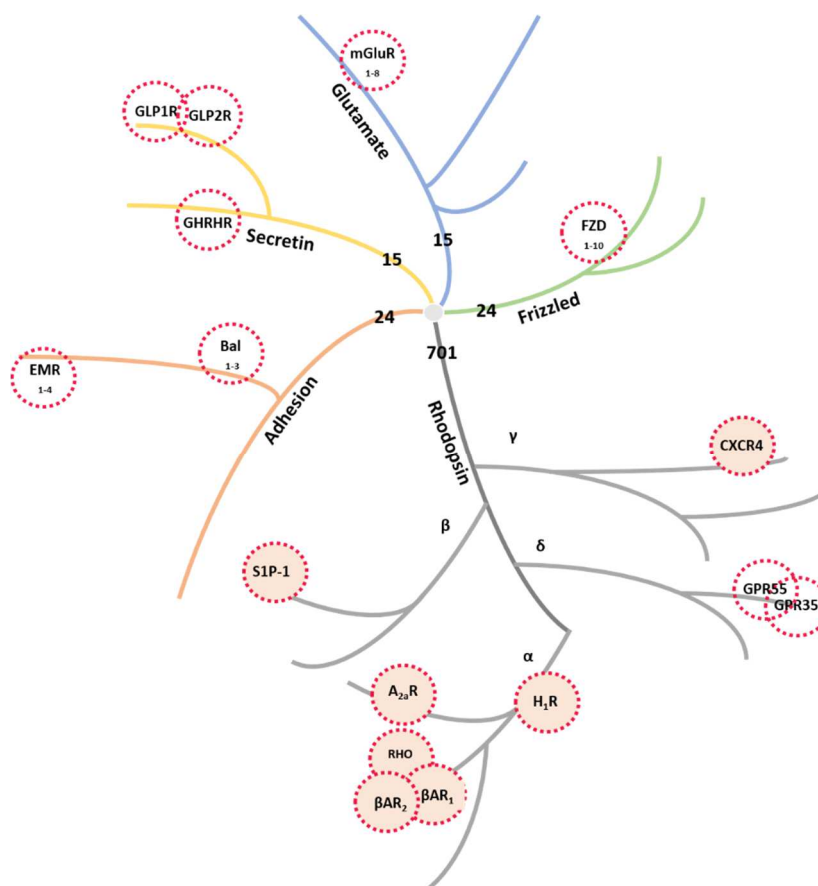
Figure 1-1. The human GPCR superfamily.

Representative diagram based upon the phylogenetic analysis of the broad superfamily of GPCRs which are sub-divided into 5 distinct categories relating to their homogeneity within the 7TMD region. The grey branch represents the 'Rhodopsin-like/ Class A family', composed of 701 GPCRs it is further categorised into 4 groups; α, β, γ and δ. The yellow branch relates to the 15 'Secretin/ Class B' receptors. The 'Glutamate/ Class C' receptors constitute a family of 15 which are denoted by the blue tree branches. The orange tree branch relates to the 'Adhesion' receptors, of which there are 24 and finally, the 'Frizzled' family of 24 are represented by the yellow branches. Exemplar receptors are highlighted; GPR35, GPR55, Bal $_{1-3}$ - brain-specific angiogenesis inhibitor 1-3, EMR $_{1-4}$ - EGF-like module-containing mucin-like hormone receptor 1-4, GHRHR - growth-hormone-releasing hormone receptor, GLP1R/2R - glucagon-like peptide 1/2 receptor, mGluR$_{1-8}$ - metabotropic glutamate receptor 1-8 and FZD$_{1-10}$ – frizzled receptor 1-10. GPCRs highlighted in pink are exemplar GPCRs with atomically solved structures; βAR$_1$/ βAR$_2$ – β$_1$/ β$_2$ adronergic receptor, RHO – rhodopsin receptor, A$_{2a}$R – adenosine A$_{2a}$ receptor, H$_1$R – histamine$_1$ receptor, CXCR4 – CXC chemokine receptor-4 and S1P-1 - sphingosine-1-phosphate receptor 1 (Diagram adapted from (Stevens *et al.*, 2013)).

The 'rhodopsin-like/ class A' GPCRs comprise the largest family (87.6%) and have varied agonists and physiological roles (Fredriksson *et al.*, 2003). This family is readily identifiable via their short extracellular N-termini and ligand binding pockets that lie predominantly within the TMD regions (Nordstrom *et al.*, 2009). Due to the large number of members, the rhodopsin-like family are further sub-categorised into 4 distinct groups; α, β, γ and δ, based upon phylogenetic similarities. The second group of receptors constitute the 'secretin' or 'class B' receptors and comprise a small family of some 15 members. Secretin family receptors are regulated primarily by large peptide hormones which interact, at least in substantial part, with the extracellular N-terminal domain and importantly, contain hormone binding domains (HBD) (Nordstrom *et al.*, 2009). In recent times, the first atomic level structures of class B receptor family members have been described (Hollenstein *et al.*, 2013, Siu *et al.*, 2013), providing a much more detailed insight into the basis of recognition of such peptide hormone ligands. This includes the identification of novel orthosteric binding pockets located deep within TMD regions (Hollenstein *et al.*, 2014). Of a similar size to the 'secretin' receptor family, the 'glutamate' or 'class C' receptors also constitute a small group of some 15 members. Unlike the class A receptors, the N-terminal domain of members of this group consists of a large 'venus flytrap' region, and the members of the family exist as constitutive dimers, an organisational feature which is intrinsic to their function. Although to date no atomic level structure of a full length 'class C' receptor has been reported this has been achieved individually for both the extracellular domain (Kunishima *et al.*, 2000, Muto *et al.*, 2007) and the 7TMD segments (Wu *et al.*, 2014) and, by linking these, models of the mode of ligand activation are well established (Chun *et al.*, 2012, Yin and Niswender, 2014). The 'Adhesion' receptors are a family of 24 members, and hence they constitute the second largest family of GPCRs (Yona *et al.*, 2008). Although similar to the 'Secretin' family, they are distinguished by markedly extended N-termini which can be structurally diverse (Lagerstrom and Schioth, 2008). However, they often containing common structural domains which are involved in cellular adhesion and protein interactions for downstream

signalling; these are present in epidermal growth factor (EGF)-like, lectin-like and immunoglobulin (Ig) secretin GPCRs (Yona *et al.*, 2008). Finally, the 'Frizzled' sub-category is also a family of some 20 receptors. These are primarily activated by Wnt glycoproteins which bind to cysteine-rich, extracellular domains on the GPCR (Bjarnadottir *et al.*, 2006).

This method of comparative sequence homology is widely employed. However, recent protocols to classify GPCR sub-families have taken other approaches. For example, when categorising receptor families, some approaches have begun to consider a combination of structural homology, ligand specificity and physiochemical hierarchy (Klabunde, 2007, Gao *et al.*, 2013). The integration of these approaches may be useful in exploring the evolutionary history and conserved nature of ancient receptors and successive relatives (Nordstrom *et al.*, 2009, Krishnan *et al.*, 2012). Indeed, the quest for an accurate system to define the molecular signatures of GPCR families is becoming more evident, particularly as the structural details of a greater number of GPCRs becomes available (Venkatakrishnan *et al.*, 2013).

1.1.3 GPCR crystallisation

In order to better understand GPCR structure-function relationships, immense efforts have focused upon obtaining atomic level structures of GPCRs in both inactive (R) and active (R*) states. These structures provide a wealth of information relating to the key residues which are involved in mediating GPCR flexibility and thereby facilitate the conformational changes which occur during ligand binding, receptor activation and subsequent G-protein coupling (Nakamura *et al.*, 2013).

The first GPCR crystal structure, bovine Rhodopsin, was solved over a decade ago (Palczewski *et al.*, 2000) and following this an increasing stream of structural information has become available for class A receptors (Stevens *et al.*, 2013). This includes the high

resolution structural identity of the β_2AR in 2007 and the chemokine receptor, CXCR4 in 2010 (Rasmussen *et al.*, 2007, Wu *et al.*, 2010).

Despite this progress, the conformational instability of an activated GPCR within a lipid rich, hydrophobic membrane hindered many early attempts to capture the GPCR in an active form (Kobilka, 2007, Kobilka and Schertler, 2008). This improved following development of highly specific antibodies and GPCR stabilising ligands (Maeda and Schertler, 2013). In 2011, details of the β_2AR, A_{2A} adenosine and rhodopsin receptors in agonist-bound, active states were published, the first such descriptions (Rasmussen *et al.*, 2011, Xu *et al.*, 2011, Standfuss *et al.*, 2011). These data provided much sought after comparative structural insights relating to the basal conformational status, ligand specificity and conserved domains which are essential in potentiating the R* state of rhodopsin-like/ class A GPCRs (Maeda and Schertler, 2013, Costanzi, 2013). Most notably, the leading collaborators in this field - Professors Brian Kobilka and Robert Lefkowitz, were jointly awarded the Nobel Prize in Chemistry in 2012 for their outstanding contributions to GPCR research.

1.2 GPCR signalling

1.2.1 G-proteins

The fundamental roles of GPCRs are to regulate various physiological signalling processes involved in maintaining homeostasis and to mobilise responses to pathological stimuli within the extracellular environment. Following ligand binding, GPCRs undergo unique conformational changes which promote their coupling to heterotrimeric guanine nucleotide binding proteins (G-proteins) and it is by these means that they can regulate intracellular signalling pathways in canonical fashion (Milligan and Kostenis, 2006).

G-proteins are freely distributed across eukaryotic cell membranes and may be preferentially expressed within cells and tissues depending upon their physiological relevance and functional role (Wettschureck and Offermanns, 2005). For effective activation by GPCRs, they are required to be closely anchored to the plasma membrane and this is facilitated via covalent lipid modifications and additional plasma membrane targeting factors, including palmitoylation and/or myristoylation (Marrari *et al.*, 2007). In an inactive state, G-proteins exist as a single, heterotrimeric unit comprising three sub-components; Gα, Gβ and Gγ (Milligan and Kostenis, 2006). It is well established that upon GPCR coupling and activation, the newly GTP bound Gα subunit dissociates from the Gβγ complex following the release of guanosine diphosphate (GDP) and its exchange for guanosine triphosphate (GTP). This activation process is accelerated by guanine nucleotide exchange factors (GEFs), with GPCRs being key examples of such GEFs, and decelerated by GTPase activating proteins (GAPs) such as Regulators of G-protein signalling (RGS) proteins (Suzuki *et al.*, 2009). Inactivation is associated with hydrolysis of the terminal phosphate of GTP, catalysed by the GTPase activity intrinsic to the Gα subunit and this allows re-association with the Gβγ complex. Figure 1-2 displays a schematic representation of GPCR activation and G-protein coupling mechanisms.
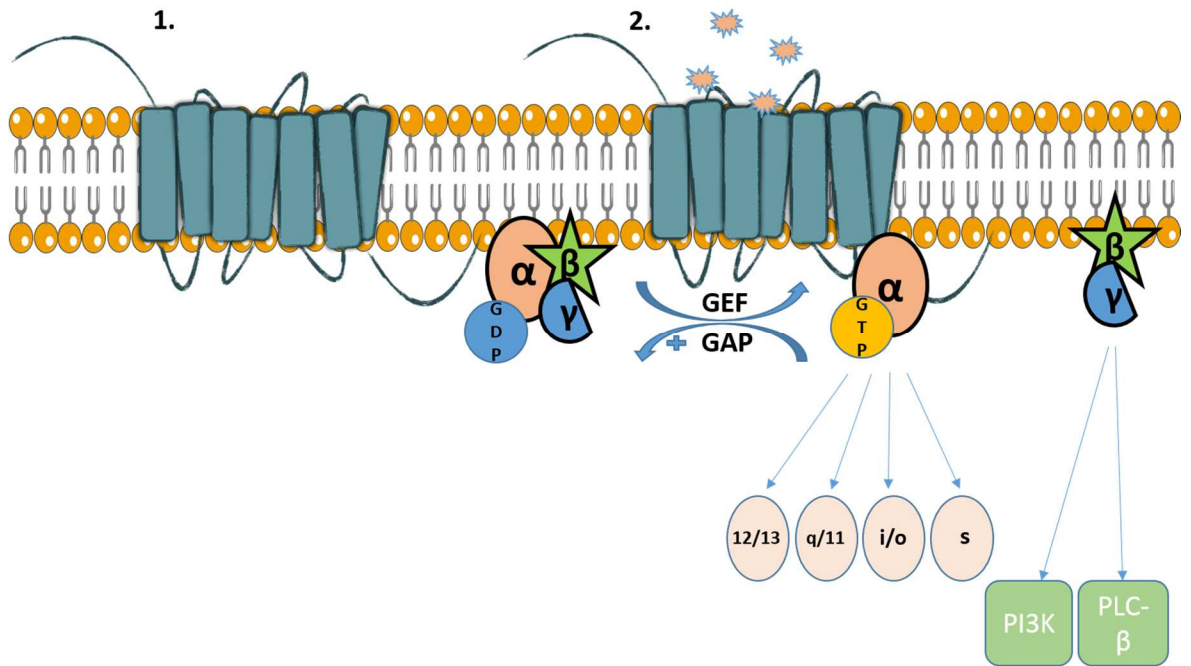
Figure 1-2. GPCR-G-protein coupling and activation.

1. A GPCR and a heterotrimeric G-protein unit in the inactive state with bound GDP and anchored to the lipid plasma membrane. **2.** GPCR and G-protein complexes in the active state. Guanine nucleotide exchange factors (GEF) promote the dissociation of GDP. Following receptor activation, conformational changes couple a select Gα subunit; Gα$_{12/13}$, Gα$_{q/11}$, Gα$_{i/o}$ or Gα$_s$. The newly GTP bound Gα subunit dissociates from the Gβγ complex, by exchanging guanosine diphosphate (GDP) for guanosine triphosphate (GTP). Gα and Gβγ complexes may then initiate distinct, intracellular signalling pathways. Two enzymes frequently linked to Gβγ-mediated control of activity are phosphatidylinositol-3 kinase (PI3K) and various isoforms of phospholipase-C β (PLCβ). This process is terminated via the GTPase activating proteins (GAP) which serve to promote the hydrolysis of the active GTP-Gα subunit.

1.2.1.1 G-protein families

In a similar fashion to GPCRs, G-proteins also comprise a collection of families and sub-families. In mammals, Gα proteins are encoded by 21 genes, categorised within 4 broad signalling families primarily based upon their sequence homology and central functional roles (Cabrera-Vera *et al.*, 2003). Collectively, Gα protein signalling families have been well characterised, consisting of; Gα$_s$ (G$_{s(S)}$^{a}α, G$_{s(L)}$^{a}α and G$_{olf}$α), Gα$_{i/o}$ (G$_{i1-3}$α, G$_{oA/B}$^{a}α, G$_z$α, G$_{t1/2}$α and G$_g$α), Gα$_{q/11}$ (G$_q$α, G$_{11}$α, G$_{14}$α and G$_{15/16}$α) and Gα$_{12/13}$ (G$_{12}$α and G$_{13}$α) (Cabrera-Vera *et al.*, 2003, Kostenis *et al.*, 2005).

There are 5 genes which code for Gβ subunits 1-5, and with the exception of Gβ$_5$, these subtypes share close homology, ranging between 79-90% (Khan *et al.*, 2013). Contrastingly, Gγ subunits are more diverse in sequence and are coded by 12 genes, Gγ$_{(1-12)}$. The role of specific isoforms in 'active' Gβγ complexes is comparatively less well understood than the Gα family. However, the diverse range of Gβγ subunits is also highly conserved amongst species (Khan *et al.*, 2013) and research in this area of G-protein signalling is steadily progressing (Garland, 2013).

1.2.1.1.1 The Gα$_s$ family

The G$_s$ family of α-subunits are, with the exception of *G$_{olf,}$* ubiquitously expressed within human tissue (Offermanns, 2003). Their central role and effectors are well characterised, given that the nomenclature of the *G$_s$* family signifies their ability to stimulate adenylyl cyclases – a family of enzymes responsible for catalysing production of 3'5' cyclic-AMP from ATP (Kostenis *et al.*, 2005). Hence, via activation of isoforms of protein kinase A (PKA) or EPAC (exchange proteins activated by cAMP), a vast range of proteins are phosphorylated or transcriptionally regulated, respectively (McCormick and Baillie, 2014). These actions range from the regulation of endothelial gap-junctions in the maintenance of vascular permeability and integrity via EPAC-induced Rap signalling and subsequent E-cadherin regulation (Gloerich and Bos, 2010), to the control of voltage gated Ca^{2+}

sensitive Ryanodine receptors (RyR) via PKA phosphorylation in excitation-contraction coupling in functional cardiomyocytes (Marx *et al.*, 2000).

Many class A GPCRs expressed within cardiac tissue, including the β-adrenoceptors and histamine receptor subtypes couple to this pathway (Tang and Insel, 2004). Notably, the G_s subunit recently became the first G-protein to be successfully crystallised in an activated and GPCR-coupled state; a highly anticipated development in the field of GPCR research which provided insights into the marked displacement in the proximities of binding domains; Ras (αRas) and α-helical (αAH) (Rasmussen *et al.*, 2011), which is important for the efficiency of nucleotide binding pockets following activation and coupling to the β-adrenoceptor (Rasmussen *et al.*, 2011).

1.2.1.1.2 The Gα$_{i/o}$ family

The role of the $G_{i/o}$ family of G-proteins is, in many aspects, to counter that of the G_s family in that they are generally viewed as direct inhibitors of adenylyl cyclase isoforms (Neves *et al.*, 2002). Although ubiquitously expressed within human tissue, many of the individual $G_{i/o}$ family members including G_z and G_{td-1}, are preferentially expressed in neuronal tissue and retinal rods and cones (Offermanns, 2003). For example, G_{td-1} acts to link opsins to the regulation of a cGMP phosphodiesterase and therefore acts to control levels of the secondary messenger cGMP (Tsang *et al.*, 1998).

The GPCR coupling profile and physiological roles of the $G_{i/o}$ family are very well characterised in health and disease. In large part this has been facilitated by the sensitivity of most members of the family to pertussis toxin (PTX) (Katada and Ui, 1982), a bacterial toxin produced by *Bordetella pertussis* which has the ability to catalyse the addition of ADP-ribose to the G_i subunit and thus prevent dissociation and downstream signalling (Kostenis *et al.*, 2005).

Further to its direct Gα subunit signalling pathway, the $G_{i/o}$ family are also understood to promote the dissociation and thus signalling of the Gβγ complex to a higher degree than

others; leading to direct interactions with other signalling pathways, including the regulation of phosphodiesterases (PDEs) and potassium channel activation (Wettschureck and Offermanns, 2005, Leaney and Tinker, 2000).

1.2.1.1.3 The $G\alpha_{q/11}$ family

The $G_{q/11}$ family comprises four distinct α-subunits that are best known for their ability to couple GPCRs to the β1-isoform of phospholipase-C (PLC-β), an enzyme which promotes hydrolysis of phosphatidylinositol 4,5-bisphosphate (PIP_2) at the plasma membrane, generating the second messengers inositol 1,4,5-trisphosphate (IP_3) and sn-1,2 diacyl glycerol (DAG) (McCudden $et\ al.$, 2005). Unlike the $G_{i/o}$ family of proteins, this family is not PTX sensitive and, therefore, characterisation of this pathway has involved the use of assays which target downstream signalling proteins. The second messengers IP_3 and DAG collectively stimulate the mobilisation of intracellular calcium (Ca^{2+}) and activate protein kinase C (PKC) isoforms, leading to diverse signalling properties and functional outcomes in a variety of cells including regulation of the actin cytoskeleton, gene transcription and cell proliferation (Kostenis $et\ al.$, 2005, Hubbard and Hepler, 2006).

The G_q and G_{11} subunits are widely expressed within human tissue. However, expression of the other family members G_{14} and $G_{15/16}$, is limited to lung, kidney and hematopoietic cells (Offermanns, 2003). Surprisingly, any distinct variations in the activation of signalling pathways or functional role of alternative subunits in the $G_{q/11}$ family remain to be elucidated despite significant sequence variations in the N-terminal regions of G_{14} and $G_{15/16}$, in comparison to G_q (65% and 35%, respectively) (Hubbard and Hepler, 2006).

1.2.1.1.4 The $G\alpha_{12/13}$ family

The final G-protein family, identified in 1991, is the $G_{12/13}$ family of proteins and for a variety of reasons, these remain the least well understood (Strathmann and Simon, 1991). Primarily, the absence of tools, such as bacterial toxins, which directly interact or interfere with the $G_{12/13}$ family – has hampered efforts to differentiate $G_{12/13}$ signalling from that of

other G-protein families. Furthermore, the downstream small monomeric GTP-bound Rho proteins which are activated via the $G_{12/13}$ pathway are particularly difficult to quantify efficiently or accurately (Maguire and Davenport, 2005). These initial drawbacks are further hampered by the limited means available to discriminate between endogenous G_{12} and G_{13} signalling, particularly *in vivo* and, therefore, their differential actions also remain poorly understood (Worzfeld *et al.*, 2008). Lastly, it is well understood that GPCRs coupling to this family of G proteins often simultaneously couple to $G_{q/11}$ and in some cases to $G_{i/o}$ (Siehler, 2009), albeit at different efficiencies (Riobo and Manning, 2005). Taken together, it is understandable that the process of characterising the $G_{12/13}$ family has been extremely difficult (Wettschureck and Offermanns, 2005).

As with many other G-proteins, $G_{12/13}$ family members are ubiquitously expressed within human tissues. They are classically reported to mediate formation of actin stress fibres and activation of serum response factor (SRF) in cells (Worzfeld *et al.*, 2008). Consequently, this pathway has been implicated in the proliferation and survival in cells overexpressing sphingosine kinase type-1 (Olivera *et al.*, 2003), the migration of an ovarian cancer cell line, SK-OV3, following LPA stimulation and subsequent activation of the $G\alpha_{12/13}$/Rho A axis (Bian *et al.*, 2006), and finally transcriptional regulation via ROCK1/2 activation and subsequent engagement with the SRF (Siehler, 2009). Interestingly, $G_{12/13}$ double-knockout mice are subject to embryonic lethality, and this is primarily attributed to the underdeveloped nature of both neural and vascular networks, suggestive of a pertinent role for $G_{12/13}$ in vascular and cardiac development (Offermanns *et al.*, 1997).

1.2.2 Gβγ signalling

The Gβγ complex is an essential signalling component of G-protein: receptor interactions and is activated simultaneously with the classical Gα pathway (Hamm, 1998). Despite its importance, the Gβγ complex was initially dismissed as a passive regulator of G-protein

signalling, in which isoprenylation modifications on the Gγ subunit merely facilitated a close proximity to the plasma membrane (Johnston and Siderovski, 2007). It was also thought that this proximity promoted the re-association of the heterotrimeric unit and in turn, readied Gα for more cycles of receptor-mediated activation. However, in 1987, following the infusion of purified Gβγ protein into embryonic atrial cells, it was first discovered that the Gβγ complex interacted directly with Kir3 channels to promote inward potassium (K^+) movement (Logothetis *et al.*, 1987). Following this, it was also demonstrated that Gβγ interacted directly with a number of effector molecules to promote downstream signalling pathways closely linked to the MAPK signalling cascade including PI-3 kinase (PI3K) (Stephens *et al.*, 1994) and PLC-$β_2$ (Hawes *et al.*, 1996), as well as alternative pathway initiators such as adenylyl cyclases (AC) (reviewed in (Khan *et al.*, 2013)). Interestingly, research also suggests a role for Gβγ in structural protein trafficking (Dupre *et al.*, 2009) and endosomal sorting (Hynes *et al.*, 2004). However, these roles are currently less well established.

Unlike the specific nature of Gα isoforms, it is still unclear if the combination of Gβ and Gγ isoforms to form functional complexes are highly specific in relation to their roles or cell types (Dupre *et al.*, 2009). However, an early characterisation study demonstrated this may be the case, as evidence suggested the $Gγ_1$ isoform is highly expressed within retinal rod cells and, following the activation of the rhodopsin receptor within these cells, $Gγ_1$ was shown to preferentially promote $Gβγ_1$ signalling (Kisselev and Gautam, 1993). Isoform selectivity was further highlighted in a study which demonstrated that the $Gγ_1$ isoform is favoured over $Gγ_5$ for efficient trafficking of the Gβγ complex to the Golgi network following receptor internalisation (Akgoz *et al.*, 2004). Initially, the authors related this finding to differing lipid modifications amongst isoforms. However, subsequent mutational analysis suggested that phosphorylation sites located on the c-terminus were the influencing factor (Akgoz *et al.*, 2004). Taking these findings together, future research

relating to the selectivity of the Gβγ isoform may provide further insight in relation to the functional consequences of targeting individual Gβγ subunits.

1.2.3 GPCR desensitisation, internalisation and trafficking

Following the activation of a GPCR, multiple molecular mechanisms are in place to terminate the signalling process. Firstly, the GPCR must be uncoupled from the Gα subunit to become desensitised, internalised and trafficked into endosomal compartments for recycling, or become lysosome-bound for degradation (Magalhaes *et al.*, 2012). This process is vital for sustained sensitivity in GPCR signalling and there are several key molecular facilitators, primarily initiated via the activity of GPCR kinases (GRKs) (Magalhaes *et al.*, 2012). There are only seven members of the GRK family (1-7) and, considering the uneven ratio of GRKs to GPCRs, it is anticipated that each isoform has the ability to bind numerous GPCR subtypes - although their specificity for receptor families remains poorly understood (Gurevich *et al.*, 2012). The majority of GRK isoforms are localised to the plasma membrane via their interactions with the Gβγ complex or phospholipids such as phosphatidylinositol 4,5-bisphosphate (PIP$_2$), whereas others, specifically GRK 5 and 6, are targeted there via palmitoylation (Gurevich *et al.*, 2012).

When GPCRs are activated, changes in the conformational state present the opportunity for GRKs to recognise and rapidly phosphorylate the c-terminal tail and/ or third intracellular loop of the GPCR (Shenoy and Lefkowitz, 2011) (Ribas *et al.*, 2007). Following phosphorylation by GRKs, the GPCR is rapidly recognised by a family of cytosol localised arrestin proteins; of which arrestin 2 and arrestin 3 (often still designated β-arrestin 1 and 2) are the predominant forms and are expressed widely (Walther and Ferguson, 2013). Sharing 78% sequence homology, the arrestin isoforms are thought to be relatively interchangeable in their roles, which involves GPCR binding, an event that is enhanced by GRK mediated receptor phosphorylation (Walther and Ferguson, 2013). By so doing this, blocks access of the Gα subunit and thus prevents further G protein-

mediated signalling (DeWire *et al.*, 2007). The stability of the bound β-arrestin-GPCR complex can be indicative of the speed and outcome of the internalisation and recycling process (Shukla *et al.*, 2011) and research suggests that this stability is variable amongst individual GPCR subtypes, for example, Class A GPCRs have been shown to bind transiently to β-arrestin and are recycled rapidly whereas, Class B GPCRs are more firmly bound and thus the process is comparatively slower (Oakley *et al.*, 2000). Following recruitment of a β-arrestin, receptor endocytosis is stimulated by attracting clathrin, various adapter proteins (e.g. AP-2) and dynamin - molecules responsible for the development of clathrin coated pits (CCPs) and molecular trafficking of GPCRs (Jean-Alphonse and Hanyaloglu, 2011). A further role of β-arrestins is to recruit the small GTPases required for intracellular trafficking of the receptor; these include Rab 4, 5, 7 and 11 – the specificity of which is determined by the fate of the receptor in relation to whether it will be recycled back to the membrane or become degraded (Moore *et al.*, 2007).

1.2.4 The role of β-arrestin in cell signalling

Interestingly, in addition to their roles in GPCR desensitisation and internalisation, in recent years it has come to light that β-arrestins can also promote signalling via alternative pathways, facilitated by their role as scaffolding and adapter molecules for other proteins and hence, other signalling pathways (Shukla *et al.*, 2011). Essentially, this function is non-canonical and G-protein independent and can span multiple molecular pathways, many of which are linked to the MAPK-mediated signalling cascades; c-Src, c-Jun and ERK1/2 (Luttrell *et al.*, 1999). Collectively, c-Src, c-Jun and ERK1/2 are understood to recruit β-arrestins as chaperone complexes for the regulation of cellular mitogenesis (Reiter and Lefkowitz, 2006). Furthermore, research has also demonstrated that β-arrestins can enhance the process of GPCR ubiquitination and, in the first such instance, β-arrestin was shown to facilitate targeting of the β-2AR for degradation by acting as an

adapter molecule for an E3 ubiquitin ligase (Shenoy *et al.*, 2001). Interestingly, for the β-2AR, ubiquitination was specifically mediated via β-arrestin-2, rather than β-arrestin-1, and this may be suggestive of preferential roles for specific isoforms, an aspect of β-arrestin research which remains poorly understood in relation to internalisation and trafficking (Shenoy *et al.*, 2001, Shukla *et al.*, 2011).

The therapeutic potential of 'biased' GPCR ligands, which preferentially signal via β-arrestin controlled pathways, has become an increasingly important aspect of recent research and the actions of many GPCR targeted ligands or medicines, are being reconsidered in this respect (Reiter *et al.*, 2012). For example, it has been demonstrated that TRV120023, a β-arrestin biased agonist at the angiotensin type-I receptor (AT$_1$R), stimulates cell survival following ischemic injury in cardiomyocytes via the promotion of MAPK signalling in the setting of congestive heart failure (Kim *et al.*, 2012). Most astonishingly, TRV120023 proved more effective than losartan in protecting cardiomyocytes from ischemic injury *in vitro*. This is a valuable finding, given that losartan is a gold standard antagonist at the AT$_1$R and is used to prevent cardiac remodelling in heart failure, as well as vascular remodelling in the treatment of hypertension and diabetic neuropathy (Kim *et al.*, 2012, Violin *et al.*, 2013). Taking this evidence alongside two recent reports which detail the atomic level structures of β-arrestins in their active confirmation it is evident that the future of β-arrestin research is promising (Borshchevskiy and Buldt, 2013).

1.3 G protein-coupled receptor 35

G protein-coupled receptor 35 (GPR35) is a member of the 'rhodopsin-like' family of GPCRs discovered more than 15 years ago (O'Dowd *et al.*, 1998). It remains poorly characterised in relation to the identification of its endogenous activator, its downstream role in signalling and thus, its wider physiological function in health and disease.

GPR35 was first identified within an intronless open reading frame (ORF) corresponding to 309 amino acids, located on chromosome 2, region q37.3 in human genomic DNA (O'Dowd *et al.*, 1998). In the following six years, it was discovered that GPR35 also produced an alternatively spliced version in humans, for which there was an extended N-terminus of 31AA - although the TMD and C-terminal tail were identical (Okumura *et al.*, 2004). Referring to the short version as *GPR35a* and the extended version as *GPR35b*, this initial report suggested that *GPR35b* was preferentially expressed in both healthy gastric mucosa tissue and in NIH3T3 fibroblasts which exhibited transforming capabilities (Okumura *et al.*, 2004). This report was the first to propose a functional role for GPR35 and, although evidence suggests that there may be an affiliation between GPR35 isoform expression and gastric tumour progression, the significance of the N-terminal extension remains unresolved in relation to the pathophysiology of tumour progression, ligand recognition or GPR35 function (Guo *et al.*, 2008, Mackenzie *et al.*, 2014).

Ultimately, deciphering the roles for GPR35 has been hampered by limited knowledge of the endogenous ligand(s). Although a number of potent synthetic ligands have been identified which include pamoic acid (Zhao *et al.*, 2010), amlexanox and lodoximide (Mackenzie *et al.*, 2014), GPR35 displays very marked differences in ligand pharmacology between species (Milligan, 2011). Moreover, as noted above, the true endogenous ligand(s) of GPR35 remains uncertain. Whilst some reports argue that it should still be considered as an 'orphan' receptor, at least in man (Milligan, 2011), others have proposed two possible endogenous ligands; kynurenic acid (KYNA) and 2-acyl lysophophatidic acid (2-acyl LPA) (Wang *et al.*, 2006a, Oka *et al.*, 2010). Regardless of these issues and limitations, continued efforts to identify novel, surrogate agonists which activate or block GPR35 have provided investigators with the tools to question its physiological function and possible roles in disease, albeit to a limited extent. Current evidence, derived from mouse knock-out models and studies utilising synthetic ligands, strongly suggests a role

for GPR35 in a range of diseases including heart failure, inflammation and nociception (Mackenzie *et al.*, 2011).

1.3.1 GPR35 expression

In addition to the initial discovery of GPR35 in 1998 – O'Dowd and colleagues were also first to report endogenous RNA expression of GPR35 within a range of healthy tissues (O'Dowd *et al.*, 1998). Using northern blot RNA analysis, robustly detected levels were shown to be present only in the small intestine of the rat, with negligible levels in the lungs, liver, heart, spleen and kidney (O'Dowd *et al.*, 1998). As interest in GPR35 developed, publications began to speculate on roles for GPR35 and investigators further quantified expression, mainly using quantitative PCR, in human, rat and mouse derived tissues. Studies have confirmed high expression levels of GPR35 in gastrointestinal tissue (Taniguchi *et al.*, 2006). Moreover, further studies have also reported significant expression levels in the spleen, kidneys, and also in specialised immune cell populations such as peripheral leukocytes, monocytes and neutrophils in both humans and rodents (Wang *et al.*, 2006a, Barth *et al.*, 2009, Lattin *et al.*, 2008). Also, IgE antibody-challenged human mast cells displayed enhanced GPR35 expression levels (Yang *et al.*, 2010). Moreover, both *a* and *b* GPR35 isoforms are readily detected in the central and peripheral nervous system, specifically in the whole human brain and rodent dorsal root ganglia, respectively (Taniguchi *et al.*, 2006, Cosi *et al.*, 2011, Guo *et al.*, 2008). Most recently, GPR35 demonstrated robustly high expression in isolated mouse neonatal cardiomyocytes following exposure to hypoxic conditions via the activation of hypoxia inducible factor-1 (HIF-1) (Ronkainen *et al.*, 2014). Importantly, this finding was evident in ischemic primary neonate cells and whole cardiac tissue isolated from a mouse model of acute ischemia induced via a transverse aortic constriction procedure (Ronkainen *et al.*, 2014). This is in agreement with an earlier study which reported increased expression of

GPR35 in ischemic myocardial tissue obtained from a small subset of heart failure patients (Min *et al.*, 2010).

The majority of these latter studies employed quantitative, reverse transcription-polymerase chain reaction (qRT-PCR) analysis to assess GPR35 expression levels. By quantifying DNA corresponding to a gene of interest at an early, exponential phase of the PCR cycle, qRT-PCR provides a precise measurement whilst requiring comparatively less cDNA than other techniques (Bustin *et al.*, 2005). It is, therefore, widely considered to be both more sensitive and more accurate than northern blot analysis, suggesting that the initial expression analysis employed by O'Dowd and colleagues may have lacked sufficient sensitivity, accuracy and molecular material to produce conclusive results. Given that GPCRs are often expressed at modest levels (Regard *et al.*, 2008), specificity and sensitivity are imperative for effective expression analysis.

Despite the initial contrasting reports, tissue-wide GPR35 distribution has been robustly validated in subsequent investigations and, aside from preferential gastrointestinal expression, there are also consistent reports of significant expression in spleen and immune cells (Wang *et al.*, 2006a, Lattin *et al.*, 2008). Furthermore, owing to the diverse range of tissues which have demonstrated GPR35 expression, future expression analysis and investigation of GPR35 function in relevant models of health *and* disease is clearly required to comprehensively elucidate its role.

1.3.2 GPR35 polymorphic variation/SNPs

In addition to the elusive N-terminally extended form of human GPR35, numerous polymorphic isoforms of human GPR35 have been identified and may have consequential implications within various disease states (Mackenzie *et al.*, 2011).

1.3.2.1 Type-2 diabetes

In some cases, reports have highlighted a link between the increased expression of a single nucleotide polymorphism (SNP) in GPR35 and the incidence of diabetes. For example, an identified SNP in GPR35 demonstrated increased expression in a Mexican-American population with type-2 diabetes (Horikawa et al., 2000). However, this report also established an association with the incidence of type-2 diabetes and a range of alternative genes also expressed in the 'NIDDM1' loci of chromosome 2 and, therefore, the specificity of the association between expression of the GPR35 SNP and type-2 diabetes remains unclear (Horikawa *et al.*, 2000). A further population study found GPR35 to be highly polymorphic within an Italian subset of diabetic patients. However, these authors described a non-significant association between GPR35 variation and type-2 diabetes (Vander Molen *et al.*, 2005). Evidently, more population research is required in order to decipher a link between polymorphic variations of GPR35 and the incidence of diabetes.

1.3.2.2 Coronary artery disease

The first indication that GPR35 could be involved in the progression of coronary artery disease (CAD) originated from a genetic study in patients which aimed to identify potential gene-markers relating to hypertension and subsequent end-organ damage (Sun *et al.*, 2008). These investigators also assessed the progression of coronary artery calcification (CAC) burden, via computed tomography scanning whilst accounting for multiple risk factors including plasma glucose, cholesterol, and fibrinogen levels (Sun *et al.*, 2008). Employing an elegant study design, two initial data sets of 360 hypertensive sib-ships were screened for 471 SNPs from candidate biological pathways, or positional candidate genes which might influence CAC. Using Random Forest prediction for various risk factor importance and RuleFit analysis to prioritise variable-variable interactions, a SNP in GPR35 was recognised to have significant association with increased CAC burden (Sun

et al., 2008). This SNP, within GPR35, was non-synonymous and resulted in an amino acid variation between serine and arginine at position 294 (Sun *et al.*, 2008). Upon closer examination, it was discovered that the Ser294Arg polymorphism is located at one of the four conserved c-terminus potential phosphorylation domains on GPR35 and the authors of this publication hypothesised that this may have implications for G-protein coupling, but failed to specify a pathway which might facilitate its role in calcification or atherosclerotic burden (Sun et al., 2008).

1.3.2.3 Gastrointestinal disease

Given the robust expression of GPR35 within gastrointestinal tissue, the identification of polymorphisms implicating GPR35 in gastrointestinal diseases may be expected. A SNP in GPR35 has been implicated in the early on-set of inflammatory bowel disease (IBD) (Imielinski *et al.*, 2009). In this study, a SNP was highly expressed in a subset of patients with ulcerative colitis however, the authors did not comment on the structural location of the SNP or hypothesise a functional role for GPR35 in IBD (Imielinski *et al.*, 2009). However, taking this evidence together with a recent report which demonstrates a strong association between the expression of a SNP located within the TMDIII at position 3.44 of GPR35 [a TMD potentially involved in signalling (Jenkins *et al.*, 2011)] and the incidence of primary sclerosing cholangitis (PSC) with concurrent ulcerative colitis (UC) (Ellinghaus *et al.*, 2013), future investigation relating to the role of various GPR35 polymorphisms in gastrointestinal disease is warranted.

1.3.3 Putative functions of GPR35

Information relating to species and tissue selective expression is valuable in early receptor characterisation and can often be indicative of physiological function (Kenakin, 2004). As a result of widely reported GPR35 expression, a few publications have begun to examine

putative functions for GPR35 *in vitro* and even at an *in vivo* level, in the treatment of inflammation, pain, hypertension, and cardiac hypertrophy in heart failure (Barth *et al.*, 2009, Zhao *et al.*, 2010, Cosi *et al.*, 2011, Min *et al.*, 2010, Ronkainen *et al.*, 2014).

1.3.3.1 Inflammation

Given the evidence of high expression levels of GPR35 within immune cell populations (Wang *et al.*, 2006a), Barth and colleagues examined the role of GPR35 in the early stages of inflammation within the vasculature (Barth *et al.*, 2009). Hypothesising that GPR35 might act in a similar fashion to a chemoattractant-like receptor, these authors quantified the attachment of leukocytes to a human umbilical vein endothelial cell (HUVEC) monolayer following exposure to shear stress conditions (Barth *et al.*, 2009). Importantly, the shear stress conditions were equivalent to those routinely demonstrated in the vasculature within a temperature controlled, fibronectin coated flow-chamber (Barth *et al.*, 2009). In doing this, Barth and colleagues demonstrated that GPR35 activation contributed to β_1 integrin-mediated leukocyte adhesion to an endothelial cell monolayer, increasing monocyte adhesion levels by 13-fold, following 300nM KYNU stimulation (Barth *et al.*, 2009). Importantly, these effects were attenuated by the knockdown of GPR35 via short-hairpin RNA (shRNA) and in the presence of an α_4-integrin blocking-antibody, which specifically interferes with β_1-mediated cell arrest (Barth *et al.*, 2009). These findings led authors to speculate that GPR35 activation may be implicated in the setting of early phase inflammation. However, it was ultimately concluded that further investigation was warranted in alternative settings, using a diverse range of ligands with high specificity for GPR35 (Barth *et al.*, 2009). Thus far, there are no additional publications which address the role of GPR35 in the setting of acute inflammation.

1.3.3.2 Pain

Alternatively, authors have explored a functional role for GPR35 within the central nervous system (CNS), specifically in the setting of pain. In the first instance, GPR35

demonstrated high expression in dorsal root ganglion (DRG) neurons of the rat (Guo et al., 2008) and following this, demonstrated negative regulation of cAMP via activation of $G\alpha_{i/o}$ and subsequently appeared to co-localise with transient receptor vanilloid receptor (TRPV1) channels (Ohshiro *et al.*, 2008). Notably, TRPV1 is a cation channel involved in hyperalgesia (Lawson, 2002) and researchers hypothesised that the evidence of potential interactions between TRVP1 and GPR35 may be suggestive of a role for GPR35 in the setting of pain. Following this evidence, Zhao et al. investigated the effect of administering increasing doses of the GPR35 ligand pamoic acid in a mouse model undergoing an acetic acid-induced abdominal constriction test, considered the gold standard model of nociception (Zhao *et al.*, 2010). Interestingly, the administration of increasing dosages of pamoic acid (25-100mg/kg/animal) and the number of writhes exhibited by the animal negatively correlated (Zhao *et al.*, 2010), leading authors to conclude that GPR35 activation may contribute to anti-nociception *in vivo* (Zhao *et al.*, 2010). However, although these findings correlate with the hypothesis put forward by Oshiro and colleagues (Ohshiro *et al.*, 2008), they conflict with reports from Jenkins et al., who demonstrated that whilst pamoic acid is an extremely potent agonist at human GPR35, it displays negligible potency at mouse GPR35 (discussed later) (Jenkins *et al.*, 2012). Therefore, without successful employment of a second agonist or an antagonist to block GPR35 activation, we cannot be sure that the anti-nociceptive effect following pamoic acid administration is not an off-target effect (Zhao *et al.*, 2010).

Subsequently, another report examining nociceptive properties of GPR35 shortly followed (Cosi *et al.*, 2011). Here, it was demonstrated that zaprinast and KYNA significantly attenuated, but did not completely abolish, forskolin-induced increases in cAMP via the $G\alpha_{i/o}$ signalling path in primary mouse glial cells (Cosi *et al.*, 2011); providing a potential explanation for anti-nociception in spinal cord tissue following GPR35 activation. Further to this, authors examined this hypothesis *in vivo,* demonstrating that systemic administration of 100-300mg/kg of L-kynurenine (a precursor of KYNA, see Figure 1-4, for

a schematic diagram of the kynurenine pathway) or 20mg/kg of zaprinast, decreased the number of writhes exhibited by mice undergoing an abdominal constriction test by up to 42%, inferring a level of anti-nociception following GPR35 ligand administration (Cosi *et al.*, 2011). Remarkably, systemic administration of L-kynurenine together with probenecid, a molecule which blocks excretion and disposal of KYNA (Santamaria *et al.*, 1996) increased spinal cord and plasma KYNA levels by up to 8000% compared to saline infused controls (Cosi *et al.*, 2011). Whilst it is highly probable that these levels of KYNA may produce off-target effects via antagonism of the NMDA receptor *in vivo* (Chen *et al.*, 2009), the anti-nociceptive effects demonstrated here are in agreement with those previously reported by Zhao et al. (Cosi *et al.*, 2011, Zhao *et al.*, 2010).

1.3.3.3 Hypertension

GPR35 has also been implicated in the regulation of blood pressure *in vivo* (Min *et al.*, 2010). Min and colleagues (2010) examined the haemodynamic parameters of a commercially obtained transgenic GPR35 knockout mouse strain (Deltagen, San Mateo, CA) alongside other in-house generated strains which included global knockout models of orphan GPCR, GPR37like-1 (GPR37L1) and myosin light chain kinase-3 (MLYK3) (Min *et al.*, 2010). Importantly, GPR35 and GPR37L1 were chosen for further analysis following their high expression profile in myocardial tissue derived from heart failure patients and their orphan status (Min *et al.*, 2010). Following PCR genotyping to ensure that appropriate gene deletions were evident, systolic and diastolic ventricular pressure were measured via Millar catheterisation of the right carotid artery in anesthetised mice (Min *et al.*, 2010). Most notably, GPR35 knockout mice demonstrated a significant, 37.5 mmHg, increase in systolic ventricular pressure compared to wild-type littermates (C57 BL/6) (Min *et al.*, 2010). There were no measurable differences in the heart weight/ body weight (HW/ BW) ratio between strains. However, the authors fail to report the age of the mice at the onset of hypertension and, therefore, the development of cardiac hypertrophy is unaccounted for (Min et al., 2010). Moreover, the data presented in this study were low in

power (n≤9). However, there are to date few studies that have begun to explore the role of GPR35 at an *in vivo* level and given that this study was the first to highlight a potential role of GPR35 in the regulation of blood pressure, further exploration is warranted (Min *et al.*, 2010).

1.3.3.4 Heart Failure

Within the same publication, Min and colleagues (2010) also proposed an association between GPR35 and development of heart failure (HF). In a screen of twelve failing and two healthy human myocardial tissue samples, a selection of up-regulated genes was chosen for further analysis via a global expression microarray and these included GPR35 and GPR37L1 (Min *et al.*, 2010). Other chosen genes, which included MLYK3, peroxiredoxin 4 (PRDX4) and SPARC related modular calcium binding 2 (SMOC2), also demonstrated increased expression. However, these also demonstrated a positive correlation with traditional heart failure biomarkers such as plasma brain natriuretic peptide (BNP), ejection fraction (EF) and pulmonary arterial pressure (PAP), facilitating a degree of adjustment for disease severity (Min *et al.*, 2010). Authors examined physiological parameters in global knockout *in vivo* models (discussed above), as well as changes to the morphology of cardiomyocytes in response to the over-expression of a selection of twelve up-regulated genes (Min *et al.*, 2010). Most interestingly, adenovirus mediated over-expression of GPR35 promoted a hypertrophic phenotype in primary neonatal cardiomyocytes and this was quantified via [^{3}H] phenylalanine incorporation (Min *et al.*, 2010). Interestingly, only over-expression of GPR35 led to a hypertrophic morphology amongst the chosen candidates, including genes which displayed high expression within the myocardium such as GPR37L1 and those which positively correlated with traditional heart failure biomarkers such as MLYK3 expression (Min *et al.*, 2010).

Additionally, a very recent publication demonstrated that the expression of GPR35 is significantly increased in ischemic myocardial tissue derived from mice and in primary mouse neonatal cardiomyocytes exposed to hypoxia *in vitro*, and that this response is mediated via the activation of hypoxia inducible factor-1 (HIF-1) (Ronkainen *et al.*, 2013). Using an experimental system which employed a hypoxic chamber to induce ischemia in cultured primary neonatal cardiomyocytes, these authors were able to elegantly demonstrate the up regulation of GPR35 mRNA from the onset of hypoxic exposure and, furthermore, that this was increased with time together with an alternative hypoxic marker; EGL nine homolog 3 (PHD3) (Ronkainen *et al.*, 2014). Importantly, increased expression of GPR35 could be induced independently of hypoxia, given that HIF-1α was activated and this was demonstrated via the expression of a constitutively active form of HIF-1α in primary neonatal cardiomyocytes in normoxia (Ronkainen et al., 2014). Consequently, these authors were able to identify a putative binding site for HIF-1α, located on the promoter region of mouse GPR35, via chromatin immunoprecipitation, and the interaction between GPR35 and HIF-1α was evident following the use of a luciferase assay (Ronkainen *et al.*, 2014). Moreover, these authors also demonstrated that GPR35 expression and HIF-activation are concomitantly up-regulated in ischemic ventricular tissue derived from experimental mice which have undergone ligation of the left anterior descending (LAD) coronary artery (an acute model of myocardial infarction and pathological hypertrophy) or transversal aortic constriction (TAC) which represents acute ischemic injury (Ronkainen *et al.*, 2014). Results from these procedures indicated that GPR35 is up regulated in ventricular tissue in the compensatory and de-compensatory stages of heart failure represented by LAD and TAC procedures, respectively (Ronkainen *et al.*, 2014). Finally, this publication also demonstrated zaprinast-induced GPR35 internalisation and the alteration of actin stress fibre formation in mouse cardiomyocytes, this is consistent with literature relating to GPR35-$G\alpha_{13}$ coupling (Jenkins *et al.*, 2011, Jenkins *et al.*, 2012, Mackenzie *et al.*, 2014) and subsequent activation of the Rho A/ ROCK1/2 axis (Ronkainen *et al.*, 2013).

1.3.4 G protein coupling profile of GPR35; Gα$_{i/o}$ and Gα$_{12/13}$

Alongside the initial discovery of the activity of zaprinast at GPR35 (discussed in section 1.4.2), Taniguchi and colleagues employed an aequorin assay, utilising chimeric constructs of Gα$_q$ and reported that both rat and human orthologues of GPR35 coupled to the Gα$_{i/o}$ family of G-proteins (Taniguchi *et al.*, 2006). Further evidence suggesting PTX sensitive interactions between GPR35 and Gα$_{i/o}$ have been highlighted by studies on monocytes (Barth *et al.*, 2009) and mouse glial cells activated by KYNA (Guo *et al.*, 2008, Ohshiro *et al.*, 2008) and human iNKT cells endogenously expressing GPR35 (Fallarini *et al.*, 2010). However, evidence also demonstrates that GPR35 is able to couple effectively to the Gα$_{12/13}$ G-protein family, indeed selectively to Gα$_{13}$ in assays ranging from chimeric aequorin assays, through GTP-Gα$_{13}$ immunoprecipitation experiments, to IP1 accumulation assays (Jenkins *et al.*, 2011, Jenkins *et al.*, 2012, Mackenzie *et al.*, 2014). As a result of varying reports, it has been suggested that cell/ ligand bias may exist following GPR35 activation and, whilst this has not shown to be the case for any previously identified GPR35 ligands (Jenkins *et al.*, 2012, Deng *et al.*, 2012a), gathering evidence relating to KYNA activation and subsequent activation of the Gα$_{i/o}$ family of proteins may require further investigation.

1.3.4.1 The role of Gα$_{13}$ in Cardiovascular Disease

Evidence that GPR35 selectively couples to Gα$_{13}$ (Jenkins *et al.*, 2011, Mackenzie *et al.*, 2014) is a prominent finding in relation to GPR35 and its potential role in cardiovascular disease (CVD). However, Gα$_{13}$, along with the related Gα$_{12}$ is, as noted earlier, by far the least studied mammalian G-protein. This is largely due to the reality that activation of Gα$_{13}$ does not directly regulate easy-to-measure secondary messengers and is unaffected by bacterial toxins, such as cholera toxin and pertussis toxin, which are well established tools that modify other G-protein families (Wettschureck and Offermanns, 2005).

In a range of studies, it has been demonstrated that Gα$_{13}$ plays significant regulatory roles in embryonic development, cell migration, proliferation and contraction (Suzuki *et al.*, 2009). Most recently, Gα$_{13}$ has been implicated in the regulation of angiogenesis via the promotion of expression of the vascular endothelial growth factor (VEGF) receptor via activation of transcription factor NF$_κ$B (Sivaraj *et al.*, 2013); thus establishing Gα$_{13}$ as an important mediator linked to signalling pathways relating to the pathology of CVD. Interestingly, Ruppel and colleagues generated a vascular endothelial cell-specific knockout mouse model for Gα$_{13}$ via the CreLoxP recombination system and demonstrated a loss of appropriate vascular development which proved to be fatal in embryos at mid-gestation (Ruppel *et al.*, 2005). The CreLoxP viral recombination system is an effective tool utilised to selectively abolish gene expression in specific cell types and is established by breeding two transgenic model lines; the first of which expresses a 'floxed' gene of interest (flanked by LoxP recombination sites) and a second that expresses a cell/ tissue specific Cre recombinase enzyme which has been virally introduced, encoding a promoter region. By crossing these strains, the cells which express Cre recombinase undergo recombination and the floxed allele is excised and, thus, selective gene deletion has been engineered to establish a new transgenic strain. Importantly, Ruppel et al. (2005) demonstrated that neonatal fatality and abnormal vascular development did not occur in transgenic models which only expressed a Gα$_{13}$ 'floxed' allele, suggesting that targeting of vascular endothelial cells using the CreLoxP system is not harmful in itself and, therefore, the abnormal vascular development could be attributable entirely to the elimination of Gα$_{13}$ in endothelial cells (Ruppel *et al.*, 2005). This report was consistent with previous studies which had also demonstrated vascular defects and embryonic lethality in response to Gα$_{13}$ deficiency (Offermanns *et al.*, 1997) and others which implicated Gα$_{13}$ in the regulation of morphogenesis and capillary assembly in angiogenesis via Rho GTPase activation (Connolly *et al.*, 2002). Convincingly, introducing Gα$_{12/13}$ knockout specifically to cardiomyocytes in adult mice is not detrimental to life. However, it does lead to protection from pressure overload heart failure (Takefuji *et al.*, 2012). This suggests that, while the

$G\alpha_{12/13}$ pathway is essential for growth and angiogenesis in the early stages of development, its activation may contribute to cardiac pathophysiology and heart failure in later life (Takefuji *et al.*, 2012).

The activation of the Rho A pathway following $G\alpha_{13}$ activation has been extensively reported. An early publication by Hart and colleagues in 1998 was the first to identify a specific RhoGEF, p115 RhoGEF, which was sensitive to $G\alpha_{13}$ activation (Hart *et al.*, 1998). This was also reported elsewhere within the same year (Kozasa *et al.*, 1998). Hart and colleagues reported substantial quantification of p115RhoGEF bound to $G\alpha_{13}$ following stimulation via autocrine motility factor (AMF) in co-immunoprecipitation assays and radioisotope based GDP-dissociation assays. Moreover, this study also reported that p115RhoGEF contains an RGS binding domain and, therefore, could be an effector GEF in the stimulation of Rho A activation, but also a decelerator of $G\alpha_{13}$ activation via GAP activity (Hart *et al.*, 1998). A more recent study also focusing on p115RhoGEF quantification to assess ligand-receptor-$G\alpha_{13}$ interactions, employed receptor mediated visualisation of fluorescent p115RhoGEF translocation from the cytosol to the plasma membrane following transfection of constitutively active isoforms of both $G\alpha_{12/13}$ (Meyer *et al.*, 2008). Coupling this technique with cell fractionation and subsequent immunoblotting; compartmentalisation of active G-protein and Rho A was elegantly visualised and quantified at the cell membrane (Meyer *et al.*, 2008).

Rho A is understood to mediate a range of cellular responses which include smooth muscle cell contraction, polarity and migration and is, therefore, implicated in the pathology of hypertension and vessel remodelling (Wirth, 2010, Cotton and Claing, 2009). A number of studies also demonstrate that the expression and activation of Rho A is increased in hypoxic conditions in a wide range of cell types which include porcine and human pulmonary artery ECs (PAECs) (Wojciak-Stothard *et al.*, 2005, Wojciak-Stothard *et al.*, 2012) and human mesenchymal stem cells (MSC) (Vertelov *et al.*, 2013). These cellular responses are largely produced via activation of the Rho A effectors, Rho

associated kinases (ROCK1/2). However, Rho A has also been shown to cross-talk with c-Jun NH_2-terminal kinase (JNK) in the setting of angiogenesis and cardiac hypertrophy (Maruyama *et al.*, 2002) (Figure 1.3). ROCK1/2 is understood to exert its contractile action by phosphorylating myosin light chain (MLC) and inhibiting myosin light chain phosphatase (MLCP) (Barandier *et al.*, 2003). Furthermore, ROCK1/2 up-regulates a selection of myofilament proteins, including Lim kinases 1 and 2, adducin and profilin, to regulate assembly of the actin cytoskeleton via the serum response factor (SRF) (Wirth, 2010). Inhibition of ROCK using the small molecule Y-27632 has been shown to prevent vascular endothelial growth factor (VEGF)-induced behaviours in endothelial cells such as increased migration and permeability (Bryan *et al.*, 2010) and to lower blood pressure in spontaneously hypertensive rats (SHR) (Moriki *et al.*, 2004).
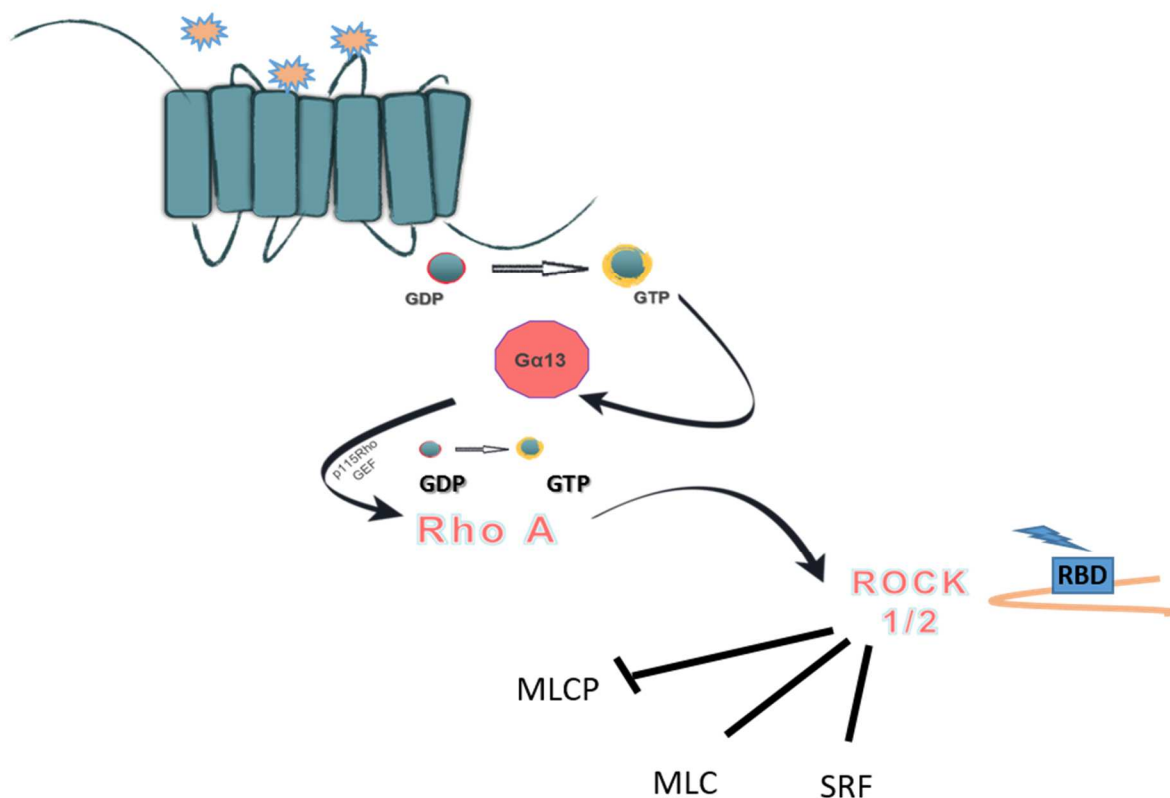
Figure 1-3. Gα13-mediated signalling via Rho A upon ligand binding to a GPCR.

Following the activation of Gα$_{13}$, p115RhoGEF can translocate from the plasma

membrane to the cytosol where it facilitates Rho A activation via the exchange of GDP for

GTP. Active GTP-Rho A then binds to the RBD domain of ROCK1/2 to allow the

previously closed, auto-inhibitory loop to unfold and become active. ROCK1/2 inhibits

myosin light chain phosphatase (MLCP), directly phosphorylates myosin light chain (MLC)

at serine 19 and activates serum response factor (SRF) for transcriptional regulation of

cytoskeletal genes.

1.4 Small molecule screening of orphan GPCRs

It has been recently estimated that 27% of medications available on the market target

various classes of GPCRs, with the majority targeting members of the 'rhodopsin/ class A'

family (Garland, 2013). As research within this field continues to progress, the

requirement for novel, potent and highly specific ligands has become of utmost importance in modern drug development. It has become common practise to employ high-throughput *in vitro* screening technologies in the initial search for novel and efficacious ligands. To promote this, extensive and well-defined chemical libraries are now broadly available and are frequently utilised to screen small-molecule compounds against both well-characterised and therapeutically validated GPCRs as well as lesser studied and even 'orphan' GPCRs, often within an academic setting. The following sections will discuss various screening techniques which have been used to identify both potential endogenous and surrogate synthetic ligands with affinity at GPR35. For 'orphan' GPCRs, where the endogenous ligand remains unidentified or disputed, screening studies can provide surrogate tool molecules to study the function of otherwise poorly defined GPCRs. According to the International Union of Clinical and Basic Pharmacology (IUPHAR) database, there are currently 57 GPCRs within the 'rhodopsin/ class A' family which remain 'orphan' (Davenport and Harmar, 2013). However, it has been estimated that up to 6 GPCRs become 'de-orphaned' per year (Foord *et al.*, 2005). To explore the mechanisms by which GPR35 mediates signalling endogenously, natural ligand identification has fundamental importance.

1.4.1 Endogenous ligand identification for GPR35

1.4.1.1 Kynurenic acid

The kynurenine metabolite, kynurenic acid (KYNA) was the first endogenously produced ligand reported to activate GPR35 (Wang *et al.*, 2006a). In addition to the tryptophan pathway, which facilitates the conversion of L-tryptophan (an essential amino acid) to 5-hydroxytryptamine ((5-HT, serotonin), an essential aminergic neurotransmitter); the kynurenine pathway is also a major facilitator of L-tryptophan degradation and conversion

(Ruddick *et al.*, 2006). In the kynurenine pathway, the degradation of L-tryptophan commences via stimulation of indoleamine-2,3-dioxygenase, an enzyme which is up regulated following the release of interferon-γ (INF-γ) in inflammation (Chen and Guillemin, 2009); please refer to Figure 1-4 for a schematic representation of the kynurenine pathway. Following this initial conversion, various intermediates are generated and subsequently implicated in a variety of signalling pathways and diseases including cancer, cerebral-inflammation and schizophrenia (Stone *et al.*, 2013b). To this end, metabolites of the kynurenine pathway are attractive therapeutic targets (Schwarcz, 2004). As an example, the metabolite 3-hydroxyanthranilic acid is understood to exert neuroprotective effects in glial cells via transcriptional suppression of the pro-inflammatory molecule tumour necrosis factor (TNF)-α and this could be targeted via alteration of the kynurenine pathway (Krause *et al.*, 2011). KYNA is a direct metabolite of kynurenine and was initially shown to act as a non-competitive antagonist of the N-methyl-D-aspartate (NMDA) receptors, which are predominantly expressed in neuronal synapses (Stone, 1993, Perkins and Stone, 1982). However, it was later discovered that KYNA is also a potent antagonist at the α7-nicotinic cholinoceptors (α7NR) (Hilmas *et al.*, 2001). Interestingly, the dysregulation of KYNA levels in disease, and subsequently decreased antagonism at this level, has been linked to various neurological and psychiatric conditions, including Huntington's disease and schizophrenia (Albuquerque and Schwarcz, 2013).
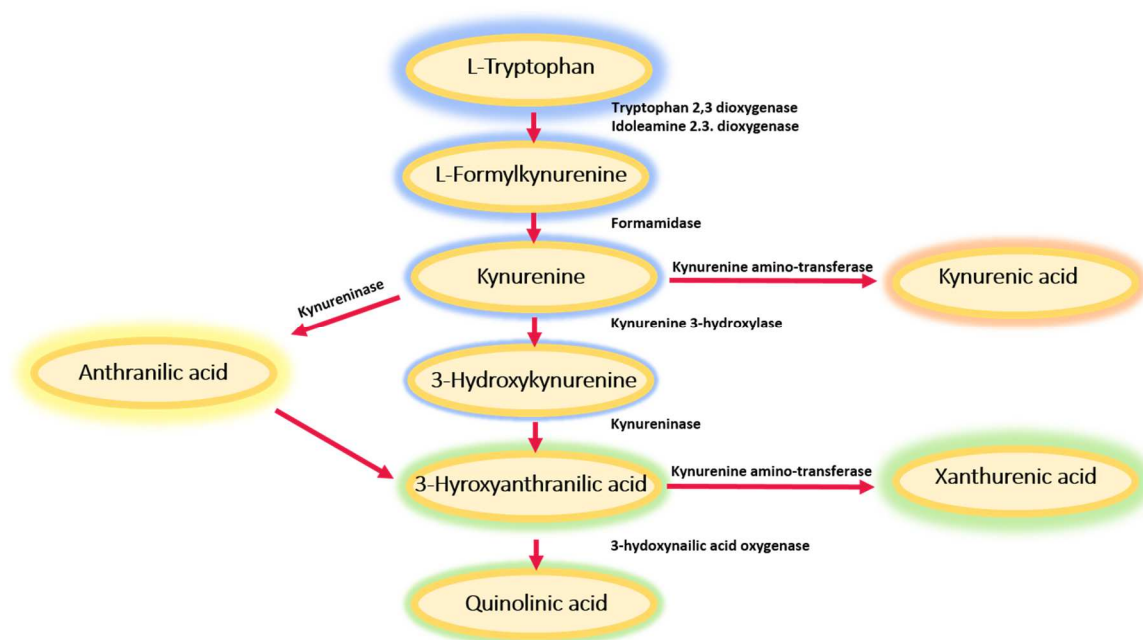
Figure 1-4. The kynurenine pathway.

A schematic representation of the kynurenine pathway and the enzymes which are involved in the degradation of L-tryptophan and conversion of metabolites to produce kynurenic acid (KYNA), a proposed endogenous activator of GPR35.

Acknowledging that numerous pathway metabolites have been discovered to activate and thus de-orphan various GPCRs (Civelli *et al.*, 2006), Wang and colleagues (2006) screened a chemical library comprising 300 metabolic intermediates for activity at GPR35 (Wang *et al.*, 2006a). The ability of KYNA to activate and internalise each of the human, rat and mouse orthologues of GPR35 with micromolar (µM) potency was reported. This was the only metabolite within the screen to elicit a response at GPR35 (Wang et al., 2006a). Upon reflection, it has been suggested that the acidic moiety of KYNA may facilitate its interaction with GPR35, given that this is the most prominent differential feature between KYNA and alternative tryptophan metabolites (Zhao *et al.*, 2014). In utilising an experimental system which incorporates G_q-protein chimeras and employs an aequorin assay to measure signals via a Ca^{2+} sensitive dye upon agonist stimulation, it

was reported that GPR35 coupled to $G_{i/o}$ following KYNA stimulation (Wang *et al.*, 2006a). Most interestingly, however, comparative Ca^{2+} transients revealed that there were significant potency differences between the species orthologues - ranging from those of rat GPR35 (EC_{50} 7.4μM), followed by mouse GPR35 (EC_{50} 10.3μM) and to human GPR35 (EC_{50} 39.2μM) (Wang *et al.*, 2006a). Importantly, these results established two central issues that have hampered subsequent GPR35 research; the variation in ligand potency between species and the fact that, for a 'natural' ligand, KYNA displays only modest potency at GPR35 (Wang *et al.*, 2006a).

Despite consistent observations that plasma KYNA is present at nanomolar levels in normal physiological conditions (Amirkhani *et al.*, 2002, Turski *et al.*, 2013), it has been argued these can reach micromolar levels in inflammatory states and this could, therefore, prove sufficient for GPR35 activation (Wang *et al.*, 2006a). It has indeed been reported that circulating KYNA levels are elevated in patients with IBD and this may be linked to the disease association of GPR35 and IBD (see section 2-3-2 on GPR35 polymorphic variations). However, there is limited other evidence for this association (Forrest *et al.*, 2002). Analysis of pancreatic, bile and intestinal secretions also demonstrated higher concentrations of KYNA, but these remain within nanomolar concentration ranges (Paluszkiewicz *et al.*, 2009). By contrast, a study conducted in 2008 assessed endogenous KYNA in various rodent tissues and reported concentrations of up to 16μM in the small intestine of the rat (Kuc *et al.*, 2008). These levels are the highest reported and together with the clear evidence of robust GPR35 expression within gastrointestinal tissue, the hypothesis that KYNA is an endogenous ligand remains strong in relation to rat GPR35 (Milligan, 2011).

In the human context, evidence of GPR35 activation via KYNA remains ambiguous. For example, Oka and colleagues were unable to generate a response at human GPR35 to KYNA when measuring changes in intracellular Ca^{2+} levels, nor were they able to demonstrate receptor internalisation following transfection of a fluorescently tagged form

of human GPR35 (Oka et al., 2010). However, in a study which assessed the adhesion properties of mononuclear cells under flow conditions, a 2-fold increase in leukocyte arrest in endothelial cells stimulated with KYNA was observed and, interestingly, this difference was abolished following knockdown of human GPR35 via short-hairpin RNA (shRNA) transfection (Barth et al., 2009). Furthermore, the authors reported functionally significant effects following treatment with 300nM KYNA (Barth et al., 2009), a comparatively low concentration compared to those required to elicit GPR35 activation in various transfected cell studies (Wang et al., 2006a, Jenkins et al., 2010). Subsequently, Jenkins and colleagues were only able to report a minor response at human GPR35 after assessing a KYNA dose-stimulation for β-arrestin recruitment in transiently transfected cells via bioluminenscence resonance energy transfer (BRET) analysis (Jenkins et al., 2010). This remains one of the few studies to directly compare ligand potency of KYNA at various GPR35 species orthologues and reproduced the previously demonstrated effects (Wang et al. 2006); although the latter study showed that activation of human GPR35 by KYNA was 100-fold less potent than for rat GPR35 (Jenkins et al., 2010). Similar results were also published by Zhao and colleagues, who reported 217µM (EC_{50}) KYNA potency at hGPR35 (Zhao et al., 2010). Finally, a recent short publication outlining results from a screen of ligands against various orphan GPCRs reported no effect at human GPR35 following KYNA addition (Southern et al., 2013).

Notably, screening technologies based upon β-arrestin recruitment were used routinely in these latter publications and, whilst it is possible that the differences observed may be attributable to the use of varied techniques across data sets, it is also possible that a degree of functional selectivity or ligand bias may exist following GPR35 activation via KYNA. Failing to account for functional selectivity can be a limiting factor in the initial stages of ligand screening and may result in an inaccurate reflection of ligand potency or even future therapeutic value (Reiter et al., 2012). It has been suggested that the identification of endogenous ligands for GPR35 may have been hampered by the use of

second messenger assays which are solely dependent upon Gα signalling (Southern *et al.*, 2013). Therefore, future experimental strategies which account for both β-arrestin recruitment and secondary signalling events may help to disentangle some of the conflicting evidence which exists in relation to GPR35 activation.

To employ a β-arrestin based strategy, Jenkins and colleagues modified human and rat GPR35 by introducing both an N-terminal epitope tag and C-terminal in-frame fusion of enhanced yellow fluorescent protein (eYFP) and co-transfected these into HEK293 cells along with *Renilla* luciferase-tagged β-arrestin-2 (Jenkins *et al.*, 2010). (See Figure 1.5).
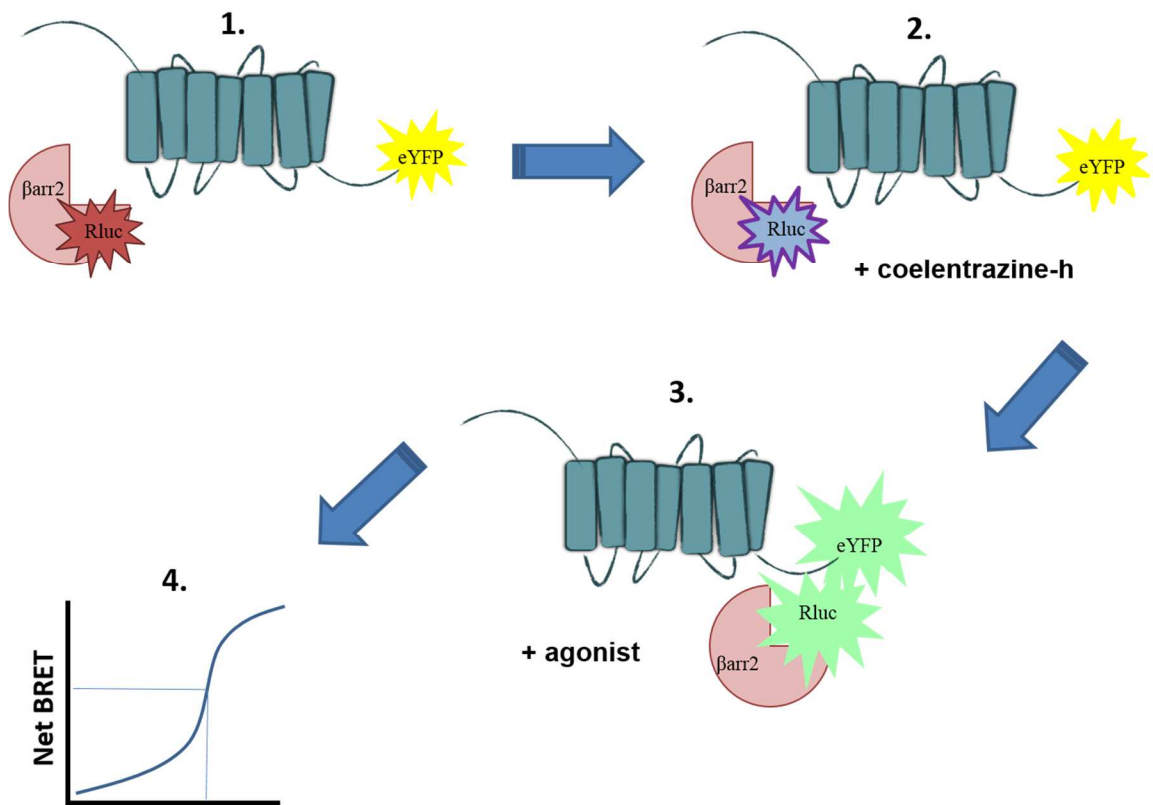
Figure 1-5. Bioluminescence Resonance Energy Transfer (BRET) assay.

1. HEK 293T cells are co-transfected with FLAG-hGPR35-eYFP and β-arrestin-2-*Renilla* luciferase-6 (βarr2-Rluc). **2.** Following the addition of the *Renilla* luciferase substrate, coelentrazine-h, cells are incubated in the dark at 37°C. **3.** Upon the addition of agonists, cells are incubated for a further 5 minutes. **4.** BRET ratio is calculated from the emission at 530 nm/485 nm minus the BRET ratio of cells expressing only the *Renilla* luciferase construct within the same experiment.

1.4.1.2 Lysophosphatidic acid

Whilst Oka and colleagues were unable to generate a GPR35 response upon KYNA addition, they did report a second potential endogenous ligand for human GPR35, 2-acyl lysosphophatidic acid (2-acyl LPA) (Oka *et al.*, 2010). The LPA family is a group of bioactive phospholipids which are present in serum, often in excess of micromolar levels

(Mills and Moolenaar, 2003). Various isoforms of LPA are able to activate the $LPA_{(1-5)}$ receptors and these promote coupling to several G-proteins including $G_{i/o}$, $G_{q/11}$ and $G_{12/13}$, and they have been implicated in cardiovascular disease, cancer and inflammation (Lin *et al.*, 2010). Classical $LPA_{(1-3)}$ receptors are not closely related to GPR35. However, novel LPA receptors including GPR55, GPR23 (LPA_4) and GPR92 (LPA_5) share significant homology with GPR35, (Lin *et al.*, 2010, Zhao and Abood, 2013, Milligan, 2011). On this basis, Oka and colleagues screened various lysophospholipids which are structurally similar to lysophosphatidylinositol (LPI), the natural ligand at GPR55, with which GPR35 shares 27% identity (Sawzdargo *et al.*, 1999).

Various forms of LPA were found to activate human GPR35 to a minor degree, though, further analysis proved 2-acyl LPA to be most efficacious (EC_{50} 30-50nM) (Oka *et al.*, 2010). Following stimulation with 1-10µM 2-acyl LPA, HEK293 cells transiently expressing human GPR35 exhibited greater intracellular Ca^{2+} mobilisation, ERK 1/2 phosphorylation (pERK), active GTP-bound Rho A protein and receptor internalisation than vector-only transfected controls. Conversely, stimulation with 1-100µM of KYNA failed to produce any response at human GPR35 (Oka *et al.*, 2010) which is largely in agreement with Jenkins and colleagues (Jenkins *et al.*, 2010). Despite the strength of these findings, the identification of 2-acyl LPA as an endogenous activator of GPR35 has had limited impact on subsequent GPR35 research. Whilst investigators have since employed various screening strategies in a bid to identify additional GPR35 ligands these findings have yet to be confirmed (Southern *et al.*, 2013, Deng *et al.*, 2012a). A reluctance to investigate further may reflect the potential difficulties which are involved in disentangling signalling pathways mediated exclusively via GPR35 activation following LPA stimulation, given the ability of forms of LPA to mediate signalling via multiple alternative LPA receptors that are widely expressed (Lin *et al.*, 2010). Despite these issues, the homology which exists between the newly identified LPA receptors and GPR35, and the robust experimental protocol employed by Oka et al. provide strong

evidence that LPA may be an endogenous activator of GPR35 (Oka *et al.*, 2010). What is more, the recent identification of antagonists which block activation of human GPR35 (Jenkins *et al.*, 2012) may prove useful in confirming the activity of 2-acyl LPA specifically via GPR35 in future studies.

1.4.2 Synthetic ligand identification for GPR35

Although natural ligands can be advantageous tools in the process of receptor characterisation, the ability of synthetic ligands to modulate GPCR signalling should not be discounted as an effective means to elucidate receptor function. Whilst GPR35 remains a poorly characterised receptor in relation to its physiological function, the identification and exploration of various structurally distinct agonist sets is extensive and complex.

1.4.2.1 Zaprinast

The first synthetic surrogate ligand identified to activate GPR35 was zaprinast (Taniguchi *et al.*, 2006). Like many other agonists at GPR35, zaprinast also has other physiological targets and is better known as a selective inhibitor of cyclic guanosine monophosphate-phosphodiesterases (cGMP-PDEs), specifically PDEs 5 and 6 (Gibson, 2001). Since the actions of zaprinast may produce increases in cGMP and other off-target effects, its use to explore the role of GPR35 in functional experimental systems is significantly limited. Alternatively, zaprinast has proven an excellent gold-standard reference compound in an array of GPR35 screens, demonstrating robust activation in multiple assay systems, in an unbiased manner, and with moderate potency (Jenkins *et al.*, 2010, Zhao *et al.*, 2010, Deng and Fang, 2012b, Mackenzie *et al.*, 2014, Southern *et al.*, 2013). However, as with previously identified GPR35 ligands such as KYNA, zaprinast displays selective potency amongst species and is 50-fold more potent at rat than human GPR35 (Taniguchi *et al.*, 2006, Jenkins *et al.*, 2010).

1.4.2.2 Identifying GPR35 ligands within the Prestwick Chemical library

Three independent publications simultaneously performed a screen of the Prestwick Chemical Library® (Yang *et al.*, 2010, Zhao *et al.*, 2010, Jenkins *et al.*, 2010). This commercially available small scale chemical library is composed of 1120 small molecule drugs which are clinically marketed and pre-approved by the Food and Drug Administration (FDA) (Wermuth, 2004). These are principally advantageous in relation to potential *in vivo* investigation and human trials as substantial information is available on ligand toxicity and both pharmacodynamics and pharmacokinetics. Most crucially, the aforementioned publications all independently identified and verified a substantial number of hits in their primary screens and re-confirmation assays. These included pamoic acid (Zhao et al., 2010), an 'inactive' salt component of many clinically marketed drugs, and the anti-asthma medication, cromolyn disodium (Yang et al., 2010).

1.4.2.3 Pamoic acid

Until recently, pamoic acid was the most potent agonist reported at GPR35, displaying nanomolar potency (Zhao *et al.*, 2010, Jenkins *et al.*, 2011). Upon first identifying pamoic acid as a potent activator via a range of assays which included receptor internalisation, ERK1/2 phosphorylation and β-arrestin translocation, Zhao and colleagues did not report any discrepancy in potency between species; demonstrating that pamoic acid effectively induced receptor internalisation of both human and mouse GPR35 (Zhao *et al.*, 2010). They also reported a dose-dependent increase in nociception following pamoic acid infusion in a mouse model undergoing an abdominal constriction test (Zhao *et al.*, 2010). However, these findings were contradicted in subsequent publications from Jenkins and colleagues who consistently report that pamoic acid is virtually inactive at both rat and mouse orthologues of GPR35; measured via β-arrestin interaction, receptor internalisation and IP1 accumulation assays *in vitro* (Jenkins *et al.*, 2010, Jenkins *et al.*, 2012). Furthermore, Jenkins and colleagues reported pamoic acid to be a partial agonist (~50%

efficacy compared to zaprinast) at human GPR35 and investigated this further via competition assays using increasing concentrations of zaprinast. Results revealed that high concentrations of pamoic acid reduced the effectiveness of zaprinast, consistent with this notion (Jenkins *et al.*, 2011). Of course, without testing a potent, endogenous agonist at human GPR35, it is impossible to fully investigate the implications of using pamoic acid as a surrogate ligand at GPR35 and, therefore, a comparative study to assess the mode of binding for both ligands may be useful.

Most intriguingly, prior to its identification as a GPR35 agonist pamoic acid was considered by drug manufacturers as an inactive 'salt', often utilised to increase the longevity of commercially marketed drug formulations, including a range of antihistamine and antipsychotic medications (Neubig, 2010). Considering its recently identified potential to evoke signalling via GPR35, the continued use of pamoic acid in such formulations may have to be carefully considered.

1.4.2.4 Flavonoids, phenolic acids and aspirin metabolites

Other agonists of micromolar potency identified via the Prestwick Chemical Library screen included the anti-inflammatory bio-flavonoids luteolin and quercetin, which displayed substantial selectivity for rat GPR35, but had little efficacy at human GPR35 (Jenkins *et al.*, 2010). By contrast, niflumic acid, a potassium and chloride ion channel blocker, displayed significant selectivity for human GPR35 (Jenkins *et al.*, 2010). To account for possible ligand bias towards β-arrestin recruitment, the ligand hits which were identified via β-arrestin translocation assays were further verified using a $G\alpha_{13}$ [^{35}S]GTP[S] binding assay, for human GPR35.   Importantly, there were no discrepancies between assays - indicating an absence of ligand bias (Jenkins *et al.*, 2010).

Finally, the most recent screen of the Prestwick Chemical Library® produced results in agreement with the earlier publications, confirming luteolin, quercetin and niflumic acid as GPR35 agonists via a multi-assay protocol (Deng et al., 2012a). However, these authors

also identified an additional agonist at human GPR35; ellagic acid. Ellagic acid is a natural phenol and displayed potency comparable to, or slightly lower than, zaprinast, and furthermore acted as a partial agonist (Deng et al., 2012a). Ellagic acid is present in high concentrations in fruit and vegetables, particularly in berries, and is known to exert powerful anti-oxidant effects in cardiovascular disease and cancer (Lesca, 1983). Following these findings, the authors postulated that additional phenolic acids may also be ligands for GPR35 and subsequently demonstrated that this is true for gallic acid, an anti-inflammatory and anti-allergenic natural phenol, which also displayed micromolar potency at human GPR35 (Deng and Fang, 2012a).

Despite the extensive evidence for multiple GPR35 ligands with known bioavailability and powerful anti-oxidative effects, there have been no functional studies to examine a potential role for GPR35 in the modulation of redox status. However, in hypothesising a role for GPR35 in the treatment of inflammation, these authors further highlighted the fact that oxygenated products of aspirin are structurally related to phenolic acids (Deng and Fang, 2012b). Moreover, these authors identified a further set of human GPR35 ligands in aspirin metabolites. Two of those identified; 2,3,4 THB and 2,3,5 THB, demonstrated moderate potencies ranging between 8-11µM (EC_{50}). However, it is notable that these were not equivalent between assay systems, underlining a potential degree of ligand bias (Deng and Fang, 2012b). The molecular mode of action of aspirin is well-understood and involves the acetylation and suppression of cyclooxygenase (COX) 1/2 enzyme expression, and subsequent down regulation of the production of prostaglandins, to exert its effect (Vane *et al.*, 1998). The studies of Deng and Fang. (2012b) demonstrated that aspirin does not activate GPR35 directly but instead they hypothesised a supporting role for GPR35 activation in the anti-nociceptive and anti-inflammatory effects which ensue following aspirin administration and subsequent oxidation of the ligand

1.4.2.5 Cromolyn disodium and other mast cell stabilisers

Yang and colleagues first identified cromolyn disodium as an agonist at GPR35 and
reported selective potency for rodent GPR35 at micromolar levels using an aequorin and
an IP-1 accumulation assay in their screen of the Prestwick Chemical Library (Yang *et al.*,
2010). Although, Jenkins and colleagues reported similar potency values in their screen,
they demonstrated equipotent activation between rat and human orthologues using the
BRET assay system (Jenkins *et al.*, 2010). Cromolyn disodium is a well-known anti-
asthma medicine which exerts its action via inhibition of the degranulation of mast cells,
thus preventing the release of histamine and other mediators of type I hypersensitivity
reactions. However, the fundamental molecular mechanism of action (MMA) of this
inhibition is unknown (Howell and Altounyan, 1967). Yang and colleagues included an
additional mast cell stabilising compound within their screen, and consequently
demonstrated that nedocromil sodium also activated GPR35 at equivalent potency to
cromolyn disodium, despite their chemical formulations being distinct (Yang *et al.*, 2010).
Given the significant lack of information regarding the MMA of these drugs, these authors
hypothesised a role for GPR35 (Yang *et al.*, 2010).

These initial findings prompted further investigation of mast cell stabilising compounds as
GPR35 agonists, resulting in the identification of brufolin and lodoxamide; two anti-allergic
medications which activate both human and rat GPR35 with low nanomolar potency and
are, therefore, the most potent activators identified to date (Mackenzie *et al.*, 2014). In
examining the pharmacological and structural similarities of GPR35 activating-mast cell
stabilising compounds, this publication highlighted an obvious commonality in that the two
most potent ligands shared a symmetric, di-acid structure. It was evident therefore that it
was not merely the presence of carboxylic acid containing structures within chemicals
which were GPR35 agonists, but that it may further relate to mirror-image structures.
Although this may not provide a functional explanation of their possible role in the
stabilisation of mast cells, it is an intriguing finding (Mackenzie *et al.*, 2014).

Further screening also identified amlexanox, doxantrazole and permirolast as nanomolar potency agonists at GPR35 (Mackenzie et al., 2014). Although not symmetrical di-acids, each of these ligands displays anti-allergenic pharmacology and have similar chemical properties to previously identified ligands at GPR35 in that they also possess a fixed negative charge (Mackenzie *et al.*, 2014). Ultimately, these studies have begun to define common structural components for synthetic GPR35 agonists and this information will be useful in future screening studies.

1.4.2.6 Tyrophostin analogues

Although displaying limited potency at human GPR35, the identification of tyrophostin analogues was the first of many efforts to identify GPR35 agonists by researchers at Corning, NY (Deng *et al.*, 2011a). Notably, the human colon cancer cell line HT-29, that endogenously express GPR35, was utilised in their initial screening process. By measuring changes in dynamic mass redistribution (DMR), a label-free cell biosensor assay (Schroder *et al.*, 2010), tyrophostin analogues were identified and flagged hits were then subject to further analysis, including receptor internalisation, ERK phosphorylation and use of a commercially available β-arrestin recruitment assay, Tango® (Deng *et al.*, 2011a). Fourteen tyrophostin analogue hits were identified. The most potent of these were Tyrophostin-51, which displayed potencies similar to zaprinast across all assays, and also entacapone, a tyrophostin analogue used in the treatment of Parkinson's disease (Rascol *et al.*, 2000). Tyrophostins are inhibitors of receptor tyrosine kinases, the molecules responsible for regulating cellular functions via transmembrane induced protein tyrosine phosphorylation (Levitzki and Gazit, 1995). The authors postulated that the moderate potency of entacapone at GPR35 may be indicative of clinical relevance, despite the primary clinical action of entacapone being well understood (Deng *et al.*, 2011a)

Following this, an additional compound screen was performed using the same range of experimental assays (Deng *et al.*, 2011b). Unusually, these compounds were synthesised in-house, and with unknown pharmacology and/ or containing malononitrile groups, which are structurally similar to the previously identified tyrophostins (Deng *et al.*, 2011a, Deng *et al.*, 2011b). Here activity of two high potency ligands at human GPR35 was demonstrated, the first being 2-(4-methylfuran-2(5H)-ylidene) malonitrile (EC$_{50}$ 32nM) and the second being thieno[3,2-b]thiophene-2-carboxylic acid (EC$_{50}$ 63nM) . These researchers were able to compare the chemical and structural properties with the exhibited pharmacology to deduce that the presence of the carboxylic acid and malonitrile group was important for potent GPR35 activation (Deng *et al.*, 2011b). This is in agreement with previous observations, relating to the presence of one or more carboxylic acid groups in GPR35 activating compounds (Jenkins *et al.*, 2010, Milligan, 2011, Mackenzie *et al.*, 2014, Funke *et al.*, 2013).

1.4.2.7 Catecholics

Another recently identified group of GPR35 ligands is a family of catechol-containing compounds. Catecholics are known free-radical scavengers which protect against lipid peroxidation and are utilised in an array of FDA approved drugs (Deng and Fang, 2013). Deng and colleagues initially identified 10 catecholic compounds which activated GPR35. However, only pyrogallol, propyl gallate and benserazide displayed moderate to low potency, ranging between EC$_{50}$ 1-11µM (Deng and Fang, 2013). It was noted that this group of GPR35 active compounds was lacking a carboxylate function and, therefore, this may indicate a distinct mode of binding in comparison to previously identified GPR35 agonists that contain a formal negative charge.

1.4.3 Receptor mutagenesis studies

Despite the evident structural diversity which exists between GPR35 agonists, only a handful of studies has addressed the basis of ligand binding, either in relation to the importance of the acidic moieties or the wide ranging species selectivity.

The first insights into amino acids critical for ligand-binding or activation of GPR35 resulted from a mutagenesis study carried out by Jenkins and colleagues (Jenkins *et al.*, 2011). An earlier publication highlighted that an arginine in TMDIII, located at position 3.36 [according to the Ballesteros and Weinstein (1995) numbering system], was of critical importance for the binding of small ligands containing a carboxylate moiety, including lactate, to GPR81 (Liu *et al.*, 2009). Given that residues crucial for ligand binding are often conserved amongst closely related 'rhodopsin-like' GPCRs and that GPR35 ligands are generally negatively charged and contain a carboxylate moiety or a related bioisoteric group; Jenkins and colleagues (2011) carried out a similar mutagenesis study (Jenkins *et al.*, 2011). The substitution of arginine - a positively charged basic residue, for an alanine – a non-polar residue, at position 3.36 in both rat and human GPR35, eliminated efficacy and potency of zaprinast, KYNA and a newly identified ligand, compound 10, at GPR35 in both species whilst membrane expression of these mutants remained unaffected. Moreover, a second mutant, this time substituting tyrosine for leucine (a non-polar residue) at position 3.32 had a similar effect in that both human and rat GPR35 essentially lost responsiveness to both zaprinast and KYNA (Jenkins *et al.*, 2011). A series of competition assays was then performed to assess allosteric binding potential and results suggested that increasing concentrations of either ligand had no effect on the ability of the other to reach a maximal response at GPR35. These findings, and those relating to mutagenesis, are consistent with zaprinast and KYNA sharing an overlapping, orthosteric binding site to which the positively charged arginine located within TMDIII at position 3.36 contributes (Jenkins *et al.*, 2011).

Alongside the identification of the high potency GPR35 agonists lodoxamide and brufolin, MacKenzie et al. (2014) also explored the importance of site specific residues within the GPR35 ligand binding pocket (Mackenzie *et al.*, 2014). Computational modelling and ligand docking studies helped to generate a series of GPR35 mutants designed to define additional crucial arginine residues within the boundaries of TMDIII and VII, a suggested area of ionic interaction. Mutation of two arginines at positions 6.58 and 7.32 significantly reduced the potency of lodoxamide, whilst having little effect upon zaprinast, suggesting that the binding sites of these ligands are distinct (Mackenzie *et al.*, 2014). This may not be surprising, given that lodoxamide and brufolin possess a di-acid structure. However, in contrast to many high potency GPR35 ligands containing a carboxylate moiety, which often exhibit rodent GPR35 selectivity, these compounds show equivalent potency between rodent and human orthologues. This led MacKenzie et al. (2014) to generate and examine a series of cross-species amino acid substitutions. Interestingly, the results suggested that whilst the majority of these ligands share a central, arginine-based binding domain, those ligands possessing additional carboxylate groups require a further binding site and this may facilitate high potency interactions with GPR35. Furthermore, these additional binding sites are often poorly conserved between species and may explain the frequency of species selective ligands, with the exception of lodoxamide and brufolin (Mackenzie *et al.*, 2014).

These findings are largely in agreement with a study recently published by Zhao and colleagues (2014). These authors also performed computational modelling and more restricted site-directed mutagenesis to identify crucial amino acid residues essential for the binding of zaprinast and pamoic acid to human GPR35 (Zhao *et al.*, 2014). Their findings suggest, like MacKenzie et al. (2014) that key positively charged arginine residues residing within TMD 3, 4, 5 and 6 are most prominently involved in ligand recognition (Zhao *et al.*, 2014). Furthermore, this study also assessed the importance of arginines located within the second extracellular loop (ECL) of GPR35 and discovered

that, whilst several of these are common recognition sites for zaprinast and pamoic acid, the mutation of one arginine, R(167) selectively reduced pamoic acid potency by 4-fold (Zhao *et al.*, 2014). Despite the highly conserved nature of 'rhodopsin-like' GPCRs, the second ECL is understood to be most variable in relation to both receptor type and species (Katritch *et al.*, 2013) and, therefore, this publication is the first to demonstrate that differential binding sites exist within the second ECL for GPR35 ligands and this also may contribute to human orthologue selectivity displayed by pamoic acid (Zhao *et al.*, 2014).

1.4.4 Identification of GPR35 Antagonists

Two antagonists of GPR35 have been described; CID-2745687 (methyl-5 [(tertbutylcarbamothioylhydrazinylidene) methyl]-1-(2, 4-difluorophenyl) pyrazole-4-carboxylate) (Zhao *et al.*, 2010) and ML-145 (2-hydroxy-4-[4-[(5Z)-5-[(E)-2-methyl-3-phenylprop-2-enylidene]-4-oxo-2- sulfanylidene-1,3-thiazolidin-3-yl]butanoylamino] benzoic acid) (Heynen-Genel *et al.*, 2010). Both demonstrate nanomolar potency at GPR35, and are highly selective for the human orthologue and elicit little or no effect at rodent orthologues (Zhao *et al.*, 2010, Heynen-Genel *et al.*, 2010, Jenkins *et al.*, 2012). First identified by Zhao and colleagues (2010), CID-2745687 demonstrated an ability to block agonist induced β-arrestin translocation and ERK1/2 phosphorylation with high affinity with a reported K_i of 12.8nM and 18nM, respectively (Zhao *et al.*, 2010). Furthermore, these authors noted that this compound only elicited an antagonistic response at human GPR35, with no effect upon the mouse orthologue. This is in agreement with findings published by Jenkins and colleagues, who have consistently demonstrated nanomolar potency of CID-2745687 at the human orthologue, with negligible effects at rodent forms of GPR35 (Jenkins *et al.*, 2012). A short time later a second high affinity GPR35 antagonist, ML-145, was identified (Heynen-Genel *et al.*, 2010). This compound was highlighted via a probe report from the NIH Molecular Libraries Program and resulted from a screen for antagonists against both GPR35 and GPR55.

Importantly, ML-145 demonstrated >1000-fold affinity for GPR35 over GPR55 (Heynen-Genel *et al.*, 2010). Following this, Jenkins and colleagues examined the molecular pharmacology of ML-145 more closely using multiple assay systems, which included β-arrestin translocation, receptor internalisation and IP-1 accumulation (Jenkins *et al.*, 2012). Notably, ML-145 was also a human GPR35-selective antagonist and, like CID-2745687, a competitive inhibitor of zaprinast and cromolyn disodium but a non-competitive antagonist of pamoic acid (Jenkins *et al.*, 2012) at this receptor. The molecular basis for the species selectivity of these compounds has not yet been reported.

1.5 Cardiovascular Disease

Recent epidemiological evidence highlights that cardiovascular disease (CVD) is the predominant cause of mortality within western civilisation and it is estimated that one person will die every 37 seconds of a cardiovascular related disease in the USA alone (Lloyd-Jones *et al.*, 2010). CVD is a multifaceted condition and incorporates various diseases including hypertension, atherosclerosis and resulting end-organ damage of the kidneys, brain and heart (Wald *et al.*, 2009). Hypertension and subsequent atherosclerosis are thought to be significant hallmarks of CVD and up to 11% of all deaths in developed countries are attributed to the hypertensive state (Lloyd-Jones *et al.*, 2010). In order to target multiple disease pathologies treatment often constitutes a combination of medications including β-blockers, Ca^{2+} channel inhibitors, angiotensin converting enzyme (ACE) inhibitors and diuretics (Wald *et al.*, 2009).

As research within this field progresses and diagnostic biomarkers become increasingly more accurate (Wang *et al.*, 2006b, Vasan, 2006), it is expected that the prevalence of conditions stemming from CVD will continue to rise. It is unsurprising, therefore, that translational medicine remains at the forefront of research directed toward the development of new therapies to treat CVD and its related conditions.

1.5.1 A role for GPR35 in the pathology of CVD

As discussed in section 1-3-3 *(Putative functions of GPR35)*, GPR35 has been implicated in numerous disease pathologies since its discovery almost 15 years ago (O'Dowd *et al.*, 1998). However, despite various investigations, such links remain uncertain. Collectively, evidence, although in many cases circumstantial, strongly suggests that GPR35 may play a part in the pathology of CVD, particularly in hypertension and heart failure (Barth *et al.*, 2009, Min *et al.*, 2010, Ronkainen *et al.*, 2014). Moreover, data from genome wide association studies (GWAS) have further implicated GPR35 in multiple disease states which include the identification of a polymorphic isoform which strongly and positively correlates with the incidence of CAD in man (Sun *et al.*, 2008). The following section aims to discuss the pathologies of the various diseases which affect the cardiovascular system, the treatment options which currently exist and evidence of a requirement for the development of novel interventions and therapeutics.

1.5.1.1 Hypertension, its treatment and limitations

The World Health Organisation (WHO) defines the diagnosis criteria for human essential hypertension as a reading of systolic blood pressure (SBP) ≥140mmHg and/ or diastolic blood pressure (DBP) ≥90 (Whitworth, 2003). Most recent guidelines categorise this in to three fields of severity; 'pre-hypertension' (SBP 120-139mmHg, DBP 80-89mmHg), 'stage I hypertension' (SBP 140-159mmHg, DBP 90-99mmHg) and the most severe, 'stage II hypertension' (SBP≥160mmHg, DBP≥100mmHg) (Weber *et al.*, 2014). Before a diagnosis is confirmed, it is common for patients to receive two consecutive readings on separate occasions, 1-4 weeks apart, or in some cases, 24-hour ambulatory monitoring is required (Weber *et al.*, 2014).

The etiology of human essential hypertension is complex and its development is often idiopathic in nature. However, factors such as age, gender, environment and genetics highly influence its prevalence (Whitworth, 2003, Egan *et al.*, 2010). For example, it has

been estimated that genetic factors may account for up to 15-40% of hypertensive pathophysiology (Staessen *et al.*, 2003). To this end, genetic disorders which relate to ethnicity, geographical location and gender are well documented (Carretero and Oparil, 2000). However, the contribution of specific genetic interactions in human essential hypertension remains largely unknown (Delles *et al.*, 2010). Ultimately, if uncontrolled, hypertension can lead to an increased pulse pressure and arterial stiffness translating to end-organ damage of the heart, kidney, vasculature and brain (Safar *et al.*, 2012). Consequently, undiagnosed hypertension can significantly increase cardiovascular risk and is thought of as a silent killer (Korhonen *et al.*, 2013).

As previously noted, the conventional mode of treatment for patients with essential hypertension is often a combination of two or more medications (Staessen *et al.*, 2003, Gradman *et al.*, 2010). Practically, combination treatment is designed to address several fundamental mechanisms that regulate BP; total blood volume, vascular tone and cardiac function (Lifton *et al.*, 2001). Therefore, a representative treatment regimen may constitute a diuretic to increase sodium excretion; an angiotensin converting enzyme (ACE) inhibitor to prevent the conversion of angiotensin-I (Ang I) to angiotensin-II (Ang II), (a potent vasoconstrictor) and, finally, β-blockers are also prescribed to reduce total cardiac output via the dual antagonism of the $β_1AR$ in heart tissue and kidneys, reducing heart rate and the release of renin, respectively (Gradman *et al.*, 2010). Information gained from randomised clinical trials indicate that the development of combination treatment has significantly improved the number of patients with 'controlled hypertension' by up to 25% in the recent decade (Egan *et al.*, 2010, Turnbull, 2003). Despite these outstanding achievements, on a population scale it is estimated that between 30-55% of hypertensive patients remain resistant to existing therapies or have poor adherence levels as a result of unwanted side-effects to medication and are therefore classed as having 'resistant' or 'uncontrolled' hypertension, respectively (Calhoun *et al.*, 2008a, Egan *et al.*, 2010). Unfortunately, poor control of BP, for whichever reason, significantly increases

mortality risk and therefore, the treatment of hypertension is an area of unmet clinical need and further investigative research is warranted towards the discovery and development of new therapies (Persell, 2011).

1.5.1.2 Atherosclerosis and CAD, interventions and treatment

Together with hypertension, the presence of atherosclerosis is a significant hallmark of the cardiovascular disease state (Lloyd-Jones *et al.*, 2010). The pathophysiology of atherosclerosis involves a progressive inflammatory cascade within the vasculature and ultimately results in the formation of a 'fatty streak' which can develop into a fibrotic plaque or 'fibroatheroma' (Weber and Noels, 2011). This process is initiated following endothelial cell damage and activation caused by exposure to increased biomechanical forces within the vasculature, often specifically at 'pro-atherosclerotic' artery bifurcation points (Moore and Tabas, 2011, Sima *et al.*, 2009). Once activated, endothelial cells express vascular cell adhesion molecule-1 (VCAM-1) and pro-inflammatory chemokines which attract circulating low-density lipids (LDLs); a process which is greatly exacerbated in hypercholesterolemia (Khan *et al.*, 1995, Dansky *et al.*, 2001). The atherosclerotic process is advanced following the adhesion of circulating leukocytes, namely monocytes and neutrophils, to the endothelium via interactions between α/β-integrins and adhesion molecules (Weber and Noels, 2011). Following this, intercellular adhesion molecule-1 (ICAM-1) and VCAM-1 promote the lateral migration of monocytes into the sub-endothelial space (Dansky *et al.*, 2001) where, due to their high level of plasticity, they are able to differentiate into macrophages which scavenge oxidised LDL (oxLDL) and other cell debris (Woollard and Geissmann, 2010). These become macrophage 'foam cells' and form the initial lipid laden 'fatty streak' evident in early atherosclerosis. However, as atherosclerosis advances macrophages become apoptotic, giving rise to the development of a necrotic core (Moore and Tabas, 2011). Advanced atherosclerosis involves plaque stabilisation via the deposition of extracellular matrix (ECM) proteins and migration of smooth muscle cells (SMCs) into the sub-endothelial space (Moore and Tabas, 2011).

However, over time, destabilisation and rupture may occur following plaque exposure to shear stress, macrophage-specific protease enzymes which can degrade the fibrotic cap [matrix metalloproteinase (MMP)] and further vascular cell apoptosis, enlarging the necrotic core (Moore and Tabas, 2011). Critically, mobilisation of a plaque or subsequent thrombus formation may cause cerebral stroke or myocardial infarction (MI), depending on the origin of the lesion (Virmani *et al.*, 2005).

Atherosclerotic lesion formation and calcification burden can be quantified in patients using non-invasive imaging techniques such as intravascular ultrasound (IVUS) (Taylor *et al.*, 2003) and hypercholesterolemia can be identified via assessment of total cholesterol and HDL:LDL ratio (Stone *et al.*, 2013a). Primary prevention strategies encompass the control of hypertension, a modified lifestyle regimen and the use of statin therapy to inhibit cholesterol synthesis and reduce inflammation of the endothelium (Weber and Noels, 2011, Charo and Taub, 2011). Unfortunately, following a major adverse cardiovascular event (MACE) such as MI, primary prevention strategies are not singly appropriate and must be applied alongside secondary prevention revascularisation procedures such as the deployment of percutaneous transluminal coronary angioplasty (PTCA) and drug eluting stents or coronary artery bypass grafting (CABG), depending on the site and severity of vessel occlusion (Thygesen *et al.*, 2012).

Patients receive PTCA treatment following the narrowing of one or more vessels and the procedure involves the advancement of a balloon tipped catheter via the groin and into the heart where it is inflated at the location of vessel occlusion in order to the 'clear' the obstructive plaque. Following this, a metal framed cylinder (stent) is deployed to stabilise the vessel and the catheter is removed. Although 5 year survival rates are high; 89.5-95%, associated with the number of vessels affected, a major contributor to failure rates is restenosis of the vessel and this occurs following 30-40% of stent deployments (Smith *et al.*, 2001). Restenosis occurs following loss and dysfunction of the vascular endothelium and subsequent injury to the internal elastic lamina following balloon inflation and stent

deployment can damage the medial layer of the vessel wall, collectively promoting the stimulation of vascular SMC proliferation, migration and inflammatory reactions (Otsuka *et al.*, 2012). To prolong longevity, researchers have developed drug-eluting stents (DES) as opposed to bare metal stents (BMS), which utilise coated polymers including, for example, sirolimus and paclitaxel to prevent the induction of proliferative and migratory SMCs (Van der Heiden *et al.*, 2013, Otsuka *et al.*, 2012). However, it became evident that DES were subject to severe late restenosis and this was related to a 50% reduction in re-endothelialisation up to 5-40 months following the deployment of drug eluting stents in comparison to BMS, highlighting the importance of endothelial cell viability in the prevention of restenosis (Joner *et al.*, 2006).

CABG is the most widely elected procedure following MI which involves multi-vessel occlusion. According to recent statistics, it has been estimated that >400,000 CABG procedures are performed in a single year in the USA alone (Rosamond *et al.*, 2008). Despite the investment of time and resources to treat this disease, and the use of alternative vessel sources such as radial and mammary arteries in the bypass procedure, autologous saphenous vein is still widely utilised, especially when multi-bypass procedures are required. The effective patency rates of vein grafts are severely reduced over time and, currently, failure rates are as high as 50%, 10 years post CABG (Rienstra *et al.*, 2008) and previous evidence has shown that 5 years post CABG, >25% of vein grafts will fail (Eagle *et al.*, 1999). In order to effectively prevent vein graft failure, it is important to understand its causal mechanisms. Intimal hyperplasia plays an important role in vein graft occlusion, with neointima formation resulting from vascular smooth muscle cell (VSMC) proliferation and migration to the sub-endothelial intima alongside the deposition of circulating monocytes and neutrophils. The most common source for coronary artery bypass vessels is the human saphenous vein (HSV) due to its ready availability, autologous nature and the frequent requirement for bypassing multiple vessel occlusion in many patients. However, shear stress presented by the coronary circulation

can cause damage to, and potential loss of, endothelial cells (ECs) or induce EC

activation, resulting in the secretion of inflammatory cytokines and growth factors that

promote VSMC proliferation and migration (Rienstra *et al.*, 2008). Furthermore, ischemia

and subsequent reperfusion result in reactive oxygen species (ROS) production

contributing to EC and VSMC death and inflammation via activation of the NFkB pathway

(Eltzschig and Eckle, 2011). NFkB is also integral to VSMC migration and proliferation via

modulating matrix metalloproteinases (MMPs) and their endogenous inhibitors, the tissue

inhibitors of metalloproteinases (TIMPs) (Wan *et al.*, 2012b). Given that the nature of the

bypass procedure presents a short therapeutic window for *ex vivo* vessel treatment,

investigators have begun to assess the potential of adenoviral mediated gene delivery

alongside drug exposure in this setting (Wan *et al.*, 2012a). Despite this progress, limited

novel therapies have successfully reached the clinic and there remains a requirement for

new interventions in the setting of vein graft failure.

1.5.1.3 Heart failure and treatment

Of the many pathologies which lead to heart failure, a 5 year prognosis following

myocardial infarction indicates it is fatal for 65% of patients (Passier *et al.*, 2008).

Ischemic heart disease results from a single coronary artery occlusion or multi-vessel

disease which prevents adequate blood perfusion to the surrounding myocardium, further

resulting in cardiomyocyte death and the formation of scar tissue via fibrosis (Maillet *et al.*,

2013). Cardiac hypertrophy and remodelling is an adaptive response which enables

cardiac output to be maintained and stabilises the heart, reducing its acute vulnerability to

rupture. However, following prolonged cardiac remodelling and fibrosis, progressive scar

formation and lack of functional cardiomyocytes detracts from the overall pump function of

the heart, resulting in severely diminished contractile function (left ventricular ejection

fraction <35%) (Keteyian, 2013). This leads to detrimental effects upon vital organs to

which a limited oxygen supply is being delivered, ultimately resulting in end-organ

damage. Moreover, when large areas of the myocardium become ischemic, cell-cell

interactions may become disrupted resulting in an uncoupling of electrical activity, potentially giving rise to ventricular-arrhythmias and sudden cardiac death (Cascio *et al.*, 2005).

Thus far, treatment options for heart failure are challenging and pharmacological interventions are designed to reduce pre- and after-loads which are exacerbated by hypertension, as well as total cardiac output (McMurray *et al.*, 2012). This can be managed via therapies such as diuretics, ACE inhibitors and β-blockers. However, due to the non-regenerative nature of the human heart, progressive heart failure ultimately requires heart transplant and thus, patient mortality rates are high (Passier *et al.*, 2008). Therefore, the importance of developing novel pharmaceuticals which have improved specificity in relation to patient and disease whilst presenting minimal risk of cardiac-toxicity, is becoming increasingly evident (Matthews and Frid, 2010).

1.6 Hypothesis and aims

Taking together the evidence which suggests a role for GPR35 in disease, a robust cardiovascular element exists within the current literature. Whilst evidence from genome-wide association and gene expression studies has linked GPR35 to both CAD (Sun *et al.*, 2008) and heart failure (Min *et al.*, 2010), respectively, subsequent investigation of the phenotypic profile of mice lacking the GPR35 gene has highlighted that systolic blood pressure is significantly increased in these models, suggesting that GPR35 expression and thus, activation, may be essential for the maintenance of blood pressure. Moreover, a recent study, investigating the expression of GPR35 *in vitro* and *in vivo* following exposure to acute and chronic ischemia within cardiomyocytes and tissue, reported GPR35 as a prominent and novel biomarker in the development of acute heart failure, directly promoted by the binding of hypoxic marker, HIF-1 (Ronkainen *et al.*, 2013). Therefore, to

investigate the potential role GPR35 may play in the development of cardiovascular diseases, a series of aims were devised:

- To pharmacologically characterise and identify potent agonists and antagonists of GPR35 which activate multiple species orthologues, providing the opportunity to realistically target GPR35 in both an *in vitro* and *in vivo* setting, for the first time.

- To investigate the role GPR35 might play in human saphenous vein smooth muscle and endothelial cell migration, proliferation and morphology, which demonstrate high expression levels of GPR35.

- Further to this, an additional aim will be to dissect the role of GPR35 and $G\alpha_{12/13}$ mediated signalling in vascular cell culture models, using a multiple assay system approach.

- Finally, we hope to elucidate a role for GPR35 in the setting of hypertension and related end-organ damage by measuring the effects of GPR35 activation on haemodynamic and cardiac properties in the spontaneously hypertensive stroke prone rat (SHRSP).

2 Materials and Methods

2.1 Pharmacological reagents

Zaprinast *(2-(2-Propyloxyphenyl)-8-azapurin-6-one),* **CID-2745687** *(1-(2,4-Difluorophenyl)-5-[[2-[[(1,1-dimethylehyl)amino]thioxomethyl]hydrazinylidene]methyl]-1H-pyrazole-4-carboxylic acid methyl ester), and* **ML-145** *(-Hydroxy-4-[4-(5Z)-5-[(E)-2-methyl-3-phenylprop-2-enylidene]-4-oxo-2-sulfanylidene-1,3-thiazolidin-3-yl]butanoylamino]benzoic acid):*

Tocris Bioscience, Bristol, UK.

Pamoic acid *(1, 1'-Methylene-bis(2-hydroxy-3-naphthoic acid)),* **cromolyn disodium** *(disodium;5-[3-(2-carboxylato-4-oxochromen-5-yl)oxy-2-hydroxypropoxy]-4-oxochromene-2-carboxylate) and* **amlexanox** *(2-Amino-7-(1-methylethyl)-5-oxo-5H-[1]Benzopyrano[2,3-b]pyridine-3-carboxylic acid):*

Sigma-Aldrich Company, Dorset, UK

Y-27632 *(R)-(+)-trans-4-(1-Aminoethyl)-N-(4-Pyridyl)cyclohexanecarboxamide dihydrochloride:*

Calbiochem, UK

Y-16 *(4-{3-[(3-methylbenzyl)oxy]benzylidene}-1-phenyl-3,5-pyrazolidinedione):*

ChemBridge, CA, US

2.2 Chemical reagents

Coelentrazine-h:

Promega, Southampton, UK

Hygromycin-B and Zeocin:

Roche, West Sussex, UK

Blasticidin:

Life Technologies, Thermo Fischer Scientific, Renfrew, Scotland, UK

Polyethylenimine (PEI):

Polysciences, Warrington, PA, USA

Tetramethylrhodamine (TRITC) actin phalloidin stain and dimethyl sulfoxide (DMSO):

Sigma-Aldrich Company, Dorset, UK

ProLong® Gold Antifade Mountant with DAPI and Immumount:

Life Technologies, Thermo Fischer Scientific, Renfrew, Scotland, UK

2.3 Buffers and solutions

Hank's Balanced Salt Solution (HBSS) and Phosphate Buffered Saline (PBS):

GIBCO® Life Technologies, Thermo Fischer Scientific, Renfrew, Scotland, UK

0.25% Trypsin-ethylenediaminetetraacetic acid (EDTA) and poly-D-lysine:

Sigma-Aldrich Company, Dorset, UK

Tris-EDTA (TE) buffer:

5mM Tris-base, 5mM EDTA in 5 Litres in H_2O (pH 7.4)

DNA loading dye (5X):

QIAGEN, West Sussex, UK

Laemmli Buffer (5X):

0.4M DTT, 0.17M sodium dodecyl sulphate (SDS), 50mM Tris-base, 5M urea and 0.01% bromophenol blue. Stored at 4°C.

Tris-Buffered Saline with Tween 20 (TBST) Buffer:

50mM Tris, 150mM sodium chloride (NaCl), 0.05% Tween 20 in 500mL of H_2O.

Competent bacteria:

Buffer 1: 1M potassium acetate, 1M rubidium chloride ($RbCl_2$), 1M calcium chloride ($CaCl_2$), 1M manganese chloride ($MnCl_2$), 80% (w/v) glycerol = 100mL de-ionised water (pH 5.8). Stored at 4°C.

Buffer 2: 100mM 3-(N-morpholino)propanesulfonic acid (MOPS) (pH 6.5), 1M $CaCl_2$, 1M $RbCl_2$, 80% (w/v) glycerol = 40mL de-ionised water (pH 6.5). Stored at 4°C.

Radioimmunoprecipitation assay (RIPA) buffer (1X): 50mM Hepes, 150mM NaCl, 1% (v/v) Triton-X-100, 0.5% (w/v) NaDeoxycolate, 0.1% (w/v) SDS, 10mM sodium fluoride (NaF), 5mM EDTA, 10mM monosodium phosphate (NaH_2PO_4), 5% (v/v) ethylenglycol (pH 7.3) + protease inhibitor cocktail. Stored at -20°C.

Paraformaldehyde (4%): 40g polyoxymethylene, 800ml PBS at 60°C (pH 6.9). Stored at -20°C.

Luria-Broth (LB): 1% Tryptone, 0.5% yeast extract and 10g NaCl = 1L H_2O (pH 7.0)

Autoclaved at 126°C and used within 24 hours.

Luria-agar (LA): 1% (w/v) Tryptone, 0.5% (w/v) yeast extract, 1% (w/v) NaCl and 1.5%

(w/v) Bacto-agar = 1L H_2O (pH 7.0) and autoclaved at 126°C. Once cooled, 50mg/mL

ampicillin was added and the agar broth was poured into $10cm^3$ dishes and solidified

before storage at 4°C.

Krebs solution: 0.25M NaCl, 0.001M KCL, 2mM magnesium sulphate ($MgSO_4$), 50mM

sodium bicarbonate ($NaHCO_3$), 2mM potassium dihydrogen orthophosphate (KH_2PO_4),

2mM $CaCl_2$ (pH 7.4). Oxygenated with 95% O_2 and 5% CO_2.

2.4 Molecular biology and cloning techniques

2.4.1 Preparation of competent bacteria

XL1 Blue competent cells were streaked out on an agar plate without antibiotics and

grown overnight at 37°C. A single colony was grown in 5mL of L-broth overnight at 37°C

within a shaking incubator and this was sub-cultured into 100mL of L-broth and grown

until optical density at 550nM was 0.48 using a spectrophotometer. After chilling on ice for

5 minutes, the cells were subjected to centrifugation at 1000 *g* for 10 minutes at 4°C.

Each pellet was re-suspended in 20mL of 'buffer 1' (see *2-3 Buffers and Solutions*), then

chilled on ice for 5 minutes and the centrifugation step repeated. Each pellet was then re-

suspended in 2mL of 'buffer 2' (see *2-3 Buffers and Solutions*) by gentle pipetting and

chilled on ice for a further 15 minutes. Cells were then aliquotted into 220μL volumes and

were stored at -80°C. Once thawed, these were not re-used.

2.4.2 DNA Transformation

50ng of plasmid DNA was incubated with 50µL of competent cells on ice for 15 minutes. The cells were heat treated for 90 seconds at 42°C in a water bath (to make them porous) and were returned to ice for 2 minutes prior to addition of 450µL sterile L-broth. Cells were then recovered at 37°C for 45-60 minutes within a shaking incubator. Next, 50-200µL was then added to an agar plate containing 50mg/mL Ampicillin. The plates were incubated overnight at 37°C and transformed colonies were selected and cultured overnight in 5mL of L-broth containing 50mg/mL Ampicillin. The resulting cultures were either DNA mini-prepped or sub-cultured within 100mL of L-broth containing 50mg/mL Ampicillin to produce larger amounts of plasmid DNA.

2.4.3 DNA mini prep

Small cultures of plasmid DNA were purified using the Wizard® Plus SV Minipreps DNA Purification System (Promega, Southampton, UK) as per manufacturer's instructions. Briefly, plasmid culture was subjected to centrifugation at maximum speed for 5 minutes at room temperature (RT) and the remaining pellet was gently re-suspended in 250µL of re-suspension buffer [50 mM Tris-hydrogen chloride (HCl), 10 mM EDTA, 100 µg/mL RNase A (pH 7.5)]. Cells were then lysed following the addition of 250µL of lysis buffer (0.2M sodium hydroxide (NaOH), 1% SDS). After 5 minutes, the lysis buffer was neutralised by the addition of 350µL of neutralisation buffer [4.09M guanidine hydrochloride, 0.76M potassium acetate, 2.12M glacial acetic acid (pH 4.2)]. 850µL of cultured plasmid DNA was then transferred to a spin column and subjected to centrifugation at maximum speed for 1 minute at RT. The flow-through was discarded and 750µL of wash solution [162.8mM potassium acetate, 22.6mM Tris-HCl (pH 7.5), 0.109mM EDTA (pH 8.0) (diluted with 95% ethanol)] was added to the spin column and it was again subjected to centrifugation at maximum speed for 1 minute at RT. This step

was then repeated using 250µL of wash solution and centrifugation was at maximum speed for 2 minutes at RT using a new collection tube. The column was transferred into a new, sterile 1.5mL Eppendorf tube and plasmid DNA was eluted by adding 50-100µL of nuclease-free water and subjecting to centrifugation at maximum speed for 1 minute at room temperature. Plasmid DNA was quantified by measuring the absorbance of a 1:00 dilution in H_2O at 260nm and 280nm using a spectrophotometer. Ratios of A_{260}/A_{280} between 1.7 and 2.0 were considered pure and plasmids were then stored at $-20°C$ or below for future use.

2.4.4   DNA maxi prep

Larger volumes of plasmid cultures were purified using a QIAGEN plasmid maxiprep kit (QIAGEN, West Sussex, UK) according to the manufacturer's instructions. Briefly, 50mL aliquots of cultured plasmid were harvested via centrifugation at 6000 x g for 15 min at 4°C and the remaining pellet was then vigorously re-suspended within suspension 'buffer P1' [50mM Tris·Cl, 10mM EDTA and 100µg/ml RNase A (pH 8.0)] and then lysed by adding 10mL of lysis buffer P2 [200 mM NaOH, 1% SDS (w/v)], gently inverting (so as not to shear genomic DNA) the tube to mix and it was then incubated for 5 minutes. The lysis reaction was stopped by addition of 10mL neutralisation 'buffer P3' [3.0M potassium acetate (pH 5.5)] and the solution was chilled on ice for 15 minutes. Next, samples were added to QIAfilter Maxi Cartridges which enable filtration and lysate was cleared. Using a QIAGEN-tip 100 which had been 'primed' with 10mL of equilibration 'buffer QBT' [750mM NaCl, 50mM MOPS, 15% isopropanol (v/v), 0.15% Triton X-100 (v/v) (pH 7.0)], the remaining supernatant was added and passed through the membrane via gravity flow. The QIAGEN-tip was then washed twice with 10mL of 'buffer QC' [1.0M NaCl, 50mM MOPS, 15% isopropanol (v/v), (pH 7.0)] to remove all contaminants. Finally, the DNA was eluted with 5mL of 'buffer QF' [1.25M NaCl, 50mM Tris-Cl and 15% isopropanol (v/v) (pH

8.5)] and was precipitated by adding 3.5mL of isopropanol and subjected to centrifugation at ≥15,000 x g for 30 minutes at 4°C. Once the supernatant was removed, the remaining pellet was washed with 2mL ethanol (70%) to remove precipitated salt and centrifugation performed at ≥15,000 x g for 10 minutes. Again, removing the supernatant, the pellet was air dried and re-dissolved in 1mL of nuclease-free water. Plasmid DNA was quantified by measuring the absorbance of 1:00 dilution at 260nm and 280nm using a spectrophotometer. Ratios of A_{260}/A_{280} between 1.7 and 2.0 were considered pure and plasmid preps were then stored at –20°C or below for future use

2.4.5 Polymerase Chain Reaction (PCR)

To amplify specific sections of DNA or to introduce terminal sequences, PCR was routinely performed within PCR Eppendorfs in a total reaction volume of 50µl;

- 20ng of DNA template (e.g. genomic DNA)
- 0.8mM dNTPs (0.2 mM each deoxyadenosine triphosphate (dATP), deoxycytidine triphosphate (dCTP), deoxyguanosine triphosphate (dGTP) and deoxythymidine triphosphate (dTTP))
- 25pmole/µL of forward oligonucleotide primers
- 25pmole/µL of reverse oligonucleotide primers
- 1x PFU buffer (20mM Tris-HCl, pH 8.2, 10mM potassium chloride (KCl), 6mM ammonium sulfate $((NH_4)_2SO_4)$, 2mM $MgCl_2$, 0.1 % Triton X-100, 10mg/mL BSA)
- 2.5U PFU enzyme

Reaction mixtures underwent specific thermic cycle reactions designed to break down hydrogen bonds to create single-stranded DNA by heating, then allowing the primers to anneal at a cooler temperature. The reaction was re-heated to promote elongation of the DNA strands. This reaction underwent many repetitions to create an abundance of DNA copies. Finally, these were cooled to allow for the hydrogen bonds to reform, once again

creating stable, double-stranded DNA. The following protocol was carried out on an

Eppendorf Gradient Thermocycler PCR machine:

1. Preheating 95°C - 5 minutes

2. Denaturation 95°C - 1 minute

3. Annealing 50-60°C [depending on primer melting temperature (Tm)] - 1 minute

4. Extension 72°C - 3 minutes

5. Repeat step 2-4 (X 29)

6. Final extension 72°C - 10 minutes

7. Hold at 4°C

2.4.6 Protein purification

Following PCR reactions, samples were then purified using a QiaQuick PCR purification

kit (QIAGEN, West Sussex, UK) according to the manufacturer's instructions. DNA was

eluted from the purification column using 30-50µL of sterile H_2O.

2.4.7 Agarose gel electrophoresis

To isolate specifically amplified PCR products from DNA templates, gel electrophoresis

was used. The samples were diluted in a DNA loading buffer (x5) and were loaded onto a

1% (w/v) agarose gel with 1X TAE buffer and 1% (w/v) SYBR Safe gel stain (Life

Scientific). Once gels were set within moulds, they were immersed in 1X TAE buffer and

the samples were subjected to electrophoresis at a 75 milliamp voltage alongside a

molecular weight marker (Rainbow™, Sigma-Aldrich). The appropriately sized fragments

were then visualised using ultraviolet light and excised for purification. DNA fragments

were then purified using QiaQuick gel extraction kit (QIAGEN, West Sussex, UK),

according to the manufacturer's instructions and were eluted into 30µL sterile H_2O.

2.4.8 DNA restriction endonuclease digest

To clone newly generated DNA fragments into existing vectors, restriction endonuclease digestion was performed to create 'sticky' ends for ligation into pcDNA3.1. Samples were prepared in 50µL volumes using 16-40U of the appropriate enzyme, 5µL buffer for each restriction site, 5µg of DNA or vector and sterile H_2O to 50µL.

Rat and Mouse FLAG-GPR35eYFP:

pcDNA3.1 - *Bam*HI – FLAG-GPR35 – *Not*I – eYFP – *Xho*I– pcDNA3.1

Human GPR35 FLAG-GPR35eYFP:

pcDNA3.1 – *Hin*DI – FLAG-GPR35 – *Not*I – eYFP – *Xho*I– pcDNA3.1

2.4.9 DNA ligation

Following digestion of DNA fragments and vectors, ligation reactions were performed using T4 DNA ligase. A ratio of 1:4 and 1:6 (vector: DNA) was incubated with 1U T4 ligase and 1µL ligase buffer (X10) to make a final volume of 10µL in H_2O and these were incubated at 4 °C for 16 hours.

2.4.10 DNA sequencing

DNA sequencing was performed by DNA Sequencing & Services (MRCPPU, College of Life Sciences, University of Dundee, Scotland, www.dnaseq.co.uk) using Applied Biosystems Big-Dye Ver 3.1 chemistry on an Applied Biosystems model 3730 automated capillary DNA sequencer. The resulting sequences were aligned with published DNA nucleotide sequences using online Multiple Sequence Alignment software 'ClustalW2'.

2.5 Generation of the mouse FLAG-GPR35-eYFP construct

To compare the pharmacology of ligands at mouse orthologues of GPR35 using bioluminescence resonance energy transfer (BRET) analysis, a mouse FLAG-GPR35-eYFP construct was generated. PCR primers were designed to incorporate an N-terminal epitope FLAG tag and a stop codon was removed at the C-terminal tail to allow for eYFP expression within the vector.

FLAG-Mouse forward primer with *Bam*HI:

5'TTTT<u>GGATCCG</u>CCACCATGGATTACAAGGATGACGACGATAAGATGAATAGTACAACCTGTAACAGCACC-3'

FLAG-Mouse reverse primer with *Not*I:

5' TTTT<u>GCGGCC</u>GCGGTGAGGCTCAGGATCTGG-3'

These were applied using a standard PCR protocol (described in section 2.5.5) using a mouse genomic DNA template. Following purification, PCR products were ligated into a pcDNA3.1 expression vector containing eYFP with *Bam*HI and *Not*I restriction endonuclease sites which are underlined in the primer sequences. These products were sequenced to identify the correct mouse FLAG-GPR35eYFP construct sequence.

2.6 Site-directed mutagenesis:

To identify the crucial residues involved in receptor interaction with ligands, site-directed mutagenesis was performed, whereby one nucleotide within either the fourth or seventh transmembrane domain (TMD) regions was swapped for an alternative nucleotide in the human and rat FLAG-GPR35eYFP constructs. To introduce these single-point mutations, the Quickchange™ Method (Strategene) was used and primers were designed according to the manufacturer's instructions:

Human GPR35 R$^{4.60}$A Forward:

5' – GGCTCCCTGGTGGCT<u>GCC</u>TGGCTCCTGGGGATTC – 3'

Human GPR35 R$^{4.60}$A Reverse:

5' – GAATCCCCAGGAGCCA<u>GGC</u>AGCCACCAGGGAGCC – 3'

Human GPR35 R$^{4.60}$M Forward:

5' – GGCTCCCTGGTGGCT<u>ATG</u>TGGCTCCTGGGGATTC – 3'

Human GPR35 R$^{4.60}$M Reverse:

5' – GAATCCCCAGGAGCCA<u>CAT</u>AGCCACCAGGGAGCC – 3'

Human GPR35 R$^{6.58}$Q Forward:

5' – GTGGGGCTGACAGTGC<u>AAC</u>TCGCAGTGGGCTGG – 3'

Human GPR35 R$^{6.58}$Q Reverse:

5' – CCAGCCCACTGCGAG<u>TTG</u>CACTGTCAGCCCCAC – 3'

Human GPR35 R$^{6.58}$A Forward:

5' – GTGGGGCTGACAGTGG<u>CCC</u>TCGCAGTGGGCTGG – 3'

Human GPR35 R$^{6.58}$A Reverse:

5' – CCAGCCCACTGCGAG<u>GGC</u>CACTGTCAGCCCCAC – 3'

Rat GPR35 R$^{4.60}$A Forward:

5' – CACCTCCCTGGTACT<u>GGC</u>CTGGCGCCTGGGGATAC – 3'

Rat GPR35 R$^{4.60}$A Reverse:

5' – GTATCCCCAGGCGCCAG<u>GCC</u>AGTACCAGGGAGGTG – 3'

Rat GPR35 R$^{4.60}$M Forward:

5' – CACCTCCCTGGTACT<u>GAT</u>CTGGCGCCTGGGGATAC – 3'

Rat GPR35 R$^{4.60}$M Reverse:

5' – GTATCCCCAGGCGCCAC<u>ATC</u>AGTACCAGGGAGGTG – 3'

Rat GPR35 Q$^{6.58}$R Forward:

5' – GATCCTGACAGTGAG<u>GGT</u>CTCCCTGAACC- 3'

Rat GPR35 Q$^{6.58}$R Reverse:

5' – GGTTCAGGGAGACCCTCACTGTCAGGATC – 3'

To introduce site-specific mutagenesis, PCR was performed within PCR Eppendorfs in a total reaction volume of 50µL using the primers outlined above:

- 5µL of 10× reaction buffer

- 5–50ng of dsDNA template

- 125ng of oligonucleotide forward primer

- 125ng of oligonucleotide reverse primer

- 0.2mM of each dNTP

- 1µL of PfuTurbo DNA polymerase (2.5 U/µL)

The following protocol was then carried out on an Eppendorf Gradient Thermocycler PCR machine:

1. 95°C for 30 secs (repeat step 1-2 X30)

2. 50°C for 1 min

3. 68°C for 7 min

To digest the parental methylated dsDNA, the PCR reaction was then incubated with 1µL of *Dpn*I restriction enzyme for 60 minutes at 37°C. PCR products were then transformed, 3 colonies were cultured, DNA extracted and then sequenced to identify the appropriate receptor mutations underlined above.

2.7 Generation of Flp-In™ T-REx™ HEK293 inducible mouse FLAG-GPR35-eYFP cell line

Flp-In™ T-REx™ HEK293 cells were co-transfected with 0.8µg of the mouse FLAG-GPR35eYFP construct within a pcDNA5/FRT/TO vector and 7.2µg pOG44 vector using

Lipofectamine (*see section 2.9.3*). After 48 hours, Opti-mem™ medium (GIBCO® Fisher

Scientific) was changed to Flp-In™ T-REx™ HEK293 media with 200µg/mL hygromycin-B

to select cells harbouring the construct. Cells which had not incorporated the receptor did

not have resistance to hygromycin-B and died. To prevent cell-death related cytotoxicity,

the medium was changed regularly. After 2-weeks, established colonies were evident and

these were gently passaged using Trypsin-EDTA and sub-cultured to new T25cm^2 culture

flasks to grow in replenished medium without hygromycin-B. When the cell line was

established and growing optimally, a titration of doxycycline was performed to determine

the optimal concentration of doxycycline required to initiate uniform receptor expression

by examining eYFP expression across cells (Figure 2-1.)

Doxycycline Titration (ng/ml)
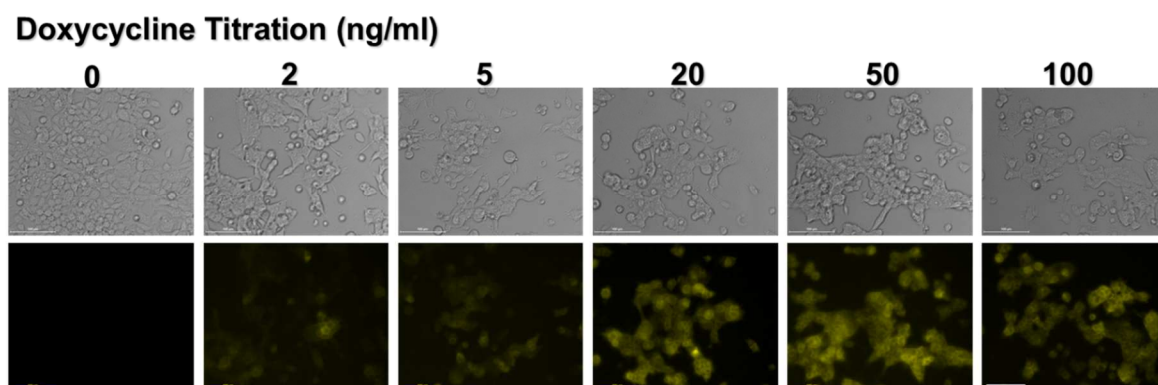
Figure 2-1. Doxycycline titration of the mouse FLAG-GPR35-eYFP cell line.

Flp-In™ T-REx™ HEK293 cells were plated on clear, 6-well plates and grown until 80% confluent. To stably express mouse FLAG-GPR35eYFP, increasing concentrations of doxycycline (0-100ng/mL) were added to fresh media and 24 hours later, these were imaged for eYFP expression using an epifluorescence microscope. Magnification = X10, scale bar = 100µm.

2.8 Culture of cell lines

All cell lines were cultured within sterile, laminar flow hoods and were grown in a humidified incubator (5 % CO_2/ 95% air at 37°C).

2.8.1 Maintenance of HEK293t cells

Human embryonic kidney-293 cells expressing the large T-antigen of SV40 (simian virus 40) (HEK293T cells) were maintained in Dulbecco's modified Eagle's medium (DMEM) (GIBCO® Life Technologies) supplemented with 0.292 g/L L-glutamine and 10% (v/v) foetal calf serum (FCS). Cells were passaged every 2-3 days using 0.25 % Trypsin-EDTA when they reached 80% confluence.

2.8.2 Maintenance of Flp-In™ T-REx™ HEK293 cells

Flp-In TREx HEK293 cells were maintained in DMEM without sodium pyruvate (GIBCO®
Life Technologies), supplemented with 10% (v/v) FCS, 1IU penicillin, 100μg/mL
streptomycin, and 10μg/mL blasticidin. Cells were passaged every 2-3 days using 0.25 %
Trypsin-EDTA when they reached 80% confluence.

2.8.3 Maintenance of H9c2 cardiomyocytes

H9c2 cardiomyocytes were maintained in DMEM (GIBCO® Life Technologies)
supplemented with 10% (v/v) FCS, 2mM L-glutamine and 1IU penicillin, 100μg/mL
streptomycin (Life Technologies, Paisley, UK). H9c2 Cells were passaged every 1-2 days
using 0.25 % Trypsin-EDTA when they reached 50% confluence.

2.9 Cell transfection

2.9.1 Polyethylenimine (PEI)

For BRET analysis, HEK293T cells were transfected with the *Renilla*-luciferase (Rluc)
tagged β-arrestin-2 and either human, rat or mouse GPR35eYFP-tagged constructs in
$10cm^2$ dishes. The DNA ratio of Rluc:eYFP was 1:8. 5μg of DNA was used in a total
transfection and following the addition of 30μg of PEI (ratio 1:6), these were incubated for
10 minutes at RT. The mixture was then added drop-wise to the dishes containing 10mL
of fresh medium and incubated for 16 hours before being used for experiments.

2.9.2 Lipofectamine

For the transfection of constructs for microscopy or the generation of Flp-In™ T-REx™ HEK293 cells, Lipofectamine and Opti-mem™ medium were used. Once cells had reached 60-70 % confluence, 5µg of DNA was diluted in Opti-mem™ to a final volume of 600µL and 20µL of Lipofectamine diluted in 580µL Opti-mem™ was added drop-wise (this could be scaled up or down for the appropriate culture plate or flask). Following a 30 minute incubation at RT, these were added to a $10cm^2$ dish with 5mL of fresh Opti-mem™ and these were incubated at 37°C. After 4-8 hours, the transfection mixture was removed and replaced with the appropriate growth media and the cells were used for experiments within 24-48 hours.

2.9.3 X-fect™

To transfect H9c2 cardiomyocytes with rat GPR35eYFP, we used the X-fect™ transfection protocol. The cells were seeded on sterile poly-D-lysine coated 6mm glass coverslips within 6-well clear plates at a density of $3x10^4$ cells/well. 0.3µL of X-fect polymer was used per 1µg of plasmid DNA and for 6-well plates, 4µg of DNA was added to each well plus 1.2µL of X-fect polymer and the total volume was made up to 100µL with X-fect reaction buffer. Following a 10-minute incubation at RT, this mixture was gently added drop-wise to the cells. Cells were incubated for 4-6 hours at 37°C, after which time the media was replenished and the experiment was carried out 12-24 hours later.

2.10 The chemical structures and properties of key GPR35 ligands

The species-selective properties displayed by various GPR35 ligands has provided challenges for pharmacological assessment and despite reports of endogenous activation via KYNA and LPA (Wang *et al.*, 2006a, Oka *et al.*, 2010), literature suggests that it is still considered an orphan GPCR, at least in human (Milligan, 2011). The chemical composition of key reference GPR35 ligands used in this chapter are structurally defined in Figure 2-1**.** These are the agonists zaprinast, cromolyn disodium and pamoic acid, and the antagonists CID-2745687 and ML-145. Importantly, these are representative of several chemical characteristics often typical of GPR35 ligands highlighted across the literature. For instance, cromolyn disodium and pamoic acid hold a formal negative charge via their carboxylic moiety and zaprinast possesses an acid bioisostere, in line with the majority of identified GPR35 ligands (Jenkins *et al.*, 2010, Mackenzie *et al.*, 2011, Mackenzie *et al.*, 2014). Another feature of high potency ligands at human GPR35 is the characteristic di-acid, mirror image structure common to both cromolyn disodium and pamoic acid (inverted mirror image, in the case of pamoic acid) (Mackenzie *et al.*, 2014). Furthermore, aside from cromolyn, which displays species neutrality - zaprinast and pamoic acid display differential species-selective properties. For zaprinast, a >50-fold difference in potency favours rat GPR35 over human; and pamoic acid is an example of extreme ligand selectivity in that it displays virtually no activity at rat, whilst reported potencies for human GPR35 are within the nanomolar range (Jenkins *et al.*, 2010). In this respect, these are exemplar GPR35 ligands. Interestingly, the GPR35 antagonists CID-2745687 and ML-145 also display extreme human-GPR35 selectivity and research suggests these share overlapping binding positions with zaprinast and cromolyn disodium (Jenkins *et al.*, 2012).
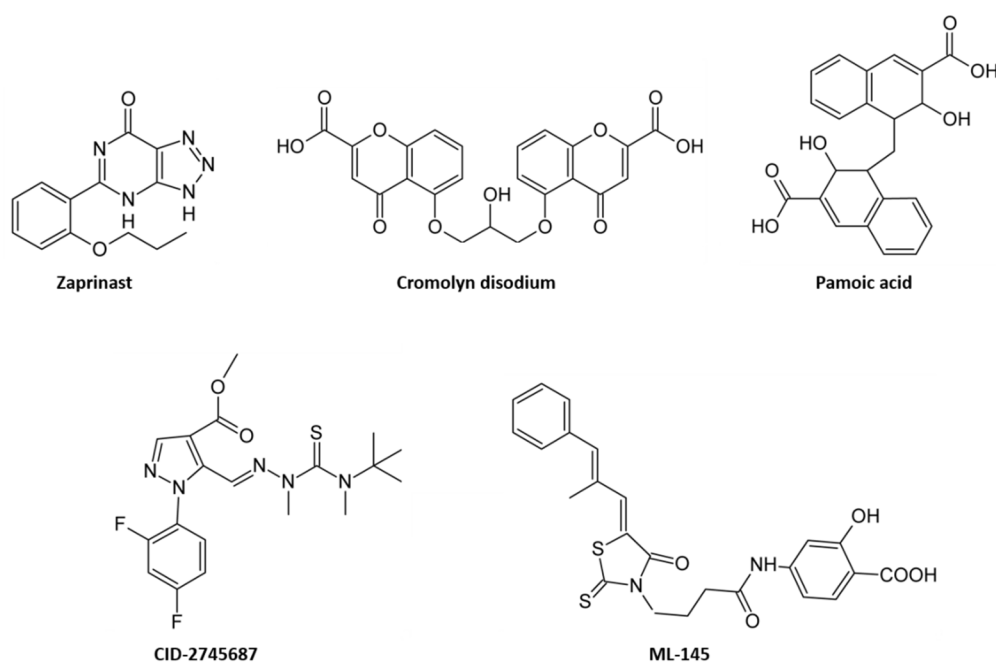
Figure 2-2. The chemical structures of key GPR35 ligands.

The structural properties of GPR35 agonists; zaprinast, cromolyn disodium and pamoic acid and human selective GPR35 antagonists CID-2745687 and ML-145 (adapted from Jenkins et al., 2012).

2.11 Bioluminescence Resonance Energy Transfer (BRET)

HEK293T cells were transfected with human, rat or mouse FLAG-GPR35-eYFP and β-arrestin-2-*Renilla* luciferase (ratio 4:1), using the PEI transfection method (*described in section 1.9.1*). After 24 hours, the cells were plated in triplicate onto a poly-D-lysine-coated white 96-well plates at a density of $1x10^6$cells/well and were further incubated for up to 16 hours at 37°C. One triplicate condition of 'mock' pcDNA3.1 + β-arrestin-2-*Renilla* luciferase was used as a control. One hour before BRET analysis, the cells were washed twice with HBSS (37°C) and incubated in the remaining volume of 70-80µL per well. While the cells recovered, serial drug dilutions were made in HBSS at 10X concentrations and each was equalised for DMSO content. Prior to the beginning of the experiment,

eYFP expression was measured across all wells using a PHERAstar FS reader (BMG-Labtech, Offenburg, Germany). First, 10µL of coelentrazine-h (Promega), the substrate for *Renilla*-luciferase, was added to each well to give a final concentration of 5µM and cells were incubated in darkness for 10 minutes at 37°C prior to the addition of an agonist. Alternatively, if antagonists were being examined, these were added 10 minutes prior to the addition of coelentrazine-h. Cells were incubated for a further 5 minutes at 37°C before BRET measurements were performed using a PHERAstar FS reader (BMG-Labtech, Offenburg, Germany). The BRET ratio was calculated as wavelength emission at 530/485 nm for eYFP and Rluc expression, respectively, and the values were normalised to Rluc only control. These 'BRET units' were then expressed as a percentage of the maximal signal of zaprinast.

2.12 Quantitative receptor internalisation

To quantify receptor internalisation following agonist and antagonist exposure, we employed an 'ArrayScan' High Content Analysis method. Flp-In T-Rex 293 cells containing either human FLAG-GPR35-eYFP or mouse FLAG-GPR35-eYFP were seeded into poly-D-lysine-coated, clear-bottomed 96-well plates at a density of $6x10^4$ cells per well. 24 hours later, these were treated with 100 ng/mL doxycycline to induce receptor expression. Up to 24 hours later, the cells were washed twice in HBSS, leaving a remaining 50µL of HBSS per well and were incubated with 50µL of 2X concentrated ligands for 1 hour at 37°C. Cells were then incubated for another 30 minutes with ligands and 10µg/mL Hoechst nuclear stain at 37°C. Images were acquired immediately by using a Cellomics ArrayScan II high content imager (Thermo Fisher Scientific, Waltham, MA), and internalised receptors were quantified by using a proprietary algorithm designed to identify the number of endosomal recycling compartments per cell. Internalisation was

normalised to the number of nuclei present and these were expressed as a percentage of unstimulated, basal receptor internalisation.

2.13 Inositol Phosphate-1 (IP1) accumulation

To examine the coupling profile of human GPR35 following pamoic acid stimulation, HEK293T cells were transiently co-transfected with the human FLAG-GPR35-eYFP and chimeric G proteins $G\alpha_{q/12}$, $G\alpha_{q/13}$, $G\alpha_{q/i}$ or full $G\alpha_q$ in $10cm^2$ dishes using PEI (*see section 2.9.1*) and IP1 accumulation was quantified using a HTRF IP-One Tb kit (Cisbio Bioassays, MA, USA). Following a 16-hour incubation at 37°C after transient transfection, the cells were removed from the dishes using trypsin-EDTA in cell dissociation buffer subjected to centrifugation at 5000 *g* for 5 minutes, were re-suspended in IP-One stimulation buffer (10 mM HEPES, 1mM $CaCl_2$, 0.5mM $MgCl_2$, 4.2mM KCl, 146mM NaCl, 5.5mM glucose, and 50mM lithium chloride (LiCl), pH 7.4). Samples were added to white, round-well, 384-well plates at a density of $1x10^4$ cells/well within 7µL of stimulation buffer. Serial dilutions of pamoic acid were made at X2 concentration in stimulation buffer according to the manufacturer's instructions. The cells were then exposed to 7µL of pamoic acid (10nM-100µM, final concentration) for 2 h at 37°C. Following this, d^2-conjugated inositol monophosphate (IP1) was exogenously added alongside an anti-IP1 Lumi4-Tb cryptate, diluted in lysis buffer. The high-throughput format of the IP1 accumulation assay employs the use of a Lumi-4® IP1 antibody and this competitively binds to increasing concentrations of endogenously produced IP1 rather than dye d^2-tagged IP1, which has been added exogenously. Following ligand administration, GPCR activation and subsequent IP1 accumulation produces an inverse signal. Following a further incubation for 1 hour at RT, homogeneous time-resolved fluorescence was measured using a PHERAstar FS plate reader at wavelengths of 665nm and 620nm to create a ratio which was multiplied by 1000 to produce IP1 signal units.

2.14 Quantification of Rho A activation in HSV SMCs

2.14.1 GTP-Rho A pull down-assay

To investigate if pamoic acid stimulation of endogenously GPR35 expressing HSV SMCs resulted in the activation of Rho A following coupling to $G\alpha_{13}$, we employed a RhoA Activation Assay Kit (CellBiolabs, inc) according to the manufacturer's instructions. To minimalize basal Rho A activation, HSV SMCs were plated at a low density of $5x10^4$ cells/well within 6-well, clear plates. Prior to the experiment, cells were quiesced for 48-hours and serial dilutions of pamoic acid in serum free media were incubated with the cells at 37°C for 5 minutes. Positive and negative controls for Rho A activation were 5% serum and 0% serum, respectively. Following stimulation, the cells were placed on ice to inhibit physiological processes and were washed twice with ice-cold PBS. 500μL of ice-cold 1XRIPA buffer was used to lyse the cells and these were placed in a rocking incubator at 4°C for 15-minutes. The cells were then collected using a cell scraper and the cell lysates were subjected to centrifugation at 14,000 x g at 4°C. The supernatant was removed and adjusted to 1mL with 1XRIPA buffer. Before addition of the agarose beads, 200μL of sample was snap frozen and stored at -70°C for later analysis of total Rho A protein. Next, 30μL of Rhotekin RBD Agarose bead slurry was then added to each sample and these were incubated at 4°C for 1 hour on a rotating wheel. The beads were pelleted by centrifugation at 14,000 x g for 10 seconds and then were washed three times in 500μL of 1XRIPA buffer. The beads were then re-suspended in 2X Laemmli buffer (containing 5% β-mercaptoethanol) and boiled for 5 minutes using a temperature controlled heating block. Finally, the beads were pelleted by centrifugation at 14,000 x g for 10 seconds and the supernatant was transferred into fresh Eppendorf tubes for electrophoresis.

2.14.2 Electrophoresis and protein transfer

Samples were loaded onto a precast 12-well NuPage Novex Bis-Tris gel (12 %

acrylamide) and were electrophoresed alongside a molecular weight marker (Rainbow™)

within a XCell Surelock mini-cell gel tank at 160-200V in NuPage MOPS 20X running

buffer (diluted to 1 X with H_2O). Once samples reached approximately 90% of the gel

length, the transfer was stopped and gels were placed in a transfer cassette with

nitrocellulose membranes, sandwiched between layers of sponge and Whatman paper.

Protein was transferred for 1 hour at 35V, submerged in 1 X transfer buffer (14.4g glycine,

3g Tris, 800mL H_2O and 200mL methanol (MeOH)).

2.14.3 Immunoblotting

To visualise active and total Rho A protein, nitrocellulose membranes were washed with

1X TBST (*see section 2.3*) and then incubated in blocking buffer (5% milk in TBST) for 1

hour at RT with gentle agitation. The primary Rho A antibody was diluted 1:500 in 3%

blocking buffer and incubated for 16-hours at 4°C with gentle agitation. The membranes

were then washed three times with TBST for 5 minutes and a secondary α-rabbit-

hydrogen peroxide (HRP) conjugated antibody was diluted 1:1000 in 5% blocking buffer

and applied for 1 hour at RT with constant agitation. The membranes were again washed

three times in TBST and chemiluminescence reagents SuperSignal West Pico (Pierce

Biotechnology) were applied at a ratio of 1:1 for 5 minutes for detection of protein and

these were exposed and developed on Kodak film over a time-course of 5-15 minutes.

2.15 Qualitative cell trafficking

2.15.1 Receptor internalisation

Flp-In™ T-REx™ 293 cells harbouring human and rat FLAG-GPR35eYFP were grown on cover slips in 6-well plates coated with poly-D-lysine until they were 70-80% confluent and were induced to stably express human FLAG-GPR35-eYFP by treatment with 25-100ng/mL of doxycycline for 24 hours. For live cell imaging, coverslips were placed in a temperature controlled (37°C) chamber within HBSS. Next, 100µM concentrations of GPR35 agonists zaprinast, pamoic acid and cromolyn disodium diluted in HBSS were gently added to the chamber to give a final concentration of 10µM for each ligand. eYFP was imaged at emission wavelengths of 495nm. Images were acquired at 5 minutes intervals over a 45-minute time-course using a spinning disk structured illumination Viva Tome device (Zeiss, Germany) to observe receptor internalisation in the presence of GPR35 ligands.

2.15.2 p115-RhoGEF trafficking

To visualise the trafficking of p115-RhoGEF from the cytosol to the plasma membrane upon $G\alpha_{12}$ or $G\alpha_{13}$ activation, HEK293T cells were grown on glass coverslips in 6-well plates until they were approximately 70-80% confluent. These were transiently transfected with constitutively active (CAM) or wild-type (WT) versions of $G\alpha_{12}$ or $G\alpha_{13}$ alongside a GFP tagged p115-RhoGEF construct using Lipofectamine (described in section 1.9.3). After 16-24 hours, the cells were washed with PBS and fixed for 5 minutes using 4% paraformaldehyde (PFA) in the presence of 0.001% (v/v) CellMask® Orange plasma membrane stain (Invitrogen, Life Technologies). Cells were then washed five times using PBS and mounted onto glass slides with Immumount™ (Invitrogen, Life Technologies). GFP and CellMask® Orange were captured at emission wavelengths of 495nm and

567nm, respectively, using a spinning disk structured illumination Viva Tome device (Zeiss, Germany).

2.16 Phalloidin staining

To visualise cytoskeletal architecture of cells, a phalloidin stain which binds to F-actin on the actin filament within cells was used. HSV EC, SMC and H9c2 cardiomyocytes were seeded on 30mm coverslips and quiesced for 24 hours (EC) and 48 hours (SMC and H9c2). Following exposure to GPR35 ligands at 37°C, cells were fixed using 4% (w/v) PFA for one hour at RT and for optimal staining, the cells were then permeabilized using PBS with 0.1% Triton X-100 for 20 minutes at RT. Cells were then washed with PBS and stained with TRITC F-actin phalloidin stain at 5µg/mL for 1 hour at RT (Sigma-Aldrich, UK). The unbound F-actin stain was then removed with two PBS washes and the coverslips were mounted onto glass coverslips with Prolong® Gold Antifade reagent with 4',6-diamidino-2-phenylindole (DAPI) (Invitrogen). Cells were then imaged at emission wavelengths of 610nm and 461nm for TRITC and DAPI, respectively, using a spinning disk structured illumination Viva Tome device.

2.17 Hypertrophy assay

H9c2 cardiomyocytes were seeded on sterile, poly-D-lysine coated glass coverslips within 6-well plates at a density of $3x10^4$ cells/ well. Once attached, the cells were quiesced for 48-hours in serum free media. After this, cells were transfected with rat FLAG-GPR35eYFP using X-fect (as described in section 1.9.3) and were stimulated with 200nM of GPR35 ligands zaprinast or amlexanox for 48-hours in triplicate. H9c2 cells were also stimulated with 200nM of AngII or maintained in serum free media to provide a positive and negative control for hypertrophy, respectively. H9c2 cardiomyocytes were then fixed,

stained and imaged for F-actin using the protocol described in section 1.15. Cell size was quantified by measuring the length of at least 100 cells per condition using Image J software.

2.18 Isolation and maintenance of primary vascular cells

Following application for patient consent and ethical approval, we received excess tissue from patients undergoing a coronary artery bypass grafting (CABG) using human saphenous vein (HSV), at the Golden Jubilee Hospital in Clydebank, Scotland. Once the vein tissue was received, a note of the patient number, date and how the vein was used was noted in a log book. Immediately following this, primary endothelial and smooth muscle cells were then isolated from the vein tissue within sterile conditions.

2.18.1 Human saphenous vein endothelial cells (HSV EC) isolation

Firstly, the endothelial cell layer was isolated via collagenase digestion whereby the vessel was bathed in wash media (DMEM, 100 IU/mL penicillin, 100µg/mL streptomycin and 2mM L-glutamine) and then the lumen bathed with 2µg/mL of collagenase solution diluted in wash media. This was incubated within the vessel at 37°C for 15-20 minutes and a fresh collagenase dilution was then subsequently used for another 10 minutes. Following this, the endothelial cells were collected by pelleting the remaining solution by gentle centrifuging at 2000 x g for 15 minutes. The cells were then re-suspended in Large Vessel Endothelial Basal Cell Medium (TCS Cellworks Ltd, Bucks, UK) which was supplemented with 20% (v/v) FCS, 100 IU/mL penicillin, 100µg/mL streptomycin and 2mM L-glutamine and were seeded in T25 culture flasks within a humidified incubator (37°C, 5% CO_2) before the application of fresh medium and future passaging.

2.18.2 Human saphenous vein smooth muscle cells (HSV SMC)

To isolate SMC from the remaining medial layer following collagenase digestion, the vein was cut longitudinally and small sections were pinned out with the lumen-side exposed. Any remaining HSV ECs were removed by gently buffing the vessel with a rubber policeman. Latitudinal scores were then made across the vessel using a scalpel blade and strips of smooth muscle cells were peeled from the adventitia using forceps. These were placed in wash buffer (as above) and then together, all of the isolated strips were cut into small sections using a McIlwain tissue chopper. After washing with wash medium twice, the cells were transferred into Smooth Muscle Cell Growth Medium 2 containing 0.5 ng/mL epidermal growth factor, 2ng/mL basic fibroblast growth factor and 5µg/mL insulin (PromoCell, Heidelberg, Germany) and supplemented with 15% FCS, 100 IU/mL penicillin and 100µg/mL streptomycin. These were transferred into a T25cm^2 cell culture flask to grow and the media was replaced the following day. When HSV SMC became fully confluent, they were passaged 1:5 using trypsin.

2.19 Migration assay

HSV EC and SMCs were seeded in 6-well plates, grown to confluence and then quiesced for 24 or 48 hours for SMC and EC, respectively. Three horizontal scratches were created in each well using a 200µL pipette tip and the cells were gently washed twice with warm PBS to remove cell debris. A straight line was drawn on the bottom of each well on the outside of the plate to act as an area marker whilst imaging migrating cells. Cells were then stimulated with pamoic acid (Sigma-Aldrich) at concentrations of 10nM, 100nM and 300nM or zaprinast at 100nM, 500nM and 1µM in serum free DMEM or were co-administrated with 100nM of either GPR35 antagonist CID-2745687 or ML-145. To assess the involvement of the Rho A signalling axis in pamoic acid induced migration, cells were

also incubated with 10µM Rho A pathway inhibitor Y-16, or ROCK inhibitor Y-27632, alongside 100nM pamoic acid in serum free conditions. All conditions were performed in triplicate and on at least three occasions. Images of the cells were acquired at time zero, followed by incubation at 37ºC and imaged at 12-hour time points for the following 36-hours. Importantly, images were taken at the same area following alignment with the guideline on the plate and therefore, migration was directly comparable across images. Migration was then quantified by measuring the distance (µm) between cells migrating into the wound area at approximately 10 areas within each field of view, using Image J software. These were then averaged and expressed as percentage migration, compared to migration at time point 0.

2.20 Assessment of cell proliferation

HSV EC and SMC were seeded in clear 96-well plates at a density of 5×10^3 cells/well and quiesced in serum free media for 24 and 48 hours, respectively. To optimise the concentration of serum required for a positive proliferative response, each cell type was first exposed to 0-20% serum conditions, and it was found that 5% serum was sufficient to induce maximal cell proliferation for both HSV EC and SMCs. Cells were then stimulated with a range of concentrations of GPR35 ligands +/- 5% serum, over a period of 24 hours (EC) and 48 hours (SMC). Cell proliferation was assessed using either Cell Titer 96 Aqueous NonRadioactive Cell Proliferation Assay (MTS) (Promega, WI, USA) or the 5-bromo-2'-deoxyuridine Cell Proliferation Assay Kit (BrdU), (Cell Signalling Technology, UK), according to manufacturer's instructions. Colorimetric output was measured on a Wallac VICTOR2 plate reader at absorbance values of 490nm or 450nm for MTS and BrdU assays, respectively.

2.21 Gene expression analysis

2.21.1 RNA extraction of cells and tissues

To isolate ribonucleic acid (RNA) cells were harvested from 6-well plates which were washed using PBS and then removed using 700µL of cell lysis reagent, QIAzol® (QIAGEN). The cells were homogenised via pipetting and the lysates were stored in RNase free tubes at -80°C until extraction. To isolate RNA from tissues, samples were immediately snap frozen in liquid nitrogen upon harvest and were homogenised in 700µL of QIAzol® and with the addition of one stainless steel bead (5mm) (QIAGEN), these were processed via vigorous mechanical shaking in a TissueLyser System (QIAGEN) at 25Hz. RNA from both cells and tissue were then extracted using an RNeasy mini kit (QIAGEN) according to the manufacturer's instructions. Briefly, 700µL of 70% (v/v) ethanol was added to each sample and these were applied to an RNeasy spin column which binds the cell lysate, these were cleared via centrifugation at 8,000 g. The samples were washed with 350µL RW1 buffer and to eliminate genomic DNA contamination, were treated with 70µL of DNaseI, diluted in buffer RDD. After a 30 minute incubation period at RT, the samples were washed again with 350µL RW1 buffer and twice with 500µL of RLT buffer before being eluted into a fresh RNase free tube with 30µL of RNase free H_2O. RNA was immediately quantified as outlined in section 2.20.2 and then stored at -80°C for future analysis.

2.21.2 Nucleic acid quantification

To quantify RNA, a NanoDrop 1000 Spectrophotometer (Thermo Scientific) was used. This equipment is able to quantify RNA via measuring its absorbance at 260nm and provides a reading of RNA in ng/µL. Furthermore, a ratio of absorbance at 260/280nm indicated the quality of RNA and this was considered 'pure' if the reading was close to 2.0.

2.21.3 Reverse Transcription (RT)

To reverse transcribe the RNA into complementary DNA (cDNA), a Taqman® Reverse Transcription Kit (Applied Biosystems) was used according to the manufacturer's instructions. Briefly, 750ng of RNA was added to a reaction mixture containing 1X reverse transcriptase buffer, 5.5mM $MgCl_2$, 0.5mM each of dATP, dCTP, dGTP and dTTP, 2.5µM random hexamers, 0.4 U/µL RNase inhibitor, 1.25 U/µL Multiscribe™ and RNase free H_2O was added to each sample mixture for a final volume of 50µL. These were then added to PCR reaction plates and thin, thermogenic film (Thermo Scientific) sealed the plate. The following protocol was then performed to transcribe cDNA from RNA:

- 25ºC for 10 minutes (primer annealment)

- 48ºC for 30 minutes (reverse transcription)

- 95ºC for 5 minutes (inactivation of transcriptase)

- Hold at 4ºC

The samples were then stored at 4ºC for use within 24-hours or at -20ºC for longer-term storage.

2.21.4 Quantitative real-time polymerase chain reaction (qRT-PCR)

mRNA expression of GPR35, $G\alpha_{13}$, collagen I and III in cells and tissues, was quantified via real-time PCR using TaqMan chemistries (Applied Biosystems, Warrington, UK). Each of the selected TaqMan assays have a fluorescent reporter dye incorporated within the 5' to 3' primer and this 'quenched' by an incorporated inhibitor within the 3' to 5' primer. In the presence of the Taq™ polymerase enzyme, the inhibitor is cleaved following primer annealling and a fluorescent signal is produced. Importantly, this fluorescence signal is measured during the exponential phase of each PCR cycle and upon the application of a set cycle threshold (CT), mRNA expression level is quantified. All gene expression

analysis was subject to the quantification of a ubiquitously and endogenously expressed 'housekeeping' gene, such as ribosomal 18s or β-actin. The CT value for each gene was normalised for the appropriate housekeeper and the data were expressed as ΔCT values, or as fold-expression relative to a control condition (ΔΔCT). For a 10μL total reaction volume, a master mix containing 0.5μL of Taqman probe and H_2O was added to 3μL of cDNA for GPCR expression or 0.5μL of cDNA for either housekeeping gene. All conditions were carried out in biological triplicates with technical replicates. These were then analysed on an Applied Biosystems ABI Prism 7000 sequence detection system operated according to manufacturer's instructions:

- 95ºC for 10 min X40 cycles (to denature)

- 95ºC for 15 sec (primer annealing)

- 60ºC for 1 minute (primer extension)

2.22 *In vivo* techniques and tissue analysis

2.22.1 Experimental plan for *in vivo* assessment of GPR35 activation in the SHRSP

10 Male SHRSPs were chosen as a model for a 6-week amlexanox dosing study. At 5-6 weeks of age, age-matched animals were randomly assigned; vehicle control (n=5) or 2.5mg/kg/day amlexanox (n=5). To measure blood pressure in young SHRSPs they underwent tail cuff plethysmography at age 5-6 weeks until 8-9 weeks of age, three times per week. Daily dosage of either amlexanox or vehicle control began at 6 weeks of age for the duration of the study. To prevent stress induced increases in blood pressure associated with oral gavage techniques, amlexanox was administered to rats in 1 mL of sweetened, blended food. At age 8 weeks, SHRSPs underwent wireless radiotelemetry probe implantation, for which the gel-tipped probe was inserted into the abdominal aorta

and sewn into the abdominal muscle wall to prevent movement. Haemodynamic parameters encompassing systolic, diastolic and mean arterial pressure were captured at 5 minutes intervals for the duration of the study. Radiotelemetry also measured locomotion activity and heart rate. At age 12-13 weeks, all animals were sacrificed and tissues were harvested for the analysis of fat deposition, vascular reactivity in isolated vessels, cardiac hypertrophy, renal fibrosis and gene expression. NB: one probe became dislodged 2-weeks following implantation and although this was not fatal for the animal, subsequent analysis of haemodynamic parameters was limited to n=4 animals per group. Please refer to Figure 2-3 below, for a schematic overview of the experimental plan.
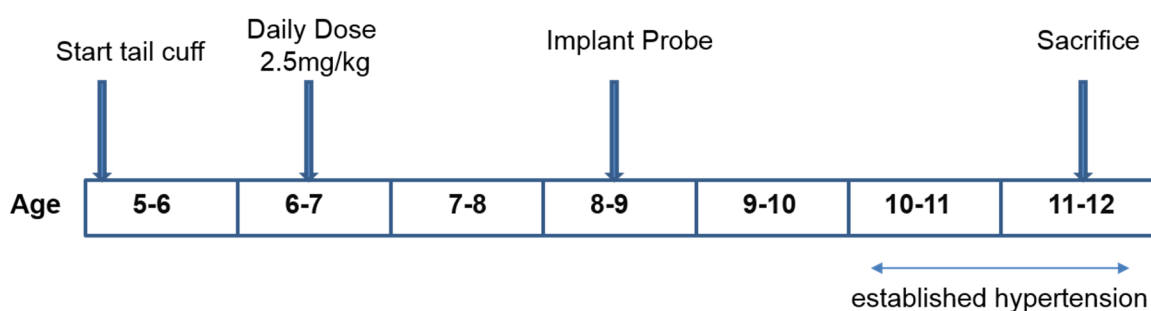
Figure 2-3. Schematic time-line, outlining the experimental plan for *in vivo* assessment of GPR35 activation in the SHRSP.

2.22.2 Experimental animals

10 male, 6-week old stroke-prone spontaneously hypertensive rats (SHRSP) were used to examine the effect of pharmacological agonism of GPR35 in this study. All of the experimental analysis of animals was subject to the Animal Scientific Procedure Act (1986) and was carried out under the project licence of Dr. Delyth Graham (60/4286). The animals were housed within the animal unit which had controlled lighting (12h-light/ 12-dark, 7am-7pm/ 7pm-7am) and temperature (21.5°C). One animal per cage was required

in this study due to the nature of drug administration. Rats were fed a standard chow diet and were able to eat and drink *ad-libitum*.

2.22.3 Drug administration

2.5mg/kg of amlexanox powder was mixed into 1mL of banana custard flavoured baby food (HEINZ). This was prepared once per week, based on animal weight and was stored at -20°C in small petri dishes before being administered daily for the trial duration. There were 5 animals per group and the group which were not administered the amlexanox were given 1mL of banana custard flavoured baby food (HEINZ) as a 'vehicle control'.

2.22.4 Tail-cuff plethysmography

To measure systolic blood pressure (SBP) in young SHRSPs (6-8 weeks), tail-cuff plethysmography was carried out every 2-3-days for the first twenty-days of the study. The animals were warmed-up in an insulated environment to improve blood-flow to the tail, they were then placed on heated mat (30°C) and gently wrapped in a towel to prevent movement or distress. Once the animal was composed, an inflatable cuff with a built in piezoceramic transducer (Hartmann &Braun) was placed on the base of the tail and to obtain a stable reading of SBP, the tail-cuff was inflated approximately 10 times per session and the pressure measurement was taken on deflation of the cuff. Following this, outlying readings were rejected and an average of the remaining readings created a single measurement of blood pressure.

2.22.5 Radiotelemetry

The SHRSPs underwent surgery to implant a wireless telemetry probe within the abdominal aorta at age 8-9 weeks under surgically sterile conditions. Following the removal of abdominal fur, the surgery was carried out under anaesthetic (2.5% Isoflurane and 1.5L/min O_2) and it was ensured that the animals were unconscious via the tail pinch method. Upon abdominal incision, the large intestinal organs were gently positioned out with the body and were kept moist using sterile, PBS soaked gauze. Using the pressure of surgical thread to prevent blood flow, a small hole was made above the lower abdominal aortic branch using a needle and the telemetry probe was gently advanced into the aorta (towards the heart). This probe was previously calibrated, re-furbished and re-gelled and was held in place using a small patch of sterile gauze and surgical glue. The probe transmitter (radio frequency transducer model TA11PA) was sutured into the abdominal muscle wall to prevent any movement. Immediately following the surgery, an analgesic (Carprofen 5mg/kg) was administered and the animals recovered in a sterile, warm environment under supervision. Following a 7-day recovery period, SBP, diastolic blood pressure (DBP), mean arterial blood pressure (MAP), heart rate (HF) and locomotion was received on a consolidation matrix 4650 receiver panel using the Dataquest IV Telemetry System (Data Sciences International). These measurements were recorded and stored every 5 minutes for the duration of the study and the results were averaged for 12-hour light and dark cycles using a previously devised macro spreadsheet (Microsoft Excel).

2.22.6 Tissue harvesting

The animals were sacrificed at age 12-13 weeks under anaesthetic (4.0% Isoflurane and 1.5L/min O_2). To sacrifice, the heart was punctured and approximately 2mL of blood was collected using a 5mL syringe. Following sacrifice, the heart and kidneys were immediately weighed and the heart was dissected to weigh the left ventricle plus septal

tissue (LV+S). Tissue from the heart, kidney and spleen were either snap frozen in liquid nitrogen for future gene expression analysis or fixed in 10% (v/v) neutral buffered formalin for paraffin embedding. The epidydymal and retroperitoneal fat pads were also excised and weighed. The thoracic aorta and large intestine (containing the mesenteric arteries) were placed in Krebs solution for large and small vessel myography.

2.22.7 Tissue mass index

Using a double-pointed drawing compass, the tibia length was measured from the knee to the ankle joint, which was exposed following scalpel incision to each area. This was then measured in millimetres using a standard 30cm ruler. This provided the opportunity to create an additional organ mass index whereby whole heart, LV+S and kidney mass were normalised tibia length or body weight.

2.22.8 Resin embedding and sectioning

Heart and kidney tissue previously fixed in formalin were placed in 0.5mL embedding cassettes and were processed in a Citadel 1000 (Thermo Scientific, UK) whereby they were exposed to a gradual water-histoclear gradient to dehydrate the tissue. These were then embedded in paraffin wax and left to solidify on a cooling block before storage at -20°C prior to sectioning. 5µm sections of LV and kidney tissue were then cut using a microtome (Leica RM2125, Leica Microsystems, UK).

2.22.9 Histology

Prior to tissue staining, the heart and kidney sections were mounted onto glass slides and were baked overnight at 40°C for 12-16 hours. To remove paraffin, the slides were immersed twice in histoclear for 7 minutes. The tissue sections were then re-hydrated using a gradual ethanol gradient [100, 95 and 75% (v/v)] for 7 minutes each and then were finally immersed in distilled H_2O for 7 minutes.

2.22.9.1   Collagen staining

To identify the presence of fibrosis within cross-sectional kidney tissue sections, picrosirius red staining, specific to collagen I and III, was used. The slides were immersed in 0.1% (v/v) picrosirius red solution (300mg sirius red F3B, 300mL saturated picric acid) in darkness for 90 minutes at RT. To wash, these slides were then twice immersed in 0.01M HCl for 5 minutes and twice in dH_2O for 5 minutes. The sections were then dehydrated using a reverse ethanol gradient (75-100%) and protective glass coverslips were mounted using DPX non-aqueous mounting medium (Merck Millipore, Germany). Collagen (red-staining) was blindly quantified by measuring pixel density in 4 areas of interest per slide (three slides per animal tissue) using ImageProPlus software.

2.22.9.2   Wheat-germ agglutinin (WGA)

Cardiomyocytes situated within the LV wall were stained using WGA-TRITC conjugate which binds N-acetylglucosamine and sialic acid residues to identify cell membranes. The tissue sections were permeablized using HBSS with 0.1% Triton X-100 for 20 minutes at RT and then were immersed in HBSS buffer + 5µg/mL WGA-TRITC for 10 minutes at RT. These were then washed twice with HBSS. The sections were then dehydrated using a

reverse ethanol gradient (75-100%) and protective glass coverslips were mounted using

Prolong® Gold Antifade reagent with DAPI (Invitrogen). These were imaged at an

emission wavelength 610nm and cardiomyocyte size was then quantified by measuring

cell length in 4 areas per slide (three slides per animal) using Image J software.

2.22.10 Wire myography

Third order mesenteric arteries and thoracic aortas were harvested upon animal sacrifice

to examine vasoreactivity in small and large vessels, respectively, using a wire myograph.

Following isolation, these were gently cleaned and excess connective tissue and fat was

removed. These were then stored in Krebs solution (*see section 2.3*) overnight at 4°C

before the experiment was conducted. Sections of mesenteric artery approximately 1.8-

2.0mm in length (n=2 per animal) were mounted onto the structure using two steel wires

and were placed into a four channel small vessel myograph (Danish Myotechnology,

Denmark). Following a 30 minute equilibration period, the tension on each vessel was

normalised for its internal diameter using Laplace's equation, where the tension is directly

proportional to vessel diameter and force applied. Changes in vessel tension were

measured via the myograph transducer and recorded using Data Acquisition Software

(Powerlab Systems). To stimulate contraction and 'wake-up' the vessel, the vessels were

pre-treated with 10mM of KCl in Krebs solution twice, and from the second treatment, the

maximum vessel contraction for potassium was obtained. The vessels were then washed

four times in Krebs solution and were left to normalise and return to basal tension for 45-

60 minutes. To examine the vasoreactive pharmacology of the vessels, they were

exposed to increasing concentrations of noradrenaline (100nM-1mM) and following the

application of the maximal concentration, the vessels were then exposed to increasing

concentrations of carbachol (10-30µM) to assess endothelium-dependent vasorelaxation.

Vessels were washed again four times using Krebs solution and left to normalise to basal

tension. The vessels were again exposed to increasing concentrations of noradrenaline (100nM-1mM), however, this time smooth muscle cell-dependent vasorelaxation was assessed by adding increasing concentrations of sodium nitroprusside (SNP) (100nM-1mM). For large vessel myography, aortic rings (3-5mm) were mounted onto two fixed steel wires within a large vessel myograph (Danish Myotechnology, Denmark) and these were left to equilibrate for 30 minutes following the application of 1.5–3.0grams of tension. Vessels were treated with the same stimulation and relaxation protocols used for mesenteric arteries, however, instead of using noradrenaline to stimulate vessel contraction, phenylephrine was used (10nM-1mM). The resulting contractile responses were plotted as a percentage of the maximal KCl response obtained at the beginning of the experimental protocol.

2.23 Statistical analysis

All data are displayed as mean +/- SEM and were analysed using GraphPad Prism® software. Student's t-test for paired data and one-way ANOVA was applied, with Dunnett's test for multiple comparisons when comparing to a control, or, with Bonferroni's correction to compare all of the conditions. Statistical significance was considered if $p<0.05$. Experiments were performed in triplicate and on at least three independent occasions. To confirm that the data were normally distributed, the Kolmogorov-Smirnov test was utilised (given its ability to account for the distribution within data of an n=5). Although, for higher sample numbers (n≥7), the D'Agostino-Pearson test would be preferable in the assessment of normality in the distribution of data. For WGA and collagen staining quantification, the sample conditions were blinded by a colleague during the quantification process.

3   Translating the pharmacology of GPR35 in multiple species orthologues

3.1 Introduction

The pharmacological characterisation of ligands which act at GPR35 has proved an intriguing and challenging process thus far. As previously described, the majority of molecules which act at GPR35 demonstrate considerable species-selectivity and the possibility of ligand bias following activation has also been discussed (Milligan, 2011). Though research has begun to elucidate a role for GPR35 using functional systems in both an *in vitro* and *in vivo* context, many questions relating to the species-selective properties of ligands remain un-resolved and therefore, targeting GPR35 within an endogenous setting has been problematic. For example, following reports that GPR35 might have therapeutic implications within the central nervous system (Ohshiro *et al.*, 2008), investigators assessed the nociceptive response of mice undergoing an acetic acid-induced abdominal constriction test in the presence of increasing doses of pamoic acid; at that time, a novel GPR35 agonist (Zhao *et al.*, 2010). A reduction in writhing behaviour correlated with increased pamoic acid dosage and led the authors to conclude that GPR35 activation may alter pain tolerance (Zhao *et al.*, 2010). However, these conclusions contrast reports demonstrating that pamoic acid is highly selective for human GPR35, displaying virtual inactivity at the rat orthologue via β-arrestin-2-receptor interaction (Jenkins *et al.*, 2010). Upon consideration of these conflicting indications, it remained unclear if the reported nociceptive response following pamoic acid administration in a mouse model was attributable to GPR35 activation (Zhao *et al.*, 2010). Furthermore, in an attempt to reverse pamoic acid induced nociception, investigators co-administered a newly identified GPR35 antagonist; CID-2745687. However, its previous *in vitro* antagonistic action was not replicated in the animal model (Zhao *et al.*, 2010). Prior to evidence published by Jenkins and colleagues (2012), which involves work presented in this chapter, it was uncertain if, like human-selective agonists, the novel antagonists CID-2745684 and ML-145 also exhibit species-selective properties. Thus far, GPR35 antagonists have demonstrated limited use in functional systems.

To understand the mode of ligand binding to a receptor, investigators often employ site-directed mutagenesis and thus, by introducing single-point mutations to areas of potential ionic interaction, it is possible to identify critical residues for receptor activation. To this end, several key binding residues crucial for ligand interaction have been successfully identified within GPR35 and these include critical residues within the third TMD, for which zaprinast and kynurenic acid share overlapping binding positions (Jenkins *et al.*, 2011). Most recently, residues within the sixth and seventh TMDs have proved critical for interaction with lodoxamide, a novel high-potency GPR35 agonist (Mackenzie *et al.*, 2014). Research has only begun to identify crucial domains within human GPR35 that mediate interaction with pamoic acid. Latterly, the effect of single residue substitutions with differential charges was investigated within TMD regions III – VI of human GPR35 (Zhao *et al.*, 2014). Without emphasis on implication for species selectivity, the authors reported that positively charged residues located within TMD III, IV, V and VI of human GPR35 are crucial for interaction with both pamoic acid and zaprinast, suggesting overlapping binding positions (Zhao *et al.*, 2014). Importantly, substitution of positively charged residues within the second ECL, specifically of arginine[167], reduced the potency of pamoic acid by four-fold in a β-arrestin-receptor interaction assay (Zhao *et al.*, 2014). Essentially, this mutation is the first to produce differential effects on ligand potency and thus, is strongly suggestive of an additional binding site for pamoic acid which may, in part, facilitate its selectivity for human GPR35. Evidently, more research is required to identify crucial differential residues which account for the species-selective properties of pamoic acid.

Another aspect to promote discussion within the field of GPR35 research has been its G-protein coupling profile. Upon identification of its two most prominent and widely utilised ligands; zaprinast (Taniguchi *et al.*, 2006) and kynurenic acid (KYNA) (Wang *et al.*, 2006a), it was reported that GPR35 coupled to the $G\alpha_{i/o}$ family of proteins and, in both cases, this was demonstrated via Ca^{2+} mobilisation following the transfection of $G\alpha_{q/i}$

chimeric constructs (Taniguchi *et al.*, 2006, Wang *et al.*, 2006a). Additional studies have also reported PTX sensitive activation in cells stimulated with KYNA (Barth *et al.*, 2009, Ohshiro *et al.*, 2008) and pamoic acid (Zhao *et al.*, 2010). On the other hand, consistent evidence that GPR35 couples to the $G\alpha_{12/13}$ family of proteins following activation by a range of ligands including zaprinast, pamoic acid and cromolyn disodium, also exists (Jenkins *et al.*, 2011, Jenkins *et al.*, 2012, Mackenzie *et al.*, 2014). Moreover, these authors report that GPR35 displays selectivity for $G\alpha_{13}$ over $G\alpha_{12}$ to elicit an intracellular Ca^{2+} response in the presence of zaprinast (Jenkins *et al.*, 2011). Given the wealth of existing and somewhat conflicting evidence, it remains unclear if multiple pathways are activated following GPR35 activation or if ligand bias promotes differential $G\alpha$ signalling.

3.1.1 Hypothesis and aims

Given that studies from our lab have demonstrated that pamoic acid is not effective at rat GPR35 (Jenkins *et al.*, 2012), it is hypothesised that this might also extend to alternative rodent species, such as mouse. Previous research also links species specificity of GPR35 ligands to differential binding positions within the GPR35 structure (Jenkins *et al.*, 2010), and therefore, it is expected that the identification and exploration of these might help to clarify the governance of ligand specificity amongst species. Likewise, it is also hypothesised that ligand-species selectively may affect recently identified GPR35 antagonists, CID-2745687 and ML-145. Finally, considering that previous research has highlighted a selective coupling between GPR35 and $G\alpha_{13}$ following activation by zaprinast (Jenkins *et al.*, 2010), it is thought that this coupling profile may also exist following stimulation with pamoic acid, to promote Rho A activation and downstream signalling. Therefore, the aim of this study was to explore the pharmacology of previously identified GPR35 ligands at human, rat and for the first time, mouse GPR35. This chapter will also endeavour to identify crucial residues responsible for pamoic acid's selectivity for

human GPR35 and clarify the G-protein coupling profile following activation with this ligand. Outlined below are a series of aims which have been devised to investigate this fully:

- To identify if pamoic acid, and other human-selective GPR35 ligands are able to activate the mouse orthologue of GPR35.

- To identify key residues within GPR35 which are crucial for activation and account for the human-selectivity displayed by pamoic acid.

- To identify if the newly identified antagonists CID-2745684 and ML-145 display GPR35 orthologue selectivity.

- To confirm that GPR35 couples selectively to $G\alpha_{13}$ following pamoic acid induced activation to promote activation of the Rho A pathway.

3.2 Results

3.2.1 Evidence of β-arrestin-2 recruitment following GPR35 activation and subsequent optimisation of the bioluminescence resonance-energy transfer assay

To begin to explore ligand function at GPR35, a β-arrestin-2-receptor interaction assay was employed. This mode of assessment is essentially G-protein independent and therefore, provides an objective assessment of immediate ligand pharmacology that allows β-arrestin-2 recruitment to the receptor complex. To demonstrate the mobilisation of β-arrestin-2 following agonist stimulation, doxycycline (DOX) inducible Flp-In™ T-REx™ cells stably expressing FLAG-humanGPR35-eYFP were transiently transfected with β-arrestin-2-mCherry using Lipofectamine™ and were then imaged in the presence and absence of 10µM zaprinast. In Figure 3-1.A, compartmentalisation of FLAG-humanGPR35-eYFP and β-arrestin-2-mCherry expression is evident in unstimulated cells. Following a sustained 45-minute stimulation with 10µM zaprinast, both humanGPR35-eYFP and β-arrestin-2-mCherry constructs cluster within the cytosol at close proximity to the plasma membrane, indicative of β-arrestin-2 recruitment to the receptor complex following ligand activation (Figure 3-1.A). To quantify β-arrestin-2 recruitment to GPR35, a bioluminescence resonance-energy transfer (BRET) assay was employed in HEK293T cells transiently transfected with β-arrestin-2-*Renilla*-luciferase (β-arrestin-2-Rluc) and FLAG-humanGPR35-eYFP (Figure3-1.B) or FLAG-ratGPR35-eYFP (Figure3-1.C). Given that GPCR activation can occur within a short time-frame, these cells were stimulated with increasing concentrations of zaprinast at time points ranging from 5 to 20 minutes. The BRET ratio was calculated at emission wavelengths of 530 nm/485 nm using a Pherastar FS plate reader and ratios were normalised to β-arrestin-2-Rluc only expressing cells. Results indicate that the potency of zaprinast at human and rat GPR35 remains unchanged following increased ligand exposure time (hGPR35 EC_{50}= 3.06-4.2µM *± 0.08-*

0.18, rGPR35 EC_{50}=74nM-94nM ± *0.04-0.07*) (p>0.05). However, maximal efficacy becomes more variable; reduced following increased ligand exposure at human GPR35 (E_{max}=107.2-70.59% ± *3.4-4.7%*) (Figure3-1.B) and increased at rat GPR35 (E_{max}=106.6-151.9% ± *1.9-2.2%*), however these effects were non-significant between time points (Figure3-1.C). From these results, it was deduced that the optimal and most comparable time point in going forward for ligand exposure in the BRET assay was 5 minutes for both species of GPR35.
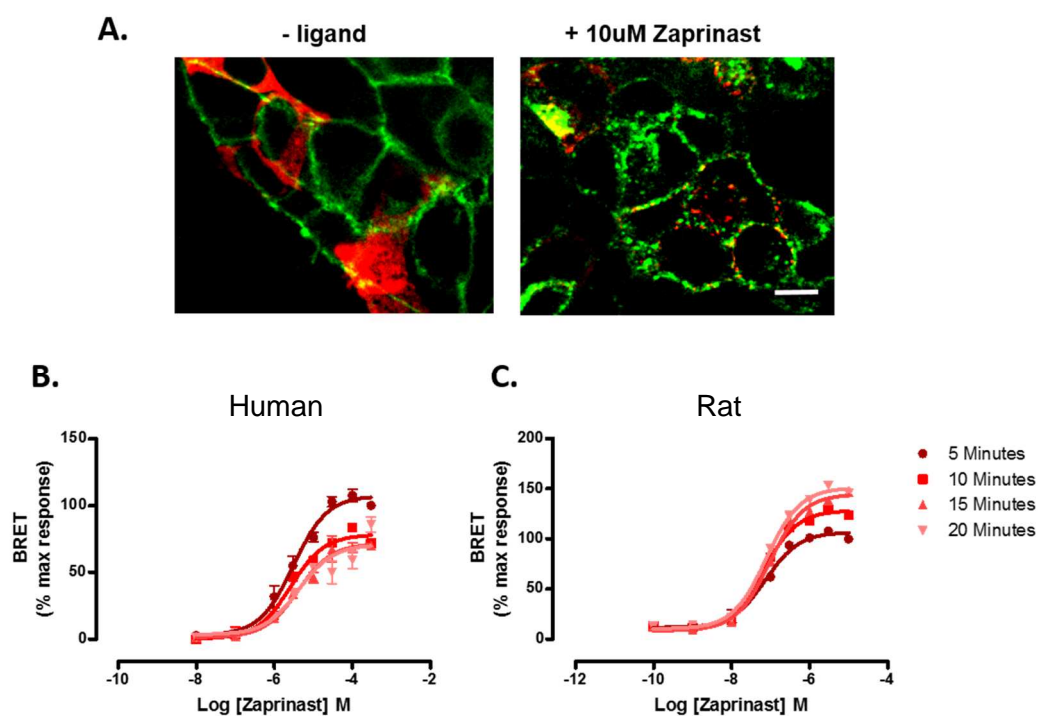
Figure 3-1. GPR35 co-localisation with β-arrestin-2 and BRET optimisation.

Doxycycline (DOX) inducible Flp-In™ T-REx™ cells stably expressing FLAG-humanGPR35-eYFP, transfected with β-arrestin-2-mCherry were fixed, mounted and imaged using Vivatome™ spinning disk confocal microscopy. A) FLAG-humanGPR35-eYFP (green) internalisation and co-localisation with β-arrestin-2-mCherry (red) ± 10μM zaprinast for 45 minutes. B & C) A comparison of β-arrestin-2 receptor interaction derived concentration-response curves in HEK293T cells transfected with β-arrestin-2-Renilla-luciferase and B) FLAG-humanGPR35eYFP or C) FLAG-ratGPR35eYFP in the presence of increasing concentrations of zaprinast for 5-20 minute incubation periods. All data are representative of n=3-4 individual experiments and each condition was performed in triplicate. Scale bar represents 20μm.

3.2.2 The assessment of key reference ligands; zaprinast, cromolyn disodium and pamoic acid at mouse GPR35 via BRET analysis

Previous research has established the potency and efficacy of the ligands zaprinast, pamoic acid and cromolyn disodium to activate human and rat orthologs of GPR35; showing rodent-selectivity in the case of zaprinast, human-selectivity for pamoic acid and equivalence for cromolyn disodium (Jenkins *et al.*, 2010). However, it was unclear if GPR35 ligands follow a trend in that they are either human or rodent specific, and therefore, it was questioned if the potency and efficacy of these ligands would were different at mouse GPR35. To make the necessary comparisons, mouse GPR35 flanked by an N-terminal epitope tag (FLAG) and C-terminally fused eYFP was cloned into a pcDNA3.1 expression vector and co-transfected into HEK293T cells with β-arrestin-2-*Renilla*-luciferase. Similar to previous research (Jenkins *et al.*, 2011), a BRET assay was performed to assess the potency and efficacy of increasing concentrations of key reference GPR35 agonists zaprinast, cromolyn disodium and pamoic acid. In Figure 3-2, the concentration-response curves indicated robust and comparable BRET signals at all GPR35 orthologs and furthermore, demonstrated that rodent orthologues of GPR35 displayed a similar ligand-activation pattern. For example, both rodent species exhibited higher potency for zaprinast; mouse GPR35 (EC_{50}=950.0 ± *0.082nM*), rat GPR35 (EC_{50}=11.0 ± *0.035nM*) compared to human GPR35 (EC_{50}=3.9 ± *0.07µM*) (Figure 3-2.). Cromolyn disodium displayed micromolar potency for the mouse ortholog (EC_{50}=48.0 ± *0.19µM*) (Figure 3-2.C), but this was also true for human GPR35 (EC_{50}=14.0 ± *0.06µM*) (Figure 3-2.A) and rat GPR35 (EC_{50}=5.0 ± *0.075µM*) (Figure 3-2.B). Most clearly in line with rat GPR35, pamoic acid demonstrated negligible activity at the mouse ortholog, contrasting nanomolar potency displayed at human GPR35 (EC_{50}=45.0 ± *0.1nM*) (Figure 3-2.A). This evidence indicated that zaprinast and pamoic acid ligands were largely rodent or human GPR35 selective, respectively. To investigate this further, the

pharmacology of alternative GPR35 ligands with distinct species selective properties was next investigated (Table 3-1.).
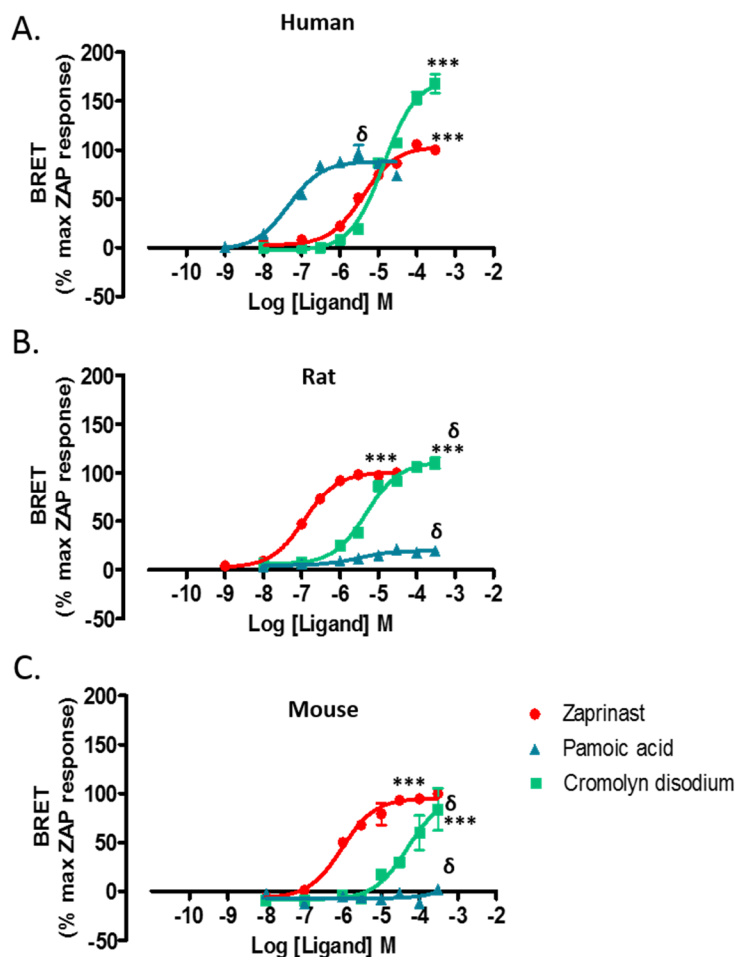
Figure 3-2. BRET analysis highlights the species selectivity of key reference ligands; zaprinast, pamoic acid and cromolyn disodium.

Representative concentration-response curves derived from a β-arrestin-2-receptor interaction assay in HEK293T cells transfected with β-arrestin-2-Renilla-luciferase and A) FLAG-humanGPR35-eYFP, B) FLAG-ratGPR35-eYFP or C) FLAG-mouseGPR35-eYFP in the presence of increasing concentrations of zaprinast, cromolyn disodium or pamoic acid. All data are representative of n=3-4 individual experiments, values are displayed as a mean % of maximal zaprinast response, +/- SEM and were performed in triplicate. Significant difference EC_{50}: *** = $p<0.001$, compared to pamoic acid or, δ = $p<0.001$, compared to zaprinast.

3.2.3 BRET analysis of GPR35 ligand hits from the Prestwick Chemical Library® screen and KYNA at mouse GPR35

Next, the potency of ligands previously identified to act at human and rat GPR35 via screening of the Prestwick Chemical Library ® (Deng *et al.*, 2012b, Jenkins *et al.*, 2010, Zhao *et al.*, 2010), as well as the rat-selective endogenous agonist, KYNA (Wang *et al.*, 2006a) were assessed at mouse GPR35 via BRET analysis. Given that zaprinast demonstrates substantial potency for mouse GPR35, it was utilised as a reference agonist for the concentration-response curves displayed and therefore, the data are presented as percentage of maximal zaprinast response. Table 3-1 displays the comparative potencies (log EC_{50}) of a range of ligands at human, rat and mouse GPR35 and the majority of these present a similar species-selective trend identified in the analysis of zaprinast, cromolyn disodium and pamoic acid. For example, Figure 3-3 demonstrates that niflumic acid (NFA) exhibits low potency (Log EC_{50}=4.01 ± *0.54*) (Table 3-1) and low efficacy (E_{max}=11.3% ± *2.96%*) at mouse GPR35 and this is similar to the actions of NFA at rat GPR35. Additionally, the data suggest that ellagic acid displays low potency at mouse GPR35 (Log EC_{50}=4.36 ± *0.18*). This is slightly lower than values previously recorded for rat GPR35 (Log EC_{50}=5.37), however, these contrast with negligible potency exhibited by NFA at human GPR35 (Table 3-1). Whereas, the bioflavonoid luteolin reaches high efficacy (E_{max}=165.4% ± *8.9%*) yet maintains low potency at mouse GPR35 (Log EC_{50}=4.35 ± *0.08*); the potency was similar to values derived from human and rat GPR35 concentration responses. Interestingly, not all ligands follow a rodent-selective trend and this is particularly evident in the response to the endogenous tryptophan metabolite, KYNA. The data suggest that KYNA has very low potency and efficacy for mouse GPR35 (Log EC_{50}=3.1 ± *0.43*, E_{max} =18.8% ± *6.2%*) and uncharacteristically, this is comparable to the negligible activity displayed at human GPR35 rather than potency displayed at rat GPR35, which was at least ten-fold higher (Log EC_{50} = 4.2) (Table 3-1).

	Human logEC$_{50}$ ± SEM	Rat logEC$_{50}$ ± SEM	Mouse logEC$_{50}$ ± SEM
Zaprinast	5.41 ± 0.06	7.13 ± 0.15	6.03 ± 0.12
Kynurenic Acid	< 3	4.17 ± 0.0615	2.9 ± 0.50
Pamoic Acid	7.29 ± 0.03	< 3	< 3
Niflumic Acid	4.84 ± 0.1	< 3	4.01 ±0.54
Luteolin	4.87 ± 0.3	5.01 ± 0.08	4.35 ± 0.08
Cromolyn Disodium	5.12 ± 0.03	5.36 ± 0.03	4.14 ±0.044
Ellagic Acid	< 3	5.37 ± 0.13	4.36 ± 0.16

Table 3-1. A comparison of the species selective properties exhibited via GPR35 agonists.

A comparison of potency values (logEC$_{50}$ ±SEM) of various Prestwick Chemical Library® GPR35 hits and the endogenous agonist kynurenic acid at human, rat and mouse FLAG-GPR35-eYFP transiently expressed in HEK293T cells and measured via a β-arrestin-2-receptor interaction BRET assay. Data are representative of n=3-4 individual experiments, values are displayed as mean LogEC$_{50}$ +/- SEM and were performed in triplicate.
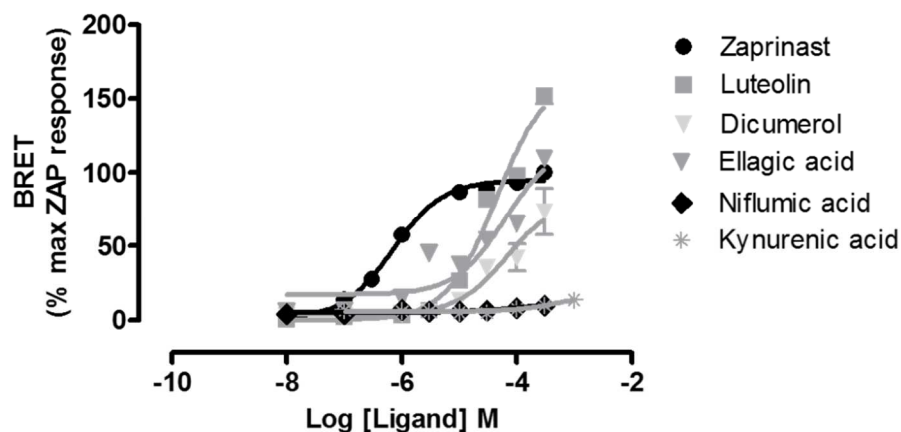
Figure 3-3. The activity Prestwick Library® hits at FLAG-mouseGPR35-eYFP.

Representative β-arrestin-2 receptor interaction concentration-response curves in the presence of GPR35 ligands in HEK293T cells transiently transfected with FLAG-mouseGPR35-eYFP and β-arrestin-2-*Renilla*-luciferase. Data are representative of n=3 individual experiments, values are displayed as mean percentage of maximal zaprinast BRET response, +/- SEM and were performed in triplicate.

3.2.4 Internalisation of FLAG-humanGPR35-eYFP and FLAG-ratGPR35-eYFP demonstrate species selectivity of zaprinast, cromolyn disodium and pamoic acid

An alternative indication of receptor activation is the visualisation of receptor internalisation following ligand administration. Here, zaprinast, pamoic acid and cromolyn disodium demonstrate the ability to effectively activate and internalise FLAG-humanGPR35-eYFP in doxycycline inducible Flp-In™ T-REx™ cells stably expressing the receptor construct following a 40 minute incubation period with each ligand. These effects are represented by live cell imaging captured via VivaTome™ spinning disk illumination microscopy at 0 and 40 minutes (Figure 3-4.A). These images clearly illustrate the ability of zaprinast, pamoic acid and cromolyn disodium to internalise FLAG-humanGPR35-eYFP (Figure 3-4.A). In contrast, internalisation of FLAG-ratGPR35-eYFP is only evident following exposure to zaprinast and cromolyn disodium (Figure 3-4.B). This is consistent with the human-selective GPR35 activation exhibited by pamoic acid via BRET analysis which also highlighted a lack of activity of pamoic acid at rodent orthologs (Figure 3-2.).
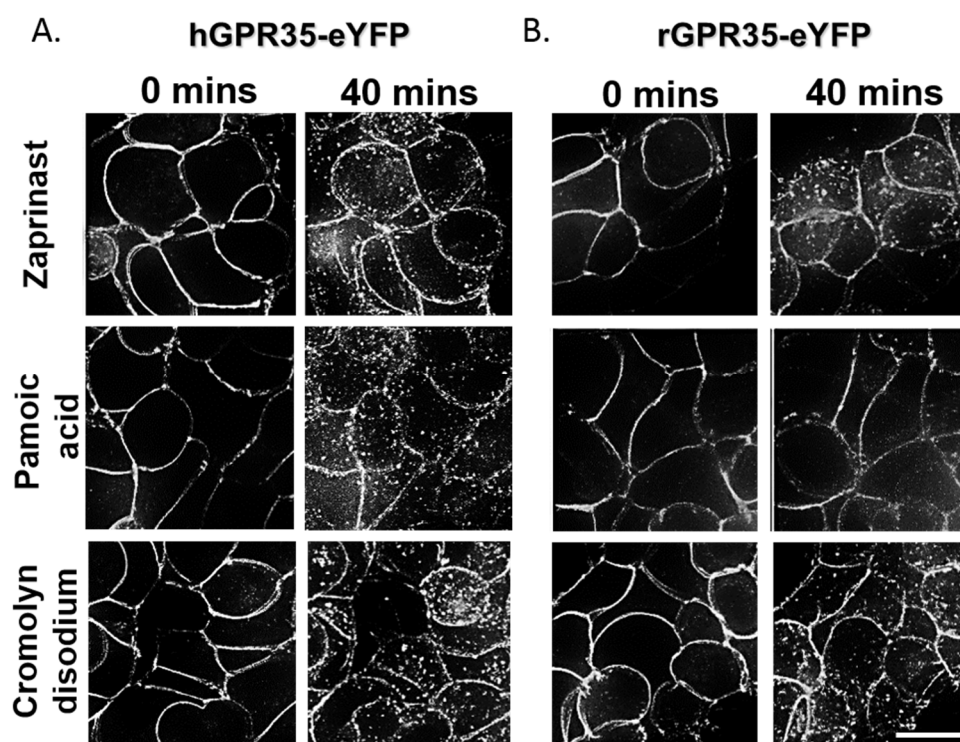
Figure 3-4. Species orthologue selectivity of GPR35 ligands is evident by examining receptor internalisation.

Live cell images of doxycycline induced Flp-In™ T-REx™ cells stably expressing A) FLAG-hGPR35-eYFP or B) FLAG-rGPR35-eYFP stimulated with either 10μM zaprinast, 10μM pamoic acid or 10μM cromolyn disodium (0 and 40 minutes, at 37°C, 5% CO_2). Live receptor internalisation was captured via VivaTome™ spinning disk illumination microscopy (x 64 objective). Images are representative of n=3 individual experiments, and conditions were performed in triplicate. Scale bar represents 20μm.

3.2.5 Identifying residues crucial for the binding of the human selective GPR35 agonist pamoic acid via site-directed mutagenesis

To address the fundamental mechanism of human GPR35 selectivity exhibited by pamoic acid, it is important to identify differential and crucial binding domains which exist between species and further examine their importance in mediating species selective GPR35 activation via site directed mutagenesis. Protein sequence alignments of human GPR35a (the first identified, short isoform of human GPR35), rat GPR35 and mouse GPR35 are detailed in Figure 3-5. GPR35 is relatively well conserved amongst these species - denoted by asterisks underneath the alignment, however, there are areas which differ in sequence and these are denoted with a semi-colon (semi-conservative) or a period (conservative) in Figure 3-5. Putative transmembrane domain (TMD) regions are also highlighted within red-dashed boxes and these are considered crucial areas for small molecule interaction with Class A/ Rhodopsin-like GPCRs. Research in this area has previously employed site directed mutagenesis to examine the significance of interactions between the positively charged arginine located within TMDIII at position 3.36 (according to the Ballesteros and Weinstein numbering system (Ballesteros *et al.*, 1998)) and GPR35 agonists zaprinast and KYNA (Jenkins *et al.*, 2011), highlighted in green in Figure 3-5. Following a collaborative exchange with researchers specialising in computational modelling and fit-docking analysis at the University of Barcelona, putative binding sites for pamoic acid within human GPR35 were identified as suggested areas of ionic interaction. To examine the relevance of these residues for human GPR35 selectivity for pamoic acid, a series of cross-species mutations were generated for both human and rat GPR35. Computational analysis carried out by collaborators suggested that two arginines (R), located at position 4.60 and 6.58, may be crucial for potential interactions between human GPR35 and negatively charged carboxylic acid groups belonging to pamoic acid (highlighted in purple in Figure 3-5). Notably, the nominated arginines are conserved between species at TMD IV but, are not within TMD VIII - resulting in a positively charged

arginine at human GPR35a and polar residue, glutamine (Q), at both rodent orthologs of GPR35.

Figure 3-5. Comparative protein sequence features of human GPR35a, rat GPR35 and mouse GPR35.

A comparison of amino-acid sequences of humanGPR35a, ratGPR35 and mouseGPR35. The putative positions of transmembrane domains (TMDs) I-VII are highlighted within red dashed boxes. The DRY motif is also highlighted within TMDIII, a highly conserved feature amongst Rhodopsin-like/ Class A GPCRs. Potential ligand binding positions are highlighted in green and purple. Arginine (R) 3.36 (green) is a reportedly crucial amino acid for zaprinast and KYNA recognition (Jenkins et al., 2010) and further computational modelling has identified R4.60 and R6.58 as potential binding positions for pamoic acid in human GPR35a (purple).

To assess if either of these arginine residues was essential for ionic interaction with pamoic acid, a series of mutations were introduced via site directed mutagenesis, predominantly replacing positively charged arginines (R) with polar, or negatively charged amino acids in FLAG- humanGPR35-eYFP at position 4.60 and 6.58 or FLAG- ratGPR35-eYFP at position 4.60 (Figure 3-6 & Figure 3-7, respectively). Alternatively, positively charged arginine (R), or non-polar residue methionine (M) substituted native glutamine (Q) in the FLAG-ratGPR35-eYFP construct at position 6.58 (Figure 3-7).

Results indicated that replacing arginine (R) with alanine (A) at both 4.60 and 6.58 eliminated agonist activity of zaprinast and the human selective agonist pamoic acid altogether in human GPR35 (Figure 3-7.B&F). However, replacing arginine (R) at position 4.60 with glutamine (Q) had no effect on the activity of zaprinast at human GPR35 and reduced the potency of pamoic acid by ten-fold and efficacy by 50%, suggesting that its presence can partially retain agonist activity of pamoic acid (Figure 3-7.C). Replacing arginine (R) with methionine (M) at position 6.58 abolished activity of zaprinast and reduced the potency of pamoic acid by ten-fold and efficacy by 50% (Figure 3-7.D), compared with WT human GPR35 (Figure 3-7.A). This suggests that the presence of an alternative, non-polar hydrophobic based residue can maintain interaction with pamoic acid, to a degree. To assess variation in cell-surface receptor delivery efficiency following the introduction of single-residue mutations, which may be indicative of alterations in protein-folding and trafficking, a cell-surface immuno-absorbance ELISA assay was performed in HEK293T cells transiently transfected with each mutant construct (Figure 3-7.E). Compared to WT-humanGPR35a, which was more highly expressed compared to vector only ($p<0.01$), the overall cell-surface expression of the mutant constructs was reduced following the introduction of single-point mutations indicating that cell surface delivery was very limited.
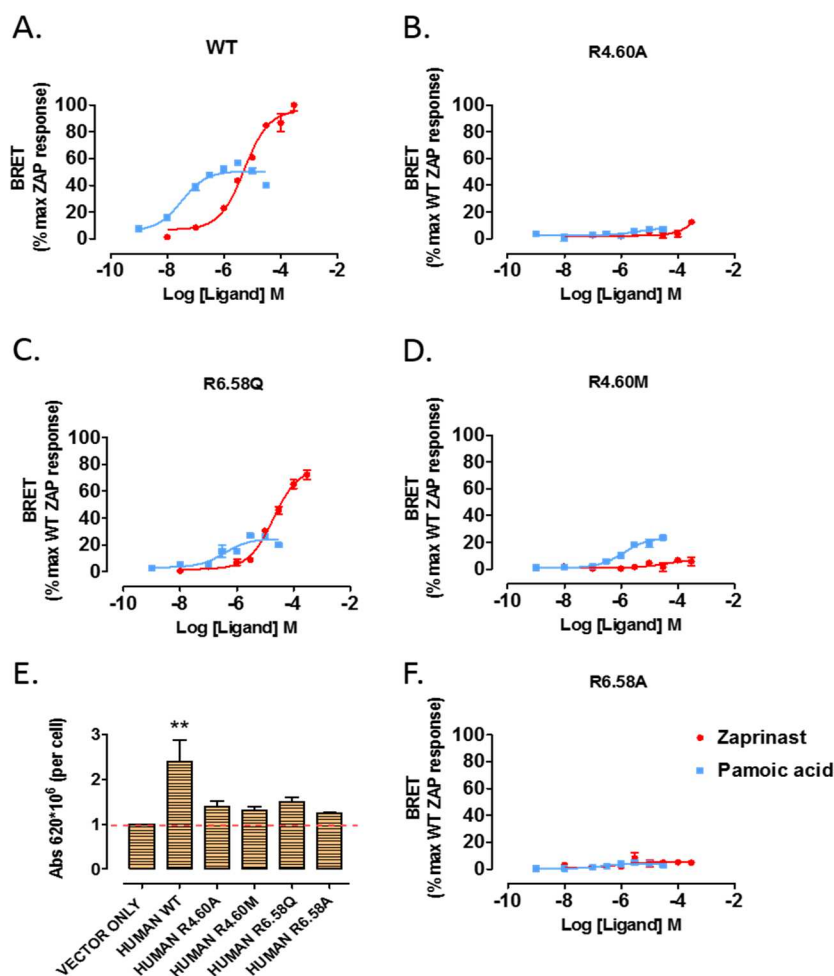
Figure 3-6. Site-directed mutagenesis suggests that positively charged arginines located at 4.60 and 6.58 are essential for agonist function at hGPR35.

β-arrestin-2 interaction assays were performed in HEK293T cells transiently transfected with A) Wild-type (WT) humanGPR35-eYFP, B) arginine (R) mutation to alanine (A) at 4.60 in hGPR35, C) arginine (R) mutation to glutamine at 6.58 (Q) in hGPR35, D) arginine (R) mutation to methionine (M) at 4.60 in hGPR35, and F) arginine (R) mutation to alanine (A) at 6.58 in human GPR35, following exposure to increasing concentrations of zaprinast or pamoic acid. E) Cell surface expression of human WT and mutant GPR35 constructs in comparison to vector only transfection (pcDNA3.1), assessed via ELISA. Data are representative of n=4 individual experiments, values are displayed as mean % of maximal zaprinast response, +/- SEM and were performed in triplicate. ** = $p < 0.01$, compared to vector only.

Interestingly, the results demonstrated that replacing arginine (R) with alanine (A) at position 4.60 generated a high level of basal activity in rat GPR35 (Figure 3-7.B). This indicates a shift in receptor conformation to produce constitutive activity and therefore, the presence of a positively charged residue at this position may be vital to sustain basal receptor confirmation (Figure 3-7.B). However, substituting methionine (M) at the same position – another hydrophobic residue – eliminated activity of both ligands (Figure 3-7.C) and a similar effect was observed following the introduction of this mutation at human GPR35, which abolished the potency of zaprinast and diminished the effect of pamoic acid (Figure 3-6.B). These results suggest that arginine (R) at 4.60 is also crucial for zaprinast interaction at human and rodent orthologues, however, less so for pamoic acid activation. Furthermore, it was hypothesised that by replacing glutamine (Q) at position 6.58 with arginine (R), it may be possible to gain potency of pamoic acid at rat GPR35, however, the activity of zaprinast and pamoic acid remain unchanged (Figure 3-7.D). This was also true of the opposite mutation in human GPR35, which did not fully abolish the activity of pamoic acid (Figure 3-6.C). In contrast to human GPR35 mutant constructs, which were not consistently well expressed at the cell surface, single-point mutations introduced into rat GPR35 remained highly expressed at the cell surface in comparison to vector only expression ($p < 0.001$), assessed via ELISA (Figure 3-7.E).
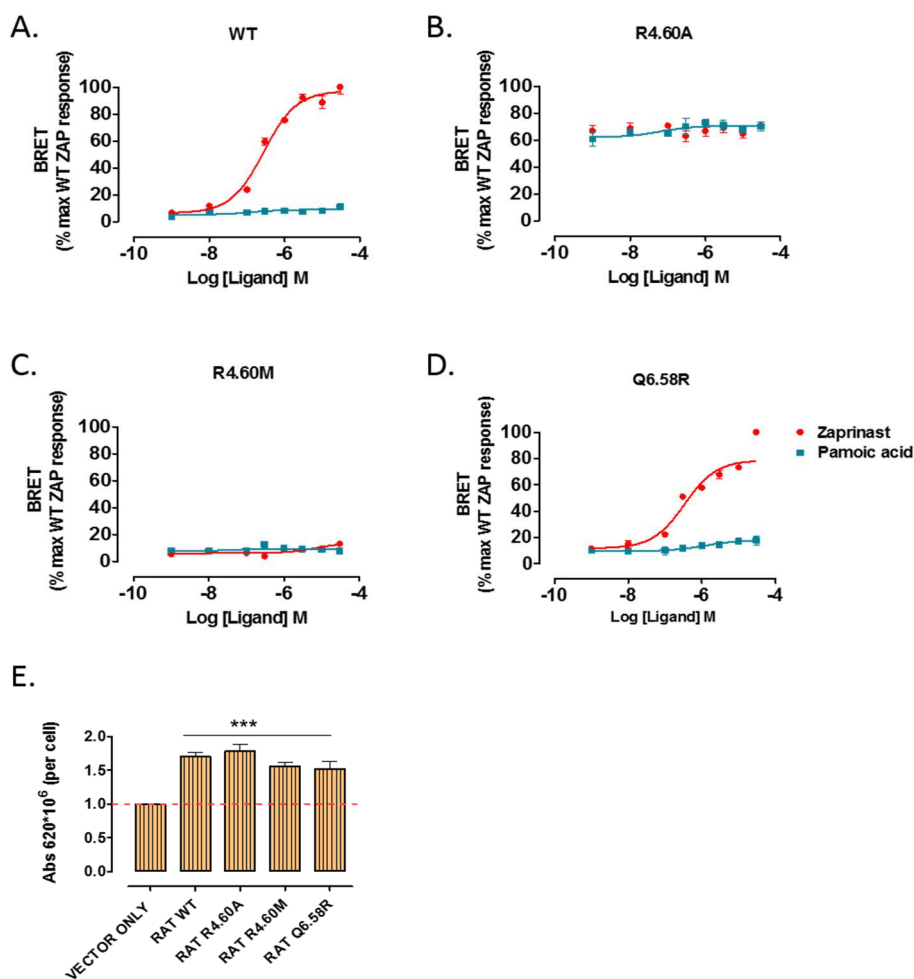
Figure 3-7. Site-directed mutagenesis suggests the positively charged arginine located at 4.60 is essential for agonist activation and basal state preservation of rat GPR35.

β-arrestin-2 interaction assays were performed in HEK293T cells transiently transfected with A) Wild-type (WT) ratGPR35-eYFP, B) arginine (R) mutation to alanine (A) at 4.60 in rat GPR35, C) arginine (R) mutation to methionine (M) at 4.60 in rGPR35, and D) glutamine (Q) mutation to arginine (R) at 6.58 in rat GPR35, following exposure to increasing concentrations of zaprinast or pamoic acid. E) Cell surface expression of WT-ratGPR35 and mutant-ratGPR35 constructs in comparison to vector only transfection (PCDNA3.1) assessed via ELISA. Data representative of n=4 individual experiments, values are displayed as mean % of maximal zaprinast response, +/- SEM and were performed in triplicate. *** = $p < 0.001$, compared to vector only.

3.2.6 Novel GPR35 ligands CID-2745687 and ML-145 are competitive antagonists, highly selective for human GPR35

Initial research to identify the GPR35 antagonists CID-2745687 (Zhao *et al.*, 2010) and ML-145 (Heynen-Genel *et al.*, 2010) failed to investigate if these ligands exhibited species selectivity, a feature often reported in GPR35 agonists. For that reason, alterations in agonist potency in the presence of increasing concentrations of either of these GPR35 antagonists across multiple species orthologues was assessed via BRET. Representative experiments shown in Figure 3-8 and Figure 3-9 demonstrate that CID-2745687 and ML-145 both exhibited a high degree of human-species selectivity. Moreover, Schild analysis indicated that CID-2745687 displays competitive and surmountable antagonism at human GPR35 ($R^2 = 0.89$-0.95) (Figure 3-8.A). Moreover, CID-2745687 demonstrates high affinity for human GPR35 (Kb = 1.1µM) (Figure 3-8.A). Conversely, zaprinast concentration curves at FLAG-ratGPR35-eYFP (Figure 3-8.B) or FLAG-mouseGPR35-eYFP (Figure 3-8.C) remained uninhibited following exposure to increasing concentrations of CID-2745687, indicating that this compound lacks significant affinity for the rodent orthologues.
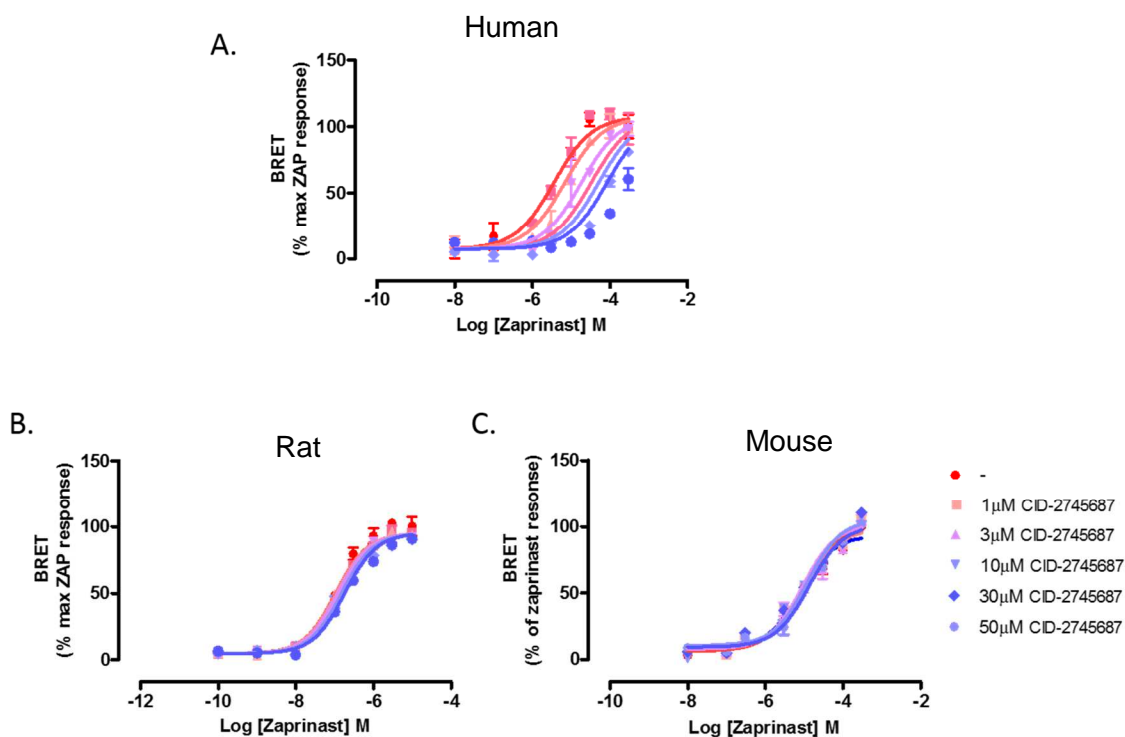
Figure 3-8. GPR35 antagonist CID-2745687 displays human selective, competitive activity.

β-arrestin-2-receptor interaction BRET assays were performed in response to various concentrations of zaprinast in the presence of fixed concentrations of CID-2745687 in HEK293T cells transfected with A) FLAG-hGPR35-eYFP B) FLAG-rGPR35-eYFP or C) Data were constrained to global fit a Schild analysis (H =1). Data are representative of n=3 individual experiments, values are displayed as mean % of maximal zaprinast response, +/- SEM and were performed in triplicate.

ML-145 also exhibited competitive antagonism of zaprinast (R^2 = 0.84-0.92) at

humanGPR35. Moreover, ML-145 demonstrated substantially higher affinity at FLAG-

humanGPR35-eYFP (Kb = 1.4nM) (Figure 3-9.A) than did CID-2745687. However, ML-

145 also displayed negligible inhibition of zaprinast induced effects at FLAG-ratGPR35-

eYFP (Figure 3-9.B) and FLAG-mouseGPR35-eYFP (Figure 3-9.C), indicating human

GPR35 selectivity.
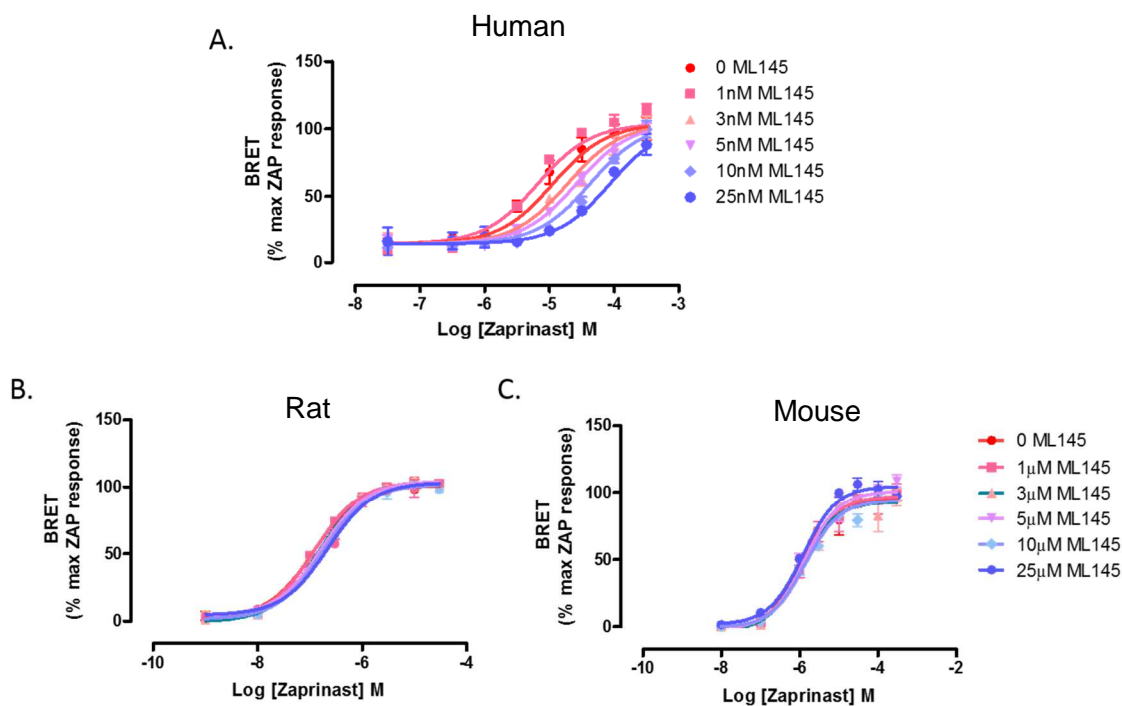
Figure 3-9. The GPR35 antagonist ML-145 also displays human selective, competitive behaviour.

β-arrestin-2-receptor interaction concentration-response curves constrained to global fit Schild analysis (H =1) in HEK293T cells transfected with A) FLAG-hGPR35-eYFP B) FLAG-rGPR35-eYFP and C) FLAG-mGPR35-eYFP in the presence of increasing concentrations of both agonist zaprinast and the antagonist ML-145. Data are representative of n=3 individual experiments, values are displayed as mean % of maximal zaprinast response, +/- SEM and were performed in triplicate.

To further investigate this apparent species selectivity of the antagonist ligand, an in-cell 'Arrayscan' of doxycycline induced Flp-In™ T-REx™ cells stably expressing FLAG-humanGPR35-eYFP and FLAG-mouseGPR35-eYFP was performed (Figure 3-10). This quantitative measurement of receptor internalisation captures live cell internalisation and subsequently applies computational algorithms to identify clusters of receptor-eYFP expression within each cell, indicative of the formation of endosomal compartments in receptor recycling. These were normalised to the number of nuclei present, identifiable via Hoescht stain and were expressed as a percentage of spots per cell (% spots/ cell). Results indicated that FLAG-humanGPR35-eYFP internalisation induced by EC_{80} concentrations of GPR35 agonists zaprinast, pamoic acid or cromolyn was inhibited in a concentration-responsive manner following the addition of increasing concentrations of CID-2745687 (Figure 3-10A) and ML-145 (Figure 3-10.B). Interestingly, results also indicated that GPR35 internalisation surpasses baseline measurements at the highest concentrations, suggesting that CID-2745687 and ML-145 may also display inverse agonism (Figure 3-10.A&B). By contrast, there was no evidence of reduced FLAG-mouseGPR35-eYFP internalisation following exposure to increasing concentrations of CID-2745687 (Figure 3-10.C) and ML-145 (Figure 3-10.D) in the presence of EC_{80} concentrations of zaprinast or cromolyn, indicating that CID-2745687 and ML-145 do not exert an antagonistic effect at mouse GPR35.
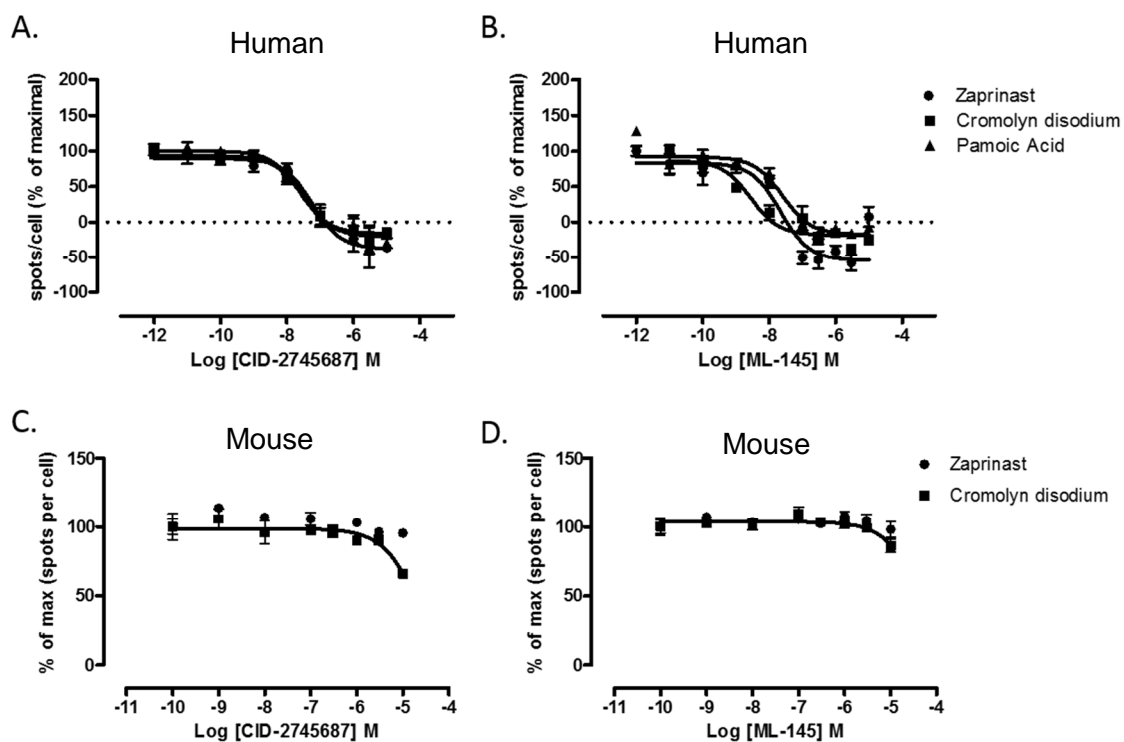
Figure 3-10. Quantitative GPR35 internalisation demonstrates human GPR35 selective antagonism of CID-2745687 and ML-145.

In-cell Arrayscan analysis performed on doxycycline induced Flp-In™ T-REx™ cells stably expressing FLAG-humanGPR35-eYFP (A&B) or FLAG-mouseGPR35-eYFP (C&D) to quantify GPCR internalisation in the presence of increasing concentrations of the purported antagonists CID-2745687 (A&C) and ML-145 (B&D) in response to zaprinast, cromolyn disodium or pamoic acid ([EC_{80}] defined for the corresponding orthologue). Data are representative of n=3 experiments, values are displayed as mean % of maximal internalisation, +/- SEM and were performed in triplicate.

3.2.7 Screening potential GPR35 antagonists via BRET analysis

In a bid to identify antagonists which are equipotent amongst species or rodent selective, competitive BRET analysis was performed using a selection of commercially available compounds, including dogoxigenin, stropanthidin, hexestrol, dienestrol and bisacodyl; that were highlighted as potential antagonists of GPR35 by screening of the Prestwick Chemical Library® in antagonist mode by collaborators from the University of Santiago de Compostela, Spain. BRET competition assays demonstrated in Figure 3-11 were performed using an EC_{80} concentration (calculated for each orthologue) of the reference agonist zaprinast, in the presence of increasing concentrations of potential antagonists in HEK293T cells transiently transfected with FLAG-humanGPR35-eYFP (Figure 3-11.A) or FLAG-ratGPR35-eYFP (Figure 3-12.B). Results from these assays indicated that three molecules, bisacodyl, dienestrol and hexestrol, exhibited potential for antagonistic activity at both human and rat orthologues of GPR35 and therefore, warranted further investigation. Schild analysis was performed in the presence of increasing concentrations of both zaprinast and either dienestrol or bisacodyl at FLAG-humanGPR35-eYFP (Figure 3-11.C&E) and FLAG-ratGPR35-eYFP (Figure 3-11.D&F). Results demonstrated that whilst the concentration-response curves to zaprinast displayed a 'rightward' shift to higher concentrations, to some degree, in response to bisacodyl, the data points poorly fit the global model of constraint within the Schild analysis (Schild slope=1) for each orthologue. Therefore, bisacodyl appeared to act as a non-competitive antagonist at GPR35, but displayed modest potency at each orthologue (Figure 3-11.C&D). Furthermore, dienestrol, a second potential GPR35 antagonist, exhibited negligible antagonistic activity in the presence of EC_{80} concentrations of zaprinast for FLAG-humanGPR35-eYFP (Figure 3-11.E) and FLAG-ratGPR35-eYFP (Figure 3-11.F). Taking this evidence together, it was clear that neither biscodyl nor dienestrol were appropriate tools for future exploration of role of GPR35 in human and rodent systems.
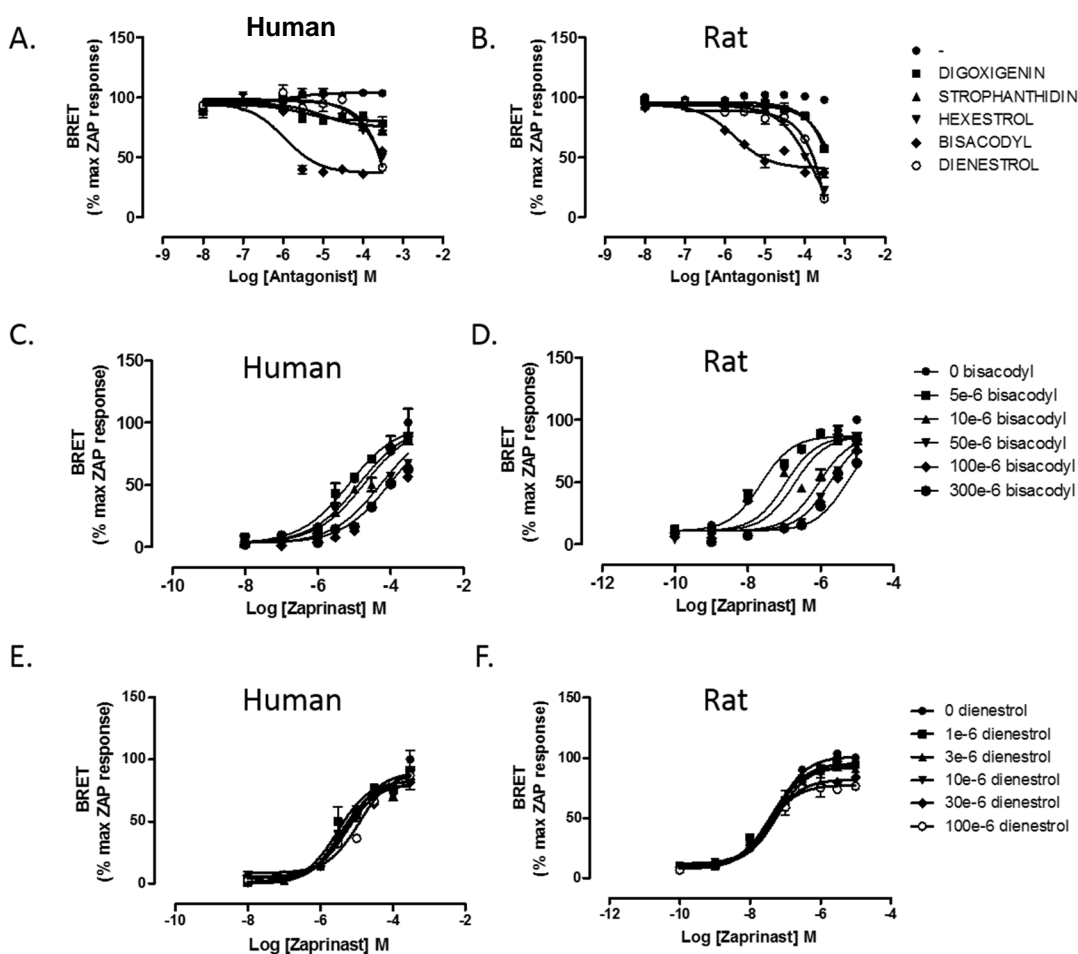
Figure 3-11. Screening potential novel GPR35 antagonists via BRET .

β-arrestin-2-receptor interaction was examined in HEK293Tcells transfected with A) FLAG-hGPR35-eYFP or B) FLAG-rGPR35-eYFP in the presence of increasing concentrations of potential GPR35 antagonists in the presence of an EC_{80} concentration of zaprinast (defined for each orthologue) and; C, D, E & F) β-arrestin-2-receptor interaction was assessed in response to varying concentrations of zaprinast, and data constrained to fit Schild slope (= 1), in HEK293T cells transfected with C&E) FLAG-hGPR35eYFP or D&F) FLAG-rGPR35eYFP in the presence of increasing concentrations the potential GPR35 antagonists bisacodyl or dienestrol. Data are representative of n=3 individual experiments, values are displayed as mean % of maximal zaprinast response, +/- SEM and were performed in triplicate.

3.2.8 The G-protein coupling profile of human GPR35 and assessment of

p115RhoGEF trafficking

By means of chimeric single-cell Ca^{2+} influx assays, Jenkins and colleagues have

previously demonstrated that GPR35 couples to the $G\alpha_{12/13}$ family of G-proteins and

indeed selectively to $G\alpha_{13}$ following zaprinast activation. However, G-protein selectivity

has yet to be explored following stimulation with alternative agonists, such as pamoic acid

(Jenkins *et al.*, 2011, Mackenzie *et al.*, 2014). Given that pamoic acid has been identified

as a high-potency agonist at human GPR35, it provides an opportunity to assess a role for

GPR35 in endogenously expressing cells of human origin and, therefore, it is important to

understand the signalling pathways it may potentiate within a functional setting. This was

next assessed via a homogeneous time resolved fluorescence (HTRF) inositol-phosphate-

1 (IP_1) accumulation assay. Following $G\alpha_q$ activation, the hydrolysis of

phosphatidylinositol 4,5-bisphosphate (PIP_2) at the plasma membrane generates the

second messenger inositol 1,4,5-trisphosphate (IP_3), which rapidly transforms into IP_2 and

in the presence of lithium chloride IP_1 formed from this is protected from further

metabolism. The high-throughput format of the IP_1 accumulation assay employs the use

of a Lumi-4® IP_1 antibody and this competitively binds to increasing concentrations of

endogenously produced IP1 rather than dye d^2-tagged IP_1, which has been added

exogenously. Therefore, following ligand administration, GPCR activation and

subsequent IP_1 accumulation; an inverse signal is produced. This assay was employed in

the presence of increasing concentrations of pamoic acid in HEK293T cells which were

transfected with FLAG-humanGPR35 alone or co-transfected with the receptor and G-

protein chimeras $G\alpha_{q/12}$, $G\alpha_{q/13}$, $G\alpha_{q/i}$ or full length $G\alpha_q$ (Figure 3-12.A). Interestingly,

results demonstrated that human GPR35 activation via pamoic acid exhibited a second

messenger IP1 response via both $G\alpha_{q/12}$ and $G\alpha_{q/13}$ chimeric constructs, indicating that

pamoic acid induced activation of human-GPR35 enabled coupling to both members of

the $G\alpha_{12/13}$ family and was not selective for one form (Figure 3-12.A). Notably, the potency

of pamoic acid was 100-fold lower (EC_{50}=3.4µM $\pm$ *0.3*) in this assay than observed

previously in the BRET assay (EC_{50}=45nM $\pm$ *0.117*) (Figure 3-12.A) and this contrasted

with recently published data which reported that pamoic acid was 10-fold more potent in

an IP_1 accumulation assay compared to BRET analysis (Jenkins *et al.*, 2012).

Moreover, given that $G\alpha_{12/13}$ activation is implicated in downstream signalling involving

Rho A and ROCK1/2, an attempt to visualise the trafficking of GFP-tagged p115RhoGEF;

a monomeric GTPase activating protein which is understood to translocate from the

cytosol to the plasma membrane to activate Rho A following $G\alpha_{12/13}$ activation was

performed (Maruyama *et al.*, 2002) (Figure 3-12.B). Unfortunately, since eYFP and GFP

produce overlapping emission wavelengths both humanGPR35-eYFP and induced

translocation of p115RhoGEF-GFP could not be imaged together effectively.

Alternatively, HEK293T cells were transiently transfected with p115RhoGEF-GFP alone,

or co-transfected with $G\alpha_{13}$ wild type (WT), $G\alpha_{13}$ constitutively active mutant (CAM), $G\alpha_{12}$

wild type (WT) or $G\alpha_{12}$ constitutively active mutant (CAM) and 24-hours later were fixed

using 4% PFA, stained with Cell Mask Orange and Hoechst and imaged using

VivaTome™ spinning disk illumination microscopy, at x 64 magnification (Figure 3-12.B).

Representative images in Figure 3-12.B demonstrate that p115RhoGEF-GFP is basally

located within the cytosol when expressed alone or in the presence of WT $G\alpha_{13}$ and WT

$G\alpha_{12}$. Conversely, co-transfection with either CAM $G\alpha_{13}$ or CAM $G\alpha_{12}$ promoted the

translocation of p115RhoGEF-GFP from the cytosol to the plasma membrane where it co-

localised with membrane stain, Cell Mask Orange (Figure 3-12.B).
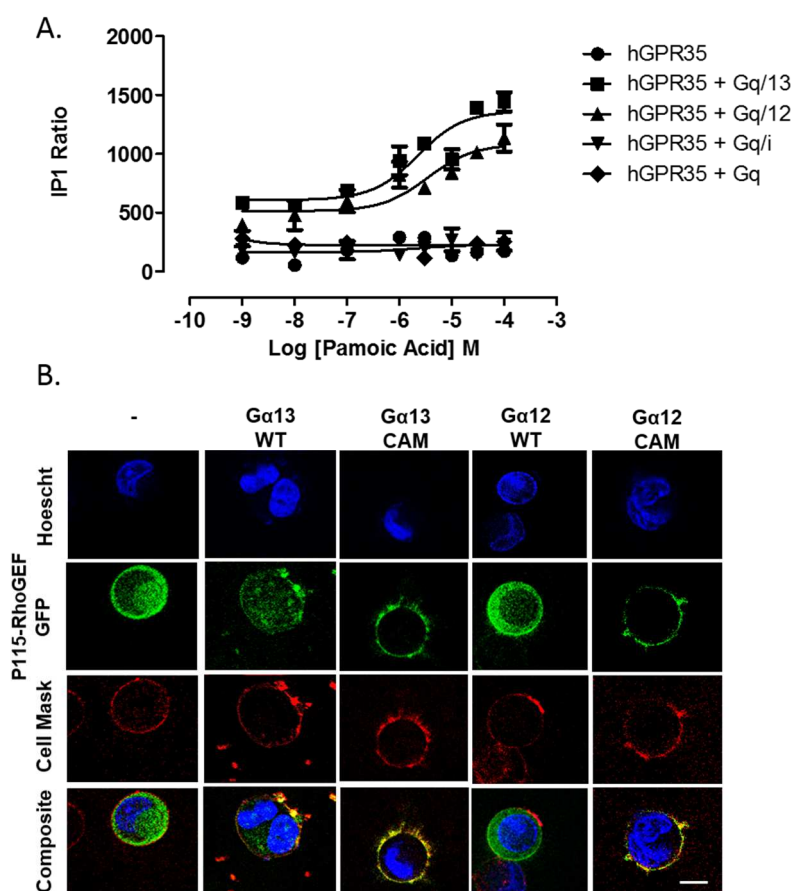
Figure 3-12. Human GPR35 couples to the Gα$_{12/13}$ family of G-proteins and these promote p115-RhoGEF translocation to the plasma membrane.

A) IP$_1$ accumulation in HEK293Tcells transfected with FLAG-hGPR35-eYFP alone or also with chimeric constructs Gα$_{q/13}$, Gα$_{q/12}$, Gα$_{q/i}$, Gα$_q$ in the presence of increasing concentrations of the GPR35 agonist pamoic acid, assessed via homogeneous time resolved fluorescence. B) p115-RhoGEF-GFP translocation in the presence of constitutively active Gα$_{12}$ or Gα$_{13}$ protein in fixed and stained (Hoescht – nuclei, Cell Mask Orange – plasma membrane) HEK293T cells transfected with p115-RhoGEF-GFP alone, or p115RhoGEF-GFP with Gα$_{13}$ wild type (WT), Gα$_{13}$ constitutively active mutant (CAM), Gα$_{12}$ wild type (WT) or Gα$_{12}$ constitutively active mutant (CAM). IP$_1$ accumulation data are representative of n=2 individual experiments, values are displayed as mean IP$_1$ ratio, +/- SEM and were performed in duplicate. Images are representative of n=3 experiments and were performed in triplicate. Scale bar represents 10μm.

3.3 Discussion

In this chapter, the pharmacology of previously identified ligands across human and rodent species of GPR35 was assessed. Earlier research has established there exists an element of species-selectivity amongst ligands which either activate (Jenkins *et al.*, 2010) or block GPR35 (Jenkins *et al.*, 2012). Prior to this latter publication – to which this study contributed (Jenkins *et al.*, 2012), it was unclear if this was true for ligand activity at the mouse orthologue of GPR35 or, if the recently identified antagonists CID-2745687 and ML-145 also displayed species-selective properties. By improving our understanding of ligand activity amongst species, it has been possible to gain further insight as to whether GPR35 ligand selectivity is evident amongst rodent species and, therefore, their future applications in functional systems can be realistically explored.

The inactivity of the human-selective agonist pamoic acid at rat or mouse GPR35 highlighted an existing trend towards ligand-selectivity for either human or rodent GPR35. Further screening of alternative GPR35 ligands confirmed this. However, the trend in ligand species-selectivity was not entirely exclusive. This was most prominently emphasised by KYNA's limited potency for mouse GPR35. This finding was unexpected, given that KYNA, the first reported endogenous agonist for GPR35 (Wang *et al.*, 2006a), demonstrates considerable selectivity for rat GPR35 (Jenkins *et al.*, 2010). Although an unexpected finding, it is important to note that species-selectivity of endogenous ligands has also been reported in cannabinoid receptors (CB1 and CB2) (Mukherjee *et al.*, 2004) and these are receptors which share close homology with GPR35 (Zhao and Abood, 2013). On the other hand, there is research to suggest that some GPCRs do not have an endogenous ligand and may be terminally orphaned (Lagerstrom and Schioth, 2008). The γ-aminobutyric acid B (GABAB1) receptor is an excellent example, reportedly forming heterodimers with GABA to mediate cell surface delivery and function, thus, replacing endogenous ligand-receptor activation (Jones *et al.*, 1998). Currently, research which addresses the potential of GPR35 to form homo- or heterodimers is lacking. Approaches

to address a mechanism for extreme species-selectivity have previously utilised site-directed mutagenesis to identify critical residues for KYNA activation. However, binding positions within TMD III at position 3.36 were demonstrated to be common to both rat and human GPR35 (Jenkins *et al.*, 2010). Species sequence alignment confirms this residue to be conserved at mouse GPR35 and therefore, it is also unlikely to be responsible for the ortholog selectivity described here (Figure 3-5.). Differential KYNA potency between rodent orthologues further suggests that additional sites of interaction exist at rat GPR35. In going forward, the investigation of residues which are different between human and murine GPR35 may prove helpful in future mutagenesis studies designed to elucidate KYNA's selective mode of binding to rat GPR35.

Of course, the findings reported here also have significant implications towards the conclusions drawn from a former publication demonstrating a dose-dependent, nociceptive effect of pamoic acid in an experimental mouse model (Zhao *et al.*, 2010). β-arrestin-2-receptor interaction demonstrates that pamoic acid is virtually ineffective at both the mouse and rat orthologues of GPR35, and this is consistent with previous evidence of inactivity at the rat orthologue (Jenkins *et al.*, 2010). The extreme human-GPR35 selective agonism of pamoic acid is also demonstrated here via receptor internalisation in cells stably expressing human or rat GPR35-eYFP. Taking this evidence together, it is possible to suggest that pamoic acid may have effects on nociception, however, it is unlikely that these effects are mediated via GPR35 (Zhao *et al.*, 2010).

It was also confirmed that CID-2745687 and ML-145 are competitive, high affinity antagonists which display surmountable activity in the presence of zaprinast, and this is in line with published evidence (Jenkins *et al.*, 2012). Given that neither CID-2745687 nor ML-145 are effective antagonists at the rodent orthologues, it is now clear that the species-selective properties displayed by the majority of GPR35 ligands also extended to antagonists. This clarification is particularly useful considering that initial reports that identified these antagonists failed to investigate this (Zhao *et al.*, 2010, Heynen-Genel *et*

al., 2010) and, therefore, CID-2745687 was employed as an antagonist of GPR35 within a mouse model - with no effect (Zhao *et al.*, 2010). Importantly, results from this chapter highlight that neither CID-2745687 nor ML-145 are appropriate tools to decipher a role for GPR35 in rodent models. Taking this information together, the differences in species-selectivity demonstrated here may have particular implications for future studies which derive associations between ligand administration, GPR35 activation and subsequent alteration of physiological parameters *in vivo*.

To further our understanding of the nature of the human-selectively displayed by pamoic acid, a series of single-point, cross-species mutations were introduced to human GPR35, substituting positively charged arginine (a potential residue which may interact with one of the carboxylate moieties in pamoic acid) for polar, neutral residues such as alanine and methionine or glutamine, the corresponding residue in both mouse and rat. Substituting arginine for alanine at both 6.58 and 4.60 resulted in a complete loss of potency and efficacy for zaprinast and pamoic acid, indicating that these ligands share an overlapping binding position which is critical for interaction. This finding is in agreement with recently published data suggesting that arginine residues within TMDs III and V are critical binding positions for pamoic acid and zaprinast (Zhao *et al.*, 2014). Most interestingly, replacing arginine at 6.58 with glutamine (the corresponding residue in rat) merely reduced the potency of both zaprinast and pamoic acid by 10-fold and the efficacy by 25%, suggesting that glutamine substitution has only a moderate effect on the interaction with either ligand.

Notably, however, the cell-surface expression for all human GPR35-mutant constructs was minimal and despite demonstrating a sustained trend towards higher expression, this was not significantly different to the vector-only control. In functional systems, single-residue mutations are understood to present post-translational modifications relating to membrane expression via an alteration in protein folding, endosomal sorting and subsequent degradation which can often result in disease and signalling modifications via GPCRs (Conn *et al.*, 2006). The repercussions of this are extensive for the gonadotropin

releasing hormone (GnRH) receptor and vasopressin type 2 receptors (V2Rs), for which single-point mutations have been implicated in hypogonadotropic hypogonadism and nephrogenic diabetes, respectively (Conn *et al.*, 2006, Conn *et al.*, 2007). However, given that the BRET assay is essentially G-protein independent in nature and its signal remained unaffected by lowered cell-surface expression, its use is advantageous to assess the pharmacology of potential ligand-receptor interaction at this level. Notably, Zhao and colleagues also employed a β-arrestin-receptor interaction assay in their assessment of single-point mutations and reported differences in potency of up to 30-fold compared to an ERK1/2 phosphorylation assay, suggesting that secondary-endpoint assays may obscure basic pharmacology at the receptor complex (Zhao *et al.*, 2014).

Though a gain in potency by pamoic acid was not demonstrated by replacing glutamine with arginine at position 6.58 in rat, this was expected, given that opposing substitutions (arginine[6.58]glutamine) in the human orthologue did not result in the loss of potency of pamoic acid. It is clear that arginine and glutamine are somewhat interchangeable at this position and this may be unsurprising, considering they are both polar, hydrophilic residues (Betts and Sternberg, 1999). Furthermore, it is clear that arginine[4.60] is a critical binding position for zaprinast at the rodent orthologues and more interestingly, when substituted for alanine, rat GPR35 becomes constitutively active. This evidence suggests an interruption of ionic constraints which have shifted GPR35 towards an active confirmation. Constitutive activity has not been reported in previously generated GPR35 mutants. However, is it understood that single-point mutations within a critical binding site can often produce constitutive activity and sustained signalling (Smit *et al.*, 2007). Given that results in secondary end-point signalling may be affected by constitutive activity, its potential use is limited in this respect. However, it could be useful for the identification of inverse agonists for GPR35 in the future. It was also important to note that unlike human GPR35 mutants, rat GPR35 mutant constructs were very well expressed at the cell surface (p<0.001, compared to vector-only control). This may indicate a propensity for

single-point mutations to disrupt protein-folding and subsequent trafficking more readily in human than rodent GPR35. Further investigation may be required to understand if this finding reflects the numerous SNPs reported to have implications for disease in man (Mackenzie *et al.*, 2011).

Despite the steady increase in newly identified synthetic ligands at GPR35 (Mackenzie *et al.*, 2014, Deng and Fang, 2013), much of the evidence of a role for GPR35 is conflicting and this is largely due to a lack of functional ligand pairs which transcend species-selectivity (Jenkins *et al.*, 2012). To this end, this study also endeavoured to identify novel GPR35 antagonists which act at both human and rodent species. Competitive BRET analysis indicated that bisacodyl, a commercially available stimulant laxative (Manabe *et al.*, 2009) and dienestrol, a synthetic estrogen, may exert antagonistic effects at both human and rat GPR35. However, baseline BRET values were not re-established following exposure to high concentrations of bisacodyl in a competitive BRET assay - indicating non-surmountable activity. This was confirmed by application of Schild analysis, for which global Schild-slope constraints equal to one were used in the assessment of dose-response curves. Given that neither compound elicited a potent or competitive antagonistic action at either orthologue, it would be impractical to utilise these ligands within a functional setting for either species. Conclusively, these results emphasise the importance of applying basic pharmacological approaches to the screening of GPR35 ligands in order to identify functional ligand pairs within a multi-orthologue setting.

Research here also investigated the coupling profile following GPR35 activation and discovered that it couples to both $G\alpha_{12}$ and $G\alpha_{13}$ isoforms following pamoic acid stimulation. This is not in dispute with reports that pamoic acid, amongst others, promotes robust coupling to $G\alpha_{13}$ via GPR35 activation in IP1 assays (Jenkins *et al.*, 2012, Mackenzie *et al.*, 2014). However, it does contrast previous research published by Jenkins and colleagues who demonstrate that GPR35 selectively couples to $G\alpha_{13}$ via Ca^{2+}

mobilisation following zaprinast activation (Jenkins *et al.*, 2011). Whilst the data presented here are initially suggestive of either assay or ligand bias, it is important to note that this study did not employ the use of an additional GPR35 agonist, such as zaprinast. Moreover, the potency reported here is 100-fold lower than those reported at BRET and IP1 assays for pamoic acid (Jenkins *et al.*, 2012). Evidently, more work is required to confirm these findings, alongside other, well-characterised, GPR35 ligands.

Lastly, trafficking of p115-RhoGEF GFP from the cytosol to the plasma membrane following co-transfection with CAM forms of either $G\alpha_{12}$ or $G\alpha_{13}$ was also assessed. Importantly, the findings are in line with previous reports of RhoGEF cell trafficking to the cell membrane in the presence of active $G\alpha_{12}$ or $G\alpha_{13}$ (Meyer *et al.*, 2008). Moreover, constitutively active $G\alpha_{13}$ has been shown to induce p115-RhoGEF translocation to promote selective activation of Rho A (Hart *et al.*, 1998) and given that GPR35 has been shown to couple to $G\alpha_{13}$ here, and in numerous other reports (Jenkins *et al.*, 2011, Jenkins *et al.*, 2012, Mackenzie *et al.*, 2014), evidence strongly indicates that GPR35 activation might lead to Rho A signalling via $G\alpha_{13}$. Importantly, this signalling pathway has been implicated in hypertension (Wirth, 2010), vessel remodelling and cardiac hypertrophy (Maruyama *et al.*, 2002, Cotton and Claing, 2009). Taking this together with research implicating GPR35 in numerous disease pathologies relating to the cardiovascular system inclusive of hypertension (Min *et al.*, 2010), heart failure (Min *et al.*, 2010, Ronkainen *et al.*, 2014) and coronary artery disease (Sun *et al.*, 2008); a potential mechanism of action is evident. To successfully identify a functional role for GPR35, this signalling axis must be investigated within an appropriate setting, relevant to cardiovascular disease.

3.3.1 Conclusions

Results from this study represent significant challenges for the elucidation of GPR35 function within rodent models, given that neither CID-2745687 nor ML-145 demonstrate

activity at rat or mouse orthologues of GPR35. Therefore, successful investigation of a role for GPR35 in rodent models will require close correlation with existing pharmacological insights derived from *in vitro* studies. Of course, whilst novel drug discovery has not always been limited by the requirement of rodent trials, existing clinical trials which have foregone this route have ultimately suffered due to a lack of information for the efficacy and bio-availability of a compound in an *in vivo* setting (Bindels *et al.*, 2013).

In conclusion, this study has contributed to the knowledge and understanding of species orthologue selectivity of GPR35 ligands and highlighted potential key binding positions for pamoic acid and zaprinast within TMD IV and VI. Importantly, information relating to species-selectivity of GPR35 agonists and antagonists will provide a secure basis to dissect the mechanism by which GPR35 might be mediating its effects, at least, within a human setting.

4 The role of GPR35 in vascular smooth muscle and endothelial cells and cardiomyocytes

4.1 Introduction

Although not widely investigated within the cardiovascular system, literature suggests that GPR35 expression and activation may have significant implications for various pathologies relating to the progression of vascular disease and cardiac dysfunction. Two such studies have highlighted a potential role for GPR35 in the development of early, acute phase vascular inflammation and consequential vessel calcification (Sun *et al.*, 2008, Barth *et al.*, 2009). First, a genetic study inclined to identify novel gene-biomarkers associated with hypertension and end-organ damage highlighted a significant association between the expression of a non-synonymous GPR35 SNP and coronary artery calcification burden within a hypertensive patient cohort, assessed by computed tomography (Sun *et al.*, 2008). Upon closer inspection, it became clear that this mutation, which resulted in a serine-arginine swap at position 294, was located within a highly conserved region of the cytoplasmic tail of GPR35 and might have consequential implications for G-protein coupling and subsequent signalling (Sun *et al.*, 2008). However, the significance of this has yet to be assessed. An alternative publication found circulating inflammatory mediator cells, inclusive of leukocytes and neutrophils, displayed robust endogenous GPR35 expression and this led investigators to assess their potential role in vascular inflammation (Barth *et al.*, 2009). In this, it was subsequently demonstrated that GPR35 activation, stimulated via KYNA, promoted β_1 integrin-mediated leukocyte arrest to an endothelial monolayer and this was quantified in a flow-chamber under vascular shear stress conditions (Barth *et al.*, 2009). Conflicting evidence for KYNA activation of human GPR35 aside, monocyte tethering, rolling and arrest to the endothelium is indicative of acute-phase inflammation within the vasculature and this study may have identified a potential role for GPR35 as an early mediator of progressive atherosclerosis (Barth *et al.*, 2009).

A role for GPR35 has also been investigated in the setting of cardiomyocyte hypertrophy and progressive cardiac remodelling, with further tentative implications for GPR35

expression in the development of hypertension. In a microarray screen of heart failure patients, GPR35 was reported to have increased expression levels in failing myocardial tissue (Min *et al.*, 2010). This study further reported that adenovirus-mediated overexpression of GPR35 induced hypertrophy and decreased cell viability in rat neonatal cardiomyocytes (Min *et al.*, 2010). Moreover, GPR35 knock-out mice were reported to have significantly increased blood pressure compared to wild-type littermates (Min *et al.*, 2010). The association between GPR35 expression and cardiomyocyte hypertrophy was more widely investigated in a recent report which recommended GPR35 as a novel gene-biomarker in the setting of progressive cardiac remodelling (Ronkainen *et al.*, 2014). Interestingly, authors demonstrated hypoxia-dependent increases in GPR35 expression within hypertrophic cardiomyocytes in an *in vitro* setting and this finding was further replicated in cardiac hypertrophy following induced acute MI in mice (Ronkainen *et al.*, 2014). Upon closer examination, it was revealed that a transcription factor, hypoxia inducible factor-1 (HIF-1), was able to bind to the promoter region of GPR35 and this resulted in an increase in GPR35 expression following exposure to hypoxic conditions (Ronkainen *et al.*, 2014). Taking this information together, it is evident that GPR35 expression and activation might have significant implications for disease pathologies relating to both vasculature and cardiac tissue and therefore further investigation is warranted.

The major challenges presented by the species-selective properties of GPR35 ligands have promoted continuous characterisation and identification of successful ligand pairs in order to elucidate a function for GPR35 (Jenkins *et al.*, 2012). The tryptophan metabolite kynurenic acid (KYNA) was the first reported endogenous GPR35 ligand (Wang *et al.*, 2006a) and whilst micromolar potency has been confirmed at rat GPR35, further analysis of β-arrestin recruitment demonstrate that KYNA activation of human GPR35 is almost undetectable (Jenkins *et al.*, 2011). Moreover, results in Chapter 3-2-4 demonstrate that KYNA also has limited activity at the mouse ortholog of GPR35. More recently, other

natural agonists of GPR35 were identified within the LPA family, specifically 2-acyl LPA (Oka *et al.*, 2010), however, there have not been any subsequent reports which explore this further. Given reports of extreme-species selectivity for KYNA and the evidence of alternative endogenous targets for both ligands (Stone, 1993, Lin *et al.*, 2010), GPR35 is still regarded as an orphan GPCR, prompting investigators to identify alternative surrogate ligands in order to successfully investigate functional roles for GPR35. The first identified and best utilised of these is zaprinast (Taniguchi *et al.*, 2006), a potent agonist at all species of GPR35, however, significantly more so at rodent orthologs and zaprinast is the customary ligand of reference in chemical screens targeting GPR35 (Deng and Fang, 2013, Mackenzie *et al.*, 2014, Jenkins *et al.*, 2011). Despite this, its use in functional assays is limited by its potency as an inhibitor of cGMP phosphodiesterase (PDE), specifically PDEs 5 and 6 (Gibson, 2001). Work from Jenkins et al, and others have reported detailed pharmacology for alternative novel, synthetic GPR35 ligands and this includes the identification of pamoic acid as a highly potent agonist at human GPR35 (Jenkins *et al.*, 2010, Zhao *et al.*, 2010). This study has also contributed to recently reported detailed species pharmacology for novel GPR35 antagonists CID-2745687 and ML-145, revealing that they are also highly selective for human GPR35 (Jenkins *et al.*, 2012). Given that pamoic acid and both GPR35 antagonists are highly potent for human GPR35 and not reported to target other receptors, they provide an excellent set of tools to assess GPR35 function in endogenously expressing cells of human origin.

The use of autologous human saphenous vein (HSV) is the most common surgical intervention for bypass of occluded multi-vessel coronary artery disease (CAD), despite use of alternative sources of graft such as internal mammary artery and advances in interventional revascularisation via coronary intervention (Anderson *et al.*, 2002). Although successful in reducing overall rates of mortality and morbidity in CAD patients, 50% of long term vein grafts become occluded due to intimal hyperplasia (Rienstra *et al.*, 2008). The pathophysiology of vein graft disease is defined by a cascade of events

leading to neointimal formation and graft occlusion; early graft failure and thrombosis can result from endothelial dysfunction and loss, due to injury by shear stress, from the coronary circulation (Shukla and Jeremy, 2012). Furthermore, ischaemia and subsequent reperfusion results in reactive oxygen species (ROS) production, contributing to endothelial and vascular smooth muscle cell (VSMC) death and inflammation via activation of the NFκB pathway. Importantly, NFκB is also integral to VSMC migration and proliferation via the modulation of matrix metalloproteinases (MMPs) and their endogenous tissue inhibitors (TIMPs) (Bond *et al.*, 2001, Bond *et al.*, 1999) (reviewed in (Wan *et al.*, 2012b). Therefore, the migration, proliferation and integrity of vascular cells, together with the deposition and activation of inflammatory mediators, is central for neointimal development and if left unchecked, can lead to graft occlusion via atheroma (Shukla and Jeremy, 2012). Current therapeutic options are limited and only by repeating the intervention is it possible to relieve an occluded graft. Therefore, vascular remodelling is an important target for the development of new therapies.

In agreement with published literature (Jenkins *et al.*, 2010), this study has shown that GPR35 couples to $G\alpha_{12/13}$, although others have reported $G\alpha_{i/o}$ coupling leading to ERK1/2 activation (Zhao *et al.*, 2010). Following its interactions with Rho A and subsequent activation of ROCK1/2 effectors, the coupling and activation of $G\alpha_{12/13}$ mediated signalling has been widely demonstrated to have significant implications for the progression of various pathologies relating to cardiovascular disease including angiogenesis, vascular remodelling, neointima formation and cardiac hypertrophy (Wirth, 2010, Moriki *et al.*, 2004, Takefuji *et al.*, 2012).

4.1.1 Hypothesis and aims

Given that GPR35 has been reported to selectively couple to the $G\alpha_{13}$ signalling pathway (Jenkins *et al.*, 2010), a coupling well understood to promote pathways governing

vasculature function via Rho A activation (Wirth, 2010), it was hypothesised that GPR35 activation might play a functional role within the vascular cell population. Therefore, this study was designed to investigate a functional role for GPR35 in the setting of acute vascular injury using *in vitro* models in human primary saphenous vein endothelial and smooth muscle cells, for the first time. Moreover, given evidence that GPR35 expression is implicated in cardiomyocyte hypertrophy and progressive cardiac remodelling, a role for GPR35 activation in the setting of cardiomyocyte hypertrophy was also explored using a novel, highly potent GPR35 ligand. To investigate these in detail, a series of aims are outlined below:

- To assess the endogenous expression levels of GPR35 in human tissue and primary vascular endothelial and smooth muscle cells.

- To investigate the effects of human-selective GPR35 ligands on actin-cytoskeleton organisation in primary human vascular smooth muscle and endothelial cells endogenously expressing GPR35.

- To investigate the effects of human-selective GPR35 agonism and antagonism on the migratory and proliferative capacity of primary human vascular endothelial and smooth muscle cells.

- To investigate the effects of GPR35 agonists on actin-cytoskeleton organisation and hypertrophy in cardiomyocytes.

4.2 Results

4.2.1 The expression of GPR35 in human tissue and vascular cells

Expression of GPR35 is widely reported in a variety of tissues. However, much of the research previously conducted focuses upon a limited range of tissue and the methods used to detect expression are inconsistent and imprecise (O'Dowd *et al.*, 1998, Wang *et al.*, 2006a). In this study, the expression of human GPR35 mRNA was comparably quantified in a wide ranging array of tissue samples and isolated primary vascular cells via real-time, quantitative reverse transcription-polymerase chain reaction (qRT-PCR). Consistent with previous literature reports (O'Dowd *et al.*, 1998, Taniguchi *et al.*, 2006), GPR35 was detected in the small intestine, colon and spleen and these were 347.3-fold, 122.4-fold and 22.5-fold higher than in heart tissue, respectively. (Figure 4-1.A). However, it is notable that GPR35 mRNA expression could also be detected in many other tissues of the body including the kidney, cervix, ovaries and prostate, albeit at lower levels (6.7-11.4-fold, relative to heart expression) (Figure 4-1.A). Most interestingly, primary human saphenous vein endothelial cells (HSV EC) demonstrated significant levels of GPR35 expression (92.7-fold, relative to heart expression), and these levels were comparable to those found in the colon (Figure 4-1.A). Of course, it was important to recognise that GPR35 expression within niche cell populations, such as HSV EC, might not be best compared to whole tissue expression which constitutes multiple cell-types. Therefore, to investigate if GPR35 was also highly expressed in alternative vascular cells, expression levels were examined in primary human saphenous vein endothelial and smooth muscle cells (HSV EC/ SMCs), and human umbilical vein endothelial cells (HUVECs) (Figure 4-1.B). To provide a positive control for GPR35 expression, a doxycycline-inducible cell line stably expressing human GPR35 and human colon adenocarcinoma cell line, HT-29, were included. Robust equivalent levels of GPR35

expression could be detected across all vascular cell types tested (Figure 4-1.B).,

Importantly, this evidence provided a strong platform to endogenously target GPR35 in

vascular cells using previously identified, high-potency, human-selective ligands.
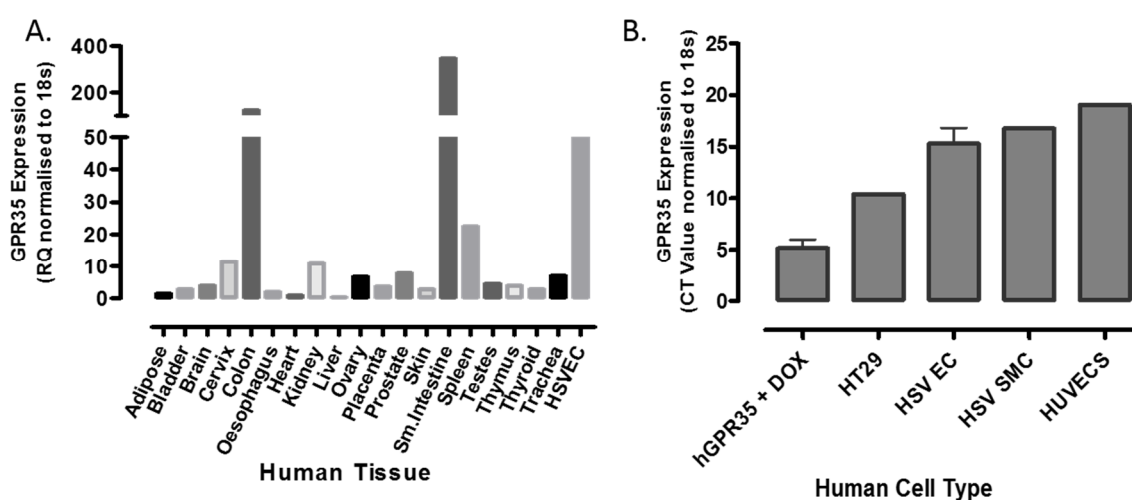
Figure 4-1. GPR35 is robustly expressed within human tissue and primary vascular cells.

A. hGPR35 mRNA expression in a commercially available, healthy human tissue panel

and primary human saphenous vein endothelial cells (HSV EC), expressed as RQ relative

to hGPR35 expression in the heart and normalised to ribosomal 18s. B. hGPR35 mRNA

expression in a range of immortalised and primary cells; stable FLAG-hGPR35-eYFP

(positive control), HT-29 cells (positive control), human umbilical vein endothelial cells

(HUVECS), HSV EC and human saphenous vein smooth muscle cells (HSV SMC).

Values are expressed as cycle threshold (CT), for which an inverse relationship is

indicative of high expression levels, and normalised to ribosomal 18s. All data are

representative of n=3-4 biological replicates and were performed in technical duplicates.

4.2.2 The effects of human-selective GPR35 ligands on the cytoskeletal arrangement of cells endogenously expressing GPR35.

It is well understood that $G\alpha_{12/13}$ activation leads to downstream signalling via RhoA and that subsequent effectors (ROCK1/2) promote the reorganisation of the actin-cytoskeletal architecture via an inhibition of MLCP and up-regulation of myofilament proteins adducin and prolifin (Wirth, 2010). In Chapter 3-2-9, it was shown that human GPR35 activation promoted $G\alpha_{12/13}$ coupling and that tonic $G\alpha_{12/13}$ activation results in the translocation of p115-RhoGEF from the cytosol to the plasma membrane where it is hypothesised to activate RhoA (Hart *et al.*, 1998, Maruyama *et al.*, 2002). Therefore, the effects of GPR35 ligand exposure on the cytoskeletal arrangement of engineered and endogenously GPR35 expressing cells was tested here. The effects of human-selective ligands were first assessed in HEK293t cells engineered to express GPR35 in a doxycycline-inducible manner (Figure 4-2). Importantly, the induction of GPR35 expression did not introduce any changes to actin cytoskeleton and the architecture of intracellular actin filaments remained consistent across the cross-sectional cell area (Figure 4-2.). On the contrary, following exposure of doxycycline-treated cells to 500nM of pamoic acid for 45 minutes, close inspection of the cytoskeletal architecture revealed a definite alteration in cell morphology whereby the cells became contracted and exhibited distinctly fewer intracellular filaments (Figure 4-2). Importantly, pamoic acid exposure to cells lacking GPR35 expression i.e. cultured in the absence of DOX, had no effect on the cytoskeleton indicating that its effects were indeed mediated via GPR35. Furthermore, co-administrating pamoic acid with either of the human-selective antagonists, CID-2745687 or ML-145, at equal concentrations (100nM) prevented any pamoic acid-induced changes in the actin cytoskeleton (Figure 4-2). Given that two distinct human-selective antagonists produced identical actions, it was clear that pamoic acid was mediating its effects on the actin cytoskeletal architecture via GPR35 activation.

To date, there have been no studies on the functional aspects of these ligands in human vascular cells. Therefore, the effects of these ligand pairs on HSV SMC morphology and cytoskeletal rearrangement were next analysed. Following 45 minutes incubation with 100nM pamoic acid, a striated, contractile and elongated morphology was evident in HSV SMCs (Figure 4-3). This phenotype was not apparent in HSV SMCs in serum free conditions or following the co-administration of pamoic acid with the antagonists CID-2745687 or ML-145 (Figure 4-3.A.). By quantifying cell length via ImageJ analysis, it was evident that pamoic acid exposure significantly lengthened HSV SMCs by up to 74 ±15.7µm, in comparison to agonist free conditions ($p < 0.001$) (Figure 4-3.B). Most importantly, this effect was blocked in the presence of equal concentrations (100nM) of CID-2745687 and ML-145 (Figure 4-3.B.). Closer inspection of the cytoskeletal architecture revealed that pamoic acid induced substantial actin filament rearrangement in comparison to serum free conditions, indicative of a migratory phenotype in HSV SMC (Figure 4-3.C).
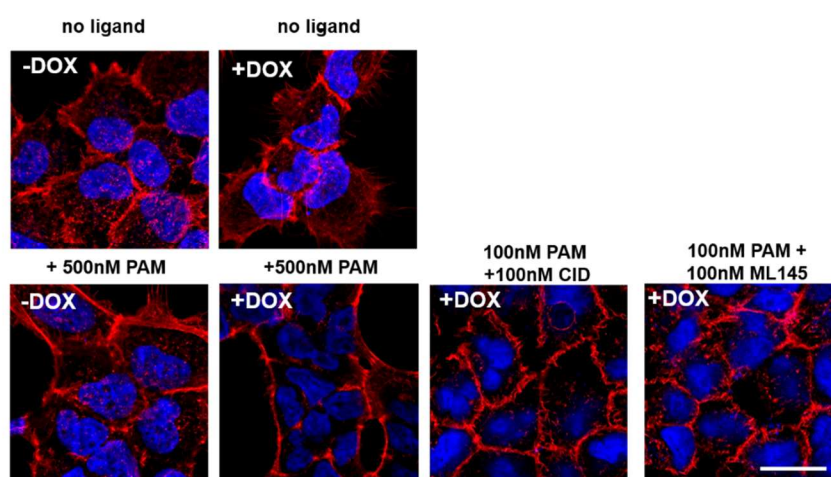
Figure 4-2. CID-2745687and ML-145 block pamoic induced actin-cytoskeletal reorganisation in cells stably expressing hGPR35.

Representative images of doxycycline (DOX) inducible Flp-In™ T-REx™ cells stably expressing FLAG-hGPR35-eYFP in the presence and absence of 100ng/mL doxycycline (i.e. +/- human GPR35eYFP). 24 hours later, cells were stimulated with 500nM pamoic acid (PAM) alone or 100nM PAM + 100nM CID-2745687 (CID) or ML-145 for 45 minutes. Cells were fixed with 4% PFA, stained for F-actin using TRITC actin phalloidin stain and mounted to glass coverslips with ProLong® Gold antifade with DAPI. Slides were imaged via spinning disk illumination VivaTome™ microscopy. Visible actin reorganisation in the presence of pamoic acid is evident and this is blocked when co-administered with antagonists CID and ML-145. All images are representative of n=3 individual experiments. Scale bar represents 20µm.
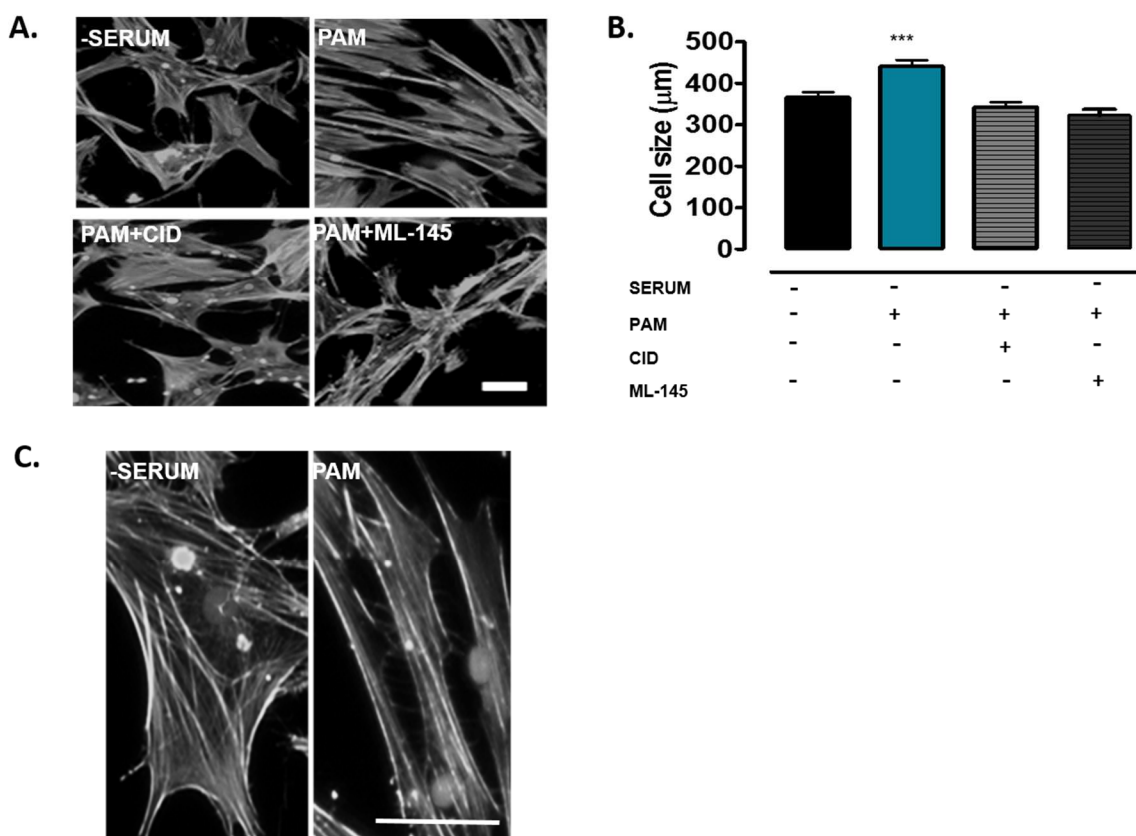
Figure 4-3. Pamoic acid induces changes in HSV SMC morphology, cytoskeletal arrangement and size and this is blocked in the presence of antagonists CID-2745687 and ML-145.

A. A comparison of the morphological differences in quiescent human saphenous vein smooth muscle cells (HSV SMC) which were fixed and stained for F-actin following stimulation with 100nM of pamoic acid (PAM) +/- antagonists CID-2745687 (CID) or ML-145 for 45 minutes. B. Quantification of HSV SMC size in the presence of 100nM pamoic acid +/- antagonists CID or ML-145. C. Comparative qualitative images, demonstrating cytoskeletal re-arrangement in response to stimulation with 100nM pamoic acid and serum free conditions, in HSV SMC fixed with 4% PFA, stained for F-actin using TRITC actin phalloidin stain and mounted to glass coverslips with ProLong® Gold antifade with DAPI. All data are representative of n=3-4 individual patient cells. Quantification of cell size was analysed using ImageJ software. Statistical significance *** $p<0.001$. Scale bar represents 100μm.

4.2.3 The effect of human-selective GPR35 ligands on HSV SMC migration

To assess a possible functional role for GPR35 in vascular remodelling, migration of HSV SMC was next assessed via a scratch and wound healing assay in the presence of GPR35 ligands zaprinast or pamoic acid. Briefly, following a 48-hour exposure to serum free conditions, horizontal scratches were applied to a confluent monolayer of quiescent HSV SMCs using a 200µL pipette tip. HSV SMCs were stimulated with ligands in serum free media and imaged at intervals of 6-8 hours in order to assess any effect of GPR35 ligands on the migration of cells into the wounded area. Both zaprinast and pamoic acid significantly enhanced migration by up to 25% in comparison to serum free conditions ($p<0.001$) and this occurred in a concentration-responsive manner for concentrations of up to 500nM for zaprinast and 100nM for pamoic acid. However, migration did not continue to increase following exposure above these concentrations for either agonist (Figure 4-4.B. and Figure 4-5.A., for zaprinast and pamoic acid respectively). Next, the effects of co-administering of GPR35 antagonists CID-2745687 and ML-145 at 100nM were assessed. Essentially, both antagonists completely abolished zaprinast and pamoic acid induced migration at 36 hours ($p>0.05$, compared to –serum) (Figure 4-4.C. and Figure 4-5.B., for zaprinast and pamoic acid respectively). Pamoic acid-induced migration was also assessed at earlier time points of 20 and 30-hours ($P<0.001$) and the ability of GPR35 antagonists to effectively block this was also observed (Figure 4-5.C.).

Importantly, neither antagonists had any effect on the basal migration of HSV SMC at these concentrations ($p>0.05$, compared to –serum) (Figure 4-6.A). However, serum induced migration of HSV VSMC was inhibited at higher concentrations of 1µM and 10µM for both antagonists (Figure 4-6.B). These data suggest that physiological factors in normal serum might mediate HSV SMC migration via GPR35 activation and highlights that GPR35 antagonism may have therapeutic utility.
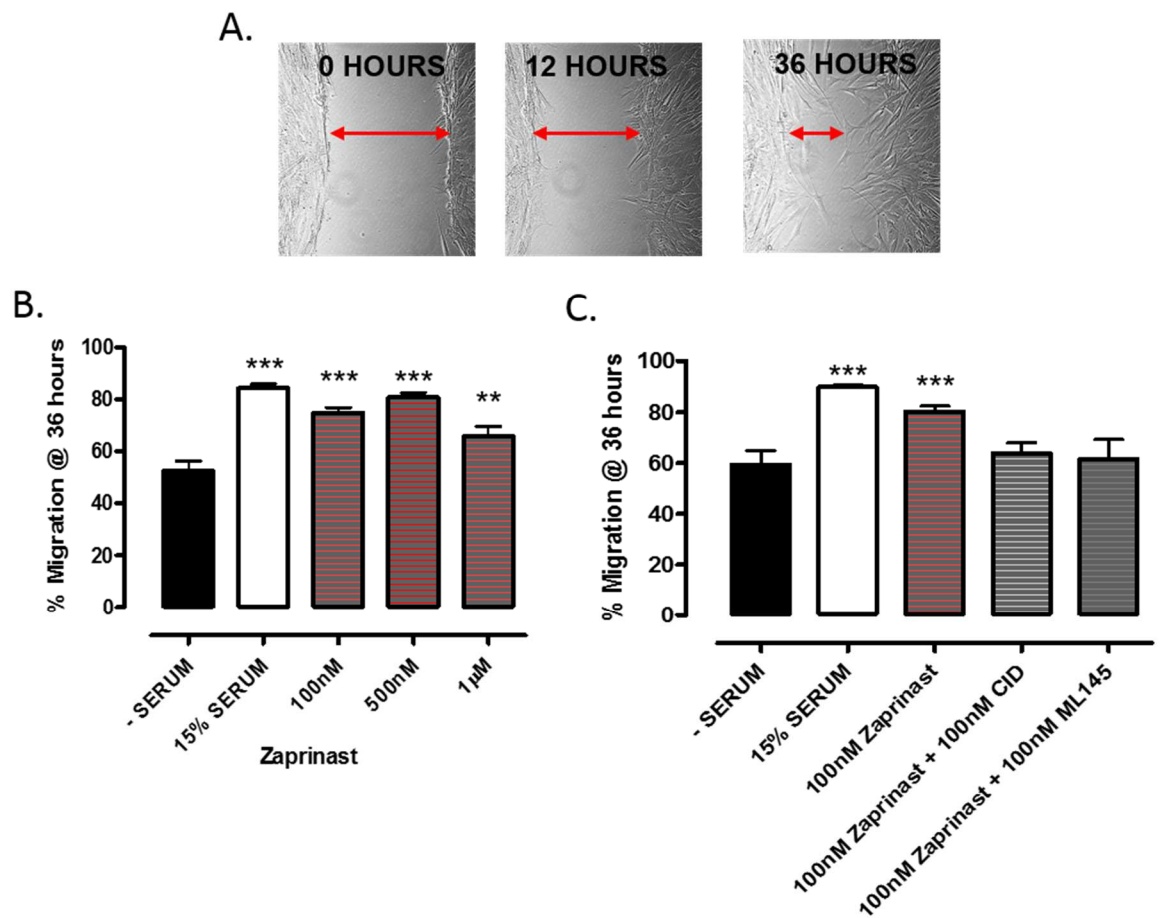
Figure 4-4. The migratory capacity of HSV SMC is increased following sustained incubation with zaprinast and this is blocked by co-administering CID-2745687 and ML-145.

A. Representative images of invading migratory human saphenous vein smooth muscle cells (HSV SMCs) into the wound following zaprinast incubation over a time course of 36 hours. B. Migration of confluent, quiescent HSV SMC in the presence of increasing concentrations of the reference GPR35 agonist, zaprinast (100nM-1µM). C. Migration of confluent, quiescent HSV SMC in the presence of agonist zaprinast and +/- CID-2745687 or ML-145. All data were acquired via scratch-wound healing assay at 36 hours, expressed as a percentage of migration at time point 0 and are representative of n=3 individual patient experiments. Statistical significance; ** $p < 0.01$, *** $p < 0.001$ (compared to –SERUM control).
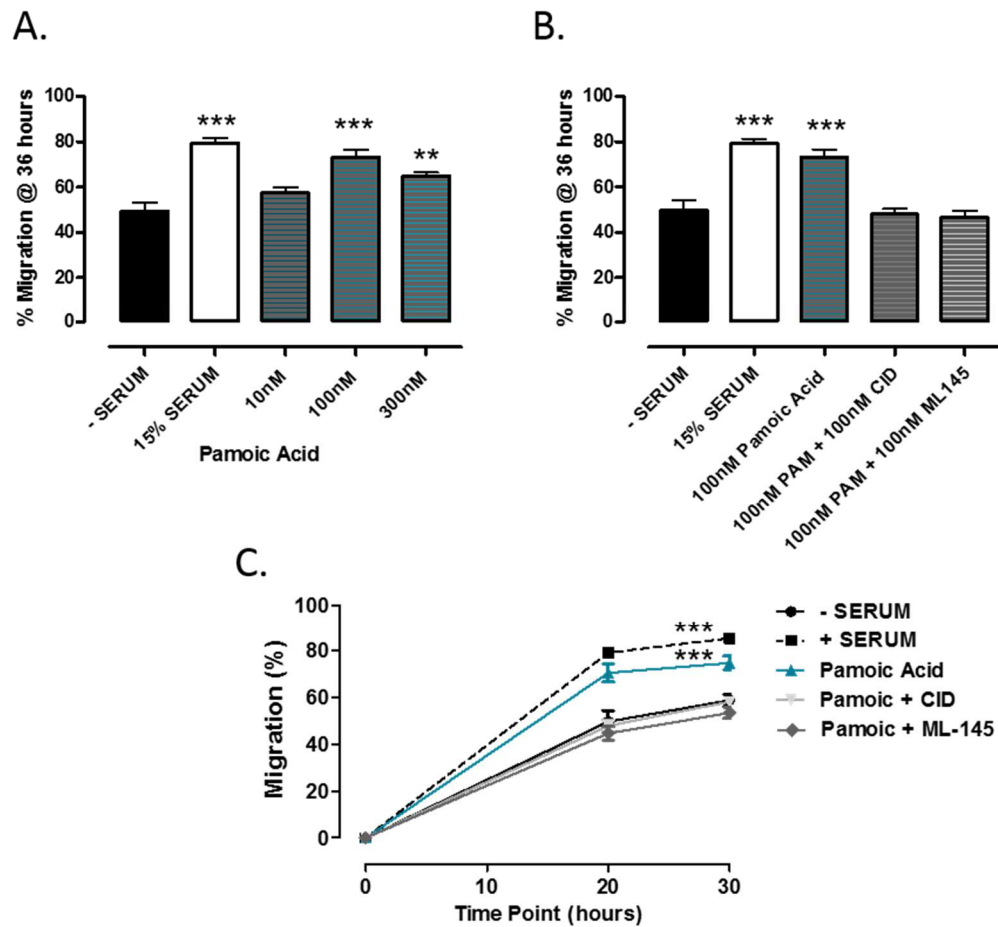
Figure 4-5. Pamoic acid induced HSV SMC migration is blocked in the presence of GPR35 antagonists CID-2745687 and ML-145.

A. Migration of confluent, quiescent HSV SMC in the presence of increasing concentrations of hGPR35 agonist pamoic acid (PAM) (10-300nM). B. Migration of confluent, quiescent HSV SMC in the presence 100nM hGPR35 agonist pamoic acid (PAM) +/- CID-2745687 or ML-145. C. Comparative migratory response of confluent, quiescent HSV SMC in the presence 100nM hGPR35 agonist pamoic acid (PAM) +/- CID-2745687 or ML-145 over a time course of 30 hours. All data was acquired via scratch-wound healing assay at 30-36 hours, expressed as a percentage of migration at time point 0 and are representative of n≥3 individual patient experiments. Statistical significance; ** $p < 0.01$, *** $p < 0.001$ (compared to –SERUM control).
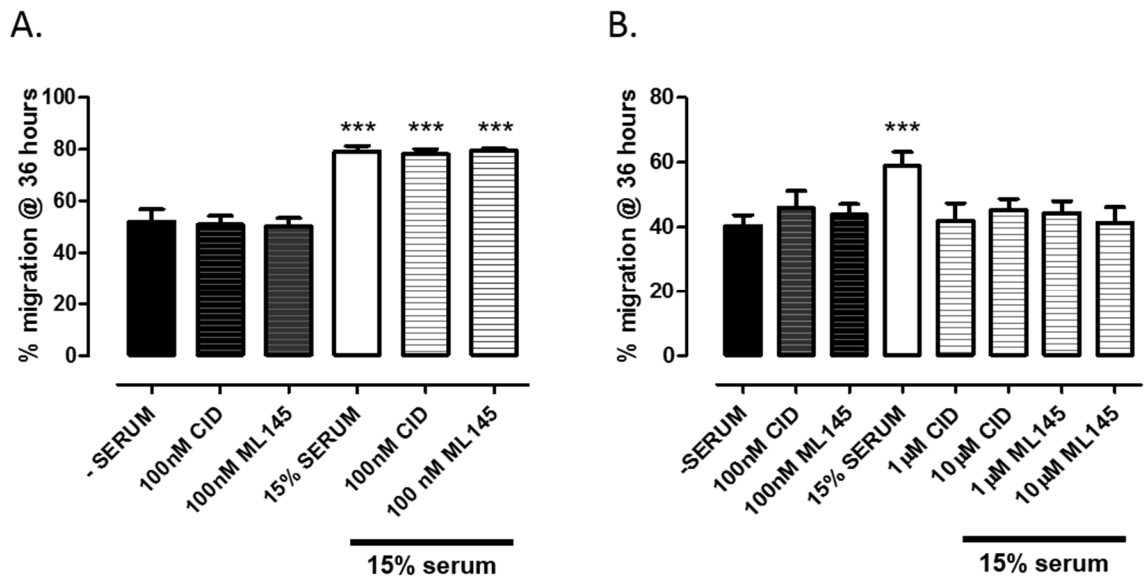
Figure 4-6. Human GPR35 antagonists CID-2745687 and ML-145 block serum induced HSV SMC migration at high concentrations.

A. Migration of confluent, quiescent HSV SMC in the presence of hGPR35 antagonists CID-2745687 and ML-145 at 100nM in the presence and absence of 15% serum. B. Migration of confluent, quiescent HSV SMC in the presence of hGPR35 antagonists CID-2745687 and ML-145 at 100nM in the absence of 15% serum and 1μM and 10μM in the presence of 15% serum. All data was acquired via scratch-wound healing assay at 36 hours, expressed as a percentage of migration at time point 0 and are representative of n=2 individual patient experiments. Statistical significance, based on 3 technical replicates, each with 10 cross-sectional wound measurements; *** $p < 0.001$ (compared to –SERUM control).

4.2.4 GPR35-induced migration of HSV SMCs is mediated via the Rho A-ROCK1/2 signalling axis.

Given that GPR35 activation in HSV SMC leads to an alteration of the actin-cytoskeleton and subsequent increased migration, the involvement of the RhoA/ ROCK 1/2 signalling axis was next assessed. To test if pamoic acid directly induced RhoA activation, an immunoprecipitation RhoA pull-down assay was employed in HSV SMCs following a short, 5 minute exposure to 10-500nM pamoic acid. Pamoic acid concentrations of 10-100nM produced an increase in GTP-bound RhoA (activated RhoA) protein in HSV SMCs (Figure 4-7.A).

To investigate the involvement of subsequent ROCK1/2 effectors on HSV SMC migration, pamoic acid was then co-administered alongside two distinct Rho A pathway inhibitors; Y-27632 and Y16, in a wound-healing assay (Figure 4-7.C&D). Both inhibitors blocked pamoic acid induced migration in line with GPR35 antagonists ($p<0.001$), suggesting that GPR35 activation mediates effects on migration via the Rho A, ROCK1/2 signalling axis. HSV SMC viability was unaffected when exposed to high concentrations of the ROCK inhibitor Y-27632 (10µm), assessed via an MTS assay (Figure 4-7.B).
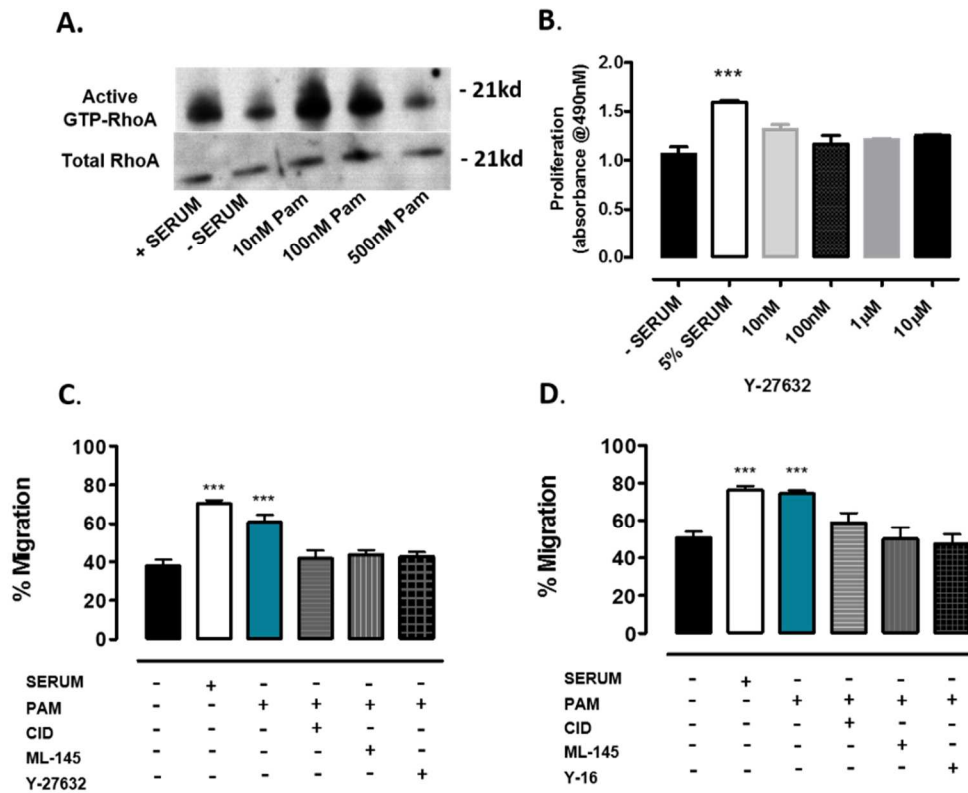
Figure 4-7. Pamoic acid induces RhoA activation in HSV SMC and pamoic acid induced migration is blocked in the presence of ROCK inhibitors Y-27632 and Y-16.

A. Expression of total and active GTP-RhoA protein in human saphenous vein smooth muscle cells (HSV SMCs) following 5 mins incubation with increasing concentrations of pamoic acid (10-500nM), measured via a RhoA pull-down immunoprecipitation assay. B. The proliferative response of quiescent HSV SMC in the presence of increasing concentrations of the ROCK inhibitor Y-27632 (10nM - 10µM) in the absence of 5% serum, measured via MTS assay at 48 hours. C&D. The migratory response of confluent, quiescent HSV SMC in the presence of hGPR35 agonist pamoic acid (PAM) +/- CID-2745687, ML-145 (100nM) or 10µM ROCK inhibitors C) Y-27632 and D) Y16, measured by scratch-wound healing assay at 36 hours. Migratory experiments are representative of n=3-5 individual patients. For RhoA protein quantification, n=1. Statistical significance; *** p<0.001 (compared to –SERUM control).

4.2.5 The effects of human-selective GPR35 ligands on HSV SMC proliferation.

To account for the possibility that increased migration following GPR35 agonist stimulation was not simply due to an increased rate of cell proliferation, an MTS assay was employed. Essentially, the MTS assay is inclusive of both proliferation status and metabolic integrity via colorimetric measurement of formazan, a breakdown product of tetrazole, reduced enzymatically in healthy and proliferating cells (Wang *et al.*, 2010). Neither zaprinast nor pamoic acid induced or prevented HSV SMC proliferation in concentrations equivalent to those used to assess migration (P>0.05) (Figure 4-8.). Moreover, it was also clear that neither CID-2745687 nor ML-145 had any effect on serum induced HSV SMC proliferation or cell-viability (Figure 4-8.D). Taking these results together, GPR35 stimulation enhances the migration of HSV SMC without affecting proliferation.
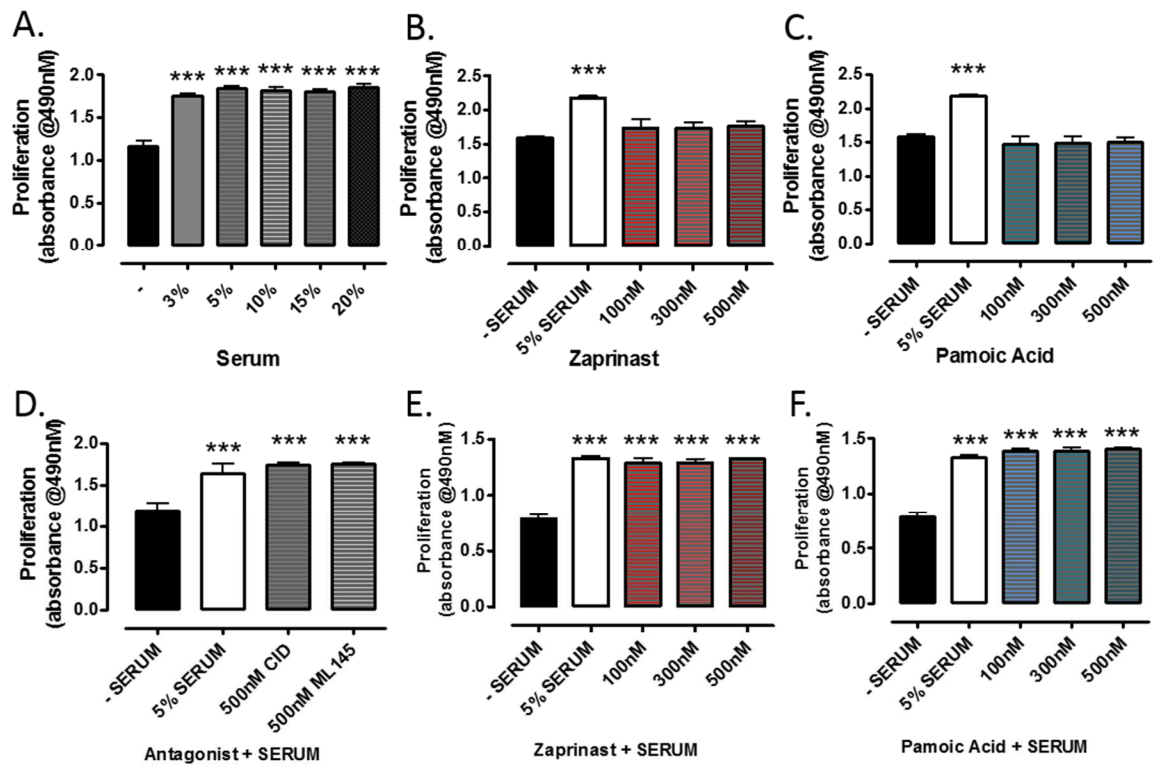
Figure 4-8. HSV SMC proliferation is unaffected by the presence of GPR35 agonists and antagonists.

A. Proliferation of HSV SMCs following exposure to increasing serum concentrations (0-20%) at 48 hours. B&C. Increasing concentrations (100-500nM) of B) zaprinast or C) pamoic acid do not elicit a proliferative response in quiescent HSV SMC in the absence of serum. D, E & F. Proliferation of HSV SMC induced by 5% serum is unaffected by D) 500nM of GPR35 antagonists CID-2745687 (CID) or ML-145 or increasing concentrations (100-500nM) of E) zaprinast and F) pamoic acid. All data were acquired via MTS assay at 48 hours and are expressed as absorbance at wavelengths of 490nm. All data are representative of n=3-4. Statistical significance; *** $p<0.001$ (compared to –SERUM control).

4.2.6 The effects of human-selective GPR35 ligands on HSV EC morphology, migration and proliferation.

Impaired vascular endothelial cell integrity is implicated in the incidence of vein graft occlusion and, given that high expression levels of GPR35 have been demonstrated in these cells, the effects of the presence of GPR35 ligands on HSV EC were assessed. In contrast to the effects of GPR35 on HSV SMCs; HSV EC morphology, actin-cytoskeletal architecture and migratory capacity remained unchanged following stimulation with increasing doses of pamoic acid ($p>0.05$, compared to –serum control) (Figure 4-9.A & B). Conversely, in assessing the proliferative capacity and viability of HSV EC via an MTS assay, a concentration-dependent increase in absorbance at 490nm following exposure to both zaprinast and pamoic acid was evident at 24 hours, $p<0.001$ (Figure 4-9.D & E). These results indicated that GPR35 agonists induced an increased metabolic response in HSV EC, suggestive of an increase in cell growth.

For a more accurate measurement of cell proliferation, a second assay was employed to measure the incorporation of 5-Bromodeoxyuridine (BrdU) (a synthetic analogue of thymidine) into cells during the progressive growth cycle. Essentially, results from BrdU incorporation directly correlated with those obtained via MTS. BrdU incorporation in HSV EC was significantly increased following exposure to concentrations of pamoic acid ranging from 50-500nM (Figure 4-10.B). Moreover, the proliferative response induced by 500nM of pamoic acid ($p<0.001$) was also examined in the presence of GPR35 antagonists and was found to be completely abolished in the presence of two concentrations of either CID-2745687 (Figure 4-10.E) or ML-145 (Figure 4-10.F). This information indicates that GPR35 activation is involved in maintaining HSV EC integrity and cell cycle progression. Notably, 24-hour incubation with CID-2745687 alone did not induce HSV EC proliferation (Figure 4-10.C), however, this was not the case for ML-145, which increased proliferation at 500nM ($p<0.01$) (Figure 3-10.D).
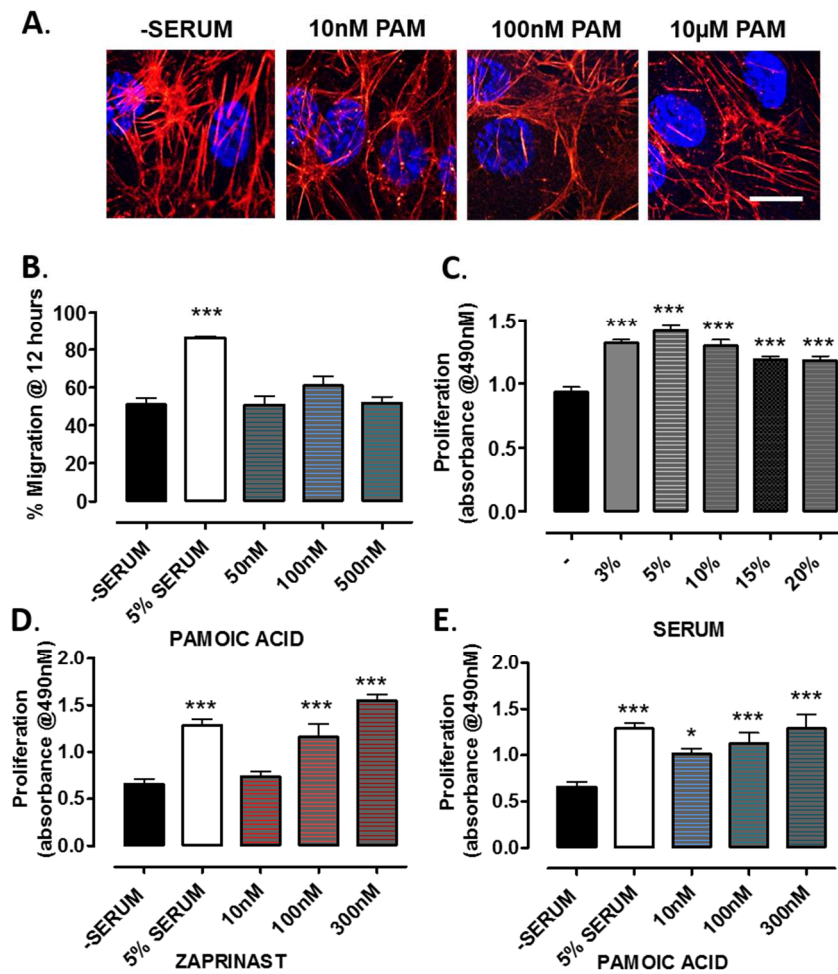
Figure 4-9. GPR35 agonist stimulation induces HSV EC proliferation.

A. Representative images of the human saphenous vein endothelial cells (HSV ECs) cytoskeleton, fixed and stained for F-actin (TRITC phalloidin) following stimulation with increasing concentrations of pamoic acid (PAM) (10nM-10µM) for 45 minutes. B. The migratory response of confluent, quiescent HSV EC was unaffected in the presence of increasing concentrations of pamoic acid (PAM) (50-500nM) measured by a scratch-wound healing assay at 12 hours. C, D & E. The increased proliferative response of HSV ECs following exposure to increasing concentrations of C) serum (0-20%), D) zaprinast (10-100nM) and E) pamoic acid (10-100nM). All data were acquired via MTS assay at 24 hours, expressed as absorbance at 490nm. All data are representative of n=3-5 individual patient experiments. Statistical significance; * $p<0.05$, *** $p<0.001$ (compared to –SERUM control). Scale bar represents 20µm.
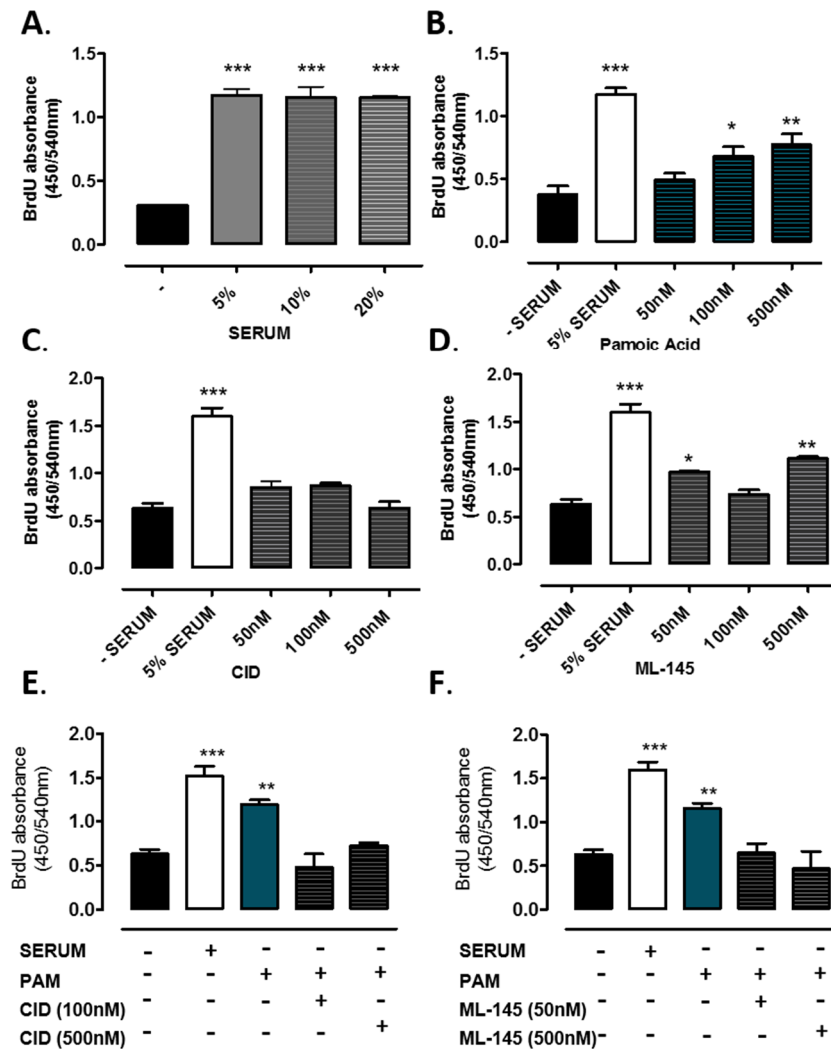
Figure 4-10. Pamoic acid-induced proliferation in HSV ECs is blocked by human-selective GPR35 antagonists CID-2745687 and ML-145.

The proliferative response of human saphenous vein endothelial cells (HSV ECs) exposed to increasing concentrations of A. serum (0-20%), B. pamoic acid, C. CID-2745687 (CID) and D. ML-145 (50-500nM). C & D. The response induced by 100nM pamoic acid was blocked by two concentrations of human selective GPR35 antagonists D. CID (100nM/500nM) and E. ML-145 (50nM/500nM). All data was acquired via BrdU incorporation at 24 hours, expressed as a ratio of the absorbance at 450/540nm. All data are representative of n=2 individual patient experiments. Statistical significance, based on 3 technical replicates; * $p<0.05$, ** $p<0.01$, *** $p<0.001$ (compared to –SERUM control).

4.2.7 The effects of zaprinast and the novel high-potency agonist amlexanox in H9c2 cardiomyocytes.

Results from this study have demonstrated that GPR35 activation leads to significant changes in the cytoskeletal architecture of vascular smooth muscle cells and given that previous studies indicate that GPR35 expression is up-regulated in the setting of heart failure and cardiac hypertrophy (Min *et al.*, 2010, Ronkainen *et al.*, 2014), it was important to assess the effect of GPR35 ligands in this setting. Given that GPR35 over expression has been demonstrated to elicit a hypertrophic response, the incorporation of a transient transfection protocol into a cardiomyocyte hypertrophy assay was first optimised. Using a rat neonatal cardiomyocyte cell line (H9c2), an appropriate positive control for cell hypertrophy was of critical importance. Published reports demonstrate that 100nM of angiotensin II (AngII) elicits a significant hypertrophic response in H9c2 cardiomyocytes, following a 96-hour incubation period (Flores-Munoz *et al.*, 2011). However, as the aim was to transfect a GPR35 expression vector into the H9c2 cardiomyocytes first optimisation of the time-frame to enable transfection and AngII stimulation was performed. AngII at 200nM effectively induced significant hypertrophy in H9c2 cardiomyocytes at 48-hours and this was measured by an increase in cell size by up to $44.8 \pm 4.2\mu m$ ($p<0.001$), and this was not significantly different to H9c2 cell size following incubation with 100nM AngII at 96-hours (Figure 4-11.A). To ensure efficient ratGPR35 transfection in H9c2 cardiomyocytes, expression levels were assessed via real-time qRT-PCR. Endogenous GPR35 expression in H9c2 cardiomyocytes was unchanged by the presence of serum or transfection reagent, x-fect (Figure 4-11.B.). However, following exposure to 200nM AngII, endogenous expression of rat GPR35 increased by >2-fold in H9c2 cardiomyocytes ($p<0.001$, compared to – serum) (Figure 4-11.B.). Most importantly, rat GPR35-eYFP transfection increased expression by >5000-fold, indicative of highly efficient transfection (Figure 4-11.B.).

With the exception of zaprinast, potent ligands to assess functional activation of GPR35 in rodent orthologs were previously lacking. However, most recently, amlexanox was identified as a high-potency agonist at rat GPR35 (Mackenzie *et al.*, 2014). Activation of GPR35 was confirmed via a β-arrestin-receptor interaction assay (Figure 4-12.), revealing similar potencies (EC_{50} = 4.5nM ± 0.173) to those previously reported for rat GPR35 (Mackenzie *et al.*, 2014).

To assess the effects of GPR35 ligands on cardiac hypertrophy, quiescent H9c2 cardiomyocytes expressing rat GPR35-eYFP remained in serum free conditions or were stimulated with 200nM of either zaprinast or amlexanox. Non-transfected cells were exposed to 200nM AngII or maintained in serum free media alone. After 48-hours, cells were fixed, stained for F-actin using TRITC-phalloidin and mounted on glass coverslips for subsequent fluorescence imaging and cell size quantification. Conflicting with established reports, there were no differences in the H9c2 cardiomyocyte size in ratGPR35-eYFP transfected cells compared to non-transfected, non-stimulated cells (128.0 ±4.9μm and 133.1 ±3.0μm, for transfected and non-transfected cells resepectively), and this was also true of cell morphology (Figure 4-13.A.). However, this was not the case following exposure to GPR35 agonists and quantification of cell size revealed that ratGPR35-eYFP expressing cells stimulated with either zaprinast or amlexanox exhibited increased cell size of up to 44 ±8μm, compared to unstimulated H9c2 cells in serum free conditions and those transfected with ratGPR35-eYFP alone (Figure 4-13.B.). Furthermore, distinct alterations in the cytoskeletal architecture in ratGPR35-eYFP expressing cells stimulated with either ligand were evident, including striated actin filaments aligning in a parallel fashion, indicative of a hypertrophic phenotype (Figure 4-13.A.). These changes were not evident in unstimulated H9c2 cardiomyocytes transfected with rat GPR35-eYFP and therefore, this evidence suggests that GPR35 ligand exposure and thus activation is required to elicit a hypertrophic response in H9c2 cardiomyocytes. Notably, following

stimulation with either zaprinast or amlexanox, internalisation and clustering of rat GPR35-eYFP is clear, representative of receptor activation (Figure 4-13.A.)
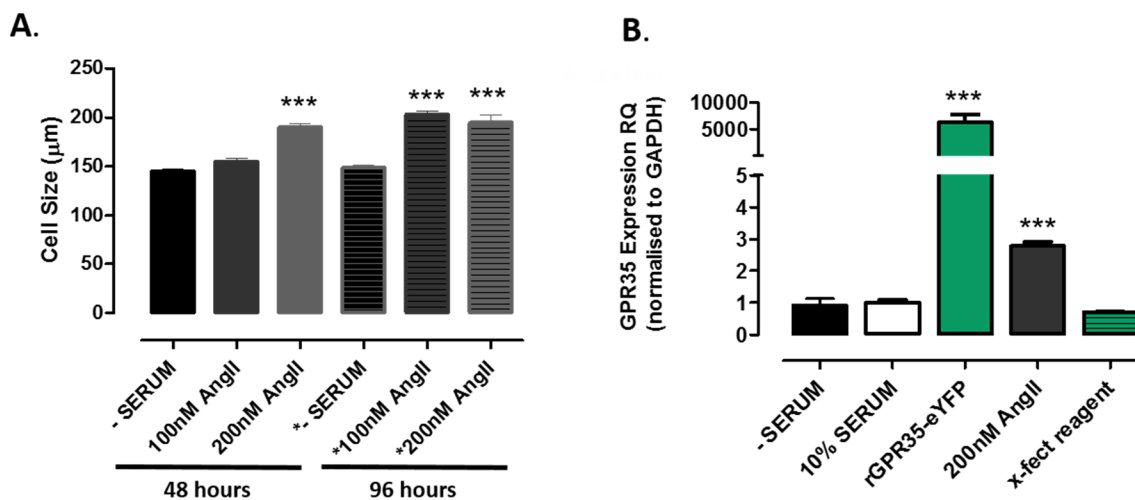
Figure 4-11. Optimisation of the hypertrophy assay for AngII incubation and rat-GPR35 transfection in H9c2 cells.

A. H9c2 cardiomyocytes were incubated with 100nM or 200nM angiotensin II (AngII) for either 48 or 96 hours. Cells were then fixed, using 4% PFA, stained for F-actin using TRITC-phalloidin and mounted on to glass coverslips with ProLong® Gold antifade with DAPI. Cell size was quantified using ImageJ software. B. H9c2 cells were plated in 6-well clear plates in serum free media. 24 hours later, cells were exposed to the following conditions; –serum, 10% serum or 200nMAngII. Alternatively, cells were transfected with ratGPR35-eYFP using X-fect reagent in serum free medium. After a 48 hour period, GPR35 expression was analysed via real-time qRT-PCR and was normalised for endogenous GAPDH expression, using respective TaqMan probes. Data are expressed as RQ, relative to serum free conditions. Data are representative of n=2 experiments. Statistical significance is based upon three technical replicates, with ten fields of view per replicate for the quantification of cardiomyocyte size; *** *p<0.001*, compared to – serum conditions.
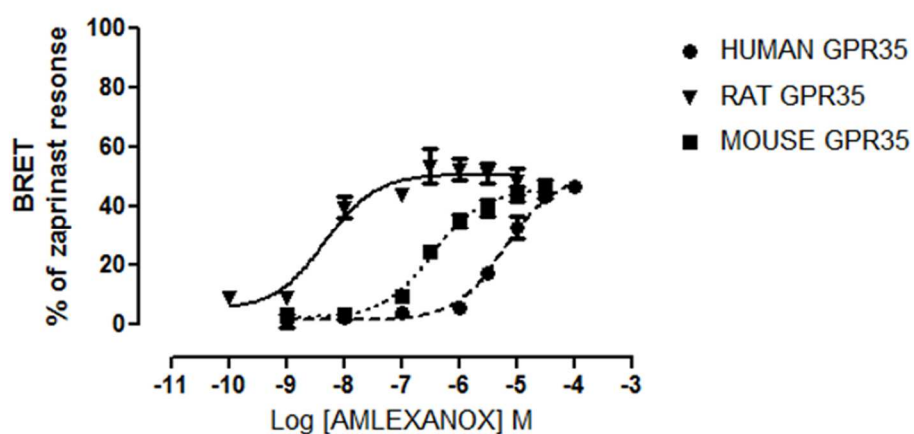
Figure 4-12. Amlexanox is a novel high-potency agonist for rat GPR35.

Representative concentration-response curves derived from a β-arrestin-2-receptor interaction assay in HEK293t cells transfected with β-Arrestin-2-*Renilla*-luciferase and either FLAG-humanGPR35-eYFP, FLAG-ratGPR35-eYFP or FLAG-mouseGPR35-eYFP in the presence of increasing concentrations of novel GPR35 agonist amlexanox. All data are representative of n=1 experiments, values are displayed as a mean % of maximal zaprinast response, +/- SEM and were performed in triplicate.

A.

B.
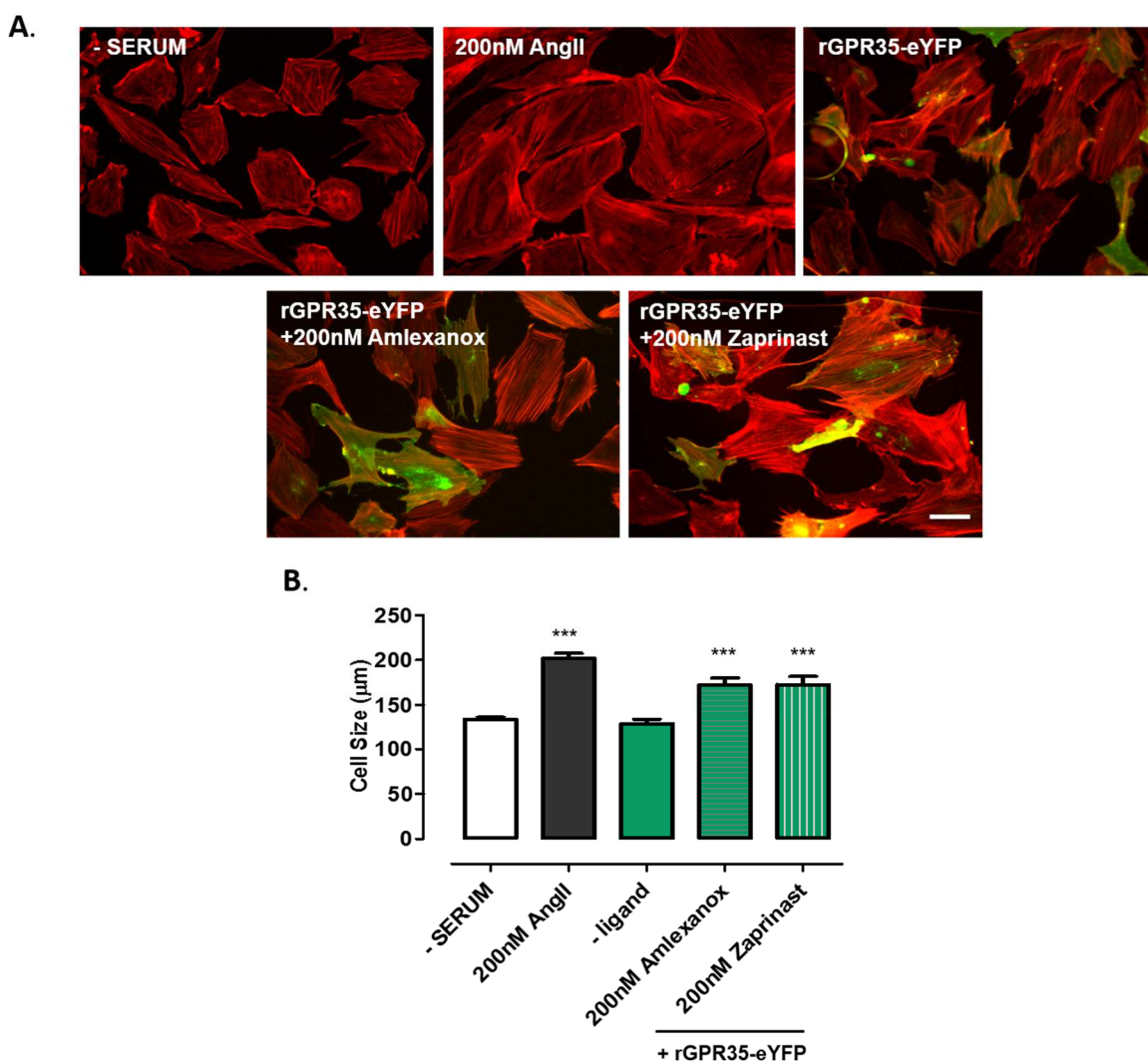
Figure 4-13. Zaprinast and amlexanox activate and internalise rat GPR35, inducing a hypertrophic response in H9c2 cardiomyocytes.

A. H9c2 cells were plated on coverslips in serum free media. 24 hours later, cells were exposed to the following conditions; –serum, 200nM AngII, or were transfected with ratGPR35-eYFP +/- 200nM amlexanox or zaprinast. After 48 hours, cells were fixed using 4% PFA, stained for F-actin using TRITC-phalloidin stain and mounted onto glass coverslips using Immu-Mount™. Cells were then imaged on a conventional fluorescence microscope. B. Cell size was quantified using ImageJ software. All data are representative of n=3 experiments. Statistical significance *** $p<0.001$, compared to – serum conditions. Scale bar = 50µm.

4.3 Discussion

Here for the first time, an integrated investigation has assessed the role GPR35 activation may play in vascular and cardiac remodelling. Recent literature has begun to highlight a potential role for GPR35 within numerous disease pathologies including hypertension and heart failure (Min *et al.*, 2010, Ronkainen *et al.*, 2014), asthma (Yang *et al.*, 2010), pain (Zhao *et al.*, 2010, Cosi *et al.*, 2011), inflammatory bowel disease (Imielinski *et al.*, 2009) and most recently; ulcerative colitis (Ellinghaus *et al.*, 2013). Even with these indications, research to define a role for GPR35 has been hampered by its challenging pharmacology, stemming from conflicting reports of the true endogenous agonist and subsequent detailing of its complicated species-selective pharmacology (Jenkins *et al.*, 2010, Milligan, 2011). Despite these difficulties, the identification of highly potent and human-selective agonists and antagonists has provided the opportunity to further dissect the functional role of GPR35 in an *in vitro* setting appropriate to vascular remodelling in cells of human origin (Jenkins et al,. 2012).

Here, it was observed that primary vascular smooth muscle and endothelial cells demonstrate GPR35 expression levels comparative to those found in the colon, spleen and small intestine. Robust detection of GPR35 expression was also evident in HUVECs, but higher levels were quantified in primary saphenous vein vascular endothelial and smooth muscle cells. In some respects, these findings contrast those from a previous study which reported low expression of GPR35 in HUVECs via qRT-PCR (Barth *et al.*, 2009). However, two robust positive controls for GPR35 expression were utilised in the study reported here, from a doxycycline inducible GPR35-stable cell line, and the colon adenocarcinoma cell line HT-29. The results in HT-29 cells are consistent with previous reports (Deng *et al.*, 2012a, Deng and Fang, 2012b) giving confidence in our own findings. One caveat of these findings is that a direct comparison between gene expression from single isolated cell populations to those in a tissue containing many different origin cell types is difficult and does not necessarily enable conclusion that the expression levels in

the cells are biologically relevant. However, the work in this chapter has highlighted a potentially important functional role for GPR35 in the migration and proliferation of primary vascular cells. Not only is this the first study to assess the functional effect of GPR35 activation in both primary vascular endothelial and smooth muscle cells, it is also the first to utilise human-selective antagonists to confirm endogenous activation. To this end, results have shown that co-incubating a wounded monolayer of HSV SMCs with human GPR35 specific antagonists CID-2745687 and ML-145 abolished a GPR35-mediated 25% increase in migration following exposure to agonists, zaprinast and pamoic acid. Given that these cells were isolated from human saphenous vein preparations used to surgically bypass multi-coronary artery occlusions, their subsequent physiological responses are relevant within the setting of vein graft remodelling, neointima formation and occlusion (Shukla and Jeremy, 2012). In essence, the evidence discussed here reveals that activation of GPR35 might promote a pro-remodelling response, at least in an *in vitro* setting, suggestive of a therapeutic potential for GPR35 antagonists and this must be explored further.

Whilst neither antagonist hindered the basal migratory capacity of HSV SMC in the absence of serum, preliminary findings demonstrated that serum induced migration of HSV SMCs was inhibited following exposure to higher concentrations (10-100-fold) of both antagonists. Due to time constrictions, this effect was not investigated further here. However, serum-induced GPR35 activation may exist, given that LPA is a reported endogenous agonist at human GPR35 (Oka *et al.*, 2010) and a well-known serum component, demonstrating micromolar concentrations (Kang *et al.*, 2004). Taking this together, it is possible to hypothesise that CID-2745687 and ML-145 might have blocked LPA mediated activation of GPR35 to inhibit migration in this study. To address these potentially confounding factors, it would be useful to utilise dialysed serum in a migration assay and, assuming that serum components would be removed (Kang *et al.*, 2004), it

may then be possible to ascertain if CID-274687 and ML-145 were blocking endogenously mediated GPR35 activation to inhibit a migratory response in serum treated HSV SMCs.

Cellular morphology and cytoskeletal rearrangement in this primary vascular cell model were also assessed and results demonstrated significant architectural reorganization which elongated the cell following agonist stimulation. This effect was also evident in a stably-expressing GPR35 cell line, for which GPR35 expression could simply be 'switched on' following exposure to doxycycline. Importantly, the exposure of non-GPR35 expressing cells to pamoic acid had no effect on the actin cytoskeleton, further supporting that pamoic acid mediated its effects on the cytoskeleton via GPR35 activation. Further to this, pamoic acid-induced changes were prevented by the co-addition of antagonists, CID-2745687 and ML-145 in both cell types. This was quantified in endogenously GPR35 expressing primary HSV SMCs, revealing cell elongation that was subsequently blocked in the presence of either antagonist. It was hypothesised that the activation of ROCK1/2 and subsequent myosin light-chain (MLC) phosphorylation were directly linked to the reorganization of the actin cytoskeleton, leading to vascular cell contraction and migration (Ai *et al.*, 2001, Surma *et al.*, 2011). Results revealed that GTP-bound Rho A protein was up regulated in HSV SMCs, following pamoic acid exposure. To examine this more closely, Rho A and ROCK 1/2 activation was assessed in migrating cells using two distinct Rho A pathway inhibitors; Y-27632, a molecule which directly inhibits ROCK 1/2 activation (Narumiya *et al.*, 2000) and Y-16, a novel RhoGEF interfering compound (Shang *et al.*, 2013). As hypothesised, GPR35 agonist-stimulated migration was found to be blocked following exposure to either compound, confirming that GPR35 mediated HSV SMC mediated migration involved the Rho A: ROCK 1/2 signalling axis. Others have reported similar effects of ROCK1/2 inhibitors in smooth muscle cell migration induced by PDGF and LPA in a collagen matrix migration model (Wirth et al, 2010). Despite ongoing efforts to target Rho A and downstream mediators in a disease setting (Barandier *et al.*, 2003, Zhou *et al.*, 2011), consensus suggests that blocking this pathway across a broad

spectrum of cell types may not be attractive therapeutically. Alternatively, compounds which mimic this effect – such as GPR35 antagonists, may have distinct therapeutic advantages in the setting of vascular injury and remodelling (Sawada *et al.*, 2000). Therapeutic interventions which are carried out in *ex vivo* setting, as required by CABG, or have the opportunity to be modified out with the body, as with and stenting, might provide further opportunities to target GPR35 effectively.

By further exploring the role of GPR35 in a proliferative capacity, it has been shown that at least in HSV SMC, neither GPR35 activation nor inhibition produced any effect on cell proliferation. Furthermore, assessment of migration was also carried out within a 48-hour time-frame within serum free conditions, so as to limit the proliferative capacity of migrating cells. Taking these together, the results clearly demonstrate that enhanced HSV SMC migration was not a consequence of increased cell number within the mono-layer wound. Conversely, HSV EC demonstrated significantly enhanced proliferation in the presence of increasing concentrations of the agonists zaprinast and pamoic acid, whilst neither cytoskeletal organisation nor migration were affected. It is well known that GPCRs often exhibit diverse effects amongst cell types (Wettschureck and Offermanns, 2005). However, such differential roles for vascular cell types was largely unexpected. Ruling out potential issues regarding receptor specificity, the proliferative response induced by pamoic acid was blocked in the presence of human selective antagonists CID-2745687 and ML-145 in a secondary assay assessing BrdU incorporation, strongly indicating that this effect was GPR35-mediated. Furthermore, it has been previously demonstrated that ML-145 displays >1000-fold selectivity for GPR35 over its most closely related receptor, GPR55 (Heynen-Genel *et al.*, 2010). Given that both antagonists produced identical effects on HSV EC proliferation at low, nanomolar concentrations it is unlikely that the specificity of ML-145 for GPR35 was compromised. This suggests that GPR35 activation may play a role in maintaining integrity and cell cycle progression in HSV EC. Fundamentally, these results suggest that GPR35 activation might exert a protective

effect upon the endothelium whist encouraging a pro-migratory response in SMCs and therefore, is counterintuitive for progressive remodelling following vein grafting. In going forward, it will be important to assess a role for GPR35 within an *in vivo* experimental setting that accounts for both EC and SMC function. For example, reports have recently detailed successful investigation of a role for endothelial and smooth muscle cell function within intact vessels, demonstrating that the regulation of microRNA-21 is essential for neointimal formation to occur following stenting (McDonald *et al.*, 2013). A similar setting might present an opportunity to further assess of a role for GPR35 activation within an *ex vivo* capacity in the future.

Results from this study not only indicate a role for GPR35 in vascular remodelling but further support existing evidence that GPR35 has significant implications for the development of cardiac hypertrophy. Two other investigations have reported a role for GPR35 in cardiac hypertrophy and subsequent progressive remodelling (Min *et al.*, 2010, Ronkainen *et al.*, 2014). Whilst the first demonstrated that adenovirus-mediated overexpression of GPR35 induced a hypertrophic phenotype in rat neonatal cardiomyocytes (Min *et al.*, 2010), the second highlighted that endogenous GPR35 expression is regulated via HIF-1 activation following exposure to hypoxia *in vitro* and this was subsequently confirmed in the setting of acute MI in mice (Ronkainen *et al.*, 2014). Indeed, these authors purported that GPR35 might be a novel, highly sensitive indicator of acute progressive cardiac remodelling (Ronkainen *et al.*, 2014). H9c2 cardiomyocytes have been extensively characterised within the setting of cardiomyocyte hypertrophy and in recent years, authors have demonstrated that their ability to exhibit hypertrophic responses, comparative to primary neonatal cardiomyocytes, following the measurement of cell size and hypertrophic gene markers such as BNP and ANP (Flores-Munoz *et al.*, 2011, Watkins *et al.*, 2011). Given that H9c2 cells revealed a limited capacity for endogenous GPR35 expression, it was necessary to transiently express GPR35 and, considering that they originate from rat neonatal cardiomyocytes, transfection of rat

GPR35-eYFP was most appropriate in this setting. This prohibited the use of CID-2745687 or ML-145, which are human-selective (Jenkins *et al.*, 2012). However, results demonstrated that zaprinast and amlexanox induced a hypertrophic response in H9c2 cardiomyocytes and they also clearly showed internalised rat GPR35-eYFP following ligand exposure. GPR35 internalisation was previously reported in cardiomyocytes, confirming receptor activation following exposure to zaprinast (Ronkainen *et al.*, 2014). Whilst the response in H9c2 cardiomyocytes in this study revealed alterations to the cytoskeletal architecture arrangement, it also increased cell size and this was not previously demonstrated in cardiomyocytes following ligand exposure (Ronkainen *et al.*, 2014). Of course, within a functional setting, cardiomyocyte hypertrophy is a resulting factor of an adaptive cardiac response to improve cardiac output and function following exposure to ischemia and increased total peripheral resistance (Keteyian, 2013). Ultimately, it cannot be sustained and leads to progressive remodelling of the cardiac tissue and heart failure (Maillet *et al.*, 2013).

It is possible that GPR35 might also mediate its effects via the Rho A: ROCK 1/2 signalling axis and reports have previously detailed its central role in $G\alpha_{13}$ mediated cardiac remodelling and heart failure (Takefuji *et al.*, 2012). Whilst previous reports showed that GPR35 up regulation resulted in cardiac hypertrophy, over expression resulted in tonic activation of GPR35 (Ronkainen *et al.*, 2014). This effect was not demonstrated here and it is important to take into consideration that experiments were performed in serum free conditions, thus eliminating potential endogenous activation following exposure to serum components, such as LPA (Oka *et al.*, 2010, Kang *et al.*, 2004). Consequently, this might explain the requirement for exogenous agonist exposure in this study.

4.3.1 Conclusions

This is the first study to demonstrate considerable expression levels and a functional role for GPR35 in the setting of vascular remodelling. Future investigations which address the mechanism of GPR35s effects on vascular endothelial cell proliferation will be integral in our understanding of its true function in vascular disease. However, the current findings strongly suggest that antagonists of GPR35 may be of beneficial therapeutic effect with respect to attenuating vascular occlusion in the setting of vein graft failure. Furthermore, this is a Gα_{13} mediated response via the Rho A-ROCK1/2 axis. Furthermore, results here also provide further evidence for a role for GPR35 in the development of cardiomyocyte hypertrophy; taking this together with reports of a role for GPR35 expression in cardiomyocyte hypertrophy and progressive remodelling (Min *et al.*, 2010, Ronkainen *et al.*, 2014), it is possible that GPR35 may also constitute a potential therapeutic target in this setting.

5 Pharmacological agonism of GPR35 modulates blood pressure in the stroke prone spontaneously hypertensive rat

5.1 Introduction

According to the most recent data from the British Heart Foundation, ≥30% of Scottish

men and women are hypertensive, with blood pressure readings exceeding 140/90mmHg

(BHF, 2012). Critically, these statistics are representative of the larger western population

which further indicate that the mortality risk associated with uncontrolled hypertension is

as high as 40.6% (Go *et al.*, 2014). Designed to target specific pathways which regulate

peripheral vascular resistance, cardiac output and kidney function, medications prescribed

to alleviate the burden of hypertension include ACE inhibitors, β-blockers and diuretics

and practitioners most often prescribe a combination of these therapies to target a wider

range of pathologies (Gradman *et al.*, 2010). A recent meta-analysis of 44 individual

clinical trials indicated that two combined therapies can provide a 5-fold improvement in

hypertension control compared to doubling the dosage of a single medication (Wald *et al.*,

2009). Despite this, it has been estimated that 20-30% of hypertensive patients remain

resistant to combination therapies (Calhoun *et al.*, 2008b). Furthermore, results from the

National Health and Nutrition Examination Survey (NHANES) 2006-2008 have highlighted

that only 50.1% of hypertensive cases are adequately controlled by the medications

currently available (Egan *et al.*, 2010). Hence, there remains an unmet clinical

requirement for improved and novel therapeutics (Egan *et al.*, 2010).

A role for GPR35 in the development of hypertension was previously explored following

results from a microarray screen of myocardial tissue from heart failure patients,

demonstrating that GPR35 expression was significantly increased in comparison to

myocardial tissue derived from healthy 'controls' (Min *et al.*, 2010). This finding led

authors to further investigate a role for GPR35 *in vivo,* subsequently assessing

haemodynamic parameters and cardiac hypertrophy in a global GPR35 knock-out mouse

model, (Min *et al.*, 2010). Whilst heart weight remained unchanged, authors reported an

increase in systolic blood pressure of up to 37.5mmHg, assessed via Millar pressure

catheterisation in GPR35 knockout mice compared to wild type (WT) litter mates (Min *et*

al., 2010). The reasons for this elevation in blood pressure were unclear; however, authors went on to assess the effects of GPR35 overexpression in primary rat neonatal cardiomyocytes via adenoviral transduction and reported that GPR35 overexpression induced a hypertrophic phenotype (Min *et al.*, 2010). Taking these findings together, it is clear that the development of hypertension and cardiac dysfunction are both sensitive to GPR35 expression, however, its mechanism of action is unknown and thus far, a role for GPR35 has not been further examined in the setting of hypertension.

A role for GPR35 in the heart was further investigated in a very recent report from Ronkainen and colleagues who suggested that GPR35 may be a prominent novel marker of early progressive cardiac remodelling (Ronkainen *et al.*, 2014). Here, authors explored the effect of hypoxia on GPR35 expression in cardiomyocytes *in vitro* and demonstrated time-dependent increases in GPR35 expression following exposure to hypoxic conditions which was concomitant with increased expression of the gold-standard hypoxic marker gene EGL nine homolog 3 (PHD3) (Ronkainen *et al.*, 2014). This effect was also confirmed in cardiac tissue from mouse models exposed to acute myocardial infarction via ligation of the left anterior descending (LAD) coronary artery. Most interestingly, closer inspection revealed that the promoter region of GPR35 contained a binding site for HIF1α and this was responsible for increased expression levels of GPR35 in the setting of progressive cardiac remodelling (Ronkainen *et al.*, 2014). *In vitro* overexpression of GPR35 in cardiomyocytes altered actin-cytoskeleton formation, however, this did not lead to hypertrophy (Ronkainen *et al.*, 2014). Essentially, the regulation of GPR35 expression within the heart is now better understood, and thus, an opportunity to further assess a role for GPR35 activation in the setting of hypoxia, remodelling and hypertrophy is evident.

Amlexanox is one of the most potent agonists identified at GPR35 to date (Mackenzie *et al.*, 2014). Like zaprinast, it has demonstrated potent activation at all three species of GPR35, however, it demonstrates substantial selectivity for rat GPR35, exhibiting potencies as high as 4.5nM (EC_{50}) (Chapter 4-2-7). However, at higher concentrations,

amlexanox has also been shown to target inflammatory pathways, as daily oral gavage administration of 25-100mg/kg amlexanox over 4-weeks resulted in rapid weight loss and improved insulin responses in mice fed a high fat diet (HFD) (Reilly *et al.*, 2013). Though its mechanism of action was not fully elucidated, authors reported that the effect resulted from increased thermogenesis and involved the inhibition of inflammatory targets of the NF-κB pathways; IKK-ε and TBK1 (Reilly *et al.*, 2013). Importantly, it was clear from this investigation that the inflammatory alterations were evident only following exposure to high concentrations of amlexanox in an *in vitro* setting. Furthermore, these effects were mimicked following exposure to similar concentrations *in vivo,* whereby the administration of 25-100mg/kg amlexanox equated to micromolar levels in serum (Reilly *et al.*, 2013). Given that amlexanox has demonstrated extremely high potency for GPR35, it has utility to test GPR35 functional effects *in vivo* at much lower concentrations, however, it is clear that careful dose administration will be required to selectively target GPR35 in this capacity.

The stroke prone spontaneously hypertensive rat (SHRSP) is a widely utilised, gold-standard model for the study of essential hypertension and investigators have detailed its use for more than three decades (Yamori *et al.*, 1976, Delles *et al.*, 2010). Its use has enabled researchers to explore pathologies relating to various pathologies of the cardiovascular system, including hypertension (McBride *et al.*, 2005), stroke (McCabe *et al.*, 2009) and cardiac hypertrophy (Flores-Munoz *et al.*, 2012). Most advantageously, hypertension is established by 10-weeks of age enabling researchers to study the progression of end-organ damage from an early time-point and therefore, the SHRSP has become the most utilised rodent model in the assessment of cardiovascular disease pathologies (Hultstrom, 2012). Furthermore, in recent years, researchers have begun to examine the differences in gene expression profiles in the SHRSP compared to the normotensive reference strain, the Wistar-Kyoto (WKY) rat (Yamamoto *et al.*, 2013, McBride *et al.*, 2003). This has led to the identification of various positional candidate

genes which might be involved in the development of hypertension, including Glutathione S-transferase Mu 1 (Gstm1), Sphingolipid G-protein-coupled Receptor 1 (Edg1) and Vascular cell adhesion protein 1 (VCAM1) (Delles *et al.*, 2010). Further exploration of a potential role for these genes has been carried out via manipulation of expression in the SHRSP, for example, a role for Gstm1 has been highlighted in pathophysiological development of hypertension with particular implications for oxidative stress in the renal system (McBride *et al.*, 2005).

5.1.1 Hypothesis and aims

Given that GPR35 is hypothesised to play a role in multiple pathologies related to cardiovascular disease (MacKenzie *et al.,* 2011), further investigation in an experimental model of essential hypertension, and related end organ damage, might help to elucidate its function. Reports of an elevation in blood pressure following the deletion of the GPR35 gene in mice has been central in driving the hypothesis that GPR35 activation may alter, or even lower, the blood pressure response. It is also hypothesised that this may have a direct impact upon vital organs, inclusive of the vasculature, heart and kidneys. Therefore, the aim of this chapter was to assess the effect of GPR35 activation on blood pressure and end-organ damage in the vasculature, heart and kidney of the SHRSP following amlexanox administration. The SHRSP is an excellent such model for this, since hypertension is established at an early age, providing the opportunity to assess if GPR35 activation offers a protective effect against the development of hypertension and progression of end-organ damage. A time-line of the events are diagrammatically outlined in Figure 2-3 (*see section 2.22.1*) and a series of aims devised to investigate this hypothesis are outlined below:

- To assess the effect of a low dose of amlexanox on body weight and fat deposition in the SHRSP.

- To assess the effect of amlexanox administration on blood pressure in the SHRSP.

- To assess the effect of sustained amlexanox administration on large and small vessel reactivity, *ex vivo*.

- To assess the effect of amlexanox administration on end-organ damage in the heart and kidney of the SHRSP.

5.2 Results

5.2.1 The effect of amlexanox administration on body weight and adipose deposition in SHRSPs

Since micromolar concentrations of amlexanox administered to mice have been reported to alter metabolism and hence body weight and fat distribution via targeting IκB kinases IKK$_{-\varepsilon}$ and TANK binding kinase-1 1 (TBK1) (Reilly *et al.*, 2013), it was hypothesised that oral administration of amlexanox at >10-fold lower doses (2.5mg/kg/day) in a larger rodent would result in comparatively lower serum levels, effectively targeting GPR35 at relevant concentrations (EC$_{50}$ =4.5 ±0.17nM). To assess if low dose amlexanox administration in the SHRSP induced any changes in body weight (BW), this was carefully monitored and recorded daily throughout the duration of the study. Importantly, no differences between the body weight of SHRSPs in the amlexanox treatment group compared to vehicle control treated animals were observed (Figure 5-1.A). Further to this, upon animal sacrifice retroperitoneal and epididymal fat pads were immediately excised, weighed and ratios were corrected for either tibia length (Figure 5-1.B) or body weight (Figure 5-1.C). Again, there were no significant differences in fat pad ratios derived from either anatomical area between conditions (Figure 5-1.C&B). Taking this together, it is clear that 2.5mg/kg/day amlexanox neither affected whole body weight nor adipose tissue deposition in the SHRSP.
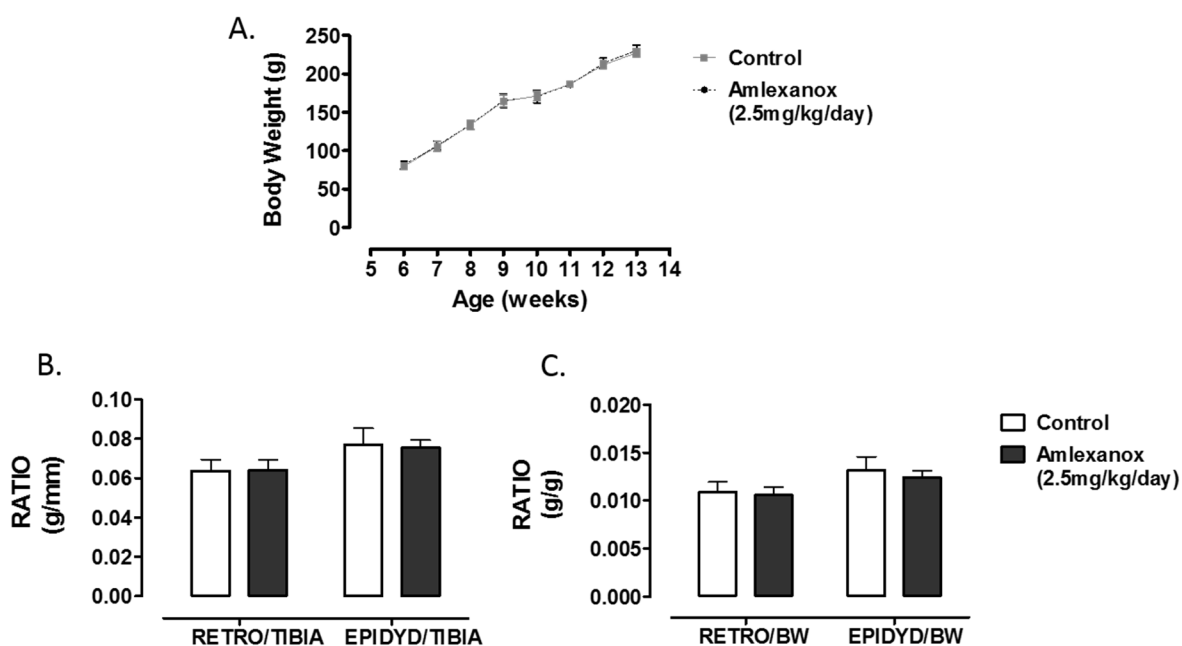
Figure 5-1. The effect of amlexanox administration on body weight and fat ratio in the SHRSP.

A. Average body weight of SHRSP following oral administration of 2.5mg/kg/day amlexanox or vehicle control, measured in grams (g) every 3 days from age 6-13 weeks

B&C. Fat ratios derived from retroperitoneal (RETRO) and epididymal (EPIDYD) regions, normalised to tibia length (TIBIA) (B) or body weight (BW) (C) following sacrifice at 12-13 weeks of age. Values are expressed as grams (g), grams/millimetre (g/mm) or grams/grams (g/g). n=5 animals per group.

5.2.2 The effects of amlexanox administration on blood pressure and haemodynamics in the SHRSP

Global knockdown of GPR35 expression has been implicated in an alteration in blood pressure, leading to increased SBP of up to 37.5mmHg in mice (Min *et al.*, 2010). However, it was not clear from these results if GPR35 activation would offer a protection from the development of hypertension in the SHRSP. Given that SHRSPs aged 6-weeks are too small for invasive radiotelemetry probe implantation, systolic blood pressure was measured via tail cuff plethysmography for the first 20 days (Figure 5-2.A). This enabled an immediate, non-invasive assessment of the effects of GPR35 agonist administration to a rodent model of hypertension at a young age. There were no immediate differences in SBP between groups using this method of assessment, however, hypertension was evident after day 10 in both groups at which point the age-matched SHRSPs were 7-8 weeks old (amlexanox; 122.0 $\pm$ *6.1* mmHg, control; 134.5 $\pm$*9.6* mmHg, p>0.05). The development of hypertension (>110mmHg) was early in comparison to alternative reports which report established hypertension in SHRSPs at 10 weeks of age (Hultstrom, 2012). Wireless telemetry probes were surgically implanted on day 14 and following a 7-day period of recovery, measurements were collected from animals in both drug and vehicle groups at 5 minute intervals for the duration of the study. Blood pressure measurements were averaged for light- (12hrs) and dark-cycles (12hrs) (Figure 5-2 and Figure 5-3). Blood pressure measurements derived from SHRSPs administered with 2.5mg/kg amlexanox daily exhibited elevated SBP throughout the study, for which the overall drug effect was significantly higher compared to vehicle treated animals (amlexanox; 164.2 $\pm$*3.6* mmHg, control; 142.3 $\pm$*5.7* mmHg; p<0.001) (Figure 5-2.A). Similarly, this was true for mean arterial pressure (MAP) (amlexanox; 144.8 $\pm$*2.5* mmHg, control; 134.3 $\pm$*3.5* mmHg; p<0.001) (Figure 5-3.A) and pulse pressure (PP) (amlexanox; 47.3 $\pm$*6.6* mmHg, control; 24.6 $\pm$*10.3* mmHg; p<0.001) (Figure 5-3.B). Contrastingly, there were no observed

differences in diastolic blood pressure between groups at any point throughout the study

(Figure 5-2.B).
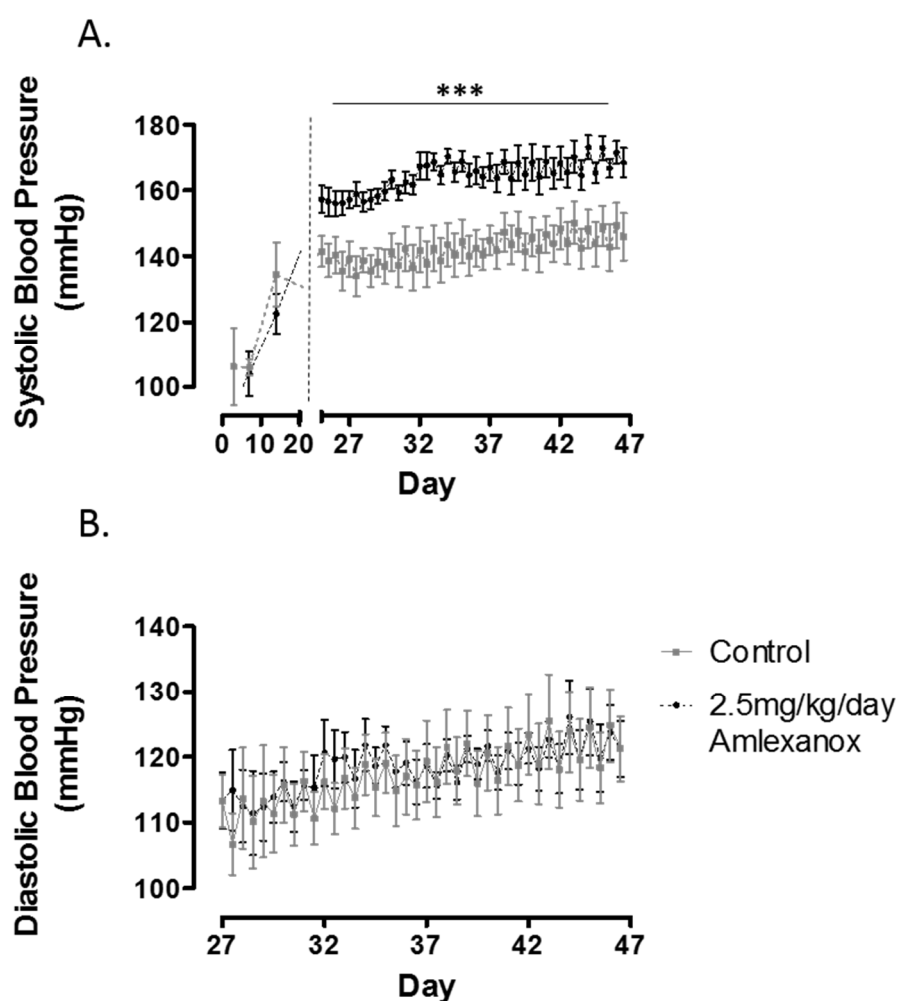
Figure 5-2. The effect of amlexanox administration on haemodynamic pressures in the SHRSP.

A. Average systolic blood pressure (SBP) and B. average diastolic blood pressure (DBP) following oral administration of 2.5mg/kg/day amlexanox or vehicle control. SBP was measured via tail cuff plethysmography on days 0-20 and following radiotelemetry implantation on day 21, both SBP and DBP measurements taken at 5-minute intervals were averaged for every 12-hours on day 27-47. Values are expressed as millimetres of mercury (mmHg). Statistical significance *** $p < 0.001$. n=4 animals per group.

A. Averaged mean arterial pressure (MAP) and B. Pulse pressure (PP) following oral administration of 2.5mg/kg/day amlexanox or vehicle control, measured via radiotelemetry implantation. Values are expressed as millimetres of mercury (mmHg). Statistical significance *** $p < 0.001$. n=4 animals per group.

5.2.3 The effect of amlexanox administration on heart rate and activity in SHRSPs

Another benefit of wireless telemetry implantation is its continuous measurement of heart rate and locomotive activity in an unrestricted, stress free environment. Unlike the induced changes in blood pressure, there were no significant differences in heart rate (amlexanox; 301.1 *±2.9* bpm, control; 306.3 ±*11.2* bpm) or activity (amlexanox; 1.6 *±0.2* A.U., control; 2.1 *±0.37* A.U.) following drug administration (Figure 5-4.A&B). However, a significant diurnal effect was evident in both amlexanox (HR night; 346 *±10.8* bpm, HR day; 308.7 *±11.5* bpm, p<0.001), (activity night; 4.1 *±0.38* A.U., activity day; 1.6 *±0.2* A.U., p<0.001) and vehicle treated (HR night; 337 *±6.5* bpm, HR day; 310 *±10.6* bpm, p<0.001), (activity night; 4.3 *±0.31* A.U., activity day; 1.61 *±0.22* A.U., p<0.001) SHRSPs. This information indicated that the SHRSPs were most active during dark-cycle periods (12h) and least active during light-cycle periods (12h), consistent with reported nocturnal behaviour in spontaneously hypertensive rats (van den Buuse, 1994).
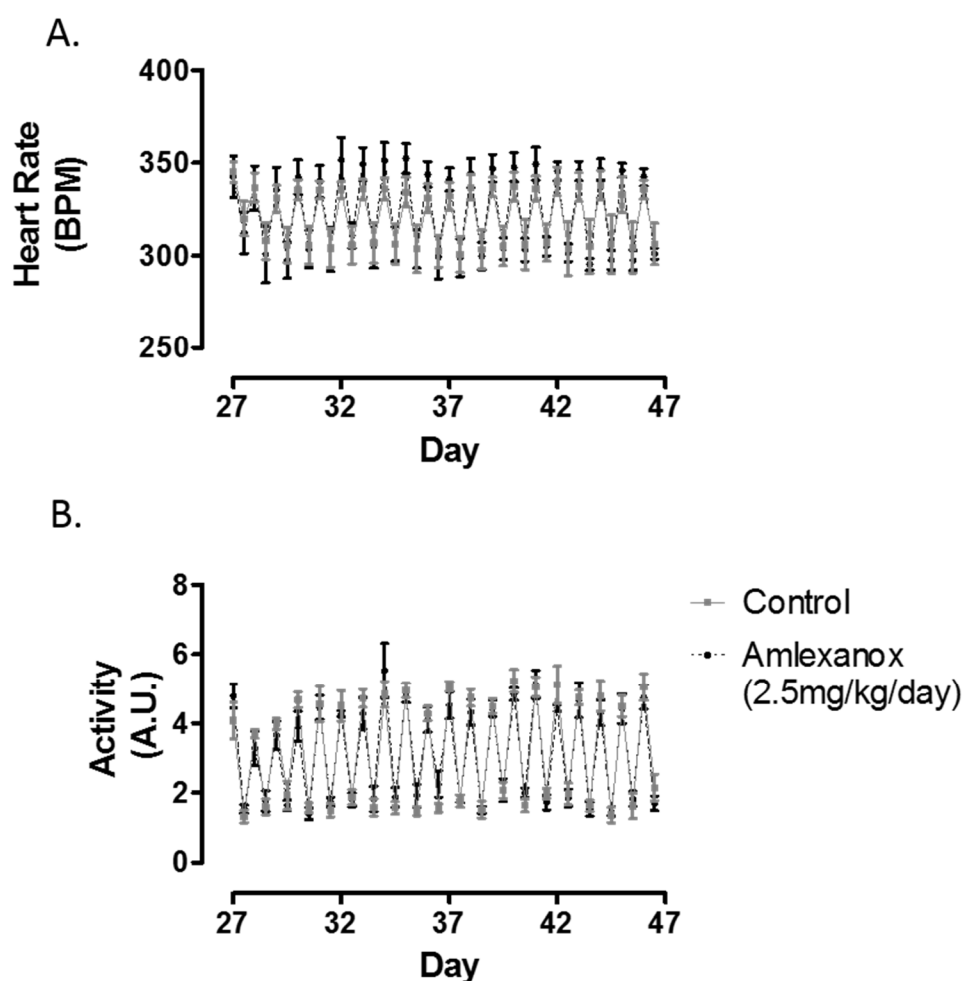
Figure 5-4. The effect of amlexanox administration on heart rate and activity in the SHRSP.

A. Averaged heart rate (HR) and B. activity following radiotelemetry implantation on day 21 (measured from day 27-47) in SHRSPs administered either 2.5mg/kg/day amlexanox or vehicle control.   Values are expressed as beats per minute (BPM) for HR and arbitrary units (A.U.) for locomotion activity. There were no significant differences between conditions. n=4 animals per group.

5.2.4 **The effect of amlexanox administration on the reactivity of large vessels and small resistance arteries**

Thus far, results from this study suggest a role for GPR35 in primary vascular endothelial and smooth muscle cell function and blood pressure regulation. Next, vasoreactivity of small and large resistance arteries were assessed in an *ex vivo* setting. Following animal sacrifice, the mesenteric artery and thoracic aorta were excised and prepared for small and large vessel wire myography. To test the effect of 6-weeks amlexanox administration on contractile vasoreactivity, isolated arteries were incubated with increasing concentrations of phenylephrine (PE) or noradrenaline (NA). Importantly, following stimulation with respective vasoconstrictors both vessels produced a concentration-response curve, indicating vessel contraction. However, there were no differences in concentration-dependent vessel contraction between amlexanox treated animals or control animals (Figure 5-5.A&B.).

To assess endothelium-dependent vasorelaxation, vessels were then incubated with cumulative concentrations of carbachol, which induces the release of nitric oxide from endothelial cells to initiate vessel dilatation (Furchgott, 1999). Contrastingly, concentration-dependent inhibition curves demonstrated impaired relaxation in both aortic and mesenteric vessels from amlexanox treated animals compared to vehicle treated controls (Figure 5-6). However, this effect was only significant in the aorta (amlexanox; 41.56 ±*6.14*%, control 18.13 ±*5.7*%, p<0.01), not in mesenteric arteries (amlexanox; 67.8 ±*15.6*%, control 53.04 ±*3.1*%, not significant) (Figure 5-6). These results suggest that continuous amlexanox administration together with an increase in blood pressure in the SHRSP might have significantly impaired endothelial function in large vessels. Interestingly, the data also suggest that this effect may also be true for mesenteric vessels and future investigation to test this effect may require a larger number of animals per condition in order to improve statistical power.

Smooth muscle cell-mediated vasodilatation was assessed following exposure to cumulative concentrations of sodium nitroprusside (SNP), an endothelium-independent vasodilator (Morris *et al.*, 2001). Both vessels exhibited a concentraion-dependent inhibition in vessel contraction to reach basal tension levels, however, there were no significant differences between vessel relaxation in amlexanox treated SHRSPs compared to vehicle treated SHRSPs (Figure 5-7). This data indicated that smooth muscle cell dependent vasoreactivity remained unaffected by amlexanox administration and subsequent increased SBP in the SHRSP.
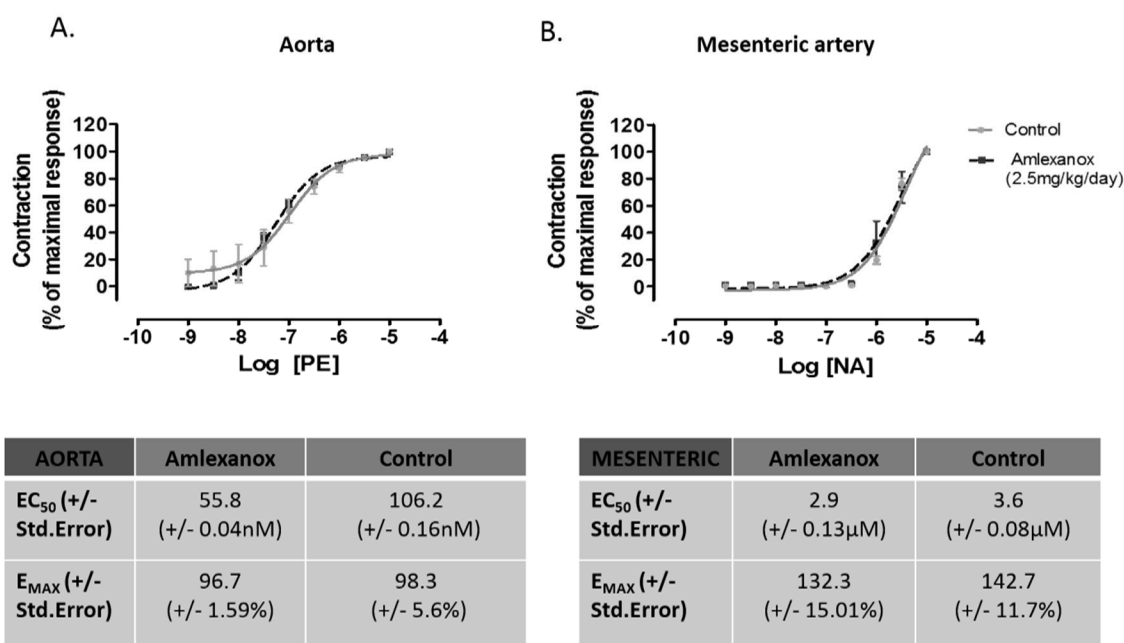
Figure 5-5. The effect of amlexanox administration on the contractile response in aortas and mesenteric arteries of the SHRSP.

A. Contractile concentration-response curve in the presence of increasing concentrations of phenylephrine (PE) in aortic rings derived from SHRSP animals upon sacrifice following 6 weeks oral administration of 2.5mg/kg/day amlexanox or vehicle control B. Contractile concentration-response curve in the presence of increasing concentrations of nor-adrenaline (NA) in mesenteric arteries derived from SHRSP upon sacrifice following exposer to 6 weeks oral administration of 2.5mg/kg/day amlexanox or vehicle control. Measurements were derived via wire-myography at 37°C. Values are expressed as percentage of maximal contractile response. There are no significant differences between conditions. n=4 animals per group (aorta) and n=3 animals per group (mesenteric artery).

AORTA	Amlexanox	Control
EC_{50} (+/- Std.Error)	55.8 (+/- 0.04nM)	106.2 (+/- 0.16nM)
E_{MAX} (+/- Std.Error)	96.7 (+/- 1.59%)	98.3 (+/- 5.6%)

MESENTERIC	Amlexanox	Control
EC_{50} (+/- Std.Error)	2.9 (+/- 0.13µM)	3.6 (+/- 0.08µM)
E_{MAX} (+/- Std.Error)	132.3 (+/- 15.01%)	142.7 (+/- 11.7%)
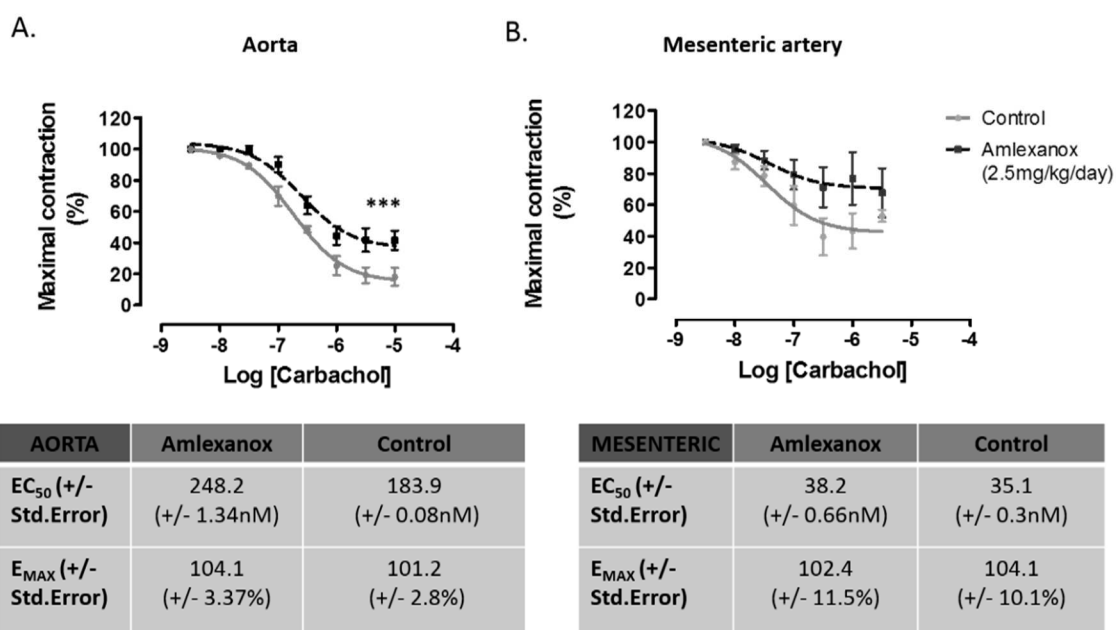
Figure 5-6. The effect of amlexanox administration on endothelial cell mediated relaxation of aortas and mesenteric arteries of the SHRSP.

The alteration of endothelial cell mediated relaxation in the presence of increasing concentrations of carbachol in aortic rings (A) and mesenteric arteries (B) derived from SHRSP upon sacrifice following 6 weeks oral administration of 2.5mg/kg/day amlexanox or vehicle control. Measurements were derived via wire-myography at 37°C. Values are expressed as percentage of maximal contractile response. Statistical significance * $p<0.05$, ** $p<0.01$. n=4 animals per group (aorta) and n=3 animals per group (mesenteric artery).

AORTA	Amlexanox	Control
EC$_{50}$ (+/- Std.Error)	50.8 (+/- 0.19nM)	21.3 (+/- 0.14nM)
E$_{MAX}$ (+/- Std.Error)	102.1 (+/- 8.5%)	105.6 (+/- 57.8%)

MESENTERIC	Amlexanox	Control
EC$_{50}$ (+/- Std.Error)	3.7 (+/- 0.17nM)	5.9 (+/- 0.17nM)
E$_{MAX}$ (+/- Std.Error)	103.8 (+/- 10.3%)	107.9 (+/- 8.9%)
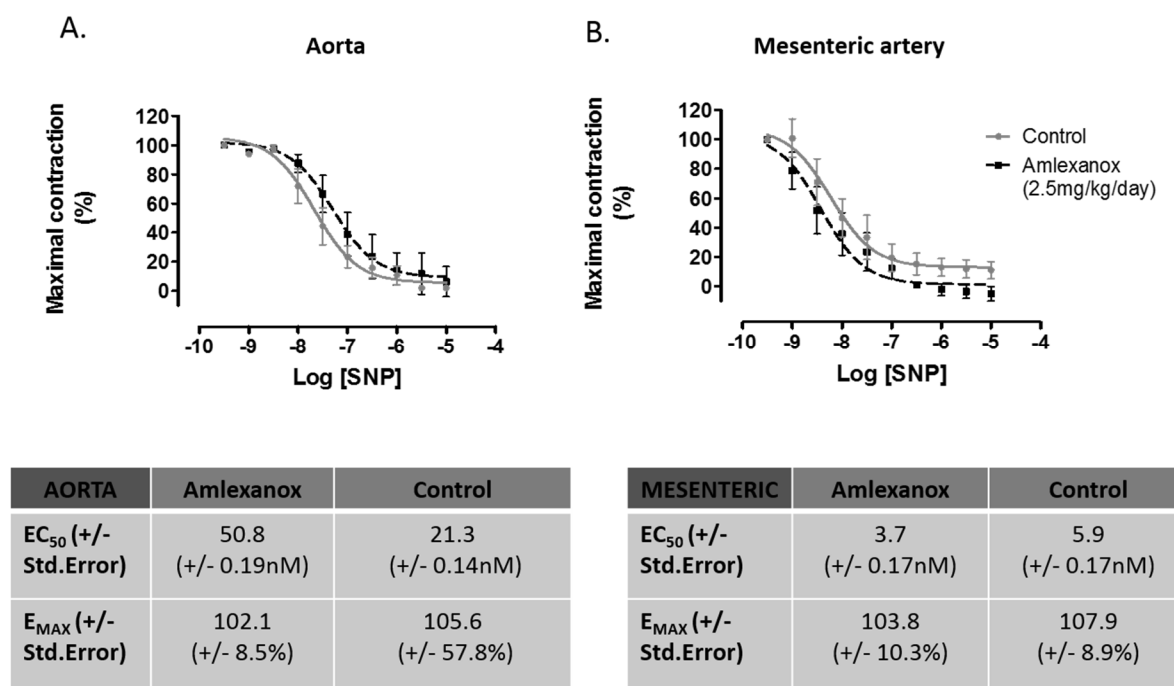
Figure 5-7. The effect of amlexanox administration on smooth muscle cell mediated relaxation of aortas and mesenteric arteries of the SHRSP.

The alteration of smooth muscle cell mediated relaxation in the presence of increasing concentrations of sodium nitroprusside (SNP) in aortic rings (A) and mesenteric arteries (B) derived from SHRSP upon sacrifice following 6 weeks oral administration of 2.5mg/kg/day amlexanox or vehicle control. Measurements were derived via wire-myography at 37°C. Values are expressed as percentage of maximal contractile response. There are no significant differences between conditions. n=4 animals per group (aorta) and n=3 animals per group (mesenteric artery).

5.2.5 The effect of amlexanox administration on cardiac tissue mass and cardiomyocyte size in the SHRSP

In Chapter 4-2-7, it was demonstrated that 200nM amlexanox and zaprinast-induced GPR35 activation mediated a hypertrophic phenotype in H9c2 cardiomyocytes, given that GPR35 expression has been most recently implicated in the development of heart failure *in vivo* (Ronkainen *et al.*, 2014), the effects of continuous amlexanox administration on cardiac tissue and cell size were also assessed here. Following animal sacrifice at 12-13 weeks of age, whole heart tissue mass was measured and upon cardiac dissection, left ventricle + septum mass were also measured. As with fat pads, cardiac tissue weight was then normalised for either BW or tibia length. The first observation was that distribution of cardiac tissue weight following amlexanox administration exhibited a more variable mass in comparison to tissue from vehicle control animals (Figure 5-8). However, amlexanox administration did lead to significantly higher whole heart weight following independent normalisation for body weight (amlexanox mean; 3.82 ±*0.08* g/g, control mean 3.61 ±*0.01* g/g*, $p < 0.05$) (Figure 5-8.C). Histological analysis of the myocardium to image cross-sectional areas of cardiomyocytes within the LV wall, stained using TRITC conjugated wheat germ agglutinin (WGA) was performed (Figure 5-9). Cardiomyocyte size was quantified by measuring the cell diameter using ImageJ software. Cardiomyocyte cross-sectional area revealed that amlexanox treatment induced a tendency for an increase in individual cardiomyocyte size, compared to vehicle controlled animals, however, the effect did not reach significance (p=0.067).
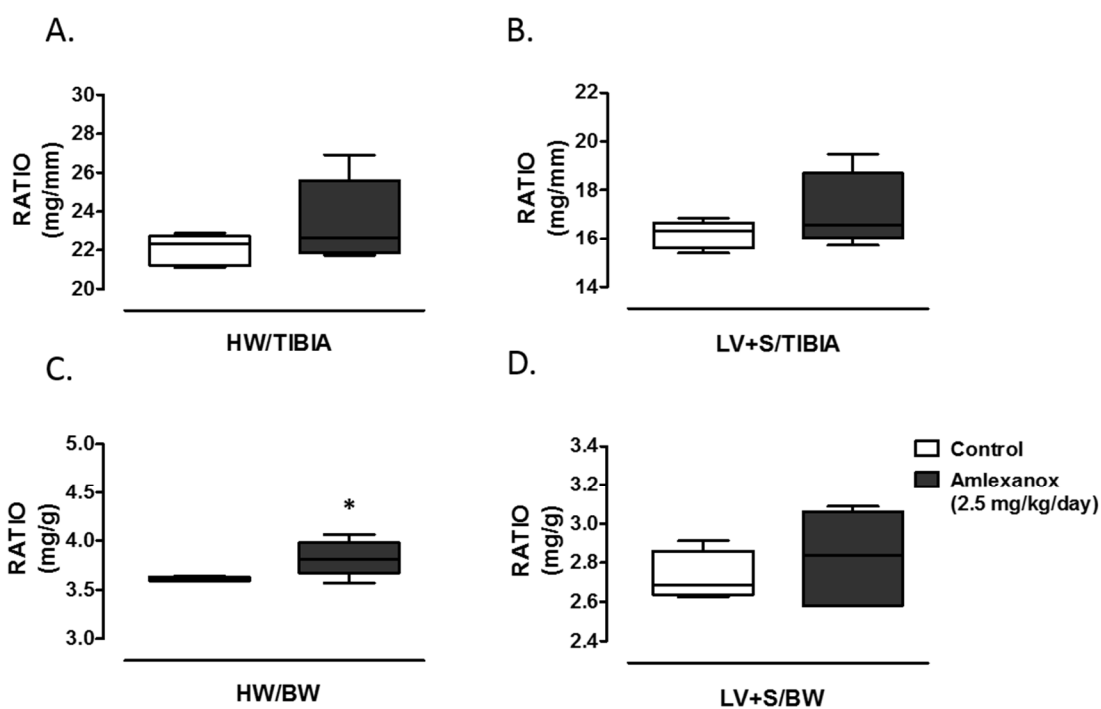
Figure 5-8. The effect of amlexanox administration on cardiac mass in the SHRSP.

Average heart weight (HW) (A) or left ventricle + septum (LV+S) (B) normalised to tibia
length in SHRSPs following oral administration of 2.5mg/kg/day amlexanox or vehicle
control upon sacrifice at 13 weeks of age. C&D. Average HW (C) or LV+S (D) normalised
to body weight (BW) in SHRSP rats following oral administration of 2.5mg/kg/day
amlexanox or vehicle control upon sacrifice at 13 weeks of age. Values are expressed as
milligrams/millimetre (mg/mm) or milligrams/grams (mg/g). Statistical significance *
p<0.05. n=5 animals per group.
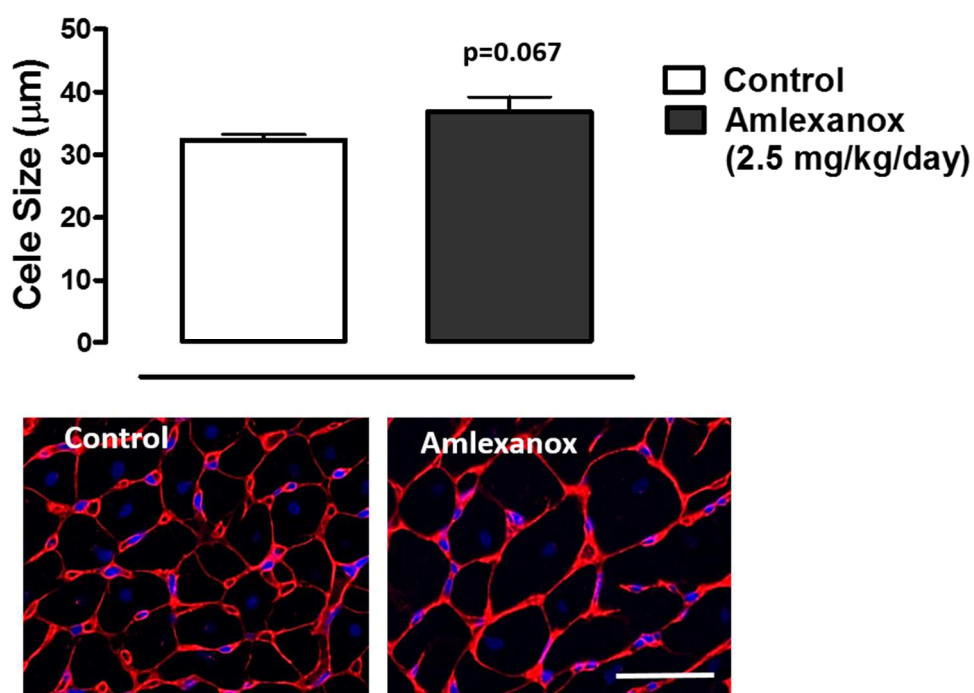
Figure 5-9. The effect of amlexanox administration on cardiomyocyte size in the SHRSP.

Average cardiomyocyte size in SHRSP rats following oral administration of 2.5mg/kg/day amlexanox or vehicle control. Upon sacrifice at 13 weeks of age, hearts were excised, weighed and left ventricle plus septum were fixed using paraformaldehyde embedded in paraffin and stained using TRITC conjugated wheat germ agglutinin (WGA) (representative images). Cardiomyocyte diameter was determined using ImageJ software and expressed as micrometres (µm). n=4 animals per group. Scale bar = 50µm.

5.2.6 The effect of amlexanox administration on renal fibrosis in the SHRSP

Hypertension is understood to contribute to end-organ damage in the SHRSP (Gelosa *et al.*, 2009), and given that amlexanox treated SHRSPs revealed elevated systolic blood pressures compared to vehicle-only treated animals, the kidney was also assessed for damage histologically. There were no significant differences in kidney weight between treatment conditions, normalised to both tibia length and BW (Figure 5-10). Histological analysis of picosirius red staining, specific for collagen type I and III to assess fibrosis, suggested that collagen deposition in kidneys from amlexanox treated SHRSPs was more uniform in comparison with vehicle-treated controls (Figure 5-11.). This was confirmed following fibrosis quantification using Image ProPlus software. Quantitative analysis of fibrosis in multiple cross-sections, specific for both interstitial and perivascular collagen deposition, revealed that amlexanox treatment significantly increased collagen deposition in both interstitial and perivascular regions ($p<0.05$ and $p<0.001$, respectively).
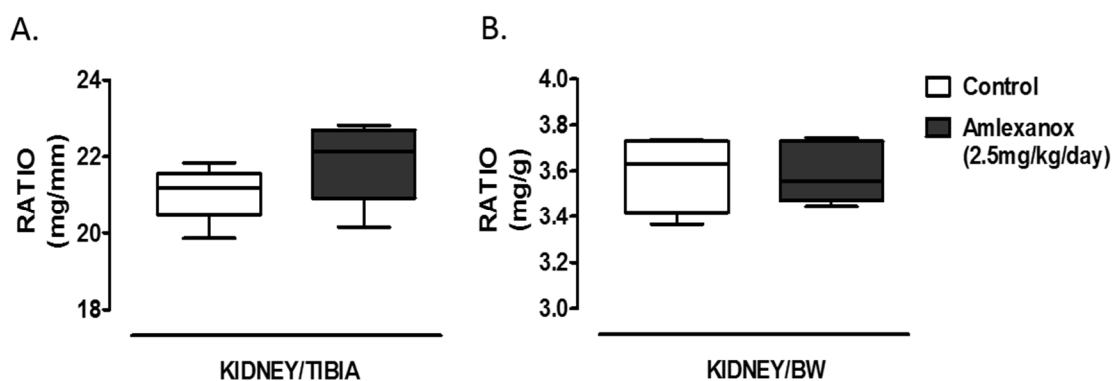
Figure 5-10. The effect of amlexanox administration on kidney mass in the SHRSP.

Average kidney weight (A) normalised to tibia (TIBIA) length in SHRSP rats following oral administration of 2.5mg/kg/day amlexanox or vehicle control upon sacrifice at 13 weeks of age. B. Average kidney weight normalised to body weight (BW) in SHRSP rats following oral administration of 2.5mg/kg/day amlexanox or vehicle control upon sacrifice at 13 weeks of age. Values are expressed as milligrams/millimetre (mg/mm) or milligrams/grams (mg/g). There were no statistical differences between conditions. n=5 animals per group.
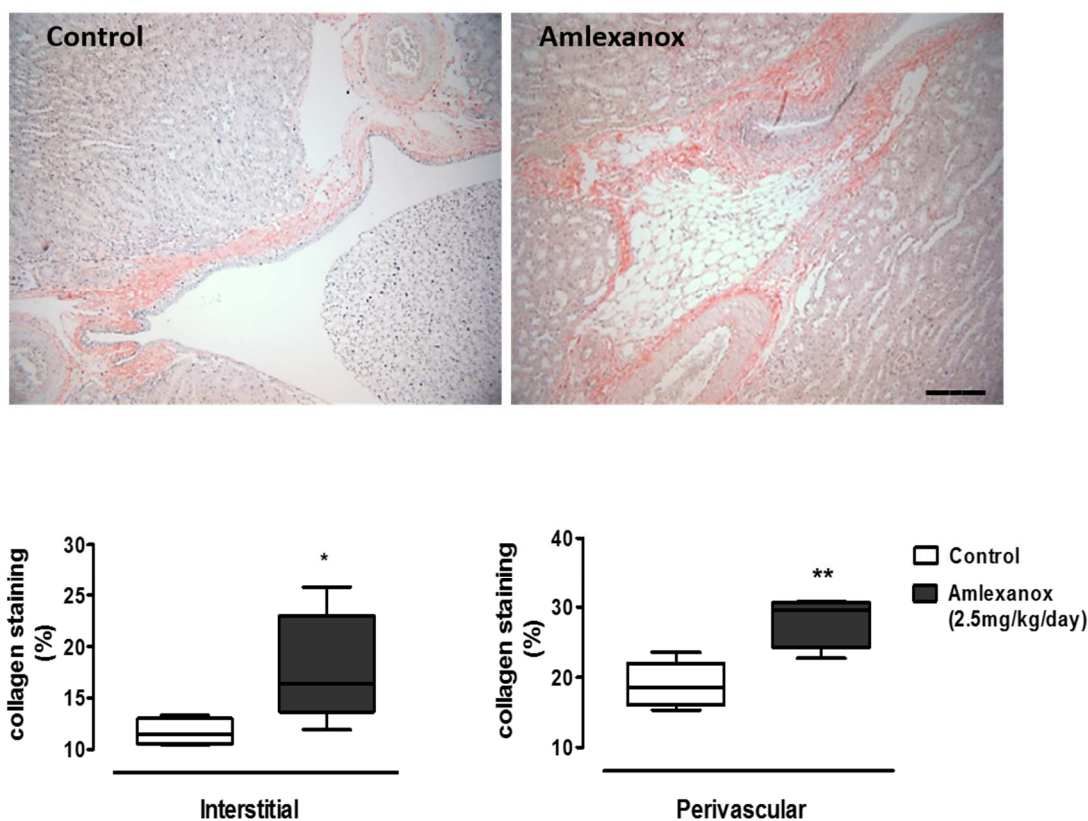
Figure 5-11. The effect of amlexanox administration on renal fibrosis in the SHRSP.

Representative images and quantification of kidney fibrosis derived from kidney tissue sections in SHRSP rats following oral administration of 2.5mg/kg/day amlexanox or vehicle control. Upon sacrifice at 13 weeks of age, kidneys were excised, weighed and were fixed using neutral buffered formalin, embedded in paraffin and sections were stained using picosirius red specific for collagen type I and III. Interstitial and perivascular collagen deposition was quantified using Image ProPlus software and values are expressed as a percentage of non-stained sections. Statistical significance * $p<0.05$, ** $p<0.01$. n=3-4 animals per group. Scale bar = 500µm.

5.2.7 The effect of amlexanox administration on gene expression in the heart and kidney of the SHRSP

Given the effect of elevated blood pressure on end-organ damage in both heart and kidney tissue following amlexanox administration to the SHRSP, we next assessed the expression of both GPR35 and $G\alpha_{13}$, its G-protein coupling partner, via real-time qRT-PCR. Spleen tissue was used as a positive control for GPR35 expression, owing to its high expression (Wang *et al.*, 2006a). Results demonstrated that neither GPR35 nor $G\alpha_{13}$ expression were altered in kidney (or spleen) following administration of amlexanox in comparison to vehicle-only control (Figure 5-12.A&B). Interestingly, GPR35 expression in the heart was elevated 2.7-fold ($p < 0.001$) following drug treatment. The mRNA expression of collagen type I and III genes were further assessed via quantitative RT-PCR in heart and kidney, revealing that collagen I and III expression were down-regulated in kidneys from amlexanox treated SHRSPs, compared to vehicle treated controls, and this effect was significant for collagen I expression ($P < 0.001$) (Figure 5-12.). This finding was unexpected, given that fibrosis was increased in kidney tissue following amlexanox treatment.
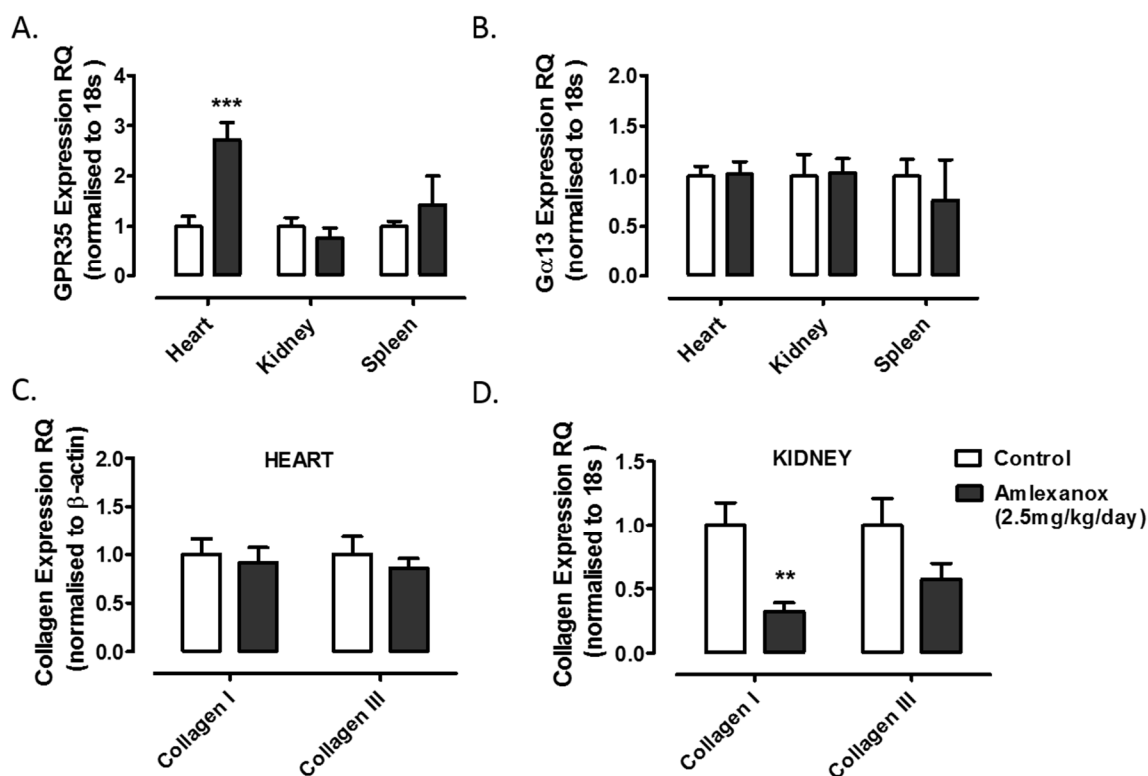
Figure 5-12. The effect of amlexanox administration on gene expression in tissues of the SHRSP.

Expression of GPR35 (A) and $G\alpha_{13}$ (B) in freshly isolated heart, kidney and spleen from SHRSP rats following oral administration of 2.5mg/kg/day amlexanox or vehicle control via real-time qRT-PCR and normalised to endogenous ribosomal 18s expression using respective TaqMan probes. C&D. Expression of collagen type I and III in freshly isolated heart (C) and kidney (D) tissue from SHRSP rats following oral administration of 2.5mg/kg/day amlexanox or vehicle control via real-time qRT-PCR and normalised to endogenous β-actin (heart) or ribosomal 18s expression (kidney) using respective TaqMan probes. Values are expressed as RQ, relative to control. Statistical significance ** $p < 0.01$, *** $p < 0.001$. n=5 animals per group.

5.2.8 The expression of GPR35 in the heart and kidney in experimental models of hypertension

To assess if GPR35 expression was altered in experimental models of hypertension compared to normotensive strains, expression levels were assessed at three ages (5, 16 and 21 weeks of age) in Wistar Kyoto (WKY; the reference strain for the SHRSP) and SHRSP in the heart and kidney. GPR35 expression in the heart was significantly reduced after 5 weeks of age ($p<0.001$), however, this was not different between strains (Figure 5-13.B). GPR35 expression was increased with age (>16 weeks) in the kidney and this was significantly higher in the SHRSP compared to the WKY strain ($p<0.05$). Therefore, this suggests that GPR35 expression in the kidney increases with age and is further exacerbated by hypertension. Next it was assessed whether changes in GPR35 expression were common in other experimental models with a hypertensive phenotype. Expression levels were assessed in heart, kidney and spleen (positive control) tissue derived from 12 week old C57BL/6 mice which have undergone continuous infusion of angiotensin II (AngII) at a dose of 400μg/kg/hr for 2-weeks via osmotic minipump compared to vehicle (dH$_2$O) control infused C57BL/6 mice. Results demonstrated that GPR35 expression was not significantly different between conditions (Figure 5-13.A). Given that AngII-induced hypertension is established 2-weeks following infusion (Zimmerman *et al.*, 2004, Clarke *et al.*, 2013), temporal differences in gene regulation may be difficult to measure here. Ultimately, these results suggest that GPR35 expression is regulated differently, depending on the mechanism of hypertension involved.
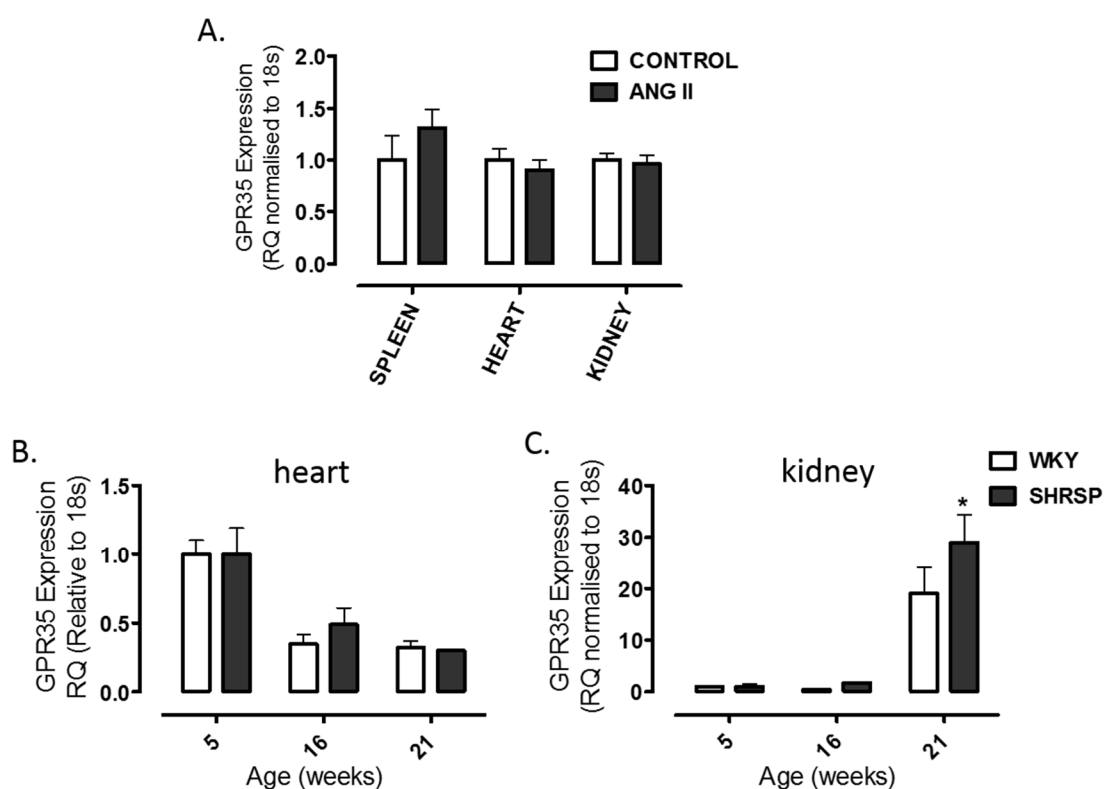
Figure 5-13. Assessment of GPR35 expression in rodent models of hypertension

A) Expression of GPR35 in freshly isolated spleen, heart and kidney tissue derived from a mouse model of hypertension, induced via angiotensin II (AngII) infusion or in control animals, assessed via real-time qRT-PCR and normalised to endogenous ribosomal 18s expression. B&C) Expression of GPR35 in freshly isolated heart (B) and kidney (C) derived from WKY and SHRSP rats at 5, 16 and 21 weeks of age, assessed via real-time qRT-PCR and normalised to endogenous ribosomal 18s expression. Values are expressed as RQ, relative to sham or vehicle control animal gene expression. Statistical significance * $p<0.05$. AngII/control n=5, WKY/SHRSP n=3

5.3 Discussion

This study has assessed the effects of stimulating GPR35 pharmacologically in a model of essential hypertension. Most evidently, results have demonstrated that low doses of the novel, highly potent GPR35 agonist amlexanox exacerbated hypertension, increasing SBP by up to 20mmHg, compared to vehicle treated controls. Furthermore, this study has also demonstrated that amlexanox administration affected end-organ damage, resulting in increased cardiac mass and renal fibrosis, and diminished endothelium-dependent vascular reactivity in the SHRSP. Thus far, confirmation of the true endogenous ligand for GPR35 has been challenging given that KYNA demonstrates extreme species-selectivity between GPR35 orthologues with low potency for rat GPR35 (Jenkins *et al.*, 2011). To this end, previous investigations as to the role GPR35 might play in the development of hypertension and cardiac hypertrophy predominantly focussed on the modulation of GPR35 expression, as opposed to its activation (Min *et al.*, 2010, Ronkainen *et al.*, 2014). However, recent advances in the identification of novel ligands for GPR35 have included a selection of mast cell stabilising compounds as high-potency agonists at GPR35 (Neetoo-Isseljee *et al.*, 2013, Mackenzie *et al.*, 2014). From this, the identification of amlexanox as a highly potent, surrogate agonist at rat GPR35 has provided an opportunity to examine the effect of GPR35 activation in the development of hypertension in a well-established model, the SHRSP (Mackenzie *et al.*, 2014, Delles *et al.*, 2010).

It was important to note, however, that alternative targets for amlexanox within the $NF_\kappa B$ pathway were recently reported, demonstrating that at serum concentrations higher than 1-2µM (IC_{50}), amlexanox inhibited IKK-kinases, IKK-ε and TBK1 (Reilly *et al.*, 2013). In a complex and extensive investigation, authors demonstrated that this led to an improved response to insulin sensitivity, reduced adipose inflammation and induced significant weight loss in mice fed a HFD (Reilly *et al.*, 2013). These findings have attracted considerable scientific interest since, in recent years, modulators of IKK-kinases have emerged as attractive therapeutic targets in the treatment of chronic inflammation and

tumour progression via their interaction with NF$_\kappa$B and subsequent modulation of gene transcription (Clement *et al.*, 2008). Importantly, the potency of amlexanox for rat GPR35 is within the nanomolar concentration range and to selectively target GPR35, a comparatively lower concentration of amlexanox would be adequate (Mackenzie *et al.*, 2014). To assess if administration of 10-fold lower dosages of amlexanox (2.5mg/kg) reflected some of the findings described by Reilly et al, SHRSP body weight and fat mass were measured and results clearly demonstrated that both parameters remained unchanged throughout drug administration. Consequently, the effects of amlexanox administration on the SHRSP could be better attributed to GPR35, which remains its only other reported target to date (Neetoo-Isseljee *et al.*, 2013, Mackenzie *et al.*, 2014).

Whilst tail-cuff plethysmography was able to detect a time-dependent increase in SBP in SHRSPs for both groups, there were no observed differences between conditions before day 20. However, following implantation of the radiotelemetry probe, pressure readings were sensitive enough to identify an increase in SBP of up to 20mmHg in amlexanox treated SHRSPs. Upon reflection, it is clear that radiotelemetry provided a more accurate blood pressure measurement than the tail-cuffing procedure owing to a less stressful and unrestrained environment. Given this, it is unsurprising that this method remains the most widely utilised in small studies of rodent hypertension (Kurtz *et al.*, 2005). First developed over two decades ago (Brockway *et al.*, 1991), radiotelemetry implantation has provided investigators with an extremely useful tool to assess the progressive development of hypertension and alternative parameters including heart rate and locomotion (Greene *et al.*, 2007). In this study, given a period of recovery following surgical implantation, radiotelemetry was sensitive enough to determine diurnal blood pressure variations related to circadian rhythms in light- and dark-cycles and this is a commonly reported effect in the SHRSP (Calhoun *et al.*, 1994). Whilst amlexanox administration did not appear to affect heart rate or locomotion in the SHRSPs, a substantial diurnal effect was clear when analysing the data for both measurements one week following surgical

implantation and this provided sufficient indication that the animals had recovered well (Greene *et al.*, 2007).

As discussed, the ambiguity related to the true endogenous agonist for GPR35 has hampered investigations to assess a role for GPR35 activation in a functional setting and therefore, the majority of studies have focused upon the regulation of its expression thus far (Min *et al.*, 2010, Sun *et al.*, 2008, Ronkainen *et al.*, 2014). Prior to this study, a role for GPR35 in the development of hypertension was highlighted for the first time in a GPR35 knock-out mouse model (Min *et al.*, 2010). Though investigators did not extensively dissect the phenotype of GPR35 KO mice, two parameters; blood pressure and cardiac mass were accounted for and via invasive Millar pressure catheter measurement in the right carotid artery, GPR35 KO mice had up to 37.5mmHg higher SBP than WT littermates (Min *et al.*, 2010). Authors did not comment on a role for GPR35 here, however, it could be hypothesised that GPR35 expression and presumably, endogenous activation provided protection against the development of hypertension or, that GPR35 might be involved in the maintenance of myogenic tone. In the current study, the SHRSP offered an excellent model to explore this hypothesis, given that hypertension is fully established at 10-weeks of age and therefore, any protection offered following GPR35 activation following amlexanox administration may well be evident from an early time point. However, results here demonstrated that GPR35 activation is not protective against the development of hypertension in the SHRSP, but rather exacerbated its development resulting in an elevated SBP which was >20mmHg higher in amlexanox treated SHRSPs, compared to vehicle treated controls and this effect was evident throughout the study.

In light of these contrasting indications, it is important to question the mechanism whereby GPR35 activation via amlexanox might lead to an increase in blood pressure. One major contributing factor stems from the uncertainty of a true endogenous ligand(s) for GPR35 or its potential concentrations in an *in vivo* setting (Milligan, 2011). It is possible that endogenous activity at GPR35 has been affected by the addition of a synthetic ligand,

altering its confirmation and thus physiological response. Allosteric modulation is understood to either potentiate or inhibit endogenous activation via receptor interaction at a distinct binding position from the orthosteric (endogenous) site (Conn *et al.*, 2009, Milligan and Smith, 2007). Given that amlexanox is a partial agonist at GPR35 and this is a common feature of allosteric agonists for class A GPCRs (Schwartz and Holst, 2007), it is possible that amlexanox is interfering with endogenous activation of GPR35 and this might promote signalling via alternative pathways to exacerbate hypertension. This mode of allosteric modulation is true for a number of GPCRs and a classic example relates to allosteric modulation of the chemoattractant receptor-homologous molecule (CRTH2) which can lead to functional selectivity resulting in the potentiation of G-protein independent β-arrestin signalling in T-helper cells (Mathiesen *et al.*, 2005). To assess if amlexanox or indeed any other agonist at GPR35 displays allosteric modulation it is essential to assess their cooperativity alongside the true endogenous ligand in a wide-range of primary and secondary endpoint assays *in vitro*, thereby identifying the mode of its potential allosterism (Smith *et al.*, 2011). Jenkins and colleagues have identified multiple overlapping binding sites belonging to KYNA and zaprinast (Jenkins *et al.*, 2011). Given this, zaprinast could theoretically provide a robust substitute for KYNA in the required assays, however, evidence that KYNA is the true endogenous ligand at GPR35 remains conflicted (Jenkins *et al.*, 2011, Milligan, 2011).

Mechanistically, peripheral resistance and vascular tone are modulated by vascular smooth muscle cell reactivity and a role for various GPCRs, including AT_1R and ET-1 R, has been well characterised in the setting of vasoreactivity following acute vascular injury and exposure to increased shear stress (Touyz and Schiffrin, 2000). Whilst $Gα_q$ activation and subsequent modulation of Ca^{2+} release is understood to be a major contributor to vasoconstriction, the activation of Rho A and subsequent ROCK1/2 signalling has also been implicated in the development of hypertension following the inhibition of MLCP via phosphorylation of MYPT-1 (Seko *et al.*, 2003, Wirth, 2010). Given that results in an

earlier chapter from this study demonstrate that GPR35 activation in primary human smooth muscle cells led to a contracted phenotype mediated via Rho A/ ROCK1/2 signalling (Chapter 4-0), it is possible that amlexanox administration has resulted in similar vascular effects to alter vascular tone in the SHRSP. Taking this together with results demonstrating increased pulse pressure following amlexanox administration, it is possible that sustained GPR35 activation mediated its vasoconstrictive effects, at least in part, via vascular SMCs. Importantly, studies have shown that pulse pressure is a precise, independent risk factor for coronary artery disease, vessel stiffness and end-organ damage, with particular implications for the renal system (Franklin *et al.*, 1999, Safar *et al.*, 2012).

Despite an increase in pulse pressure following amlexanox exposure, arterial stiffness was not fully reflected in *ex vivo* experiments as results indicated that SMC-dependent vasorelaxation remained uncompromised in large and small resistance arteries derived from amlexanox treated SHRSPs. However, endothelium-dependent relaxation was reduced by more than 20% following exposure to maximal concentrations of carbachol in aortic preparations derived from amlexanox treated animals compared to vehicle controls. However, given that amlexanox administration promoted further elevations in SBP, MAP and PP in the SHRSP, increased shear stress within the vasculature may have resulted in endothelial cell loss and dysfunction, in turn compromising signalling between vascular endothelial and smooth muscle cells (Chiu and Chien, 2011). It is well understood that vascular endothelial cell dysfunction is able to perpetuate the hypertensive response and promote vascular disease via a reduction in nitric oxide (NO) release and enhanced recruitment of inflammatory mediators (Cai and Harrison, 2000). This remains to be studied in detail in the future.

A role for GPR35 in cardiac hypertrophy was also explored in this model and while results indicated that amlexanox administration may promote an enlargement in cardiomyocytes situated within cross-sections of the LV wall, the effect was only significant for cardiac

mass at a whole tissue level. It is hypothesised that with larger sample numbers, this effect may have proved significant and future investigations may benefit from the application of a power calculation to judge the optimum sample size required to detect an effect. However, with regard to GPR35 expression, the small sample size was adequate to highlight a significant up regulation in the myocardium. Interestingly, these findings correlate with recent reports of HIF-1 mediated GPR35 expression in cardiac tissue undergoing progressive remodelling following ligation of the LAD coronary artery (Ronkainen *et al.*, 2014). Importantly, HIF-1 activation has also been implicated in the early stages of pressure overload induced cardiac dysfunction and hypertrophy (Sano *et al.*, 2007). An existing limitation of this study is that simultaneous HIF-1 activation was not assessed and therefore, it is impossible to draw parallels between HIF-1 activation and GPR35 expression directly in the SHRSP. However, taking this information together, it is possible to hypothesise that GPR35 up regulation is a result of HIF-activation following pressure overload presented by an increased SBP in the SHRSP and this would be important to investigate in future studies. Given that GPR35 expression has been repeatedly implicated in heart failure (Min *et al.*, 2010), progressive remodelling and cardiomyocyte hypertrophy (Ronkainen *et al.*, 2014) further investigation to dissect a mechanistic role for GPR35 in this setting will be required.

Amlexanox treatment also resulted in significantly increased kidney fibrosis and this was highlighted within interstitial and perivascular regions of the kidney via collagen I and III staining. Renal blood flow accounts for up to 20% of cardiac output and therefore it is understandable that kidney reperfusion apparatus is highly sensitive to alterations in blood pressure (Nangaku and Eckardt, 2007). This has been confirmed by reports of glomerular hyperperfusion and hypertrophy within juxtamedullary regions of the kidney following exposure to increased systolic blood pressure in the SHRSP (Hultstrom, 2012). Therefore, as with the heart, it is possible that exacerbated hypertension led to a progressive reduction in glomerular filtration and the resulting tubular atrophy and

apoptosis presented as increased interstitial fibrosis and perivascular remodelling in amlexanox treated SHRSP kidneys (Hultstrom, 2012). Remarkably, interstitial fibrosis is considered to be a significant hallmark in end-stage renal failure and given that both interstitial and perivascular fibrosis was evident at 12-weeks of age, GPR35 activation seems to have provoked a particularly aggressive response (Nangaku and Eckardt, 2007). There was no evidence of an alteration in GPR35 expression in the kidney following amlexanox administration. However, GPR35 expression was also assessed in the heart and kidney of alternative models of hypertension and, whilst there were no significant alterations in expression following Ang II infusion in mice for either tissue, GPR35 expression was elevated at in the kidney of the SHRSP and the WKY at 21-weeks of age, and this was significantly higher in the SHRSP strain. Though kidney damage is not often evident in the SHRSP before 30-weeks of age, it is understood that glomerular filtration starts to decline at 20-weeks as a result of sustained hypertension and therefore, this is often the earliest indicator of renal damage (Hultstrom, 2012). Given that this study has demonstrated sensitive regulation of GPR35 expression in suggested early stages of renal damage, it is possible that GPR35 may also be a highly sensitive gene-biomarker for progressive remodelling in the kidney, as well as the heart (Ronkainen *et al.*, 2014)

5.3.1 Conclusions

In conclusion, this chapter has defined a novel role for GPR35 activation in both hypertension and its related end-organ damage to the vasculature, kidney and heart. Although more work is required to dissect whether end-organ damage is a result of increased peripheral resistance or GPR35 activation (or both), this can be realistically explored and compartmentalised within individual disease models in the future. Most importantly, to fully examine a therapeutic potential for GPR35 antagonists in the setting of hypertension and progressive remodelling in the heart and kidney, a better understanding of GPR35's endogenous agonist will be required.

6 General Discussion

6.1 Summary of main findings

In this thesis I have undertaken an integrated analysis of a role for GPR35 in the progression of various pathologies related to cardiovascular disease. In the first results chapter, this study aimed to provide an in-depth characterisation of existing surrogate and endogenous GPR35 ligands, relating to their species-selectivity for both human and rodent orthologues of GPR35. In focusing on the species pharmacology of ligands, we have identified optimal tools to realistically explore a role for GPR35, both *in vitro* and *in vivo*, for the first time. In results chapter 4.0, a role for GPR35 mediated signalling was evident in the progression of vascular remodelling of primary endothelial and smooth muscle cells islolated from human saphenous veins. The final results chapter investigated pharmacological activation of GPR35 *in vivo* in the setting of hypertension and related end-organ damage in the SHRSP. The results of this research support the assertion that there is therapeutic potential for GPR35 antagonists in the setting of vascular remodelling, hypertension and end-organ damage in the heart and kidneys.

Whilst previous studies have reported low level GPR35 expression in HUVECs (Barth *et al.*, 2009), the results presented in this thesis suggest that GPR35 is robustly expressed in various vascular cell types, including HUVEC's, HSV EC and SMCs. Importantly, expression levels within HSV EC were comparable to those demonstrated in the colon, a tissue previously reported to express GPR35 highly (Taniguchi *et al.*, 2006). Previously, expression analysis of GPR35 has primarily focused upon gastrointestinal tissue, however, this investigation is the first to compare and contrast expression within tissue and individual primary cell populations to explore a potential role for GPR35 within the vasculature.

Taking this together with the characterisation of novel, highly potent and human-selective GPR35 ligands; the agonist pamoic acid, and two distinct, competitive antagonists CID-2745687 and ML-145 (Jenkins *et al.*, 2012), an opportunity to assess a role for GPR35

within functional cell culture models relevant to vascular remodelling and vein graft occlusion in cells of a human origin was evident. In the assessment of the migratory and proliferative capacity of vascular endothelial and smooth muscle cells, results demonstrated that GPR35 activation altered the arrangement of cytoskeletal actin filaments to promote a migratory phenotype in HSV SMCs, and this was blocked in the presence of either of the human-selective GPR35 antagonists. Importantly, co-incubation with either antagonist provided confirmation for endogenous GPR35 activation in primary cells. This thesis is the first to assess these novel GPR35 antagonists in a pathophysiologically relevant functional model. Moreover, the findings were further consolidated, as selective coupling of GPR35 to $G\alpha_{12/13}$ following pamoic acid stimulation was observed in both the molecular pharmacological assays and the functional assays in primary HSV SMCs. Our results demonstrated that GPR35 mediated migration was completely abolished in the presence of two distinct Rho A and ROCK pathway inhibitors, Y-16 and Y-27632, respectively. Whilst Rho A signalling has broader implications for the maintenance and regulation of vasoconstriction, atherosclerosis and vascular remodelling, their current inhibitors have displayed questionable target specificity *in vivo* (Budzyn *et al*., 2006). Therefore, blocking this pathway might not be advantageous in a wider therapeutic sense. Given that GPR35 antagonists are not reported to target elsewhere, the use of these compounds to inhibit GPR35 mediated $G\alpha_{12/13}$ signalling and subsequent activation of Rho A and ROCK1/2 may prove beneficial for clinical applications whereby a window of opportunity exists for local delivery, such as those presented during CABG surgery or PTCA strategies (Conte, 2007). Currently, intervention strategies have explored the use of polymer coated DES and adenoviral-mediated gene therapy. However, the patency rates of grafts and stents remain potentially compromised due to endothelial dysfunction and loss of the intact endothelial layer (Rienstra *et al*., 2008, Otsuka *et al*., 2012).

Moreover, results from this study have highlighted a potential role for GPR35 activation in the maintenance of endothelial cell integrity and cell-cycle progression. Using two distinct

assays, GPR35 activation produced a concentration-dependent increase in EC proliferation which was blocked upon co-administration with either GPR35 antagonist. Importantly, there remains a requirement for novel therapeutic targets which enhance re-endothelialisation following stenting; for example, DES are subject to severe late stenosis due to a 50% reduction in re-endothelialisation following deployment (Joner *et al.*, 2006). However, further research is required to truly delineate the role for GPR35 agonism/ antagonism in human ECs and SMCs. To assess if GPR35 antagonists might be useful in this setting, it would be relevant to assess if they also inhibited serum induced proliferation of HSV EC as this might reflect inhibition of endogenous GPR35 ligand mediated agonism. Of course, as with the results derived from the migratory capacity of HSV SMCs following serum stimulation, without knowledge of a true endogenous agonist, such as LPA (Oka *et al.*, 2010), these results are challenging to interpret. To understand the implications of simultaneously targeting GPR35 activation in both vascular cell types, further investigation is required. As previously noted, it would be advantageous to assess this in an assay whereby neointimal formation is quantified within intact vein tissue following exposure to ligands (McDonald *et al.*, 2013). Moreover, this setting would also be conducive to assess the effect of GPR35 mediated improvement in endothelial cell integrity and smooth muscle cell migration in the presence of hypoxia and/ or exogenously added inflammatory mediators, such as IL-β and TNF-α. These are of particular relevance, since a very recent publication demonstrated that HIF-1α activation is able to directly up-regulate GPR35 expression in myocardial tissue in a time-dependent manner following exposure to hypoxic conditions (Ronkainen *et al.*, 2014). Additionally, it has been reported that GPR35 activation in monocytes promoted firm arrest to an endothelial cell monolayer under vascular flow conditions, suggestive of a role for GPR35 in acute vascular inflammation (Barth *et al.*, 2009).

Whilst the application of basic pharmacological approaches has provided us with a degree of certainty and specificity in targeting endogenously expressed GPR35 in cells of human

origin, the varied potency of ligands at multiple species orthologues has presented distinct challenges for the use of GPR35 agonists and antagonists within rodent models of disease. Moreover, they also highlight implications for the conclusions of a role for GPR35 activation and nociception derived from a previous study employing the use of human-selective agonist pamoic acid in a mouse model which demonstrated that increasing dosages of pamoic acid reduced nociception following an acetic acid induced abdominal constriction test (Zhao *et al.*, 2010). However, following reports that blood pressure readings in mice lacking GPR35 were significantly increased by up to 37.5mmHg (Min *et al.*, 2010), it was hypothesised that GPR35 expression, and theoretically endogenous activation, might offer a protective effect against the development of hypertension or play a role in the maintenance of myogenic tone. One experimental paradigm available to test this hypothesis was to assess the effect of GPR35 activation in the SHRSP, which at 10-weeks of age develops established hypertension (SBP>110mmHg) (Hultstrom, 2012). The lack of an appropriate rodent specific antagonist was a limiting factor here, by which a reversal of the effects of GPR35-mediated signalling could not be fully dissected. In light of this, it was imperative to utilise an agonist with high potency and specificity for GPR35. The identification of amlexanox resulted from a screen of mast cell stabilising compounds at GPR35 and therefore, it was already a marketed compound with known safety and bio-availability characteristics (Mackenzie *et al.*, 2014, Neetoo-Isseljee *et al.*, 2013). However, amlexanox was also recently reported to be an inhibitor of IKK-ε and TBK1 in mice, and its administration in rodent models induced a rapid reduction in body weight and improved insulin control at serum concentrations exceeding 1-2µM following administration at doses ranging from 25-100mg/kg/day (Reilly *et al.*, 2013). Given that pharmacological assessment demonstrated that amlexanox has an EC_{50}=4.5nM for rat GPR35, we hypothesised that 10-100-fold lower doses (2.5mg/kg/day) would be optimal to target GPR35 at relevant serum concentrations. In contrast to the observations reported by Reilly et al. we observed no change in body weight throughout the study or fat deposition following animal sacrifice (Reilly *et al.*, 2013).

We were therefore confident that this low dose of amlexanox was sufficient to target GPR35 in the SHRSP and assess its effects on cardiovascular haemodynamics. To fully assess circulating concentrations of amlexanox within serum, it would have been optimal to carry out quantitative mass spectrometry in serum samples following exposure to increasing dosages of amlexanox and though serum samples were collected upon sacrifice, time constraints did not permit further exploration here (Lietz *et al.*, 2013).

Rather than exerting protection against the development of hypertension, pharmacological agonism of GPR35 exacerbated the hypertensive response and related end-organ damage in the heart and kidneys of the SHRSP. Whilst this finding disproved our original hypothesis, upon further consideration, it was clear that these results reflected our findings from functional characterisation of HSV SMCs, given that a contractile phenotype was evident following a rearrangement in F-actin filaments in HSV SMCs following GPR35 stimulation. Essentially, SMCs are integral in vasoconstriction and together, the evidence suggests that an elevation in SBP and MAP may have been mediated, at least in part, via SMC contraction (Wang *et al.*, 2009). In future studies, it might also be interesting to investigate the arrangement of cytoskeletal filaments in arterial SMCs derived from larger resistance vessels, or even cells of the microvasculature, following exposure to GPR35 ligands. Importantly, whilst there have been differences reported between ET_1R subtype Ca^{2+} handling in excitation-contraction coupling in venous SMCs compared to arterial SMCs (Claing *et al.*, 2002), there is no information to suggest that there might be any differences in the regulation of cytoskeletal architecture following ROCK1/2 mediated inhibition of MLCP between SMC subtypes.

Importantly here, PP was also increased following amlexanox administration and studies have indicated that this is a robust independent marker of arterial stiffness and end-organ damage (Safar *et al.*, 2012). These indications were partially reflected following the examination of vasoreactivity in small and large vessels and results demonstrated that endothelium-dependent relaxation in aortic samples from amlexanox treated SHRSPs

was significantly reduced by 20%, compared to vehicle treated control samples. Despite a lack of evidence for compromised SMC dependent vasoconstriction in these experiments, the results indicate a degree of endothelial damage or dysfunction in the vasculature and this may have resulted from increased shear stress to induce endothelial cell loss and dysfunction (Chiu and Chien, 2011). To further clarify this issue, it would be advantageous to directly assess the effect of ligand exposure on isometric tension in intact small and large arteries derived from normotensive animals. Whilst the SHRSP provided an excellent model to test our original hypothesis, it would now be relevant to assess if GPR35 activation also promotes hypertension in otherwise normotensive counterparts, such as the WKY, in future studies. In doing this, it may also be possible to ascertain if an elevation in SBP, and thus total peripheral resistance, is responsible for the cardiac and renal related end-organ damage observed here. Findings within this study remain difficult to dissect in this sense, given that end-organ damage is established in the SHRSP from an early age time point - regardless of ligand exposure (Camargo *et al.*, 1993).

In addition to an increase in SBP, MAP and PP, our findings suggest that amlexanox administration exacerbated damage to the heart and kidneys. This was evident following whole heart mass assessment, which was significantly larger in SHRSPs treated with amlexanox compared to vehicle controls. Moreover, GPR35 expression was elevated by 2.7-fold in the heart. Whilst there was no evidence of an alteration of GPR35 expression in the kidney, it was clear that amlexanox administration increased fibrosis in the kidney in both the interstitial and perivascular regions and these are suggested hallmarks of late-stage renal damage (Nangaku and Eckardt, 2007). While the implications of pharmacologically targeting GPR35 in the heart or kidney are currently unclear, it is possible that this effect was primarily mediated by an elevation in SBP, however, results here may also be suggestive of a role for GPR35 as a primary mediator of remodelling, at least within the myocardium. This is particularly relevant given that we also demonstrated

that H9c2 cardiomyocytes underwent hypertrophy following transient transfection of rat GPR35 and stimulation with amlexanox or zaprinast. Moreover, the elevation in GPR35 expression reported here is concurrent with a recent publication which demonstrated HIF-1α mediated up-regulation of GPR35 expression in the myocardium undergoing progressive remodelling in response to acute and chronic hypoxia (Ronkainen *et al.*, 2014) and an investigation which reported an up-regulation of GPR35 in the myocardial tissue derived from patients with heart failure (Min *et al.*, 2010). Whilst authors have recently concluded that GPR35 expression might be a sensitive biomarker for progressive remodelling in the heart, results here suggest that GPR35 expression, and subsequent signalling via the $G\alpha_{12/13}$ – Rho A – ROCK 1/2 axis, has broader implications for remodelling within the vasculature, myocardium and possibly, the kidney. Essentially, all of the functional studies conducted thus far, *in vitro* and *in vivo,* suggest a therapeutic value for GPR35 antagonists within this setting and providing that screening to identify these at rodent orthologues continues, future experimental applications to define a role for GPR35 within these systems will be of enhanced value.

Fundamentally, many of the findings reported here raise important questions relating to the ambiguity of endogenous activity of GPR35. While results from this study have confirmed previous findings of orthologue selectivity for the endogenous agonist KYNA, in that it demonstrates little efficacy or potency at human GPR35 (Jenkins *et al.*, 2010), it has also highlighted that this was similar for KYNA activity at mouse GPR35. Taking these findings together, evidence for a role for KYNA as the true endogenous agonist at GPR35 remains unconvincing. Given that GPR35-mediated signalling following endogenous activation also remains uncharacterised, as does the possibility of allosteric modulation via surrogate synthetic ligands, the interpretation of the specific effect of an exogenous, synthetic agonist on hypertension and end-organ damage is challenging. This also has implications for a role for GPR35 activation in serum induced migration, which was inhibited following exposure of high concentrations of either human-selective GPR35

antagonist. The findings described here and their relationship to each other are illustrated with relevance to the published literature (Figure 6.1).

In conclusion, this study has employed multiple approaches to pharmacologically target GPR35 in both human and rodent tissues of the cardiovascular system. Importantly, this translational approach has highlighted a role for GPR35 within a range of pathophysiological settings with relevance to cardiovascular disease and results suggest that inhibition of GPR35 mediated signalling may be therapeutically relevant in the treatment of vascular remodelling, hypertension and progressive remodelling of the heart and renal system. In the future, it will be important to assess the effect of GPR35 mediated signalling within individual disease models, however, to gain a better understanding of endogenous GPR35 activation, the identification of the true endogenous ligand for GPR35 will be key.
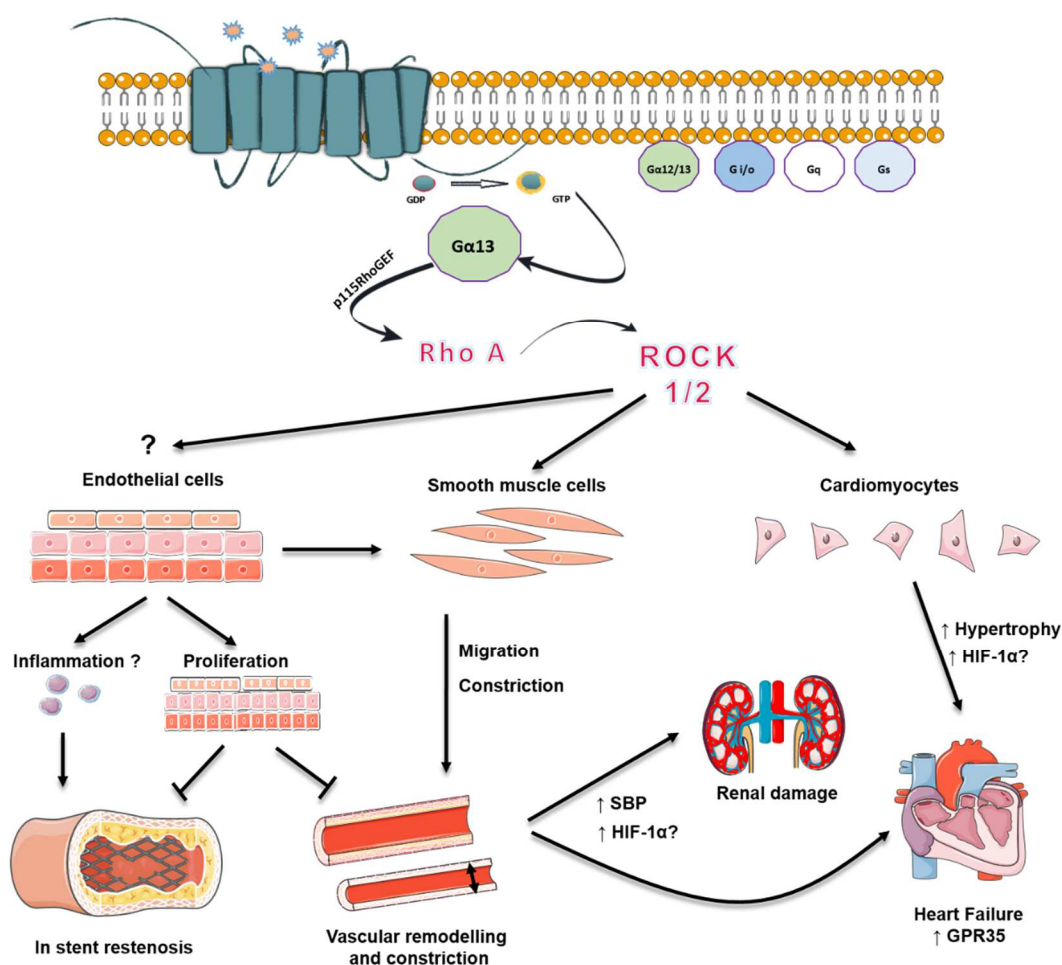
Figure 6-1. Summary of a role for GPR35 in the pathology of CVD.

GPR35 activation promoted a contracted, migratory phenotype in HSV SMCs mediated via selective $G\alpha_{12/13}$ activation of Rho A and ROCK 1/2, suggestive of a role for GPR35 in vascular remodelling and vasoconstriction. A resulting elevation in systolic blood pressure (SBP) following pharmacological GPR35 agonism *in vivo* has direct implications for renal and cardiac function following pressure overload and reports also suggest that activation of hypoxia inducible factor-1 (HIF-1) may enhance GPR35 expression in these tissues (Ronkainen *et al.*, 2014). GPR35 activation induced a proliferative response in HSV ECs, which might offer vascular protection. Others have reported an increase in monocyte adhesion to vascular ECs following GPR35 activation and together with increased SMC migration, a role for GPR35 in acute vascular inflammation and neointimal formation may also be evident (Barth *et al.*, 2009). Literature also suggests that Rho A/ ROCK 1/2 signalling is implicated in cardiomyocyte hypertrophy, which was also evident in H9c2 cells and at the whole heart level in the SHRSP following GPR35 activation.

7 List of References

AI, S., KUZUYA, M., KOIKE, T., ASAI, T., KANDA, S., MAEDA, K., SHIBATA, T. & IGUCHI, A. 2001. Rho-Rho kinase is involved in smooth muscle cell migration through myosin light chain phosphorylation-dependent and independent pathways. *Atherosclerosis,* 155**,** 321-7.

AKGOZ, M., KALYANARAMAN, V. & GAUTAM, N. 2004. Receptor-mediated reversible translocation of the G protein betagamma complex from the plasma membrane to the Golgi complex. *J Biol Chem,* 279**,** 51541-4.

ALBUQUERQUE, E. X. & SCHWARCZ, R. 2013. Kynurenic acid as an antagonist of alpha7 nicotinic acetylcholine receptors in the brain: facts and challenges. *Biochem Pharmacol,* 85**,** 1027-32.

ALEWIJNSE, A. E., TIMMERMAN, H., JACOBS, E. H., SMIT, M. J., ROOVERS, E., COTECCHIA, S. & LEURS, R. 2000. The effect of mutations in the DRY motif on the constitutive activity and structural instability of the histamine H(2) receptor. *Mol Pharmacol,* 57**,** 890-8.

AMIRKHANI, A., HELDIN, E., MARKIDES, K. E. & BERGQUIST, J. 2002. Quantitation of tryptophan, kynurenine and kynurenic acid in human plasma by capillary liquid chromatography-electrospray ionization tandem mass spectrometry. *J Chromatogr B Analyt Technol Biomed Life Sci,* 780**,** 381-7.

ANDERSON, H. V., SHAW, R. E., BRINDIS, R. G., HEWITT, K., KRONE, R. J., BLOCK, P. C., MCKAY, C. R. & WEINTRAUB, W. S. 2002. A contemporary overview of percutaneous coronary interventions. The American College of Cardiology-National Cardiovascular Data Registry (ACC-NCDR). *J Am Coll Cardiol,* 39**,** 1096-103.

BALLESTEROS, J., KITANOVIC, S., GUARNIERI, F., DAVIES, P., FROMME, B. J., KONVICKA, K., CHI, L., MILLAR, R. P., DAVIDSON, J. S., WEINSTEIN, H. & SEALFON, S. C. 1998. Functional microdomains in G-protein-coupled receptors. The conserved arginine-cage motif in the gonadotropin-releasing hormone receptor. *J Biol Chem,* 273**,** 10445-53.

BARANDIER, C., MING, X. F. & YANG, Z. 2003. Small G proteins as novel therapeutic targets in cardiovascular medicine. *News Physiol Sci,* 18**,** 18-22.

BARTH, M. C., AHLUWALIA, N., ANDERSON, T. J., HARDY, G. J., SINHA, S., ALVAREZ-CARDONA, J. A., PRUITT, I. E., RHEE, E. P., COLVIN, R. A. & GERSZTEN, R. E. 2009. Kynurenic acid triggers firm arrest of leukocytes to vascular endothelium under flow conditions. *J Biol Chem,* 284**,** 19189-95.

BETTS, M. J. & STERNBERG, M. J. 1999. An analysis of conformational changes on protein-protein association: implications for predictive docking. *Protein Eng,* 12**,** 271-83.

BHF. 2012. *British Heart Foundation - Blood pressure* [Online]. Available: http://www.bhf.org.uk/research/heart-statistics/risk-factors/blood-pressure.aspx [Accessed 23 Aug 2014].

BIAN, D., MAHANIVONG, C., YU, J., FRISCH, S. M., PAN, Z. K., YE, R. D. & HUANG, S. 2006. The G12/13-RhoA signaling pathway contributes to efficient lysophosphatidic acid-stimulated cell migration. *Oncogene,* 25**,** 2234-44.

BINDELS, L. B., DEWULF, E. M. & DELZENNE, N. M. 2013. GPR43/FFA2: physiopathological relevance and therapeutic prospects. *Trends Pharmacol Sci,* 34**,** 226-32.

BJARNADOTTIR, T. K., GLORIAM, D. E., HELLSTRAND, S. H., KRISTIANSSON, H., FREDRIKSSON, R. & SCHIOTH, H. B. 2006. Comprehensive repertoire and phylogenetic analysis of the G protein-coupled receptors in human and mouse. *Genomics,* 88**,** 263-73.

BOND, M., BAKER, A. H. & NEWBY, A. C. 1999. Nuclear factor kappaB activity is essential for matrix metalloproteinase-1 and -3 upregulation in rabbit dermal fibroblasts. *Biochem Biophys Res Commun,* 264**,** 561-7.

BOND, M., CHASE, A. J., BAKER, A. H. & NEWBY, A. C. 2001. Inhibition of transcription factor NF-kappaB reduces matrix metalloproteinase-1, -3 and -9 production by vascular smooth muscle cells. *Cardiovasc Res,* 50**,** 556-65.

BORSHCHEVSKIY, V. & BULDT, G. 2013. Structural biology: Active arrestin proteins crystallized. *Nature,* 497**,** 45-6.

BROCKWAY, B. P., MILLS, P. A. & AZAR, S. H. 1991. A new method for continuous chronic measurement and recording of blood pressure, heart rate and activity in the rat via radio-telemetry. *Clin Exp Hypertens A,* 13**,** 885-95.

BRYAN, B. A., DENNSTEDT, E., MITCHELL, D. C., WALSHE, T. E., NOMA, K., LOUREIRO, R., SAINT-GENIEZ, M., CAMPAIGNIAC, J. P., LIAO, J. K. & D'AMORE, P. A. 2010. RhoA/ROCK signaling is essential for multiple aspects of VEGF-mediated angiogenesis. *FASEB J,* 24**,** 3186-95.

BUDZYN, K., MARLEY, P. D. & SOBEY, C. G. 2006. Targeting Rho and Rho-kinase in the treatment of cardiovascular disease. *Trends Pharmacol Sci,* 27**,** 97-104.

BUSTIN, S. A., BENES, V., NOLAN, T. & PFAFFL, M. W. 2005. Quantitative real-time RT-PCR--a perspective. *J Mol Endocrinol,* 34**,** 597-601.

CABRERA-VERA, T. M., VANHAUWE, J., THOMAS, T. O., MEDKOVA, M., PREININGER, A., MAZZONI, M. R. & HAMM, H. E. 2003. Insights into G protein structure, function, and regulation. *Endocr Rev,* 24**,** 765-81.

CAI, H. & HARRISON, D. G. 2000. Endothelial dysfunction in cardiovascular diseases: the role of oxidant stress. *Circ Res,* 87**,** 840-4.

CALHOUN, D. A., JONES, D., TEXTOR, S., GOFF, D. C., MURPHY, T. P., TOTO, R. D., WHITE, A., CUSHMAN, W. C., WHITE, W., SICA, D., FERDINAND, K., GILES, T. D., FALKNER, B. & CAREY, R. M. 2008a. Resistant hypertension: diagnosis, evaluation, and treatment. A scientific statement from the American Heart Association Professional Education Committee of the Council for High Blood Pressure Research. *Hypertension,* 51**,** 1403-19.

CALHOUN, D. A., JONES, D., TEXTOR, S., GOFF, D. C., MURPHY, T. P., TOTO, R. D., WHITE, A., CUSHMAN, W. C., WHITE, W., SICA, D., FERDINAND, K., GILES, T. D., FALKNER, B. & CAREY, R. M. 2008b. Resistant hypertension: diagnosis, evaluation, and treatment: a scientific statement from the American Heart Association Professional Education Committee of the Council for High Blood Pressure Research. *Circulation,* 117**,** e510-26.

CALHOUN, D. A., ZHU, S., WYSS, J. M. & OPARIL, S. 1994. Diurnal blood pressure variation and dietary salt in spontaneously hypertensive rats. *Hypertension,* 24**,** 1-7.

CAMARGO, M. J., VON LUTTEROTTI, N., CAMPBELL, W. G., JR., PECKER, M. S., JAMES, G. D., TIMMERMANS, P. B. & LARAGH, J. H. 1993. Control of blood pressure and end-organ damage in maturing salt-loaded stroke-prone spontaneously hypertensive rats by oral angiotensin II receptor blockade. *J Hypertens,* 11**,** 31-40.

CARRETERO, O. A. & OPARIL, S. 2000. Essential hypertension. Part I: definition and etiology. *Circulation,* 101**,** 329-35.

CASCIO, W. E., YANG, H., MULLER-BORER, B. J. & JOHNSON, T. A. 2005. Ischemia-induced arrhythmia: the role of connexins, gap junctions, and attendant changes in impulse propagation. *J Electrocardiol,* 38**,** 55-9.

CHARO, I. F. & TAUB, R. 2011. Anti-inflammatory therapeutics for the treatment of atherosclerosis. *Nat Rev Drug Discov,* 10**,** 365-76.

CHEN, S. R., SAMORISKI, G. & PAN, H. L. 2009. Antinociceptive effects of chronic administration of uncompetitive NMDA receptor antagonists in a rat model of diabetic neuropathic pain. *Neuropharmacology,* 57**,** 121-6.

CHEN, Y. & GUILLEMIN, G. J. 2009. Kynurenine pathway metabolites in humans: disease and healthy States. *Int J Tryptophan Res,* 2**,** 1-19.

CHIU, J. J. & CHIEN, S. 2011. Effects of disturbed flow on vascular endothelium: pathophysiological basis and clinical perspectives. *Physiol Rev,* 91**,** 327-87.

CHUN, L., ZHANG, W. H. & LIU, J. F. 2012. Structure and ligand recognition of class C GPCRs. *Acta Pharmacol Sin,* 33**,** 312-23.

CIVELLI, O., SAITO, Y., WANG, Z., NOTHACKER, H. P. & REINSCHEID, R. K. 2006. Orphan GPCRs and their ligands. *Pharmacol Ther,* 110**,** 525-32.

CLAING, A., SHBAKLO, H., PLANTE, M., BKAILY, G. & D'ORLEANS-JUSTE, P. 2002. Comparison of the contractile and calcium-increasing properties of platelet-activating factor and endothelin-1 in the rat mesenteric artery and vein. *Br J Pharmacol,* 135**,** 433-43.

CLARKE, C., FLORES-MUNOZ, M., MCKINNEY, C. A., MILLIGAN, G. & NICKLIN, S. A. 2013. Regulation of cardiovascular remodeling by the counter-regulatory axis of the renin-angiotensin system. *Future Cardiol,* 9**,** 23-38.

CLEMENT, J. F., MELOCHE, S. & SERVANT, M. J. 2008. The IKK-related kinases: from innate immunity to oncogenesis. *Cell Res,* 18**,** 889-99.

CONN, P. J., CHRISTOPOULOS, A. & LINDSLEY, C. W. 2009. Allosteric modulators of GPCRs: a novel approach for the treatment of CNS disorders. *Nat Rev Drug Discov,* 8**,** 41-54.

CONN, P. M., JANOVICK, J. A., BROTHERS, S. P. & KNOLLMAN, P. E. 2006. 'Effective inefficiency': cellular control of protein trafficking as a mechanism of post-translational regulation. *J Endocrinol,* 190**,** 13-6.

CONN, P. M., ULLOA-AGUIRRE, A., ITO, J. & JANOVICK, J. A. 2007. G protein-coupled receptor trafficking in health and disease: lessons learned to prepare for therapeutic mutant rescue in vivo. *Pharmacol Rev,* 59**,** 225-50.

CONNOLLY, J. O., SIMPSON, N., HEWLETT, L. & HALL, A. 2002. Rac regulates endothelial morphogenesis and capillary assembly. *Mol Biol Cell,* 13**,** 2474-85.

CONTE, M. S. 2007. Molecular engineering of vein bypass grafts. *J Vasc Surg,* 45 Suppl A**,** A74-81.

COSI, C., MANNAIONI, G., COZZI, A., CARLA, V., SILI, M., CAVONE, L., MARATEA, D. & MORONI, F. 2011. G-protein coupled receptor 35 (GPR35) activation and inflammatory pain: Studies on the antinociceptive effects of kynurenic acid and zaprinast. *Neuropharmacology,* 60**,** 1227-31.

COSTANZI, S. 2013. Modeling G protein-coupled receptors and their interactions with ligands. *Curr Opin Struct Biol,* 23**,** 185-90.

COTTON, M. & CLAING, A. 2009. G protein-coupled receptors stimulation and the control of cell migration. *Cell Signal,* 21**,** 1045-53.

DANSKY, H. M., BARLOW, C. B., LOMINSKA, C., SIKES, J. L., KAO, C., WEINSAFT, J., CYBULSKY, M. I. & SMITH, J. D. 2001. Adhesion of monocytes to arterial endothelium and initiation of atherosclerosis are critically dependent on vascular cell adhesion molecule-1 gene dosage. *Arterioscler Thromb Vasc Biol,* 21**,** 1662-7.

DAVENPORT, A. P. & HARMAR, A. J. 2013. Evolving pharmacology of orphan GPCRs: IUPHAR Commentary. *Br J Pharmacol,* 170**,** 693-5.

DELLES, C., MCBRIDE, M. W., GRAHAM, D., PADMANABHAN, S. & DOMINICZAK, A. F. 2010. Genetics of hypertension: from experimental animals to humans. *Biochim Biophys Acta,* 1802**,** 1299-308.

DENG, H. & FANG, Y. 2012a. Anti-inflammatory gallic Acid and wedelolactone are G protein-coupled receptor-35 agonists. *Pharmacology,* 89**,** 211-9.

DENG, H. & FANG, Y. 2012b. Aspirin metabolites are GPR35 agonists. *Naunyn Schmiedebergs Arch Pharmacol,* 385**,** 729-37.

DENG, H. & FANG, Y. 2013. The Three Catecholics Benserazide, Catechol and Pyrogallol are GPR35 Agonists. *Pharmaceuticals (Basel),* 6**,** 500-9.

DENG, H., HU, H. & FANG, Y. 2011a. Tyrphostin analogs are GPR35 agonists. *FEBS Lett,* 585**,** 1957-62.

DENG, H., HU, H. & FANG, Y. 2012a. Multiple tyrosine metabolites are GPR35 agonists. *Sci Rep,* 2**,** 373.

DENG, H., HU, H., HE, M., HU, J., NIU, W., FERRIE, A. M. & FANG, Y. 2011b. Discovery of 2-(4-methylfuran-2(5H)-ylidene)malononitrile and thieno[3,2-b]thiophene-2-

carboxylic acid derivatives as G protein-coupled receptor 35 (GPR35) agonists. *J Med Chem,* 54**,** 7385-96.

DENG, H., HU, H., LING, S., FERRIE, A. M. & FANG, Y. 2012b. Discovery of Natural Phenols as G Protein-Coupled Receptor-35 (GPR35) Agonists. *ACS Med Chem Lett,* 3**,** 165-9.

DEWIRE, S. M., AHN, S., LEFKOWITZ, R. J. & SHENOY, S. K. 2007. Beta-arrestins and cell signaling. *Annu Rev Physiol,* 69**,** 483-510.

DEWIRE, S. M. & VIOLIN, J. D. 2011. Biased ligands for better cardiovascular drugs: dissecting G-protein-coupled receptor pharmacology. *Circ Res,* 109**,** 205-16.

DUPRE, D. J., ROBITAILLE, M., REBOIS, R. V. & HEBERT, T. E. 2009. The role of Gbetagamma subunits in the organization, assembly, and function of GPCR signaling complexes. *Annu Rev Pharmacol Toxicol,* 49**,** 31-56.

EAGLE, K. A., GUYTON, R. A., DAVIDOFF, R., EWY, G. A., FONGER, J., GARDNER, T. J., GOTT, J. P., HERRMANN, H. C., MARLOW, R. A., NUGENT, W., O'CONNOR, G. T., ORSZULAK, T. A., RIESELBACH, R. E., WINTERS, W. L., YUSUF, S., GIBBONS, R. J., ALPERT, J. S., GARSON, A., JR., GREGORATOS, G., RUSSELL, R. O., RYAN, T. J. & SMITH, S. C., JR. 1999. ACC/AHA guidelines for coronary artery bypass graft surgery: executive summary and recommendations : A report of the American College of Cardiology/American Heart Association Task Force on Practice Guidelines (Committee to revise the 1991 guidelines for coronary artery bypass graft surgery). *Circulation,* 100**,** 1464-80.

EGAN, B. M., ZHAO, Y. & AXON, R. N. 2010. US trends in prevalence, awareness, treatment, and control of hypertension, 1988-2008. *JAMA,* 303**,** 2043-50.

ELLINGHAUS, D., FOLSERAAS, T., HOLM, K., ELLINGHAUS, E., MELUM, E., BALSCHUN, T., LAERDAHL, J. K., SHIRYAEV, A., GOTTHARDT, D. N., WEISMULLER, T. J., SCHRAMM, C., WITTIG, M., BERGQUIST, A., BJORNSSON, E., MARSCHALL, H. U., VATN, M., TEUFEL, A., RUST, C., GIEGER, C., WICHMANN, H. E., RUNZ, H., STERNECK, M., RUPP, C., BRAUN, F., WEERSMA, R. K., WIJMENGA, C., PONSIOEN, C. Y., MATHEW, C. G., RUTGEERTS, P., VERMEIRE, S., SCHRUMPF, E., HOV, J. R., MANNS, M. P., BOBERG, K. M., SCHREIBER, S., FRANKE, A. & KARLSEN, T. H. 2013. Genome-wide association analysis in primary sclerosing cholangitis and ulcerative colitis identifies risk loci at GPR35 and TCF4. *Hepatology,* 58**,** 1074-83.

ELTZSCHIG, H. K. & ECKLE, T. 2011. Ischemia and reperfusion--from mechanism to translation. *Nat Med,* 17**,** 1391-401.

FALLARINI, S., MAGLIULO, L., PAOLETTI, T., DE LALLA, C. & LOMBARDI, G. 2010. Expression of functional GPR35 in human iNKT cells. *Biochem Biophys Res Commun,* 398**,** 420-5.

FLORES-MUNOZ, M., SMITH, N. J., HAGGERTY, C., MILLIGAN, G. & NICKLIN, S. A. 2011. Angiotensin1-9 antagonises pro-hypertrophic signalling in cardiomyocytes via the angiotensin type 2 receptor. *J Physiol,* 589**,** 939-51.

FLORES-MUNOZ, M., WORK, L. M., DOUGLAS, K., DENBY, L., DOMINICZAK, A. F., GRAHAM, D. & NICKLIN, S. A. 2012. Angiotensin-(1-9) attenuates cardiac fibrosis in the stroke-prone spontaneously hypertensive rat via the angiotensin type 2 receptor. *Hypertension,* 59**,** 300-7.

FOORD, S. M., BONNER, T. I., NEUBIG, R. R., ROSSER, E. M., PIN, J. P., DAVENPORT, A. P., SPEDDING, M. & HARMAR, A. J. 2005. International Union of Pharmacology. XLVI. G protein-coupled receptor list. *Pharmacol Rev,* 57**,** 279-88.

FORREST, C. M., YOUD, P., KENNEDY, A., GOULD, S. R., DARLINGTON, L. G. & STONE, T. W. 2002. Purine, kynurenine, neopterin and lipid peroxidation levels in inflammatory bowel disease. *J Biomed Sci,* 9**,** 436-42.

FRANKLIN, S. S., KHAN, S. A., WONG, N. D., LARSON, M. G. & LEVY, D. 1999. Is pulse pressure useful in predicting risk for coronary heart Disease? The Framingham heart study. *Circulation,* 100**,** 354-60.

FREDRIKSSON, R., LAGERSTROM, M. C., LUNDIN, L. G. & SCHIOTH, H. B. 2003. The G-protein-coupled receptors in the human genome form five main families. Phylogenetic analysis, paralogon groups, and fingerprints. *Mol Pharmacol,* 63**,** 1256-72.

FUNKE, M., THIMM, D., SCHIEDEL, A. C. & MULLER, C. E. 2013. 8-Benzamidochromen-4-one-2-carboxylic acids: potent and selective agonists for the orphan G protein-coupled receptor GPR35. *J Med Chem,* 56**,** 5182-97.

FURCHGOTT, R. F. 1999. Endothelium-derived relaxing factor: discovery, early studies, and identification as nitric oxide. *Biosci Rep,* 19**,** 235-51.

GAO, Q. B., YE, X. F. & HE, J. 2013. Classifying G-protein-coupled receptors to the finest subtype level. *Biochem Biophys Res Commun,* 439**,** 303-8.

GARLAND, S. L. 2013. Are GPCRs still a source of new targets? *J Biomol Screen,* 18**,** 947-66.

GELOSA, P., PIGNIERI, A., FANDRIKS, L., DE GASPARO, M., HALLBERG, A., BANFI, C., CASTIGLIONI, L., TUROLO, L., GUERRINI, U., TREMOLI, E. & SIRONI, L. 2009. Stimulation of AT2 receptor exerts beneficial effects in stroke-prone rats: focus on renal damage. *J Hypertens,* 27**,** 2444-51.

GIBSON, A. 2001. Phosphodiesterase 5 inhibitors and nitrergic transmission-from zaprinast to sildenafil. *Eur J Pharmacol,* 411**,** 1-10.

GLOERICH, M. & BOS, J. L. 2010. Epac: defining a new mechanism for cAMP action. *Annu Rev Pharmacol Toxicol,* 50**,** 355-75.

GO, A. S., MOZAFFARIAN, D., ROGER, V. L., BENJAMIN, E. J., BERRY, J. D., BLAHA, M. J., DAI, S., FORD, E. S., FOX, C. S., FRANCO, S., FULLERTON, H. J., GILLESPIE, C., HAILPERN, S. M., HEIT, J. A., HOWARD, V. J., HUFFMAN, M. D., JUDD, S. E., KISSELA, B. M., KITTNER, S. J., LACKLAND, D. T., LICHTMAN, J. H., LISABETH, L. D., MACKEY, R. H., MAGID, D. J., MARCUS, G. M., MARELLI, A., MATCHAR, D. B., MCGUIRE, D. K., MOHLER, E. R., 3RD, MOY, C. S., MUSSOLINO, M. E., NEUMAR, R. W., NICHOL, G., PANDEY, D. K., PAYNTER, N. P., REEVES, M. J., SORLIE, P. D., STEIN, J., TOWFIGHI, A., TURAN, T. N., VIRANI, S. S., WONG, N. D., WOO, D. & TURNER, M. B. 2014. Heart disease and stroke statistics--2014 update: a report from the American Heart Association. *Circulation,* 129**,** e28-e292.

GRADMAN, A. H., BASILE, J. N., CARTER, B. L. & BAKRIS, G. L. 2010. Combination therapy in hypertension. *J Am Soc Hypertens,* 4**,** 42-50.

GREENE, A. N., CLAPP, S. L. & ALPER, R. H. 2007. Timecourse of recovery after surgical intraperitoneal implantation of radiotelemetry transmitters in rats. *J Pharmacol Toxicol Methods,* 56**,** 218-22.

GUO, J., WILLIAMS, D. J., PUHL, H. L., 3RD & IKEDA, S. R. 2008. Inhibition of N-type calcium channels by activation of GPR35, an orphan receptor, heterologously expressed in rat sympathetic neurons. *J Pharmacol Exp Ther,* 324**,** 342-51.

GUREVICH, E. V., TESMER, J. J., MUSHEGIAN, A. & GUREVICH, V. V. 2012. G protein-coupled receptor kinases: more than just kinases and not only for GPCRs. *Pharmacol Ther,* 133**,** 40-69.

HAMM, H. E. 1998. The many faces of G protein signaling. *J Biol Chem,* 273**,** 669-72.

HART, M. J., JIANG, X., KOZASA, T., ROSCOE, W., SINGER, W. D., GILMAN, A. G., STERNWEIS, P. C. & BOLLAG, G. 1998. Direct stimulation of the guanine nucleotide exchange activity of p115 RhoGEF by Galpha13. *Science,* 280**,** 2112-4.

HAWES, B. E., LUTTRELL, L. M., VAN BIESEN, T. & LEFKOWITZ, R. J. 1996. Phosphatidylinositol 3-kinase is an early intermediate in the G beta gamma-mediated mitogen-activated protein kinase signaling pathway. *J Biol Chem,* 271**,** 12133-6.

HEYNEN-GENEL, S., DAHL, R., SHI, S., SAUER, M., HARIHARAN, S., SERGIENKO, E., DAD, S., CHUNG, T. D. Y., STONICH, D., SU, Y., CARON, M., ZHAO, P., ABOOD, M. E. & BARAK, L. S. 2010. Selective GPR35 Antagonists - Probes 1 & 2. *Probe Reports from the NIH Molecular Libraries Program.* Bethesda (MD).

HILMAS, C., PEREIRA, E. F., ALKONDON, M., RASSOULPOUR, A., SCHWARCZ, R. & ALBUQUERQUE, E. X. 2001. The brain metabolite kynurenic acid inhibits alpha7 nicotinic receptor activity and increases non-alpha7 nicotinic receptor expression: physiopathological implications. *J Neurosci,* 21**,** 7463-73.

HOLLENSTEIN, K., DE GRAAF, C., BORTOLATO, A., WANG, M. W., MARSHALL, F. H. & STEVENS, R. C. 2014. Insights into the structure of class B GPCRs. *Trends Pharmacol Sci,* 35**,** 12-22.

HOLLENSTEIN, K., KEAN, J., BORTOLATO, A., CHENG, R. K., DORE, A. S., JAZAYERI, A., COOKE, R. M., WEIR, M. & MARSHALL, F. H. 2013. Structure of class B GPCR corticotropin-releasing factor receptor 1. *Nature,* 499**,** 438-43.

HORIKAWA, Y., ODA, N., COX, N. J., LI, X., ORHO-MELANDER, M., HARA, M., HINOKIO, Y., LINDNER, T. H., MASHIMA, H., SCHWARZ, P. E., DEL BOSQUE-PLATA, L., ODA, Y., YOSHIUCHI, I., COLILLA, S., POLONSKY, K. S., WEI, S., CONCANNON, P., IWASAKI, N., SCHULZE, J., BAIER, L. J., BOGARDUS, C., GROOP, L., BOERWINKLE, E., HANIS, C. L. & BELL, G. I. 2000. Genetic variation in the gene encoding calpain-10 is associated with type 2 diabetes mellitus. *Nat Genet,* 26**,** 163-75.

HOWELL, J. B. & ALTOUNYAN, R. E. 1967. A double-blind trial of disodium cromoglycate in the treatment of allergic bronchial asthma. *Lancet,* 2**,** 539-42.

HUBBARD, K. B. & HEPLER, J. R. 2006. Cell signalling diversity of the Gqalpha family of heterotrimeric G proteins. *Cell Signal,* 18**,** 135-50.

HULTSTROM, M. 2012. Development of structural kidney damage in spontaneously hypertensive rats. *J Hypertens,* 30**,** 1087-91.

HYNES, T. R., TANG, L., MERVINE, S. M., SABO, J. L., YOST, E. A., DEVREOTES, P. N. & BERLOT, C. H. 2004. Visualization of G protein betagamma dimers using bimolecular fluorescence complementation demonstrates roles for both beta and gamma in subcellular targeting. *J Biol Chem,* 279**,** 30279-86.

IMIELINSKI, M., BALDASSANO, R. N., GRIFFITHS, A., RUSSELL, R. K., ANNESE, V., DUBINSKY, M., KUGATHASAN, S., BRADFIELD, J. P., WALTERS, T. D., SLEIMAN, P., KIM, C. E., MUISE, A., WANG, K., GLESSNER, J. T., SAEED, S., ZHANG, H., FRACKELTON, E. C., HOU, C., FLORY, J. H., OTIENO, G., CHIAVACCI, R. M., GRUNDMEIER, R., CASTRO, M., LATIANO, A., DALLAPICCOLA, B., STEMPAK, J., ABRAMS, D. J., TAYLOR, K., MCGOVERN, D., SILBER, G., WROBEL, I., QUIROS, A., BARRETT, J. C., HANSOUL, S., NICOLAE, D. L., CHO, J. H., DUERR, R. H., RIOUX, J. D., BRANT, S. R., SILVERBERG, M. S., TAYLOR, K. D., BARMUDA, M. M., BITTON, A., DASSOPOULOS, T., DATTA, L. W., GREEN, T., GRIFFITHS, A. M., KISTNER, E. O., MURTHA, M. T., REGUEIRO, M. D., ROTTER, J. I., SCHUMM, L. P., STEINHART, A. H., TARGAN, S. R., XAVIER, R. J., LIBIOULLE, C., SANDOR, C., LATHROP, M., BELAICHE, J., DEWIT, O., GUT, I., HEATH, S., LAUKENS, D., MNI, M., RUTGEERTS, P., VAN GOSSUM, A., ZELENIKA, D., FRANCHIMONT, D., HUGOT, J. P., DE VOS, M., VERMEIRE, S., LOUIS, E., CARDON, L. R., ANDERSON, C. A., DRUMMOND, H., NIMMO, E., AHMAD, T., PRESCOTT, N. J., ONNIE, C. M., FISHER, S. A., MARCHINI, J., GHORI, J., BUMPSTEAD, S., GWILLAM, R., TREMELLING, M., DELUKAS, P., MANSFIELD, J., JEWELL, D., SATSANGI, J., MATHEW, C. G., PARKES, M., GEORGES, M., DALY, M. J., HEYMAN, M. B., FERRY, G. D., KIRSCHNER, B., LEE, J., ESSERS, J., GRAND, R., STEPHENS, M., et al. 2009. Common variants at five new loci associated with early-onset inflammatory bowel disease. *Nat Genet,* 41**,** 1335-40.

JEAN-ALPHONSE, F. & HANYALOGLU, A. C. 2011. Regulation of GPCR signal networks via membrane trafficking. *Mol Cell Endocrinol,* 331**,** 205-14.

JENKINS, L., ALVAREZ-CURTO, E., CAMPBELL, K., DE MUNNIK, S., CANALS, M., SCHLYER, S. & MILLIGAN, G. 2011. Agonist activation of the G protein-coupled receptor GPR35 involves transmembrane domain III and is transduced via Galpha(1)(3) and beta-arrestin-2. *Br J Pharmacol,* 162**,** 733-48.

JENKINS, L., BREA, J., SMITH, N. J., HUDSON, B. D., REILLY, G., BRYANT, N. J., CASTRO, M., LOZA, M. I. & MILLIGAN, G. 2010. Identification of novel species-selective agonists of the G-protein-coupled receptor GPR35 that promote recruitment of beta-arrestin-2 and activate Galpha13. *Biochem J,* 432**,** 451-9.

JENKINS, L., HARRIES, N., LAPPIN, J. E., MACKENZIE, A. E., NEETOO-ISSELJEE, Z., SOUTHERN, C., MCIVER, E. G., NICKLIN, S. A., TAYLOR, D. L. & MILLIGAN, G. 2012. Antagonists of GPR35 display high species ortholog selectivity and varying modes of action. *J Pharmacol Exp Ther,* 343**,** 683-95.

JOHNSTON, C. A. & SIDEROVSKI, D. P. 2007. Structural basis for nucleotide exchange on G alpha i subunits and receptor coupling specificity. *Proc Natl Acad Sci U S A,* 104**,** 2001-6.

JONER, M., FINN, A. V., FARB, A., MONT, E. K., KOLODGIE, F. D., LADICH, E., KUTYS, R., SKORIJA, K., GOLD, H. K. & VIRMANI, R. 2006. Pathology of drug-eluting stents in humans: delayed healing and late thrombotic risk. *J Am Coll Cardiol,* 48**,** 193-202.

JONES, K. A., BOROWSKY, B., TAMM, J. A., CRAIG, D. A., DURKIN, M. M., DAI, M., YAO, W. J., JOHNSON, M., GUNWALDSEN, C., HUANG, L. Y., TANG, C., SHEN, Q., SALON, J. A., MORSE, K., LAZ, T., SMITH, K. E., NAGARATHNAM, D., NOBLE, S. A., BRANCHEK, T. A. & GERALD, C. 1998. GABA(B) receptors function as a heteromeric assembly of the subunits GABA(B)R1 and GABA(B)R2. *Nature,* 396**,** 674-9.

KANG, Y. C., KIM, K. M., LEE, K. S., NAMKOONG, S., LEE, S. J., HAN, J. A., JEOUNG, D., HA, K. S., KWON, Y. G. & KIM, Y. M. 2004. Serum bioactive lysophospholipids prevent TRAIL-induced apoptosis via PI3K/Akt-dependent cFLIP expression and Bad phosphorylation. *Cell Death Differ,* 11**,** 1287-98.

KATADA, T. & UI, M. 1982. Direct modification of the membrane adenylate cyclase system by islet-activating protein due to ADP-ribosylation of a membrane protein. *Proc Natl Acad Sci U S A,* 79**,** 3129-33.

KATRITCH, V., CHEREZOV, V. & STEVENS, R. C. 2013. Structure-function of the G protein-coupled receptor superfamily. *Annu Rev Pharmacol Toxicol,* 53**,** 531-56.

KENAKIN, T. 2004. Principles: receptor theory in pharmacology. *Trends Pharmacol Sci,* 25**,** 186-92.

KETEYIAN, S. J. 2013. Exercise training in patients with heart failure and preserved ejection fraction: findings awaiting discovery. *J Am Coll Cardiol,* 62**,** 593-4.

KHAN, B. V., PARTHASARATHY, S. S., ALEXANDER, R. W. & MEDFORD, R. M. 1995. Modified low density lipoprotein and its constituents augment cytokine-activated vascular cell adhesion molecule-1 gene expression in human vascular endothelial cells. *J Clin Invest,* 95**,** 1262-70.

KHAN, S. M., SLENO, R., GORA, S., ZYLBERGOLD, P., LAVERDURE, J. P., LABBE, J. C., MILLER, G. J. & HEBERT, T. E. 2013. The expanding roles of Gbetagamma subunits in G protein-coupled receptor signaling and drug action. *Pharmacol Rev,* 65**,** 545-77.

KIM, T. W., YOO, B. W., LEE, J. K., KIM, J. H., LEE, K. T., CHI, Y. H. & LEE, J. Y. 2012. Synthesis and antihypertensive activity of pyrimidin-4(3H)-one derivatives as losartan analogue for new angiotensin II receptor type 1 (AT1) antagonists. *Bioorg Med Chem Lett,* 22**,** 1649-54.

KISSELEV, O. & GAUTAM, N. 1993. Specific interaction with rhodopsin is dependent on the gamma subunit type in a G protein. *J Biol Chem,* 268**,** 24519-22.

KLABUNDE, T. 2007. Chemogenomic approaches to drug discovery: similar receptors bind similar ligands. *Br J Pharmacol,* 152**,** 5-7.

KOBILKA, B. & SCHERTLER, G. F. 2008. New G-protein-coupled receptor crystal structures: insights and limitations. *Trends Pharmacol Sci,* 29**,** 79-83.

KOBILKA, B. K. 2007. G protein coupled receptor structure and activation. *Biochim Biophys Acta,* 1768**,** 794-807.

KORHONEN, P. E., KAUTIAINEN, H., JARVENPAA, S. & KANTOLA, I. 2013. Target organ damage and cardiovascular risk factors among subjects with previously undiagnosed hypertension. *Eur J Prev Cardiol.*

KOSTENIS, E., WAELBROECK, M. & MILLIGAN, G. 2005. Techniques: promiscuous Galpha proteins in basic research and drug discovery. *Trends Pharmacol Sci,* 26**,** 595-602.

KOZASA, T., JIANG, X., HART, M. J., STERNWEIS, P. M., SINGER, W. D., GILMAN, A. G., BOLLAG, G. & STERNWEIS, P. C. 1998. p115 RhoGEF, a GTPase activating protein for Galpha12 and Galpha13. *Science,* 280**,** 2109-11.

KRAUSE, D., SUH, H. S., TARASSISHIN, L., CUI, Q. L., DURAFOURT, B. A., CHOI, N., BAUMAN, A., COSENZA-NASHAT, M., ANTEL, J. P., ZHAO, M. L. & LEE, S. C. 2011. The tryptophan metabolite 3-hydroxyanthranilic acid plays anti-inflammatory and neuroprotective roles during inflammation: role of hemeoxygenase-1. *Am J Pathol,* 179**,** 1360-72.

KRISHNAN, A., ALMEN, M. S., FREDRIKSSON, R. & SCHIOTH, H. B. 2012. The origin of GPCRs: identification of mammalian like Rhodopsin, Adhesion, Glutamate and Frizzled GPCRs in fungi. *PLoS One,* 7**,** e29817.

KUC, D., ZGRAJKA, W., PARADA-TURSKA, J., URBANIK-SYPNIEWSKA, T. & TURSKI, W. A. 2008. Micromolar concentration of kynurenic acid in rat small intestine. *Amino Acids,* 35**,** 503-5.

KUNISHIMA, N., SHIMADA, Y., TSUJI, Y., SATO, T., YAMAMOTO, M., KUMASAKA, T., NAKANISHI, S., JINGAMI, H. & MORIKAWA, K. 2000. Structural basis of glutamate recognition by a dimeric metabotropic glutamate receptor. *Nature,* 407**,** 971-7.

KURTZ, T. W., GRIFFIN, K. A., BIDANI, A. K., DAVISSON, R. L. & HALL, J. E. 2005. Recommendations for blood pressure measurement in humans and experimental animals: part 2: blood pressure measurement in experimental animals: a statement for professionals from the Subcommittee of Professional and Public Education of the American Heart Association Council on High Blood Pressure Research. *Arterioscler Thromb Vasc Biol,* 25**,** e22-33.

LAGERSTROM, M. C. & SCHIOTH, H. B. 2008. Structural diversity of G protein-coupled receptors and significance for drug discovery. *Nat Rev Drug Discov,* 7**,** 339-57.

LATTIN, J. E., SCHRODER, K., SU, A. I., WALKER, J. R., ZHANG, J., WILTSHIRE, T., SAIJO, K., GLASS, C. K., HUME, D. A., KELLIE, S. & SWEET, M. J. 2008. Expression analysis of G Protein-Coupled Receptors in mouse macrophages. *Immunome Res,* 4**,** 5.

LAWSON, S. N. 2002. Phenotype and function of somatic primary afferent nociceptive neurones with C-, Adelta- or Aalpha/beta-fibres. *Exp Physiol,* 87**,** 239-44.

LEANEY, J. L. & TINKER, A. 2000. The role of members of the pertussis toxin-sensitive family of G proteins in coupling receptors to the activation of the G protein-gated inwardly rectifying potassium channel. *Proc Natl Acad Sci U S A,* 97**,** 5651-6.

LESCA, P. 1983. Protective effects of ellagic acid and other plant phenols on benzo[a]pyrene-induced neoplasia in mice. *Carcinogenesis,* 4**,** 1651-3.

LEVITZKI, A. & GAZIT, A. 1995. Tyrosine kinase inhibition: an approach to drug development. *Science,* 267**,** 1782-8.

LIETZ, C. B., GEMPERLINE, E. & LI, L. 2013. Qualitative and quantitative mass spectrometry imaging of drugs and metabolites. *Adv Drug Deliv Rev,* 65**,** 1074-85.

LIFTON, R. P., GHARAVI, A. G. & GELLER, D. S. 2001. Molecular mechanisms of human hypertension. *Cell,* 104**,** 545-56.

LIN, M. E., HERR, D. R. & CHUN, J. 2010. Lysophosphatidic acid (LPA) receptors: signaling properties and disease relevance. *Prostaglandins Other Lipid Mediat,* 91**,** 130-8.

LIU, C., WU, J., ZHU, J., KUEI, C., YU, J., SHELTON, J., SUTTON, S. W., LI, X., YUN, S. J., MIRZADEGAN, T., MAZUR, C., KAMME, F. & LOVENBERG, T. W. 2009.

Lactate inhibits lipolysis in fat cells through activation of an orphan G-protein-coupled receptor, GPR81. *J Biol Chem,* 284**,** 2811-22.

LLOYD-JONES, D., ADAMS, R. J., BROWN, T. M., CARNETHON, M., DAI, S., DE SIMONE, G., FERGUSON, T. B., FORD, E., FURIE, K., GILLESPIE, C., GO, A., GREENLUND, K., HAASE, N., HAILPERN, S., HO, P. M., HOWARD, V., KISSELA, B., KITTNER, S., LACKLAND, D., LISABETH, L., MARELLI, A., MCDERMOTT, M. M., MEIGS, J., MOZAFFARIAN, D., MUSSOLINO, M., NICHOL, G., ROGER, V. L., ROSAMOND, W., SACCO, R., SORLIE, P., THOM, T., WASSERTHIEL-SMOLLER, S., WONG, N. D. & WYLIE-ROSETT, J. 2010. Heart disease and stroke statistics--2010 update: a report from the American Heart Association. *Circulation,* 121**,** e46-e215.

LOGOTHETIS, D. E., KURACHI, Y., GALPER, J., NEER, E. J. & CLAPHAM, D. E. 1987. The beta gamma subunits of GTP-binding proteins activate the muscarinic K+ channel in heart. *Nature,* 325**,** 321-6.

LUTTRELL, L. M., FERGUSON, S. S., DAAKA, Y., MILLER, W. E., MAUDSLEY, S., DELLA ROCCA, G. J., LIN, F., KAWAKATSU, H., OWADA, K., LUTTRELL, D. K., CARON, M. G. & LEFKOWITZ, R. J. 1999. Beta-arrestin-dependent formation of beta2 adrenergic receptor-Src protein kinase complexes. *Science,* 283**,** 655-61.

MACKENZIE, A. E., CALTABIANO, G., KENT, T. C., JENKINS, L., MCCALLUM, J. E., HUDSON, B. D., NICKLIN, S. A., FAWCETT, L., MARKWICK, R., CHARLTON, S. J. & MILLIGAN, G. 2014. The Antiallergic Mast Cell Stabilizers Lodoxamide and Bufrolin as the First High and Equipotent Agonists of Human and Rat GPR35. *Mol Pharmacol,* 85**,** 91-104.

MACKENZIE, A. E., LAPPIN, J. E., TAYLOR, D. L., NICKLIN, S. A. & MILLIGAN, G. 2011. GPR35 as a Novel Therapeutic Target. *Front Endocrinol (Lausanne),* 2**,** 68.

MAEDA, S. & SCHERTLER, G. F. 2013. Production of GPCR and GPCR complexes for structure determination. *Curr Opin Struct Biol,* 23**,** 381-92.

MAGALHAES, A. C., DUNN, H. & FERGUSON, S. S. 2012. Regulation of GPCR activity, trafficking and localization by GPCR-interacting proteins. *Br J Pharmacol,* 165**,** 1717-36.

MAGUIRE, J. J. & DAVENPORT, A. P. 2005. Regulation of vascular reactivity by established and emerging GPCRs. *Trends Pharmacol Sci,* 26**,** 448-54.

MAILLET, M., VAN BERLO, J. H. & MOLKENTIN, J. D. 2013. Molecular basis of physiological heart growth: fundamental concepts and new players. *Nat Rev Mol Cell Biol,* 14**,** 38-48.

MANABE, N., CREMONINI, F., CAMILLERI, M., SANDBORN, W. J. & BURTON, D. D. 2009. Effects of bisacodyl on ascending colon emptying and overall colonic transit in healthy volunteers. *Aliment Pharmacol Ther,* 30**,** 930-6.

MARRARI, Y., CROUTHAMEL, M., IRANNEJAD, R. & WEDEGAERTNER, P. B. 2007. Assembly and trafficking of heterotrimeric G proteins. *Biochemistry,* 46**,** 7665-77.

MARUYAMA, Y., NISHIDA, M., SUGIMOTO, Y., TANABE, S., TURNER, J. H., KOZASA, T., WADA, T., NAGAO, T. & KUROSE, H. 2002. Galpha(12/13) mediates alpha(1)-adrenergic receptor-induced cardiac hypertrophy. *Circ Res,* 91**,** 961-9.

MARX, S. O., REIKEN, S., HISAMATSU, Y., JAYARAMAN, T., BURKHOFF, D., ROSEMBLIT, N. & MARKS, A. R. 2000. PKA phosphorylation dissociates FKBP12.6 from the calcium release channel (ryanodine receptor): defective regulation in failing hearts. *Cell,* 101**,** 365-76.

MATHIESEN, J. M., ULVEN, T., MARTINI, L., GERLACH, L. O., HEINEMANN, A. & KOSTENIS, E. 2005. Identification of indole derivatives exclusively interfering with a G protein-independent signaling pathway of the prostaglandin D2 receptor CRTH2. *Mol Pharmacol,* 68**,** 393-402.

MATTHEWS, E. J. & FRID, A. A. 2010. Prediction of drug-related cardiac adverse effects in humans--A: creation of a database of effects and identification of factors affecting their occurrence. *Regul Toxicol Pharmacol,* 56**,** 247-75.

MCBRIDE, M. W., BROSNAN, M. J., MATHERS, J., MCLELLAN, L. I., MILLER, W. H., GRAHAM, D., HANLON, N., HAMILTON, C. A., POLKE, J. M., LEE, W. K. & DOMINICZAK, A. F. 2005. Reduction of Gstm1 expression in the stroke-prone spontaneously hypertension rat contributes to increased oxidative stress. *Hypertension,* 45**,** 786-92.

MCBRIDE, M. W., CARR, F. J., GRAHAM, D., ANDERSON, N. H., CLARK, J. S., LEE, W. K., CHARCHAR, F. J., BROSNAN, M. J. & DOMINICZAK, A. F. 2003. Microarray analysis of rat chromosome 2 congenic strains. *Hypertension,* 41**,** 847-53.

MCCABE, C., GALLAGHER, L., GSELL, W., GRAHAM, D., DOMINICZAK, A. F. & MACRAE, I. M. 2009. Differences in the evolution of the ischemic penumbra in stroke-prone spontaneously hypertensive and Wistar-Kyoto rats. *Stroke,* 40**,** 3864-8.

MCCORMICK, K. & BAILLIE, G. S. 2014. Compartmentalisation of second messenger signalling pathways. *Curr Opin Genet Dev,* 27C**,** 20-25.

MCCUDDEN, C. R., HAINS, M. D., KIMPLE, R. J., SIDEROVSKI, D. P. & WILLARD, F. S. 2005. G-protein signaling: back to the future. *Cell Mol Life Sci,* 62**,** 551-77.

MCDONALD, R. A., WHITE, K. M., WU, J., COOLEY, B. C., ROBERTSON, K. E., HALLIDAY, C. A., MCCLURE, J. D., FRANCIS, S., LU, R., KENNEDY, S., GEORGE, S. J., WAN, S., VAN ROOIJ, E. & BAKER, A. H. 2013. miRNA-21 is dysregulated in response to vein grafting in multiple models and genetic ablation in mice attenuates neointima formation. *Eur Heart J,* 34**,** 1636-43.

MCMURRAY, J. J., ADAMOPOULOS, S., ANKER, S. D., AURICCHIO, A., BOHM, M., DICKSTEIN, K., FALK, V., FILIPPATOS, G., FONSECA, C., GOMEZ-SANCHEZ, M. A., JAARSMA, T., KOBER, L., LIP, G. Y., MAGGIONI, A. P., PARKHOMENKO, A., PIESKE, B. M., POPESCU, B. A., RONNEVIK, P. K., RUTTEN, F. H., SCHWITTER, J., SEFEROVIC, P., STEPINSKA, J., TRINDADE, P. T., VOORS, A. A., ZANNAD, F., ZEIHER, A., BAX, J. J., BAUMGARTNER, H., CECONI, C., DEAN, V., DEATON, C., FAGARD, R., FUNCK-BRENTANO, C., HASDAI, D., HOES, A., KIRCHHOF, P., KNUUTI, J., KOLH, P., MCDONAGH, T., MOULIN, C., REINER, Z., SECHTEM, U., SIRNES, P. A., TENDERA, M., TORBICKI, A., VAHANIAN, A., WINDECKER, S., BONET, L. A., AVRAAMIDES, P., BEN LAMIN, H. A., BRIGNOLE, M., COCA, A., COWBURN, P., DARGIE, H., ELLIOTT, P., FLACHSKAMPF, F. A., GUIDA, G. F., HARDMAN, S., IUNG, B., MERKELY, B., MUELLER, C., NANAS, J. N., NIELSEN, O. W., ORN, S., PARISSIS, J. T. & PONIKOWSKI, P. 2012. ESC guidelines for the diagnosis and treatment of acute and chronic heart failure 2012: The Task Force for the Diagnosis and Treatment of Acute and Chronic Heart Failure 2012 of the European Society of Cardiology. Developed in collaboration with the Heart Failure Association (HFA) of the ESC. *Eur J Heart Fail,* 14**,** 803-69.

MEYER, B. H., FREULER, F., GUERINI, D. & SIEHLER, S. 2008. Reversible translocation of p115-RhoGEF by G(12/13)-coupled receptors. *J Cell Biochem,* 104**,** 1660-70.

MILLIGAN, G. 2011. Orthologue selectivity and ligand bias: translating the pharmacology of GPR35. *Trends Pharmacol Sci,* 32**,** 317-25.

MILLIGAN, G. & KOSTENIS, E. 2006. Heterotrimeric G-proteins: a short history. *Br J Pharmacol,* 147 Suppl 1**,** S46-55.

MILLIGAN, G. & SMITH, N. J. 2007. Allosteric modulation of heterodimeric G-protein-coupled receptors. *Trends Pharmacol Sci,* 28**,** 615-20.

MILLS, G. B. & MOOLENAAR, W. H. 2003. The emerging role of lysophosphatidic acid in cancer. *Nat Rev Cancer,* 3**,** 582-91.

MIN, K. D., ASAKURA, M., LIAO, Y., NAKAMARU, K., OKAZAKI, H., TAKAHASHI, T., FUJIMOTO, K., ITO, S., TAKAHASHI, A., ASANUMA, H., YAMAZAKI, S., MINAMINO, T., SANADA, S., SEGUCHI, O., NAKANO, A., ANDO, Y., OTSUKA, T., FURUKAWA, H., ISOMURA, T., TAKASHIMA, S., MOCHIZUKI, N. & KITAKAZE, M. 2010. Identification of genes related to heart failure using global

gene expression profiling of human failing myocardium. *Biochem Biophys Res Commun,* 393**,** 55-60.

MOORE, C. A., MILANO, S. K. & BENOVIC, J. L. 2007. Regulation of receptor trafficking by GRKs and arrestins. *Annu Rev Physiol,* 69**,** 451-82.

MOORE, K. J. & TABAS, I. 2011. Macrophages in the pathogenesis of atherosclerosis. *Cell,* 145**,** 341-55.

MORIKI, N., ITO, M., SEKO, T., KUREISHI, Y., OKAMOTO, R., NAKAKUKI, T., KONGO, M., ISAKA, N., KAIBUCHI, K. & NAKANO, T. 2004. RhoA activation in vascular smooth muscle cells from stroke-prone spontaneously hypertensive rats. *Hypertens Res,* 27**,** 263-70.

MORRIS, S. T., MCMURRAY, J. J., SPIERS, A. & JARDINE, A. G. 2001. Impaired endothelial function in isolated human uremic resistance arteries. *Kidney Int,* 60**,** 1077-82.

MUKHERJEE, S., ADAMS, M., WHITEAKER, K., DAZA, A., KAGE, K., CASSAR, S., MEYER, M. & YAO, B. B. 2004. Species comparison and pharmacological characterization of rat and human CB2 cannabinoid receptors. *Eur J Pharmacol,* 505**,** 1-9.

MUTO, T., TSUCHIYA, D., MORIKAWA, K. & JINGAMI, H. 2007. Structures of the extracellular regions of the group II/III metabotropic glutamate receptors. *Proc Natl Acad Sci U S A,* 104**,** 3759-64.

NAKAMURA, S., ITABASHI, T., OGAWA, D. & OKADA, T. 2013. Common and distinct mechanisms of activation of rhodopsin and other G protein-coupled receptors. *Sci Rep,* 3**,** 1844.

NANGAKU, M. & ECKARDT, K. U. 2007. Hypoxia and the HIF system in kidney disease. *J Mol Med (Berl),* 85**,** 1325-30.

NARUMIYA, S., ISHIZAKI, T. & UEHATA, M. 2000. Use and properties of ROCK-specific inhibitor Y-27632. *Methods Enzymol,* 325**,** 273-84.

NEETOO-ISSELJEE, Z., MACKENZIE, A. E., SOUTHERN, C., JERMAN, J., MCIVER, E. G., HARRIES, N., TAYLOR, D. L. & MILLIGAN, G. 2013. High-throughput identification and characterization of novel, species-selective GPR35 agonists. *J Pharmacol Exp Ther,* 344**,** 568-78.

NEUBIG, R. R. 2010. Mind your salts: when the inactive constituent isn't. *Mol Pharmacol,* 78**,** 558-9.

NEVES, S. R., RAM, P. T. & IYENGAR, R. 2002. G protein pathways. *Science,* 296**,** 1636-9.

NORDSTROM, K. J., LAGERSTROM, M. C., WALLER, L. M., FREDRIKSSON, R. & SCHIOTH, H. B. 2009. The Secretin GPCRs descended from the family of Adhesion GPCRs. *Mol Biol Evol,* 26**,** 71-84.

O'DOWD, B. F., NGUYEN, T., MARCHESE, A., CHENG, R., LYNCH, K. R., HENG, H. H., KOLAKOWSKI, L. F., JR. & GEORGE, S. R. 1998. Discovery of three novel G-protein-coupled receptor genes. *Genomics,* 47**,** 310-3.

OAKLEY, R. H., LAPORTE, S. A., HOLT, J. A., CARON, M. G. & BARAK, L. S. 2000. Differential affinities of visual arrestin, beta arrestin1, and beta arrestin2 for G protein-coupled receptors delineate two major classes of receptors. *J Biol Chem,* 275**,** 17201-10.

OFFERMANNS, S. 2003. G-proteins as transducers in transmembrane signalling. *Prog Biophys Mol Biol,* 83**,** 101-30.

OFFERMANNS, S., MANCINO, V., REVEL, J. P. & SIMON, M. I. 1997. Vascular system defects and impaired cell chemokinesis as a result of Galpha13 deficiency. *Science,* 275**,** 533-6.

OHSHIRO, H., TONAI-KACHI, H. & ICHIKAWA, K. 2008. GPR35 is a functional receptor in rat dorsal root ganglion neurons. *Biochem Biophys Res Commun,* 365**,** 344-8.

OKA, S., OTA, R., SHIMA, M., YAMASHITA, A. & SUGIURA, T. 2010. GPR35 is a novel lysophosphatidic acid receptor. *Biochem Biophys Res Commun,* 395**,** 232-7.

OKUMURA, S., BABA, H., KUMADA, T., NANMOKU, K., NAKAJIMA, H., NAKANE, Y., HIOKI, K. & IKENAKA, K. 2004. Cloning of a G-protein-coupled receptor that shows an activity to transform NIH3T3 cells and is expressed in gastric cancer cells. *Cancer Sci,* 95**,** 131-5.

OLIVERA, A., ROSENFELDT, H. M., BEKTAS, M., WANG, F., ISHII, I., CHUN, J., MILSTIEN, S. & SPIEGEL, S. 2003. Sphingosine kinase type 1 induces G12/13-mediated stress fiber formation, yet promotes growth and survival independent of G protein-coupled receptors. *J Biol Chem,* 278**,** 46452-60.

OTSUKA, F., FINN, A. V., YAZDANI, S. K., NAKANO, M., KOLODGIE, F. D. & VIRMANI, R. 2012. The importance of the endothelium in atherothrombosis and coronary stenting. *Nat Rev Cardiol,* 9**,** 439-53.

PALCZEWSKI, K., KUMASAKA, T., HORI, T., BEHNKE, C. A., MOTOSHIMA, H., FOX, B. A., LE TRONG, I., TELLER, D. C., OKADA, T., STENKAMP, R. E., YAMAMOTO, M. & MIYANO, M. 2000. Crystal structure of rhodopsin: A G protein-coupled receptor. *Science,* 289**,** 739-45.

PALUSZKIEWICZ, P., ZGRAJKA, W., SARAN, T., SCHABOWSKI, J., PIEDRA, J. L., FEDKIV, O., RENGMAN, S., PIERZYNOWSKI, S. G. & TURSKI, W. A. 2009. High concentration of kynurenic acid in bile and pancreatic juice. *Amino Acids,* 37**,** 637-41.

PASSIER, R., VAN LAAKE, L. W. & MUMMERY, C. L. 2008. Stem-cell-based therapy and lessons from the heart. *Nature,* 453**,** 322-9.

PERKINS, M. N. & STONE, T. W. 1982. An iontophoretic investigation of the actions of convulsant kynurenines and their interaction with the endogenous excitant quinolinic acid. *Brain Res,* 247**,** 184-7.

PERSELL, S. D. 2011. Prevalence of resistant hypertension in the United States, 2003-2008. *Hypertension,* 57**,** 1076-80.

RASCOL, O., BROOKS, D. J., KORCZYN, A. D., DE DEYN, P. P., CLARKE, C. E. & LANG, A. E. 2000. A five-year study of the incidence of dyskinesia in patients with early Parkinson's disease who were treated with ropinirole or levodopa. 056 Study Group. *N Engl J Med,* 342**,** 1484-91.

RASMUSSEN, S. G., CHOI, H. J., ROSENBAUM, D. M., KOBILKA, T. S., THIAN, F. S., EDWARDS, P. C., BURGHAMMER, M., RATNALA, V. R., SANISHVILI, R., FISCHETTI, R. F., SCHERTLER, G. F., WEIS, W. I. & KOBILKA, B. K. 2007. Crystal structure of the human beta2 adrenergic G-protein-coupled receptor. *Nature,* 450**,** 383-7.

RASMUSSEN, S. G., DEVREE, B. T., ZOU, Y., KRUSE, A. C., CHUNG, K. Y., KOBILKA, T. S., THIAN, F. S., CHAE, P. S., PARDON, E., CALINSKI, D., MATHIESEN, J. M., SHAH, S. T., LYONS, J. A., CAFFREY, M., GELLMAN, S. H., STEYAERT, J., SKINIOTIS, G., WEIS, W. I., SUNAHARA, R. K. & KOBILKA, B. K. 2011. Crystal structure of the beta2 adrenergic receptor-Gs protein complex. *Nature,* 477**,** 549-55.

REGARD, J. B., SATO, I. T. & COUGHLIN, S. R. 2008. Anatomical profiling of G protein-coupled receptor expression. *Cell,* 135**,** 561-71.

REILLY, S. M., CHIANG, S. H., DECKER, S. J., CHANG, L., UHM, M., LARSEN, M. J., RUBIN, J. R., MOWERS, J., WHITE, N. M., HOCHBERG, I., DOWNES, M., YU, R. T., LIDDLE, C., EVANS, R. M., OH, D., LI, P., OLEFSKY, J. M. & SALTIEL, A. R. 2013. An inhibitor of the protein kinases TBK1 and IKK-varepsilon improves obesity-related metabolic dysfunctions in mice. *Nat Med,* 19**,** 313-21.

REITER, E., AHN, S., SHUKLA, A. K. & LEFKOWITZ, R. J. 2012. Molecular mechanism of beta-arrestin-biased agonism at seven-transmembrane receptors. *Annu Rev Pharmacol Toxicol,* 52**,** 179-97.

REITER, E. & LEFKOWITZ, R. J. 2006. GRKs and beta-arrestins: roles in receptor silencing, trafficking and signaling. *Trends Endocrinol Metab,* 17**,** 159-65.

RIBAS, C., PENELA, P., MURGA, C., SALCEDO, A., GARCIA-HOZ, C., JURADO-PUEYO, M., AYMERICH, I. & MAYOR, F., JR. 2007. The G protein-coupled

receptor kinase (GRK) interactome: role of GRKs in GPCR regulation and signaling. *Biochim Biophys Acta,* 1768**,** 913-22.

RIENSTRA, H., ZEEBREGTS, C. J. & HILLEBRANDS, J. L. 2008. The source of neointimal cells in vein grafts: does the origin matter? *Am J Pathol,* 172**,** 566-70.

RIOBO, N. A. & MANNING, D. R. 2005. Receptors coupled to heterotrimeric G proteins of the G12 family. *Trends Pharmacol Sci,* 26**,** 146-54.

RONKAINEN, V. P., TUOMAINEN, T., HUUSKO, J., LAIDINEN, S., MALINEN, M., PALVIMO, J. J., YLA-HERTTUALA, S., VUOLTEENAHO, O. & TAVI, P. 2013. Hypoxia-inducible factor 1-induced G protein-coupled receptor 35 expression is an early marker of progressive cardiac remodelling. *Cardiovasc Res.*

RONKAINEN, V. P., TUOMAINEN, T., HUUSKO, J., LAIDINEN, S., MALINEN, M., PALVIMO, J. J., YLA-HERTTUALA, S., VUOLTEENAHO, O. & TAVI, P. 2014. Hypoxia-inducible factor 1-induced G protein-coupled receptor 35 expression is an early marker of progressive cardiac remodelling. *Cardiovasc Res,* 101**,** 69-77.

ROSAMOND, W., FLEGAL, K., FURIE, K., GO, A., GREENLUND, K., HAASE, N., HAILPERN, S. M., HO, M., HOWARD, V., KISSELA, B., KITTNER, S., LLOYD-JONES, D., MCDERMOTT, M., MEIGS, J., MOY, C., NICHOL, G., O'DONNELL, C., ROGER, V., SORLIE, P., STEINBERGER, J., THOM, T., WILSON, M. & HONG, Y. 2008. Heart disease and stroke statistics--2008 update: a report from the American Heart Association Statistics Committee and Stroke Statistics Subcommittee. *Circulation,* 117**,** e25-146.

ROVATI, G. E., CAPRA, V. & NEUBIG, R. R. 2007. The highly conserved DRY motif of class A G protein-coupled receptors: beyond the ground state. *Mol Pharmacol,* 71**,** 959-64.

RUDDICK, J. P., EVANS, A. K., NUTT, D. J., LIGHTMAN, S. L., ROOK, G. A. & LOWRY, C. A. 2006. Tryptophan metabolism in the central nervous system: medical implications. *Expert Rev Mol Med,* 8**,** 1-27.

RUPPEL, K. M., WILLISON, D., KATAOKA, H., WANG, A., ZHENG, Y. W., CORNELISSEN, I., YIN, L., XU, S. M. & COUGHLIN, S. R. 2005. Essential role for Galpha13 in endothelial cells during embryonic development. *Proc Natl Acad Sci U S A,* 102**,** 8281-6.

SAFAR, M. E., NILSSON, P. M., BLACHER, J. & MIMRAN, A. 2012. Pulse pressure, arterial stiffness, and end-organ damage. *Curr Hypertens Rep,* 14**,** 339-44.

SANO, M., MINAMINO, T., TOKO, H., MIYAUCHI, H., ORIMO, M., QIN, Y., AKAZAWA, H., TATENO, K., KAYAMA, Y., HARADA, M., SHIMIZU, I., ASAHARA, T., HAMADA, H., TOMITA, S., MOLKENTIN, J. D., ZOU, Y. & KOMURO, I. 2007. p53-induced inhibition of Hif-1 causes cardiac dysfunction during pressure overload. *Nature,* 446**,** 444-8.

SANTAMARIA, A., RIOS, C., SOLIS-HERNANDEZ, F., ORDAZ-MORENO, J., GONZALEZ-REYNOSO, L., ALTAGRACIA, M. & KRAVZOV, J. 1996. Systemic DL-kynurenine and probenecid pretreatment attenuates quinolinic acid-induced neurotoxicity in rats. *Neuropharmacology,* 35**,** 23-8.

SAWADA, N., ITOH, H., UEYAMA, K., YAMASHITA, J., DOI, K., CHUN, T. H., INOUE, M., MASATSUGU, K., SAITO, T., FUKUNAGA, Y., SAKAGUCHI, S., ARAI, H., OHNO, N., KOMEDA, M. & NAKAO, K. 2000. Inhibition of rho-associated kinase results in suppression of neointimal formation of balloon-injured arteries. *Circulation,* 101**,** 2030-3.

SAWZDARGO, M., NGUYEN, T., LEE, D. K., LYNCH, K. R., CHENG, R., HENG, H. H., GEORGE, S. R. & O'DOWD, B. F. 1999. Identification and cloning of three novel human G protein-coupled receptor genes GPR52, PsiGPR53 and GPR55: GPR55 is extensively expressed in human brain. *Brain Res Mol Brain Res,* 64**,** 193-8.

SCHRODER, R., JANSSEN, N., SCHMIDT, J., KEBIG, A., MERTEN, N., HENNEN, S., MULLER, A., BLATTERMANN, S., MOHR-ANDRA, M., ZAHN, S., WENZEL, J., SMITH, N. J., GOMEZA, J., DREWKE, C., MILLIGAN, G., MOHR, K. & KOSTENIS, E. 2010. Deconvolution of complex G protein-coupled receptor

signaling in live cells using dynamic mass redistribution measurements. *Nat Biotechnol,* 28**,** 943-9.

SCHWARCZ, R. 2004. The kynurenine pathway of tryptophan degradation as a drug target. *Curr Opin Pharmacol,* 4**,** 12-7.

SCHWARTZ, T. W. & HOLST, B. 2007. Allosteric enhancers, allosteric agonists and ago-allosteric modulators: where do they bind and how do they act? *Trends Pharmacol Sci,* 28**,** 366-73.

SEKO, T., ITO, M., KUREISHI, Y., OKAMOTO, R., MORIKI, N., ONISHI, K., ISAKA, N., HARTSHORNE, D. J. & NAKANO, T. 2003. Activation of RhoA and inhibition of myosin phosphatase as important components in hypertension in vascular smooth muscle. *Circ Res,* 92**,** 411-8.

SHANG, X., MARCHIONI, F., EVELYN, C. R., SIPES, N., ZHOU, X., SEIBEL, W., WORTMAN, M. & ZHENG, Y. 2013. Small-molecule inhibitors targeting G-protein-coupled Rho guanine nucleotide exchange factors. *Proc Natl Acad Sci U S A,* 110**,** 3155-60.

SHENOY, S. K. & LEFKOWITZ, R. J. 2011. beta-Arrestin-mediated receptor trafficking and signal transduction. *Trends Pharmacol Sci,* 32**,** 521-33.

SHENOY, S. K., MCDONALD, P. H., KOHOUT, T. A. & LEFKOWITZ, R. J. 2001. Regulation of receptor fate by ubiquitination of activated beta 2-adrenergic receptor and beta-arrestin. *Science,* 294**,** 1307-13.

SHUKLA, A. K., XIAO, K. & LEFKOWITZ, R. J. 2011. Emerging paradigms of beta-arrestin-dependent seven transmembrane receptor signaling. *Trends Biochem Sci,* 36**,** 457-69.

SHUKLA, N. & JEREMY, J. Y. 2012. Pathophysiology of saphenous vein graft failure: a brief overview of interventions. *Curr Opin Pharmacol,* 12**,** 114-20.

SIEHLER, S. 2009. Regulation of RhoGEF proteins by G12/13-coupled receptors. *Br J Pharmacol,* 158**,** 41-9.

SIMA, A. V., STANCU, C. S. & SIMIONESCU, M. 2009. Vascular endothelium in atherosclerosis. *Cell Tissue Res,* 335**,** 191-203.

SIU, F. Y., HE, M., DE GRAAF, C., HAN, G. W., YANG, D., ZHANG, Z., ZHOU, C., XU, Q., WACKER, D., JOSEPH, J. S., LIU, W., LAU, J., CHEREZOV, V., KATRITCH, V., WANG, M. W. & STEVENS, R. C. 2013. Structure of the human glucagon class B G-protein-coupled receptor. *Nature,* 499**,** 444-9.

SIVARAJ, K. K., TAKEFUJI, M., SCHMIDT, I., ADAMS, R. H., OFFERMANNS, S. & WETTSCHURECK, N. 2013. G13 controls angiogenesis through regulation of VEGFR-2 expression. *Dev Cell,* 25**,** 427-34.

SMIT, M. J., VISCHER, H. F., BAKKER, R. A., JONGEJAN, A., TIMMERMAN, H., PARDO, L. & LEURS, R. 2007. Pharmacogenomic and structural analysis of constitutive g protein-coupled receptor activity. *Annu Rev Pharmacol Toxicol,* 47**,** 53-87.

SMITH, N. J., BENNETT, K. A. & MILLIGAN, G. 2011. When simple agonism is not enough: emerging modalities of GPCR ligands. *Mol Cell Endocrinol,* 331**,** 241-7.

SMITH, S. C., JR., DOVE, J. T., JACOBS, A. K., KENNEDY, J. W., KEREIAKES, D., KERN, M. J., KUNTZ, R. E., POPMA, J. J., SCHAFF, H. V., WILLIAMS, D. O., GIBBONS, R. J., ALPERT, J. P., EAGLE, K. A., FAXON, D. P., FUSTER, V., GARDNER, T. J., GREGORATOS, G. & RUSSELL, R. O. 2001. ACC/AHA guidelines for percutaneous coronary intervention (revision of the 1993 PTCA guidelines)-executive summary: a report of the American College of Cardiology/American Heart Association task force on practice guidelines (Committee to revise the 1993 guidelines for percutaneous transluminal coronary angioplasty) endorsed by the Society for Cardiac Angiography and Interventions. *Circulation,* 103**,** 3019-41.

SOUTHERN, C., COOK, J. M., NEETOO-ISSELJEE, Z., TAYLOR, D. L., KETTLEBOROUGH, C. A., MERRITT, A., BASSONI, D. L., RAAB, W. J., QUINN, E., WEHRMAN, T. S., DAVENPORT, A. P., BROWN, A. J., GREEN, A.,

WIGGLESWORTH, M. J. & REES, S. 2013. Screening beta-arrestin recruitment for the identification of natural ligands for orphan G-protein-coupled receptors. *J Biomol Screen,* 18**,** 599-609.

STAESSEN, J. A., WANG, J., BIANCHI, G. & BIRKENHAGER, W. H. 2003. Essential hypertension. *Lancet,* 361**,** 1629-41.

STANDFUSS, J., EDWARDS, P. C., D'ANTONA, A., FRANSEN, M., XIE, G., OPRIAN, D. D. & SCHERTLER, G. F. 2011. The structural basis of agonist-induced activation in constitutively active rhodopsin. *Nature,* 471**,** 656-60.

STEPHENS, L., SMRCKA, A., COOKE, F. T., JACKSON, T. R., STERNWEIS, P. C. & HAWKINS, P. T. 1994. A novel phosphoinositide 3 kinase activity in myeloid-derived cells is activated by G protein beta gamma subunits. *Cell,* 77**,** 83-93.

STEVENS, R. C., CHEREZOV, V., KATRITCH, V., ABAGYAN, R., KUHN, P., ROSEN, H. & WUTHRICH, K. 2013. The GPCR Network: a large-scale collaboration to determine human GPCR structure and function. *Nat Rev Drug Discov,* 12**,** 25-34.

STONE, N. J., ROBINSON, J., LICHTENSTEIN, A. H., BAIREY MERZ, C. N., LLOYD-JONES, D. M., BLUM, C. B., MCBRIDE, P., ECKEL, R. H., SCHWARTZ, J. S., GOLDBERG, A. C., SHERO, S. T., GORDON, D., SMITH, S. C., JR., LEVY, D., WATSON, K. & WILSON, P. W. 2013a. 2013 ACC/AHA Guideline on the Treatment of Blood Cholesterol to Reduce Atherosclerotic Cardiovascular Risk in Adults: A Report of the American College of Cardiology/American Heart Association Task Force on Practice Guidelines. *J Am Coll Cardiol.*

STONE, T. W. 1993. Neuropharmacology of quinolinic and kynurenic acids. *Pharmacol Rev,* 45**,** 309-79.

STONE, T. W., STOY, N. & DARLINGTON, L. G. 2013b. An expanding range of targets for kynurenine metabolites of tryptophan. *Trends Pharmacol Sci,* 34**,** 136-43.

STRATHMANN, M. P. & SIMON, M. I. 1991. G alpha 12 and G alpha 13 subunits define a fourth class of G protein alpha subunits. *Proc Natl Acad Sci U S A,* 88**,** 5582-6.

SUN, Y. V., BIELAK, L. F., PEYSER, P. A., TURNER, S. T., SHEEDY, P. F., 2ND, BOERWINKLE, E. & KARDIA, S. L. 2008. Application of machine learning algorithms to predict coronary artery calcification with a sibship-based design. *Genet Epidemiol,* 32**,** 350-60.

SURMA, M., WEI, L. & SHI, J. 2011. Rho kinase as a therapeutic target in cardiovascular disease. *Future Cardiol,* 7**,** 657-71.

SUZUKI, N., HAJICEK, N. & KOZASA, T. 2009. Regulation and physiological functions of G12/13-mediated signaling pathways. *Neurosignals,* 17**,** 55-70.

TAKEFUJI, M., WIRTH, A., LUKASOVA, M., TAKEFUJI, S., BOETTGER, T., BRAUN, T., ALTHOFF, T., OFFERMANNS, S. & WETTSCHURECK, N. 2012. G(13)-mediated signaling pathway is required for pressure overload-induced cardiac remodeling and heart failure. *Circulation,* 126**,** 1972-82.

TANG, C. M. & INSEL, P. A. 2004. GPCR expression in the heart; "new" receptors in myocytes and fibroblasts. *Trends Cardiovasc Med,* 14**,** 94-9.

TANIGUCHI, Y., TONAI-KACHI, H. & SHINJO, K. 2006. Zaprinast, a well-known cyclic guanosine monophosphate-specific phosphodiesterase inhibitor, is an agonist for GPR35. *FEBS Lett,* 580**,** 5003-8.

TAYLOR, A. J., MERZ, C. N. & UDELSON, J. E. 2003. 34th Bethesda Conference: Executive summary--can atherosclerosis imaging techniques improve the detection of patients at risk for ischemic heart disease? *J Am Coll Cardiol,* 41**,** 1860-2.

TELLER, D. C., OKADA, T., BEHNKE, C. A., PALCZEWSKI, K. & STENKAMP, R. E. 2001. Advances in determination of a high-resolution three-dimensional structure of rhodopsin, a model of G-protein-coupled receptors (GPCRs). *Biochemistry,* 40**,** 7761-72.

THYGESEN, K., ALPERT, J. S., JAFFE, A. S., SIMOONS, M. L., CHAITMAN, B. R., WHITE, H. D., KATUS, H. A., LINDAHL, B., MORROW, D. A., CLEMMENSEN, P. M., JOHANSON, P., HOD, H., UNDERWOOD, R., BAX, J. J., BONOW, R. O.,

PINTO, F., GIBBONS, R. J., FOX, K. A., ATAR, D., NEWBY, L. K., GALVANI, M., HAMM, C. W., URETSKY, B. F., STEG, P. G., WIJNS, W., BASSAND, J. P., MENASCHE, P., RAVKILDE, J., OHMAN, E. M., ANTMAN, E. M., WALLENTIN, L. C., ARMSTRONG, P. W., JANUZZI, J. L., NIEMINEN, M. S., GHEORGHIADE, M., FILIPPATOS, G., LUEPKER, R. V., FORTMANN, S. P., ROSAMOND, W. D., LEVY, D., WOOD, D., SMITH, S. C., HU, D., LOPEZ-SENDON, J. L., ROBERTSON, R. M., WEAVER, D., TENDERA, M., BOVE, A. A., PARKHOMENKO, A. N., VASILIEVA, E. J. & MENDIS, S. 2012. Third universal definition of myocardial infarction. *Circulation,* 126**,** 2020-35.

TOUYZ, R. M. & SCHIFFRIN, E. L. 2000. Signal transduction mechanisms mediating the physiological and pathophysiological actions of angiotensin II in vascular smooth muscle cells. *Pharmacol Rev,* 52**,** 639-72.

TSANG, S. H., BURNS, M. E., CALVERT, P. D., GOURAS, P., BAYLOR, D. A., GOFF, S. P. & ARSHAVSKY, V. Y. 1998. Role for the target enzyme in deactivation of photoreceptor G protein in vivo. *Science,* 282**,** 117-21.

TURNBULL, F. 2003. Effects of different blood-pressure-lowering regimens on major cardiovascular events: results of prospectively-designed overviews of randomised trials. *Lancet,* 362**,** 1527-35.

TURSKI, M. P., TURSKA, M., PALUSZKIEWICZ, P., PARADA-TURSKA, J. & OXENKRUG, G. F. 2013. Kynurenic Acid in the Digestive System-New Facts, New Challenges. *Int J Tryptophan Res,* 6**,** 47-55.

VAN DEN BUUSE, M. 1994. Circadian rhythms of blood pressure, heart rate, and locomotor activity in spontaneously hypertensive rats as measured with radio-telemetry. *Physiol Behav,* 55**,** 783-7.

VAN DER HEIDEN, K., GIJSEN, F. J., NARRACOTT, A., HSIAO, S., HALLIDAY, I., GUNN, J., WENTZEL, J. J. & EVANS, P. C. 2013. The effects of stenting on shear stress: relevance to endothelial injury and repair. *Cardiovasc Res,* 99**,** 269-75.

VANDER MOLEN, J., FRISSE, L. M., FULLERTON, S. M., QIAN, Y., DEL BOSQUE-PLATA, L., HUDSON, R. R. & DI RIENZO, A. 2005. Population genetics of CAPN10 and GPR35: implications for the evolution of type 2 diabetes variants. *Am J Hum Genet,* 76**,** 548-60.

VANE, J. R., BAKHLE, Y. S. & BOTTING, R. M. 1998. Cyclooxygenases 1 and 2. *Annu Rev Pharmacol Toxicol,* 38**,** 97-120.

VASAN, R. S. 2006. Biomarkers of cardiovascular disease: molecular basis and practical considerations. *Circulation,* 113**,** 2335-62.

VENKATAKRISHNAN, A. J., DEUPI, X., LEBON, G., TATE, C. G., SCHERTLER, G. F. & BABU, M. M. 2013. Molecular signatures of G-protein-coupled receptors. *Nature,* 494**,** 185-94.

VERTELOV, G., KHARAZI, L., MURALIDHAR, M. G., SANATI, G., TANKOVICH, T. & KHARAZI, A. 2013. High targeted migration of human mesenchymal stem cells grown in hypoxia is associated with enhanced activation of RhoA. *Stem Cell Res Ther,* 4**,** 5.

VIOLIN, J. D., SOERGEL, D. G., BOERRIGTER, G., BURNETT, J. C., JR. & LARK, M. W. 2013. GPCR biased ligands as novel heart failure therapeutics. *Trends Cardiovasc Med,* 23**,** 242-9.

VIRMANI, R., KOLODGIE, F. D., BURKE, A. P., FINN, A. V., GOLD, H. K., TULENKO, T. N., WRENN, S. P. & NARULA, J. 2005. Atherosclerotic plaque progression and vulnerability to rupture: angiogenesis as a source of intraplaque hemorrhage. *Arterioscler Thromb Vasc Biol,* 25**,** 2054-61.

WALD, D. S., LAW, M., MORRIS, J. K., BESTWICK, J. P. & WALD, N. J. 2009. Combination therapy versus monotherapy in reducing blood pressure: meta-analysis on 11,000 participants from 42 trials. *Am J Med,* 122**,** 290-300.

WALTHER, C. & FERGUSON, S. S. 2013. Arrestins: role in the desensitization, sequestration, and vesicular trafficking of G protein-coupled receptors. *Prog Mol Biol Transl Sci,* 118**,** 93-113.

WAN, S., GEORGE, S. J., BERRY, C. & BAKER, A. H. 2012a. Vein graft failure: current clinical practice and potential for gene therapeutics. *Gene Ther,* 19**,** 630-6.

WAN, Y., WU, Y. L., LIAN, L. H., XIE, W. X., LI, X., OUYANG, B. Q., BAI, T., LI, Q., YANG, N. & NAN, J. X. 2012b. The anti-fibrotic effect of betulinic acid is mediated through the inhibition of NF-kappaB nuclear protein translocation. *Chem Biol Interact,* 195**,** 215-23.

WANG, J., SIMONAVICIUS, N., WU, X., SWAMINATH, G., REAGAN, J., TIAN, H. & LING, L. 2006a. Kynurenic acid as a ligand for orphan G protein-coupled receptor GPR35. *J Biol Chem,* 281**,** 22021-8.

WANG, P., HENNING, S. M. & HEBER, D. 2010. Limitations of MTT and MTS-based assays for measurement of antiproliferative activity of green tea polyphenols. *PLoS One,* 5**,** e10202.

WANG, T. J., GONA, P., LARSON, M. G., TOFLER, G. H., LEVY, D., NEWTON-CHEH, C., JACQUES, P. F., RIFAI, N., SELHUB, J., ROBINS, S. J., BENJAMIN, E. J., D'AGOSTINO, R. B. & VASAN, R. S. 2006b. Multiple biomarkers for the prediction of first major cardiovascular events and death. *N Engl J Med,* 355**,** 2631-9.

WANG, Y., ZHENG, X. R., RIDDICK, N., BRYDEN, M., BAUR, W., ZHANG, X. & SURKS, H. K. 2009. ROCK isoform regulation of myosin phosphatase and contractility in vascular smooth muscle cells. *Circ Res,* 104**,** 531-40.

WATKINS, S. J., BORTHWICK, G. M. & ARTHUR, H. M. 2011. The H9C2 cell line and primary neonatal cardiomyocyte cells show similar hypertrophic responses in vitro. *In Vitro Cell Dev Biol Anim,* 47, 125-31.

WEBER, C. & NOELS, H. 2011. Atherosclerosis: current pathogenesis and therapeutic options. *Nat Med,* 17**,** 1410-22.

WEBER, M. A., SCHIFFRIN, E. L., WHITE, W. B., MANN, S., LINDHOLM, L. H., KENERSON, J. G., FLACK, J. M., CARTER, B. L., MATERSON, B. J., RAM, C. V., COHEN, D. L., CADET, J. C., JEAN-CHARLES, R. R., TALER, S., KOUNTZ, D., TOWNSEND, R. R., CHALMERS, J., RAMIREZ, A. J., BAKRIS, G. L., WANG, J., SCHUTTE, A. E., BISOGNANO, J. D., TOUYZ, R. M., SICA, D. & HARRAP, S. B. 2014. Clinical practice guidelines for the management of hypertension in the community: a statement by the American Society of Hypertension and the International Society of Hypertension. *J Clin Hypertens (Greenwich),* 16, 14-26.

WERMUTH, C. G. 2004. Selective optimization of side activities: another way for drug discovery. *J Med Chem,* 47**,** 1303-14.

WETTSCHURECK, N. & OFFERMANNS, S. 2005. Mammalian G proteins and their cell type specific functions. *Physiol Rev,* 85**,** 1159-204.

WHITWORTH, J. A. 2003. 2003 World Health Organization (WHO)/International Society of Hypertension (ISH) statement on management of hypertension. *J Hypertens,* 21**,** 1983-92.

WIRTH, A. 2010. Rho kinase and hypertension. *Biochim Biophys Acta,* 1802**,** 1276-84.

WOJCIAK-STOTHARD, B., TSANG, L. Y. & HAWORTH, S. G. 2005. Rac and Rho play opposing roles in the regulation of hypoxia/reoxygenation-induced permeability changes in pulmonary artery endothelial cells. *Am J Physiol Lung Cell Mol Physiol,* 288**,** L749-60.

WOJCIAK-STOTHARD, B., ZHAO, L., OLIVER, E., DUBOIS, O., WU, Y., KARDASSIS, D., VASILAKI, E., HUANG, M., MITCHELL, J. A., HARRINGTON, L. S., PRENDERGAST, G. C. & WILKINS, M. R. 2012. Role of RhoB in the regulation of pulmonary endothelial and smooth muscle cell responses to hypoxia. *Circ Res,* 110**,** 1423-34.

WOOLLARD, K. J. & GEISSMANN, F. 2010. Monocytes in atherosclerosis: subsets and functions. *Nat Rev Cardiol,* 7**,** 77-86.

WORZFELD, T., WETTSCHURECK, N. & OFFERMANNS, S. 2008. G(12)/G(13)-mediated signalling in mammalian physiology and disease. *Trends Pharmacol Sci,* 29**,** 582-9.

WU, B., CHIEN, E. Y., MOL, C. D., FENALTI, G., LIU, W., KATRITCH, V., ABAGYAN, R., BROOUN, A., WELLS, P., BI, F. C., HAMEL, D. J., KUHN, P., HANDEL, T. M., CHEREZOV, V. & STEVENS, R. C. 2010. Structures of the CXCR4 chemokine GPCR with small-molecule and cyclic peptide antagonists. *Science,* 330**,** 1066-71.

WU, H., WANG, C., GREGORY, K. J., HAN, G. W., CHO, H. P., XIA, Y., NISWENDER, C. M., KATRITCH, V., MEILER, J., CHEREZOV, V., CONN, P. J. & STEVENS, R. C. 2014. Structure of a class C GPCR metabotropic glutamate receptor 1 bound to an allosteric modulator. *Science,* 344**,** 58-64.

XU, F., WU, H., KATRITCH, V., HAN, G. W., JACOBSON, K. A., GAO, Z. G., CHEREZOV, V. & STEVENS, R. C. 2011. Structure of an agonist-bound human A2A adenosine receptor. *Science,* 332**,** 322-7.

YAMAMOTO, H., OKUZAKI, D., YAMANISHI, K., XU, Y., WATANABE, Y., YOSHIDA, M., YAMASHITA, A., GOTO, N., NISHIGUCHI, S., SHIMADA, K., NOJIMA, H., YASUNAGA, T., OKAMURA, H., MATSUNAGA, H. & YAMANISHI, H. 2013. Genetic analysis of genes causing hypertension and stroke in spontaneously hypertensive rats. *Int J Mol Med,* 31**,** 1057-65.

YAMORI, Y., HORIE, R., HANDA, H., SATO, M. & FUKASE, M. 1976. Pathogenetic similarity of strokes in stroke-prone spontaneously hypertensive rats and humans. *Stroke,* 7**,** 46-53.

YANG, Y., LU, J. Y., WU, X., SUMMER, S., WHORISKEY, J., SARIS, C. & REAGAN, J. D. 2010. G-protein-coupled receptor 35 is a target of the asthma drugs cromolyn disodium and nedocromil sodium. *Pharmacology,* 86**,** 1-5.

YIN, S. & NISWENDER, C. M. 2014. Progress toward advanced understanding of metabotropic glutamate receptors: structure, signaling and therapeutic indications. *Cell Signal*.

YONA, S., LIN, H. H., SIU, W. O., GORDON, S. & STACEY, M. 2008. Adhesion-GPCRs: emerging roles for novel receptors. *Trends Biochem Sci,* 33**,** 491-500.

ZHAO, P. & ABOOD, M. E. 2013. GPR55 and GPR35 and their relationship to cannabinoid and lysophospholipid receptors. *Life Sci,* 92**,** 453-7.

ZHAO, P., LANE, T. R., GAO, H. G., HURST, D. P., KOTSIKOROU, E., LE, L., BRAILOIU, E., REGGIO, P. H. & ABOOD, M. E. 2014. Crucial positively charged residues for ligand activation of the GPR35 receptor. *J Biol Chem,* 289**,** 3625-38.

ZHAO, P., SHARIR, H., KAPUR, A., COWAN, A., GELLER, E. B., ADLER, M. W., SELTZMAN, H. H., REGGIO, P. H., HEYNEN-GENEL, S., SAUER, M., CHUNG, T. D., BAI, Y., CHEN, W., CARON, M. G., BARAK, L. S. & ABOOD, M. E. 2010. Targeting of the orphan receptor GPR35 by pamoic acid: a potent activator of extracellular signal-regulated kinase and beta-arrestin2 with antinociceptive activity. *Mol Pharmacol,* 78**,** 560-8.

ZHOU, Q., GENSCH, C. & LIAO, J. K. 2011. Rho-associated coiled-coil-forming kinases (ROCKs): potential targets for the treatment of atherosclerosis and vascular disease. *Trends Pharmacol Sci,* 32**,** 167-73.

ZIMMERMAN, M. C., LAZARTIGUES, E., SHARMA, R. V. & DAVISSON, R. L. 2004. Hypertension caused by angiotensin II infusion involves increased superoxide production in the central nervous system. *Circ Res,* 95**,** 210-6.